National Aeronautics and Space Administration

ORCAS

AS3 Report

PI: Dr. Eliad Peretz

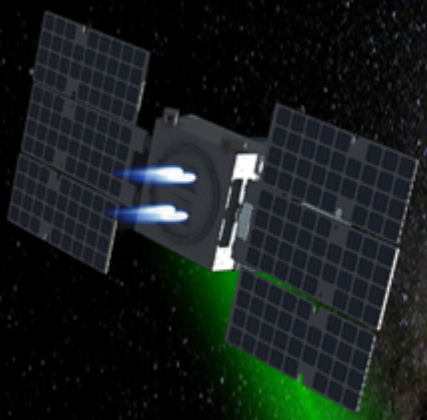

https://asd.gsfc.nasa.gov/orcas/

The Orbiting Configurable Artificial Star – ORCAS

Exploring our Universe at Unprecedented Angular Resolution & Sensitivity

ORCAS delivers superb angular resolution & sensitivity in the coming decade enabling scientific discovery

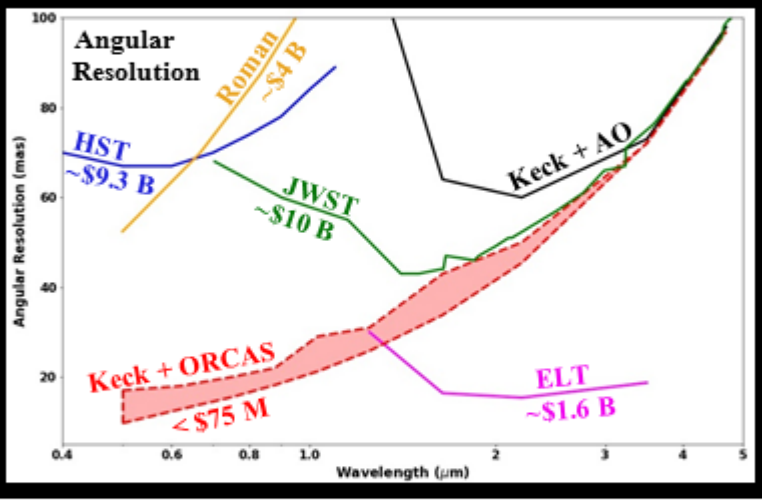

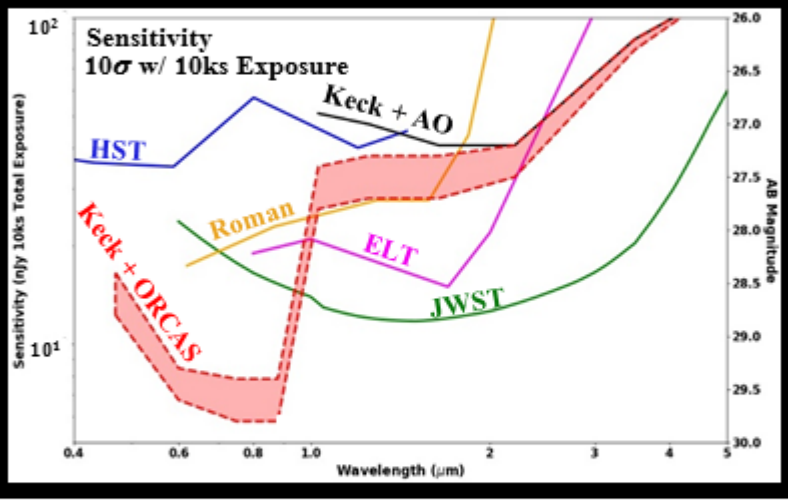

ORCAS can deliver parsec scale images unlocking the ability to detect a population of supermassive black hole binaries for the first time

10^2 10^1 1 Pair Separation [kpc] 10^{-3}

Galaxy Inspiral Dual Inspiral [Phase] Bound Binary GW

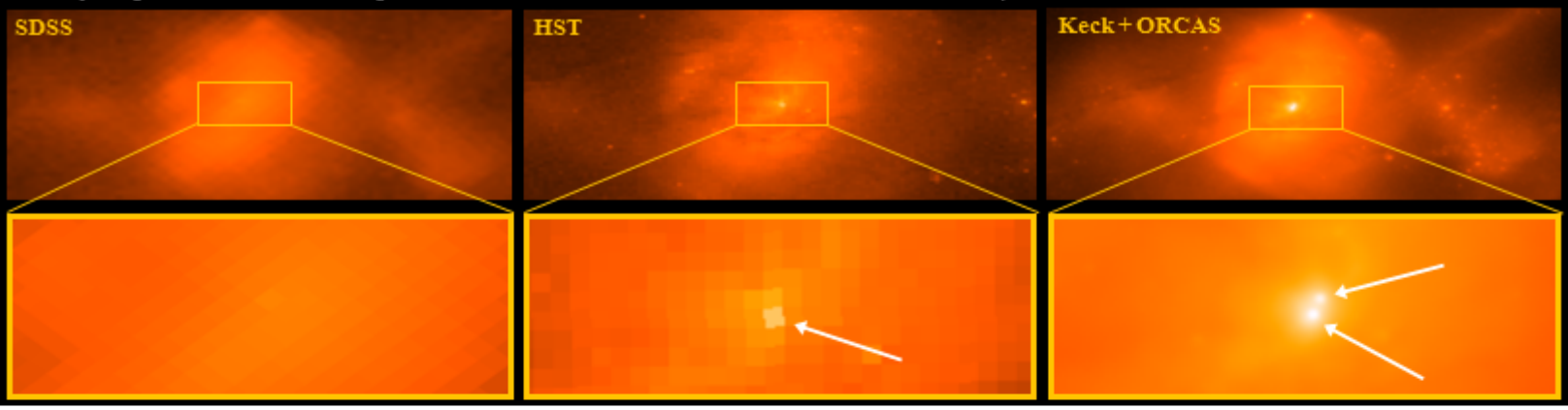

ORCAS+Keck will measure accurate distances from the light of 10 billion year old supernovae

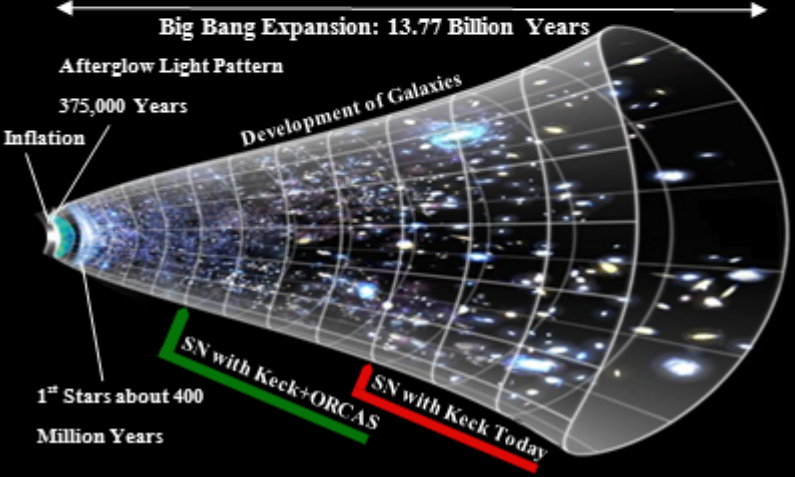

ORCAS delivers calibrated light that will vastly improve cosmology measurements

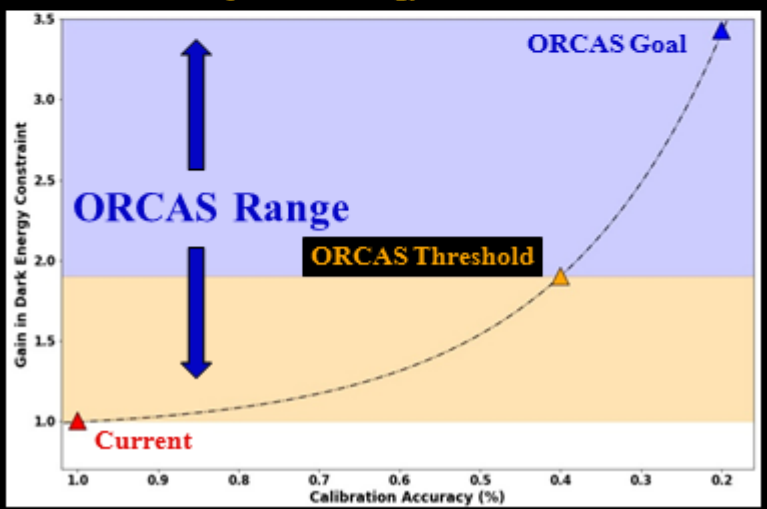

https://asd.gsfc.nasa.gov/orcas/

The Orbiting Configurable Artificial Star – ORCAS

Exploring our Universe at Unprecedented Angular Resolution & Sensitivity

By bringing together ground and space communities around common scientific goals, ORCAS answers fundamental scientific questions of the 2020's at a small sat budget, a decade ahead of its time

Mission Characteristics

Community driven observing program

10 meter nearly diffraction limited at 500 nm

Limiting Magnitude of 29 with 1 hour of exposure

Wavelength Coverage: 0.5-5μm

300 AO observations & 1500 flux-calibration sessions

Serviceable Ground Configuration

2026 Launch Date

3 years prime mission.

Sky Coverage: Keck observable sky

Can use both Keck I & II Telescopes Simultaneously

Low Mission Cost: Less than $75 Million

Highly Elliptical Orbit with ~200,000km Apogee

Solar Electric Propulsion System, > 4,000 m/s Delta-V

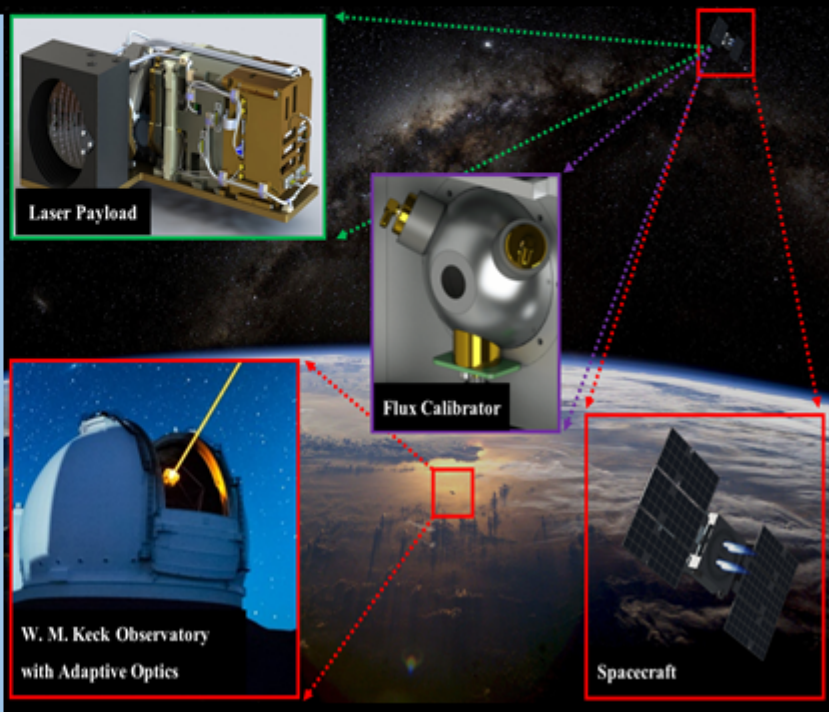

All Four Sub-Components of the ORCAS Mission

ORCAS Orbit

5 Day Period

Highly Elliptical

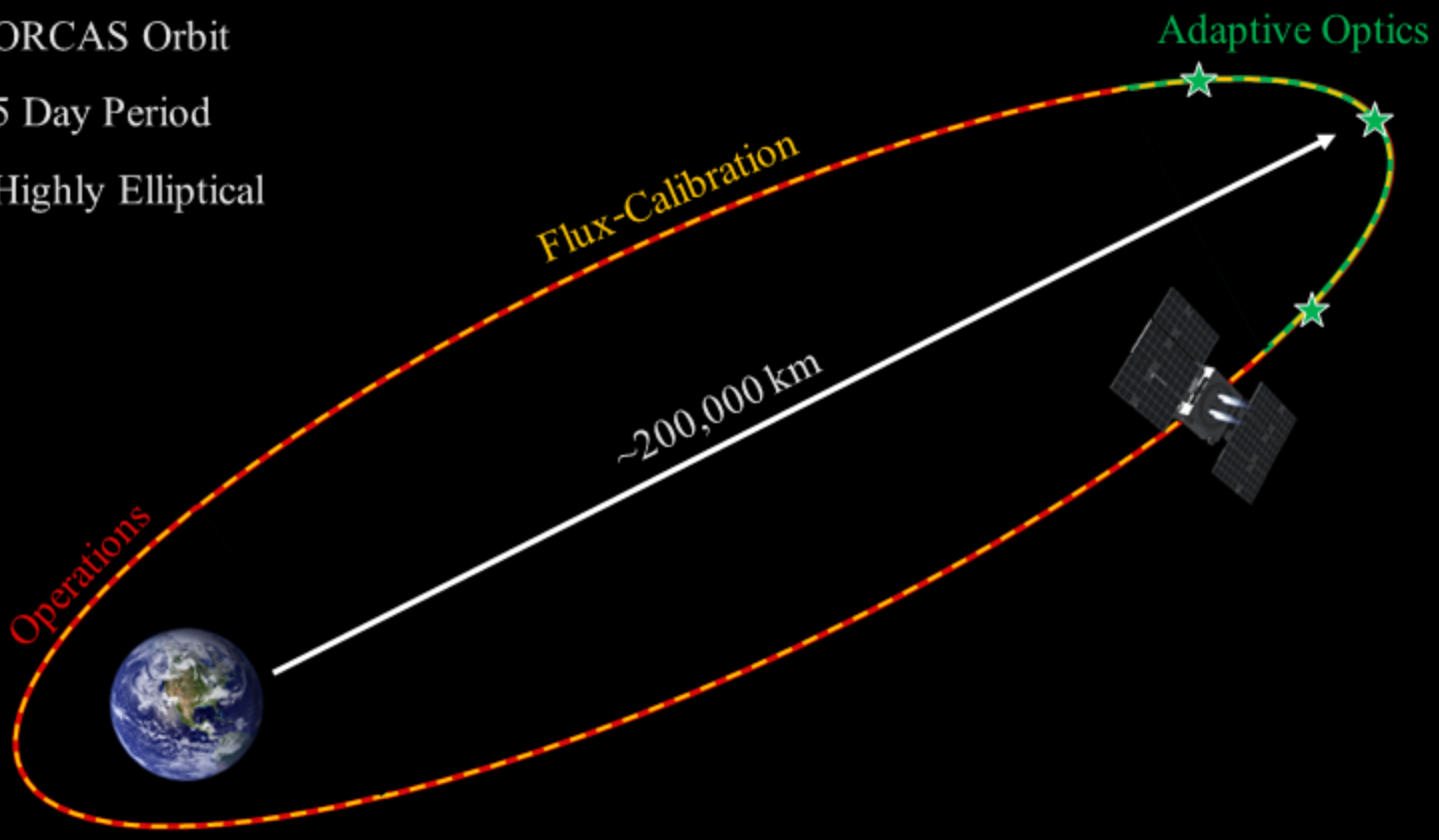

https://asd.gsfc.nasa.gov/orcas/

The Orbiting Configurable Artificial Star (ORCAS) Mission

Principal Investigator: Eliad Peretz (NASA/GSFC)
Co-Investigators: John C. Mather (NASA/GSFC), Justin Albert (University of Victoria), Greg Aldering (Lawrence Berkeley National Lab), Peter Kurczynski (NASA/GSFC), Robert Lafon (NASA/GSFC), Stefanie Milam (NASA/GSFC), John O'Meara (WMKO), Imke de Pater (University of California, Berkeley), Saul Perlmutter (University of California, Berkeley), Peter Plavchan (George Mason University), Shobita Satyapal (George Mason University), Rogier Windhorst (Arizona State University), Peter Wizinowich (WMKO)

Collaborators: Aaron Barth (University of California, Irvine), Randall Campbell (WMKO), Gabriela Canalizo (University of California, Riverside), Matt Cristina (General Atomics), Gianluca Di Rico (INAF), Josh Duncan (Blue Canyon Technologies), Aaron Freeman (General Atomics), Karl Gebhardt (University of Texas), Kelsey Gilchrist (University of Chicago), Eric Golliher (NASA/GSFC), Kevin Hall (University of Maryland), Christine Hamilton (Stanford University), Erin Hicks (University of Alaska, Anchorage), Douglas Hyland (General Atomics), Stephanie Juneau (NOAO), Marc Kassis (WMKO), Mike Koss (Eureka Scientific), Daniel Küsters (University of California, Berkeley/Deutsches Elektronen-Synchrotron), Sibasish Laha (UMBC, NASA/GSFC), Jessica Lu (University of California, Berkeley), Matthew Malkan (University of California, LA), Dimitri Mawet (California Institute of Technology), Claire Max (University of California, Santa Cruz), Kyle McCormick (General Atomics), Adam Michaels (NASA/GSFC), David Michelson (University of British Columbia), Max Millar-Blanchaer (University of California, Santa Barbara), Ellouise Moehring (Purdue University), Francisco Muller Sanchez (University of Memphis), Patrick Newman (George Mason University), Rebecca Oppenheimer (American Museum of Natural History), Lucas Pabarcius (NASA/GSFC), Piotr Pachowicz (George Mason University), Elisa Portaluri (INAF), Robert Pritchett (NASA/GSFC), Joe Rice (NIST), Barry Rothberg (LBT), Sara Seager (MIT), Richard Slonaker (NASA/GSFC), Mark Stephen (NASA/GSFC), Mark Storm (Fibertek), David Vermilion (George Mason University, NASA/MSFC), Geronimo Villanueva (NASA/GSFC), Vivian U (University of California, Irvine), Wayne Yu (NASA/GSFC)

Acknowledgements: The ORCAS team would like to extend special thanks to the following people and groups for their contributions. First we would like to thank GSFC Center Director Dennis Andrucyk and Deputy Center Director Anne Kinney, SED Director Mark Clampin, ETD Deputy director Joe Hill, and Assistant Director for Strategy Jay Pittman for their strategic advice and guidance throughout this study. We want to thank the GSFC astrophysics division, Rob Petre, Keith Jahoda, David Richardson, Padi Boyd, Rita Sambruna, Jonathan Gardner, and Erin Smith for their constructive feedback. Thanks also to the Mission Planning Lab team including Ben Cervantes and William Mast and Red Team Members Leonard Garcia and Steven Lloyd. And finally, thank you to Eric Smith and NASA's Astrophysics SmallSats officials, Michael Garcia and Heather Watson, for their support.

Contact Information: eliad.peretz@nasa.gov, **Phone: 607-882-0458.**
Submitted in response to NASA ROSES NNH19ZDA001N-AS3
(Astrophysics Science SmallSat Studies, AS3)

Contents

1 Report Summary

1.1 Executive Summary

The ORCAS mission, a first-of-its-kind hybrid space and ground observatory, will enable new science, otherwise only accessible to flagship class missions over a decade from now, at a SmallSat budget, providing unprecedented angular resolution, exquisite sensitivity and a unique flux calibrator. By enabling adaptive optics and flux calibration observations, ORCAS will deliver highly detailed images, unlocking the ability to detect a population of supermassive black hole binaries for the first time, as well as constraining the number densities of the faintest star forming clumps and understanding dark energy by measuring the distances of 10 billion year old supernovae. It will also deliver calibrated light that will vastly improve cosmology measurements, among many other advances. The low-cost ORCAS mission operating in collaboration with the W. M. Keck observatory will provide Great Observatory quality capabilities open to all US observers via a community driven observation plan. These observations will result in unique science for the mission, while also complementing and extending the science of HST, JWST, and Roman, as well as other potential future missions.

This report puts forward in detail the scientific reasoning for the ORCAS mission, and demonstrates that ORCAS could answer fundamental scientific questions of the 2020's, addressing our community goals. We do so by establishing the mission science traceability matrix and deriving the engineering requirements for each mission subsystem. We show that there is a viable and robust path for the ORCAS mission to achieve its scientific goals within a reasonable time frame and budget. Finally, the report presents technical details and major subsystems, including the spacecraft, payload, ground elements, mission operation concept, etc., and show that they could meet the science case requirements.

The ORCAS mission explicitly addresses two of the top three priorities of the 2010 Decadal Survey: "Cosmic Dawn: Searching for the First Stars, Galaxies, and Black Holes," and "Physics of the Universe: Understanding Scientific Principles." One of the great mysteries is the existence and growth of super-massive black holes through the merger of protogalaxies and the accretion of gas and stars; our ability to solve this mystery is limited by current angular resolution and sensitivity. The cosmic dark energy is likewise a mystery that has only grown deeper as measurements improve and disagreements appear. Photometric calibration is currently one of the largest error terms in dark energy measurements. ORCAS explores a new parameter regime in angular resolution and sensitivity, allowing for huge potential advances for these questions. Additionally, the flux calibrator would go far beyond our current capabilities, leading to quantitative advances in dark energy.

ORCAS is designed to both: 1) identify and characterize the velocity structures of the physical environments of Active Galactic Nuclei (AGN), especially M87* and those containing two or more nuclei, and 2) resolve discrepancies in measurements of the cosmic dark energy, both with spectroscopic observations of high redshift Supernovae (SNe) and with improvements in flux calibration for all SNe. These objectives drive the design requirements, and the design then enables investigations of high redshift galaxy structures, circumstellar disks, exoplanet formation, and Solar System objects.

These objectives are met by a new combination of space and ground hardware which will enable high performance Adaptive Optics (AO) at visible and NIR wavelengths on the Keck 10 m telescopes. We deploy low-risk flight hardware, which includes a commercial ESPA-Grande class satellite bus

with solar electric propulsion (SEP) carrying a modified commercial laser module as an AO beacon and a photometric calibrator. The spacecraft is positioned in a 5-day Highly Elliptical Orbit (HEO), enabling 3 AO observation opportunities per orbit, such that the spacecraft remains within the isoplanatic patch (region of good AO performance) for periods of up to a few hours (target declination and wavelength dependent). The available mission sky coverage is the Keck observable sky. The bus is augmented with a high-altitude GPS system demonstrated by GSFC on the MMS (Magnetospheric Multiscale) mission, enabling high precision orbit management to place the ORCAS predicted trajectory within ($\pm$ 3 milliarcsec, 3σ). ORCAS will enable $\sim$ 300 AO observations and 1,500 photometric observations throughout its 3-year mission lifetime.

The ORCAS team includes scientific and engineering expertise in all relevant areas with two Nobel Laureates (one of whom led NASA's first Explorer program mission "COBE"), an interdisciplinary science team, a space segment team led by GSFC, a ground team led by W. M. Keck Observatory, and a wide range of collaborators from academic institutions and industry partners.

1.2 How to Use this Report

This final report is provided in conclusion of the year-long ORCAS AS3 mission study. It includes all required elements as described in the study notification letter, as stated and traced to the report chapters in Table 1.

Table 1 AS3 Mission Study Requirements

AS3 Required Elements	**Section Number**
Science Objectives	2
Science Requirements, Traceable to the Science Objectives & the Proposed Complement with Supporting Rationale	3
Core Science Team Expertise & Traceability to Science Objectives	6.1
Mission Design/Architecture (Orbit, Multiple Spacecraft, etc)	5
Spacecraft Concept, Mass Budget, Power Budget, Telemetry Rates	4
Technology Needs, Quantified Gaps, & Development Required	6.5
Concept of Operations	5.1
Launch Vehicle Interface & Deployment Method	4.2
Estimated Mission Costs & Explanation of the Cost Estimation Method	6.2
Top Mission Risks & Key Mission Trades to be studied in Future	6.3

In this section (**Section 1**), we introduce the science and technology that ORCAS can complement and improve specifically relating to Adaptive Optics. **Section 2** covers all science objectives for the ORCAS mission, and also discusses how ORCAS will expand and improve current knowledge in each respective field. **Section 3** details the science traceability matrices for each of the science cases. **Section 4** presents the science implementation, which includes the engineering requirements, the flight system design, the payload design, and the telescope system design. **Section 5** discusses the mission operations, including the orbit design, observation operations concepts, and observation schedule optimization. **Section 6** presents the mission development approach including the management team, cost estimates, risks, schedule for the mission, and TRL assessment. **Section 7** concludes with remaining technology challenges and future trade studies. The remaining sections (Appendices A-B) provide supporting information.

1.3 Frequently Asked Questions (FAQs)

ORCAS FAQs (Part 1 of 2)

What are ORCAS' key science drivers?
ORCAS would provide science that would help us answer some of the great mysteries including the existence and growth of supermassive black holes through the merger of protogalaxies and the accretion of gas and stars, and cosmic dark energy. ORCAS observations would allow us to detect intermediate and supermassive black holes, measure the dark energy equation of state, reduce errors and increase accuracy in the measurement of Supernovae, and constrain the number densities of the faintest Star Forming clumps, among other science drivers. ORCAS is principally driven by the science goals above, which will be enabled through observations of AGN, the supernova cosmic distance scale, and high redshift galaxies. Observations of flux calibration, exoplanets, and the Solar System will also be enabled by ORCAS. **[Section 2, 3]**

How many targets can ORCAS observe?
A single ORCAS spacecraft will provide around 300 AO mode observations and 1,500 Flux Calibration mode observations. **[Section 5]**

How much will ORCAS cost?
We aim to propose a budget of less than $75 M (30 percent of which is contingency) to NASA for construction of the spacecraft bus, ground elements, payloads, and operations. The spacecraft and payload costs is estimated at around $40 M. **[Section 6.2]**

Can ORCAS point its laser accurately enough to W. M. Keck Telescope?
Yes; ORCAS is required to provide $<$2" pointing accuracy, where the laser system can provide 0.2" pointing accuracy, a margin of x10. The spacecraft first points the laser payload field of view to the target, followed by the laser payload optical guidance system providing the fine tuning within the field of view. **[Section 4.3.1]**

Can both Keck Telescopes use ORCAS at the same time?
Yes; ORCAS can enable simultaneous scientific investigations with multiple instruments, spanning the entire observable wavelengths in a single observation. In fact, any telescope on the summit that chooses to use ORCAS can do so as long as they are integrated to the observation program. **[Section 4]**

What is the wavelength coverage?
ORCAS will be able to use current and developed Keck instruments and will have a wavelength coverage around 0.5 - 5 microns. ORCAS will provide two calibration wavelengths to support both visible and near infrared observations. **[Section 4]**

How long will the mission operate and when will it launch?
ORCAS is required to operate for three years, yet its design implies it could operate longer than that ($\sim$ 5 years), where the mission is ultimately limited by fuel usage for target selection. ORCAS could launch four and a half years after selection. **[Section 6]**

ORCAS FAQs (Part 2 of 2)

How does ORCAS get to its orbit?
Ideally, ORCAS will ride share to a high elliptical orbit with apogee near the desired direction. However, ORCAS propulsion system and mission operation concept were developed to additionally support GTO or Artemis ride share options. **[Section 6]**

How long could an ORCAS observation last?
ORCAS can stay passively within the isoplanatic patch for up to a few hours depending on target star declination and the observable wavelength. **[Section 5]**

What is the size and mass of the propellant tank?
The spacecraft will have 112 kg of Xenon propellant. This corresponds to 18 kg of fuel for the initial maneuvers to the science orbit and 54 kg allocated for maneuvers between observation orbits. This is enough fuel for 300 AO observations during the mission lifetime. **[Section 4]**

Why not use sodium layer guide stars? They're already great!
Sodium layer "laser guide stars" work well for near IR but not for short wavelengths because:

- Sodium layer stars are faint, and photon noise is a leading term in the wavefront sensor accuracy. The required brightness scales as λ^{-6}. As wavelength decreases, the number of atmospheric turbulence cells increases, their size decreases, the speed of measurement increases, and the measurement accuracy requirement increases.
- Sodium layer guide stars are only 85 km away and do not sample the same atmospheric column as the light from a star. The solution requires multiple laser beams, multiple wavefront sensors, and complex tomography algorithms. Accuracy is limited.
- A natural guide star is required near the field of view, to stabilize the image. The sodium layer guide stars are unstable because they are produced by upgoing laser beams passing through the turbulent atmosphere. Some regions are unobservable.

What about natural guide stars? They're already achieving high Strehl at visible wavelengths.

Natural guide star AO works well but is limited because:

- It works only for targets within a few arcseconds of bright stars, a negligible fraction of the sky.
- Stray light is very bright, limiting contrast to about 10^3 or 10^4 without a coronagraph. Application is limited to relatively bright companions.
- Extreme AO achieves higher contrast of 10^5 with reduced efficiency.

1.4 ORCAS Operational Context

By bringing together ground and space communities around common scientific goals, ORCAS answers fundamental scientific questions of the 2020's at a SmallSat budget, a decade ahead of its time.

The upcoming decade will see major astronomical observatories deployed. Among them are future space observatories such as the James Webb Space Telescope (JWST) and the Nancy Grace Roman Space Telescope (NGRST), and future ground observatories including the Vera Rubin Observatory (LSST), European Extremely Large Telescope (ELT), the Giant Magellan Telescope (GMT) and the Thirty Meter Telescope (TMT). These observatories will expand upon major scientific advances made by current observatories like the Hubble Space Telescope (HST) and the W. M. Keck Observatory (WMKO). Figure 1 illustrates the advantageous position of ORCAS in the future mission landscape. ORCAS enhances U.S. competitiveness in astronomy at a time when the U.S. is increasingly challenged by other nations. The participation between Keck and NASA unlocks this high performance AO for all U.S. astronomers.

ORCAS enables unprecedented angular resolution and sensitivity as illustrated in Figure 2. Its unique mission operation concept enables near diffraction limited performance from the ground by utilizing existing large telescopes and advances made in the last decade in the development and standardization of small spacecraft and their payload. Figure 3 shows that the ORCAS budget is nearly two orders of magnitude lower than other upcoming major space observatories.

In recent decades, Hubble and other space telescopes have provided images of unprecedented clarity that have led to major advances in our understanding of astronomical phenomena. NASA relies on large ground-based telescopes to provide confirmation and follow-up observations, without which the science remains incomplete. These telescopes, such as the Keck Observatory on Maunakea, use adaptive optics (AO) to provide partial correction of the atmospheric turbulence which blurs the images. Currently, AO uses either a bright star in the vicinity of the target to provide the atmospheric correction, known as natural guide star (NGS), or lasers projected from the ground, known as laser guide stars (LGS), at a few particular wavelengths. However, for more than 99.9% of astronomical targets there is no suitable NGS bright star (magnitude of 6 or less for visible band AO) in the close vicinity of the target, and stray light from the guide star limits contrast, even with an Extreme AO coronagraph for exoplanets. The ORCAS AO system is like the NGS AO but using a laser beacon, which can be rejected by a filter, eliminating the contrast problem, and works anywhere. LGS used at near IR wavelengths are fainter and suffer from the cone effect, tip tilt instability, wavelength-dependent AO correction errors, other limiting factors, and cannot work as well at visible wavelengths.

The ORCAS mission operation concept includes observations with both WMKO telescopes, enabling simultaneous AO observations utilizing different instrument suites. With the advantage of ORCAS working in conjunction with Keck, observatory upgrades can be effectively performed. Any instrument upgrade for the ORCAS mission, including expanded wavelength coverage and extended science returns, will useful to future Keck observations, although the Strehl will be reduced if used with LGS AO. AO observations could last up to a few hours depending on wavelength and declination.

ORCAS offers the ability to work with additional observatories on the ground as long as ORCAS can be seen within its respective observable sky, which can significantly increase both the flexibility

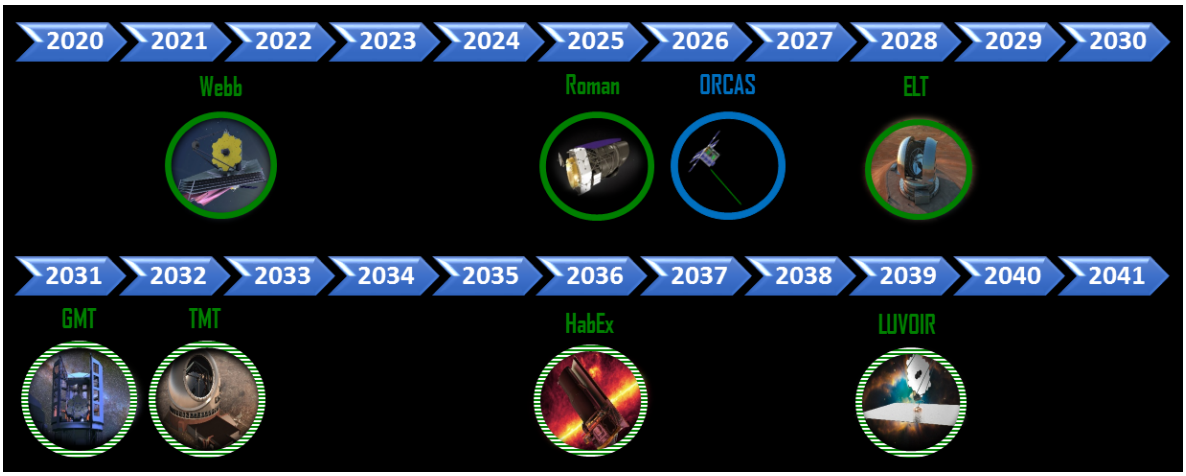

Fig 1 A timeline of future missions in the coming decades. This illustrates how ORCAS can deliver shorter wavelengths nearly a decade before future ground and space observatories. ORCAS is marked in blue while missions with a solid green circle indicate selected missions, and missions with a dashed circle indicate missions that are still in the planning mode

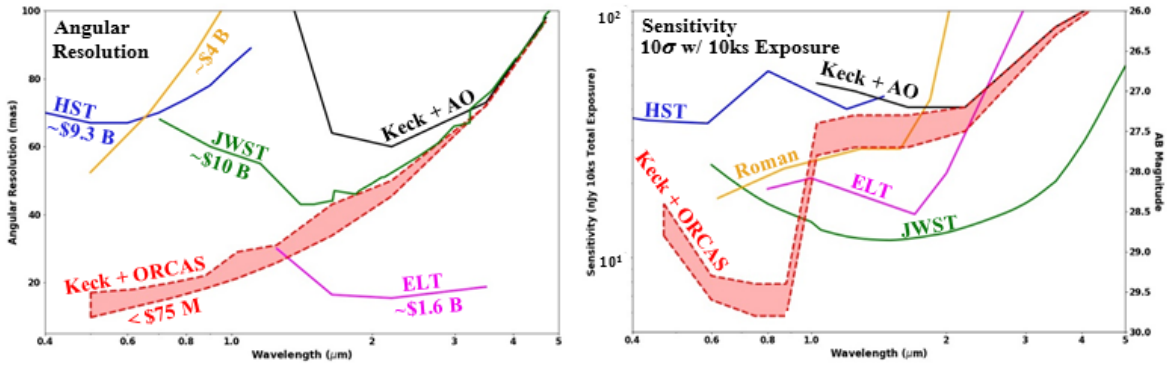

Fig 2 ORCAS performance complements other future observatories both in space and on the ground. A: The angular resolution as a function of wavelength, B: the sensitivity as a function of wavelength (for SNR = 5 in 10000 s). Note that ORCAS enables different exposure times based on the target declination. Information on the data included in these curves can be found in the Appendix A.7

.

and science output of the mission. ORCAS is an opportunity to pave a path for future satellites that work with ground observatories across the world.

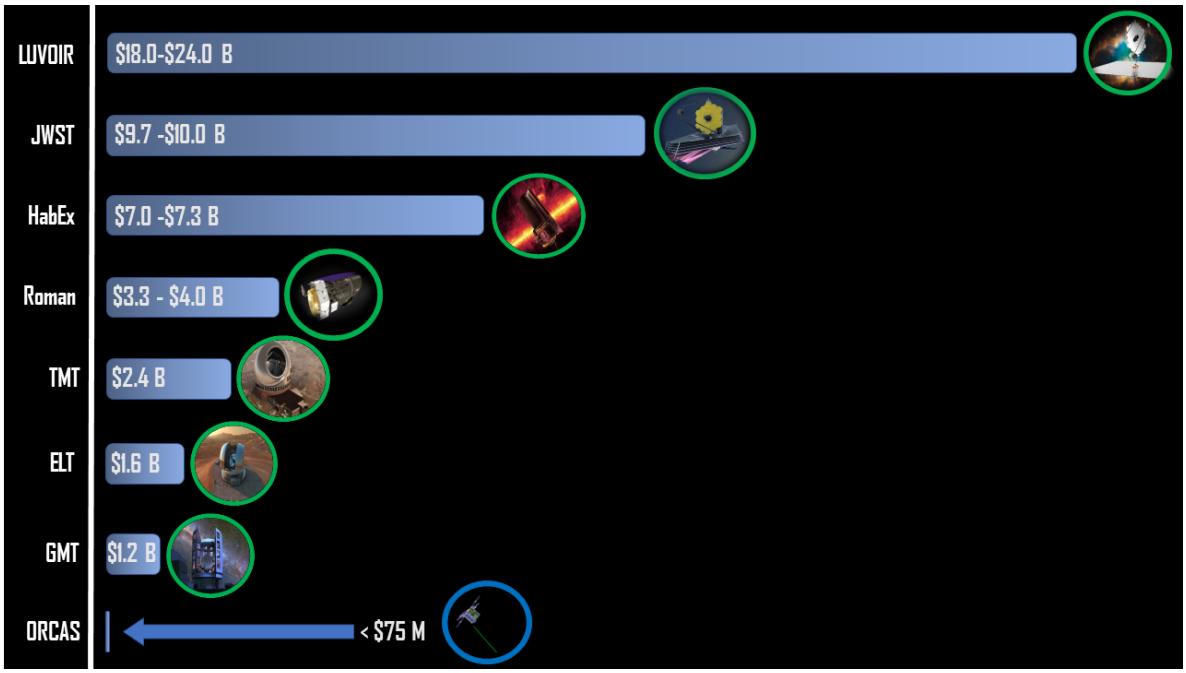

Fig 3 A comparison of US$ FY 2021 cost for future missions. The advantage of ORCAS' SmallSat cost is clearly visible when compared with future space observatories.

2 ORCAS Scientific Goals, Objectives, and Required Observations

In this section, we outline the **top priority themes for ORCAS: Active Galactic Nuclei (AGN) and Supernovae (SNe)**. We also introduce four other scientific objectives: flux calibration, the high redshift universe, exoplanets, and the Solar System. This section describes the science objectives which drive the hardware design for ORCAS. We determine key AO, imager, and spectrometer requirements from the most stressing cases, and illustrate the capabilities for all science areas. The observation requirements for each science case are discussed. Once the science team objectives are met and the equipment and systems are verified, the equipment will become a facility available for all users. In the initial proposal we assume there will be one ORCAS spacecraft, but in the future having more beacons would increase the availability of observations and would reduce fuel consumption for maneuvering to target stars in a different region of the sky. It should be noted that photometric calibration does not require specific target alignment. For this report, we propose using a highly elliptical orbit for observations. Other options include using an L2 halo orbit in the Sun/Earth system for observations, but these other options are not drivers for the initial science content. A more in-depth description of these orbits can be found in Appendix A.6.

2.1 Active Galactic Nuclei

Resolving the dynamical neighborhood of intermediate and supermassive black holes with ORCAS assisted AO.

Science Objectives: (1) Detecting intermediate mass black holes, (2) Detecting feeding and feedback signatures from the inner pc scales regions near supermassive black holes, (3) Detecting supermassive black hole binaries in the near Universe.

Observable and Measurements: (1) The proper motions of stars to find nurseries of intermediate mass black holes in the nearby universe, (2) High angular resolution imaging and spectroscopy to study in-flowing and out-flowing plasma in the inner parsecs of SMBH at the centers of AGN, (3) Imaging and spectroscopy to resolve dual and triple AGNs at parsec scale separations in the nearby Universe.

Key Functional Requirements: (1) High angular resolution ($\sim 12 - 40$ mas), (2) High spectral resolution (up to $\sim 10,000$), and (3) High sensitivity (29^{th} magnitude). (4) Wavelength coverage from 0.5–2.0 μm.

ORCAS Uniqueness: No other currently planned or commissioned instrument has sufficient angular resolution combined with spectral resolution and sensitivity to resolve the physical ($\sim$parsec) and dynamical (< 20 km/s) scales required for the above science cases.

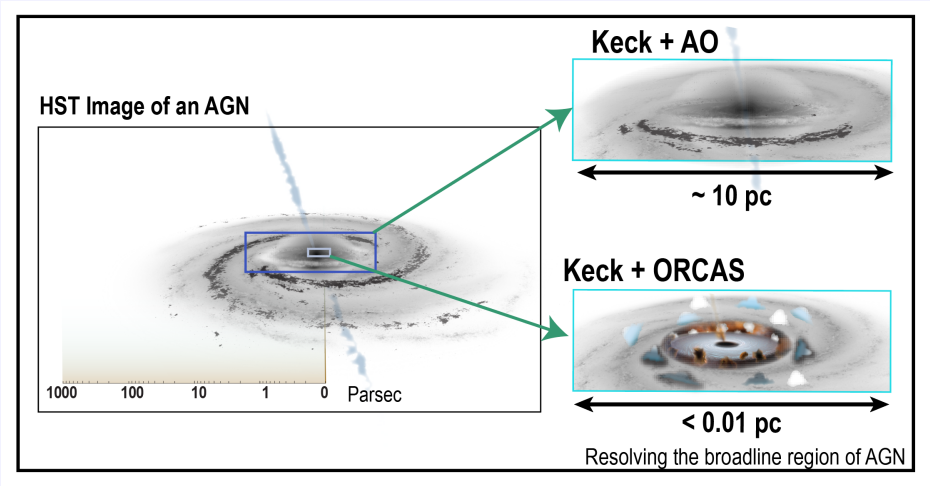

Fig 4 Schematic diagram of the AGN environment. Answering key science questions demands studying regions close to the black hole, such as the Broad Line Region (< 0.01 pc). While current Keck AO has pushed beyond HST to reveal the central tens of parsec scales in nearby AGNs, ORCAS assisted AO is crucial to resolve the critical structures close to the black hole needed to answer fundamental questions about how black holes form, grow, and shape the evolution of galaxies. This is where ORCAS can contribute unique and transformative science.

Black holes with masses from a million to up to a billion times the mass of the Sun are now known to be ubiquitous in the centers of galaxies, and their masses are known to correlate with properties of

the host in which they reside (1). When accreting, the active galactic nucleus (AGN) can in turn exercise a profound effect over the baryonic component of the Universe by driving massive energetic outflows that can suppress star formation in the host galaxy and expel as much as the entire mass of a galaxy into the intergalactic medium (2). Despite their importance in shaping the evolution of galaxies, fundamental questions remain unanswered:

- How do supermassive black holes form?
- How do supermassive black holes grow to such tremendous sizes?
- How do supermassive black holes evolve with their host galaxies?
- What fundamental physics can we learn from AGNs?

Our ability to answer these questions depends critically on resolving the central regions around the supermassive black hole. Current Keck AO capabilities on nearby AGNs have pushed beyond HST and VLT-MUSE to resolve the central structure in nearby AGNs down to the unprecedented scales of tens of parsec (3). This spatial resolution is insufficient to resolve the most fundamental structures around the black hole, such as the dusty torus, the broad line region, and the region from which AGN-driven outflows are launched, as can be seen from Figure 4. Although VLT-Gravity has made breakthroughs in spatial resolution at near-infrared wavelengths (4), the brightest emission lines are found in the optical where the most diagnostic spectral features for the AGN and the stellar population are also found. Moreover, current AO systems are hampered by crowded fields and limited sky coverage, which limits our ability to observe the most critical targets with the best possible spatial resolution. **ORCAS-assisted AO will enable the highest possible spatial resolution in the optical, where the sky brightness is the lowest and where crucial diagnostic spectral features are found, anywhere in the sky, truly exploiting the maximum science return that can be obtained from a large telescope on the ground.** The exquisite spatial resolution and sensitivity enabled by ORCAS will provide a unique and unprecedented niche in US astronomy in the study of AGNs. In this section, we highlight signature science cases in which ORCAS can have a transformative impact.

These signature science cases are:

1. Search for intermediate mass black holes in nearby globular clusters and dwarf galaxies
2. Search for dual and triple AGN in mergers
3. Study outflows and star formation in AGN host galaxies

High angular resolution is critical for advancing these science cases.

2.1.1 The Search for Intermediate Mass Black Holes

Very little is known about the existence and properties of black holes with masses less than $\approx 10^6$ $M_\odot$. In fact, there is currently no direct evidence for black holes with masses between ≈ 150 $M_\odot$ and 10^4 $M_\odot$, a gap of roughly two orders of magnitude in mass. This is a severe limitation, because black holes in this "mass desert" hold vital clues into some of the most important questions in extragalactic astronomy. In particular, **how do supermassive black holes form?** Do they form from primordial gas clouds, or do they form from the deaths of the first generation of stars? Unfortunately, it is impossible to observe SMBH seeds formed at high redshift directly. However, detecting and studying the demographics of intermediate mass black holes (IMBHs) in the local Universe can tell the story of

how SMBH formed in the early Universe. This is because most IMBHs likely reside in low metallicity dwarf galaxies, the closest analogs in the local Universe to high redshift primordial galaxies. Because of their relatively quiet cosmic histories, their mass distribution and host galaxy occupation fraction can therefore provide clues into the origins of supermassive black holes (SMBHs), potentially allowing us to discriminate between hotly debated theories of black hole seed formation in the observationally inaccessible early universe (see (5) for a recent review). If they are accreting, **IMBH-powered active galactic nuclei (AGNs) in local dwarf galaxies may give us insight into the observationally inaccessible first sources of ionizing photons and their contribution to cosmic reionization** (e.g., 6). Moreover, mergers between black holes in this mass range will give rise to the most promising sources of gravitational waves (GWs) detectable with LISA, yet black hole pairs in this mass range in the local Universe have not yet been identified and the merger rate is unknown. Finding a population of IMBHs, studying their ionizing radiation fields, measuring their masses, and understanding their connection to their host galaxies is therefore of fundamental astrophysical importance. Moreover, this is key to the interpretation of the results of the LISA mission, in which NASA partners with ESA for a launch in 2034.

To detect a black hole dynamically, the region in which the stellar motions are dominated by the gravitational influence of the black hole must be resolved. In Figure 5, we show the radius of this gravitational sphere of influence as a function of black hole mass. Detecting and measuring the mass of IMBHs is currently infeasible even in the closest galaxies, since the sphere of influence of even a $10^5 M_\odot$ black hole at a distance of 10 Mpc is only approximately 0.01 arcsecond. ORCAS-assisted AO can:

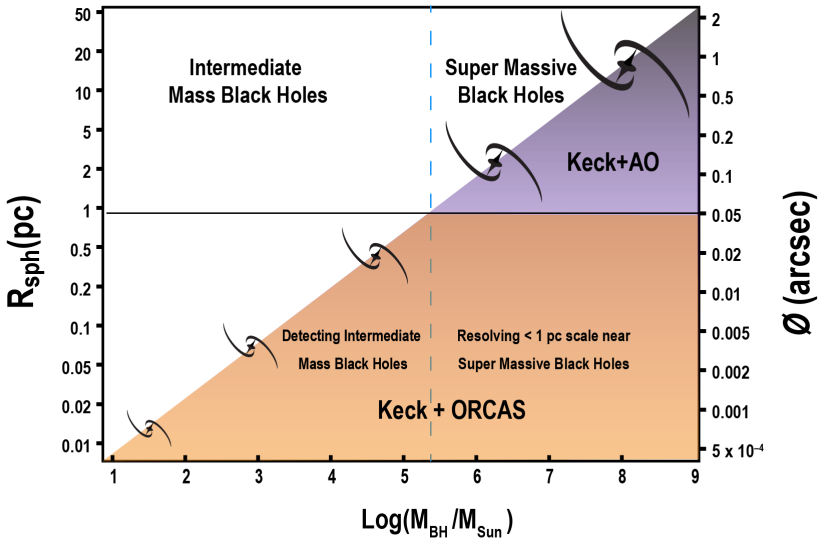

Fig 5 Black hole sphere of influence (pc) vs black hole mass ($M_\odot$) using the M-σ relation from (7). On the right axis, we show the corresponding angular resolution assuming a distance of 5 Mpc, within which there are over 100 dwarf galaxies from the Local Volume Legacy Survey (8). ORCAS-assisted AO will enable the detection and characterization of black holes in a completely uncharted mass regime (orange shaded region). In more massive black holes, ORCAS-assisted AO on Keck can resolve unprecedented spatial scales around the black hole at optical wavelengths, where the most diagnostic spectral features of the AGN radiation field, outflows, and the surrounding stellar population are found (blue shaded region). This figure shows why high resolution with ORCAS is critical for detecting intermediate mass black holes, and understanding how the AGN impacts the host galaxy across the full range in black hole mass shown.

- **Identify and determine the mass of IMBHs in globular clusters in the Milky Way.** There are 6 massive globular clusters, including M15, accessible from Keck that would be ideal candidates. With a typical distance of 10 kpc, the gravitational sphere of influence of a putative IMBH in a globular cluster is a couple of arcseconds. Identifying and measuring the mass of IMBHs requires a minimum angular resolution of 10 mas in order to resolve individual stars in the center of the cluster cores, and $\approx$ 1 km/s astrometric precision. High Strehl is critical to resolve individual stars. Key requirements include observations of the Ca II triplet line at 0.85 μm, an IFS (Integral Field Spectrometer, aka Integral Field Unit or IFU) with a 3"x3" FOV, and spectral resolution of 10,000. Note that future optical interferometry capabilities enabled by laser beacons for phase referencing can make even more transformative gains in IMBH searches using proper motions in cluster cores.
- **Identify and determine the mass of IMBHs in local dwarf galaxies.** ORCAS assisted AO equipped with a visible IFS will be able to resolve the dynamical signatures of IMBHs of 10^3 $M_\odot$ IMBHs out to approximately 1 Mpc, and 10^4 $M_\odot$ IMBHs out to 5 Mpc. Key requirements include spectroscopic observations of the Ca II 0.85 μm triplet with an IFS with a minimum FOV of 3"x3" and spectral resolution of 10,000, in order to probe stellar velocity dispersions down to 15 km/s. As a demonstration observing program, we include all 258 galaxies in the Local Volume Legacy survey, a complete survey of nearby galaxies out to 11 Mpc (Lee et al. 2007). Highest priority targets will be the closest nucleated galaxies, where a robust galactic

center can be determined.

- **Identify IMBH powered AGNs in local dwarf galaxies.** ORCAS assisted AO, equipped with a visible IFS, will be able to detect accreting IMBHs in local dwarf galaxies. The integrated light from larger aperture spectroscopic observations includes emission from surrounding star formation regions and the luminosity of an IMBH powered AGN will be low even if radiating at its maximum rate. As a result, current spectroscopic surveys of AGNs in the dwarf galaxy regime are significantly hampered. ORCAS AO can reach spatial scales of less than a parsec in local dwarfs (see Figure 4, enabling the uncontaminated emission from the AGN to be observed. Key requirements include spectroscopic observations of the brightest visible emission lines, including the [O III] 0.50 μm line with an IFS with a minimum FOV of 2"x2" and spectral resolution of 3,000. Because IMBHs are predicted to be offset from the galaxy photocenter by recent cosmological simulations (9), the IFS FOV requirement ensures that it is within the FOV and that its location relative to the galaxy photocenter can be obtained. Such observations can also be used to search for nuclear star clusters, outflows, and to study scaling relations and the impact of the AGN on the host galaxy in the unexplored low mass regime. As a demonstration observing program, we include all 258 galaxies in the Local Volume Legacy survey, a complete survey of nearby galaxies out to 11 Mpc (8). Highest priority targets will be the closest nucleated galaxies, where a robust galactic center can be determined. Integration times are expected to be less than 30 minutes per target.

Why ORCAS? Detecting IMBHs through resolved kinematics is currently unfeasible since the sphere of influence in this mass regime cannot be resolved even in the local Universe. High spatial resolution spectroscopy is crucial in order to push the mass frontier down into a regime in black hole mass never before been discovered. Diffraction limited high sensitivity spectroscopy is a game changer in IMBH searches where future ground-based spectroscopy can play a vital role. Note that this science cannot be achieved through JWST, and while ngVLA (the Next Generation Very Large Array radio telescope) has high spatial resolution, it can only detect jet dominated, weakly accreting IMBHs, which are expected to be only a small fraction of the population. Moreover, accurate masses can only be acquired through spectroscopic surveys in the near-IR or visible. Note that the unavailability of bright guide stars and an ideal NGS constellation for the prime targets limits the use of current and future LTAO (Laser Tomography Adaptive Optics) systems in carrying out this science case.

2.1.2 Observations of the AGN in galaxy M87

The galaxy M87 has as its center an AGN that is associated with a billion-plus solar mass black hole known as M87*. This system gained extraordinary notoriety due to its having the first-ever resolved image of a black hole, which was obtained by the Event Horizon Telescope (EHT) collaboration (10). Previous mass estimates of M87* were obtained from velocity dispersion of stars in the vicinity of the galaxy center (1). However, EHT observations of M87* obtained a definitive mass estimate from observations of the vicinity of the event horizon (10). This precision estimate creates a scientific opportunity that ORCAS will exploit.

ORCAS will use the EHT-obtained estimate of the mass of black hole M87* and test for the presence of a companion black hole at some point in its history, analyze the stellar dynamics close to the black hole, and test the prediction of a cusp in the stellar distribution (11) which has never before been observed. ORCAS will also measure the velocity profile of stars near the central AGN, for comparison with theoretical models of the central region of the galaxy kinematics.

Observations will use the existing OSIRIS Integral Field Spectrograph, which is IR waveband sensitive (1 - 2.5 micron), and has spectral resolution, R=3800 and spatial spatial scale: 20-100 mas/spaxel, and field of view, FOV = 3.2×6.4 arcseconds. (Kn5 filter). OSIRIS observations would target the CO bandhead at wavelength 2.3 μm. Observations with R = 3800 and 10-20 hours integration time, for which ORCAS would achieve Strehl ratio > 0.50 would yield SNR = 50 / resolution element (100 km/s spectral, 0.09 arcseconds spatial, Keck at 2.3 μm).

2.1.3 Search for dual, triple, and offset AGNs in mergers

ORCAS-assisted AO can make transformative gains in our understanding of how black holes grow, as well as place important constraints on projected gravitational wave signals in the low frequency regime. Since the vast majority of galaxies contain supermassive black holes (SMBHs) and galaxy interactions trigger nuclear gas accretion, a direct consequence of the hierarchical model of galaxy formation would be the existence of dual and triple AGNs. The existence, frequency, and characteristics of such systems have important astrophysical implications on the SMBH mass function and the interplay between SMBHs and its host galaxy. Despite decades of searching, and strong theoretical reasons that they should exist, observationally confirmed cases of dual AGNs are extremely rare, and most have been discovered serendipitously. Detections of such objects provide unambiguous confirmation of active SMBH growth during late-stage mergers, and the simultaneous fueling of both AGNs indicates that these are very efficient environments for triggering SMBH accretion. Moreover, dual AGNs are the likely precursors of SMBH mergers, which will be the loudest gravitational wave (GW) events in the Universe that will give rise to future detections with LISA. Offset AGN caused by gravitational wave and gravitational slingshot recoil kicks are also a natural consequence of supermassive black hole evolution in merging galaxies. Detection of such offset AGNs would provide key constraints on GW event rates and SMBH spin and mass evolution.

Crucial Need for High Spatial Resolution Dual and triple AGNs with spatial separations from a few kpc down to a parsec are particularly important to SMBH and galaxy coevolution as well as to predictions for future gravitational wave experiments. Because these scales correspond to the late stage of a galaxy merger, when both accretion onto the black hole and star formation are predicted to peak, the host galaxy undergoes its most dramatic morphological transformation (12), and the SMBHs are on their way to becoming bound binaries. This phase in a merger may also provide clues on the physical nature of dark matter particles, since the nature of dark matter can have a direct consequence on the orbital decay and inspiral rates on kpc scales (13). Unfortunately, it is extremely difficult to observe this population due to the required spatial resolution. To date, there have been less than ≈ 30 dual AGNs with separations less than $\approx$ 10kpc discovered, less than a handful with separations less than ≈ 3 kpc (14; 15; 16; 17), only two robustly confirmed triple AGN at close separations reported in the literature (18), and only one bound binary known in the Universe (19). While there have been numerous offset AGN candidates reported, there is still not a single offset AGN candidate confirmed in the Universe (20). This is a severe deficiency since there is a major gap in our understanding of supermassive black hole growth and binary evolution.

Fig 6 Schematic diagram showing the evolution from a galaxy merger to a close dual AGN, a bound binary and finally a black hole merger. These closely separated SMBHs in galaxy mergers are of great interest because they capture the phase in a galaxy's evolution in which the black hole experiences its peak growth and the AGN has the most impact on the host galaxy. They lead to bound SMBH binaries, which will be the loudest GW sirens in the Universe detectable in the coming years by LISA and pulsar timing arrays (PTAs). While seeing-limited observations can uncover widely separated AGN in galaxy interactions, and HST and current AO with e.g. VLT MUSE and Keck can resolve dual AGNs on kpc scales, there is a completely unexplored regime of parameter space where ORCAS can make unique and transformative advances in our understanding of SMBH binary evolution, the growth of SMBHs, and their impact on their host galaxy. From left to right are shown representative thumbnails of a widely separated galaxy merger seen by SDSS, close dual AGNs separated by a few kpc observed by VLT MUSE (21) and the closest dual probed by current Keck AO (Koss et al. 2018), and the single confirmed bound binary candidate known in the Universe observed by the VLBI (rodriguez et al. 2006).

ORCAS-assisted AO observations will make transformative advances in nearby late-stage mergers, where pair separations near the final parsec can be resolved, a completely unexplored regime of parameter space corresponding to bound binaries, and high redshift surveys of mergers, where pair separations on the order of $\approx$ 120 pc can be identified out to redshift z $\approx$ 2. Resolutions at milliarcsecond scales can identify multiple AGN in late-stage mergers in the local Universe down to the "final parsec", where binaries are expected to stall. Science objectives include identifying the AGNs, constraining their location relative to the host galaxy, measuring separations, luminosities, black hole masses, outflow velocities, central star formation rates and stellar populations. These objectives require measuring the following physical parameters: the central stellar velocity dispersion, emission line fluxes and line profiles as described. in the STM. The instrument requirements include a visible and infrared AO-fed IFS and multi-band imaging that extends to a minimum of 0.5 microns for stellar population studies.

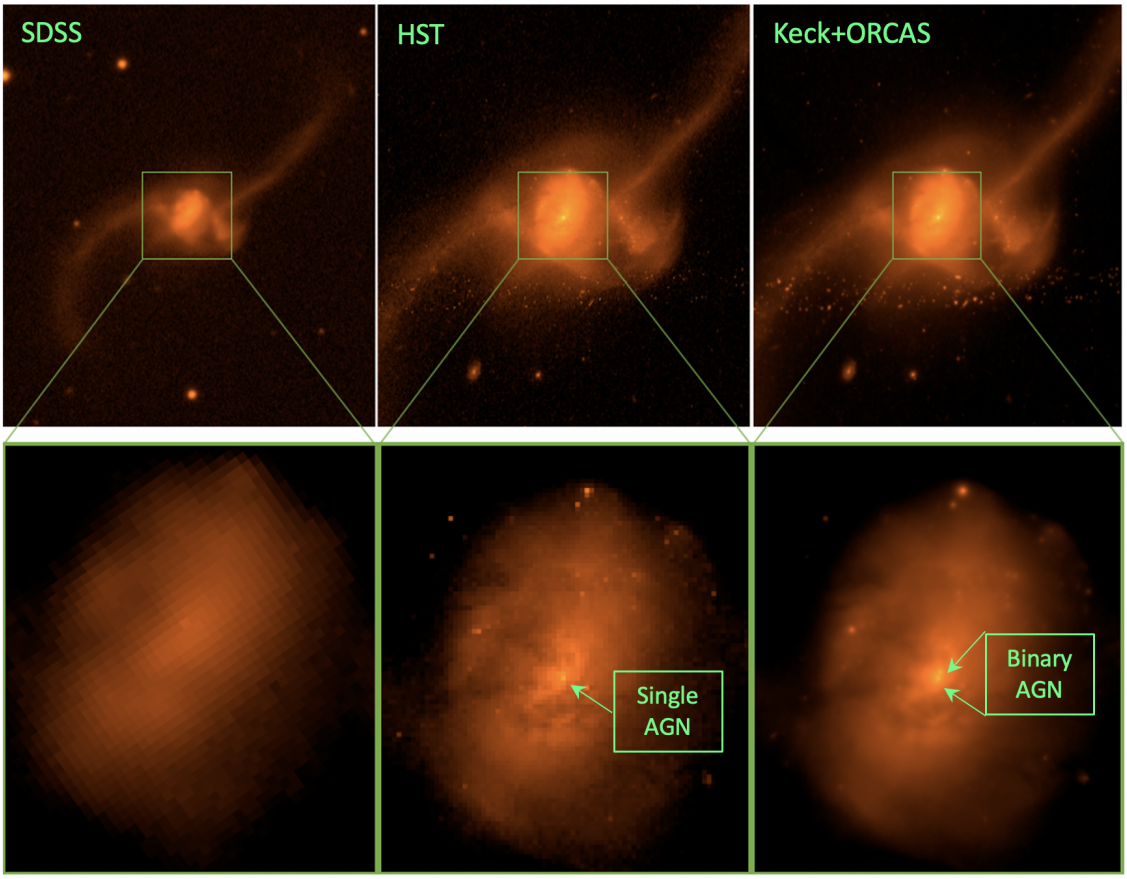

Fig 7 Seeing-limited image from SDSS of the nearby galaxy merger NGC 2623 (left panel), simulated HST image (center panel), and simulated image with Keck+ORCAS (right panel) with corresponding zoom in inserts of the central region of the merger shown in the lower panels. In this simulation, we assumed two closely separated binary AGN point sources separated by 5 pc are embedded in the single SDSS nucleus. As can be seen, HST cannot resolve the dual nuclear sources. ORCAS-assisted AO on Keck is crucial to resolve binary AGNs and the intricate nuclear structure at unprecedented spatial scales in nearby AGNs. The Keck+ORCAS simulation corresponds to a wavelength of 620 nm and a Strehl ratio of 25%.

Why ORCAS? While AO observations have demonstrated the power of uncovering a population of dual AGNs in late stage mergers (Figure 8), the number of targets with accessible guide stars is extremely limited. Using the sample of late-type galaxy mergers compiled by Galaxy Zoo in the entire SDSS survey, where close pair dual AGNs are respected to reside (see (22) and (23)), only 5% have a suitable guide star to enable LGS with Keck OSIRIS. Only a few have been observed with limited AO coverage with Strehl ratios of only 0.02, assuming optimum seeing conditions. Moreover, current Keck AO can only resolve dual AGNs down to at best 50 pc, and cannot probe the critical gravitationally bound binary phase. ORCAS-assisted AO in the optical can push the frontier for the first time into the bound binary phase in nearby galaxy mergers. To maximize spatial resolution and sensitivity, ORCAS-assisted AO will be a unique tool in identifying for the first time a key phase in galaxy and SMBH binary evolution. Suitable targets for near-infrared IFS observations in this program can be obtained from dual and triple AGN candidates from SDSS-selected late-stage mergers (e.g. Satyapal et al. 2017). Binary AGN candidates suitable for optical AO with ORCAS can be pre-selected from Gaia sources that display variability-induced ”astrometric jitter” consistent with dual or

offset AGNs (e.g. Shen et al. 2019).

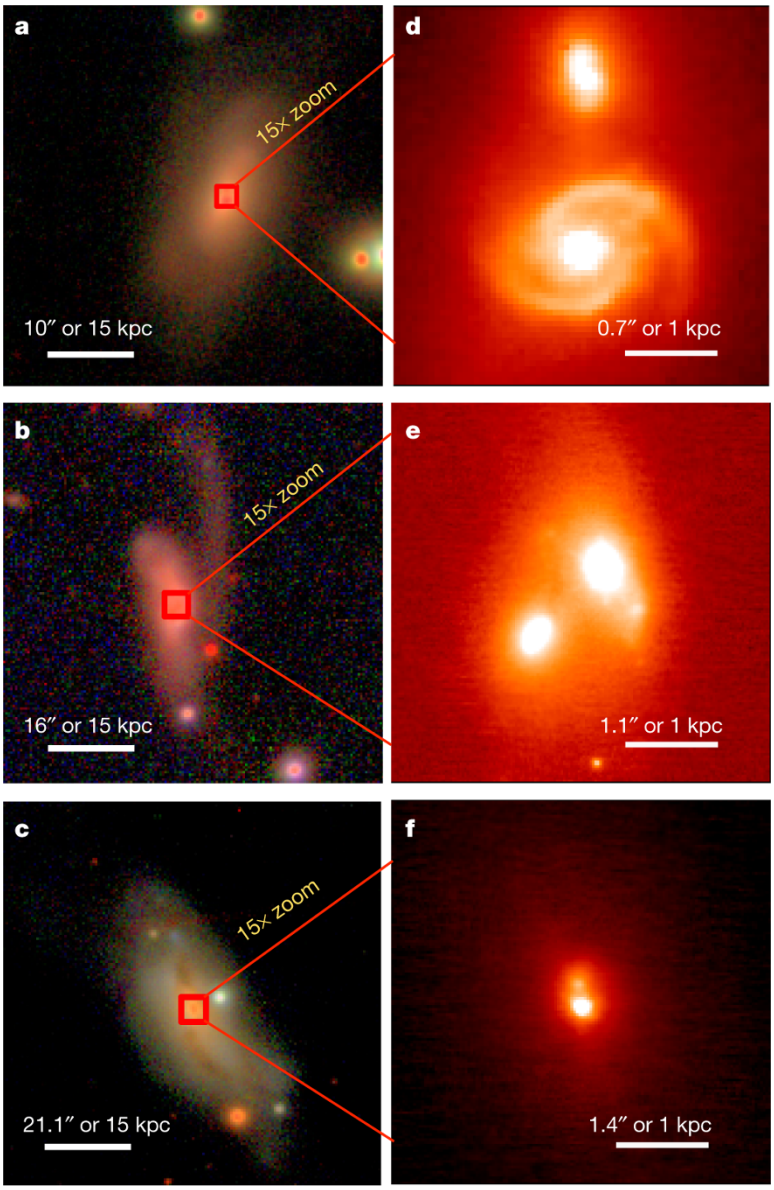

Fig 8 Near-infrared observations with Keck AO have already revealed how AO can reveal closely separated nuclei that are impossible to see in seeing-limited images. Shown on the left are SDSS images of late-stage mergers and on the right are zoom-ins of Keck-AO K-band NIRC2 images, revealing the crucial need for AO assisted observations for uncovering duals and characterizing their properties (Koss et al. 2018, Nature). Note that current AO only enables spatially resolved pairs at typically a few hundred to kiloparsec scales. ORCAS AO will enable identification of bound binaries for the first time, down to a few parsec separations in nearby galaxies.

Why now and synergy with NASA missions? Dual and offset AGNs were identified as priority science cases by two separate 2020 decadal white papers with over 25 co-authors (Koss et al. 2019, Blecha et al. 2019). Detections of binary or recoiling SMBHs prior to the launch of LISA will provide critical constraints to the LISA event rate, thereby providing crucial synergy with high priority

upcoming NASA missions. In addition, non-detections of recoiling AGNs will constrain spin evolution prior to merger and therefore, the likelihood that LISA will observe precessing waveforms. Thus, ORCAS-assisted AO searches for binary and offset AGN described here, combined with future LISA observations will transform our understanding of SMBH evolution in merging galaxies, and low-frequency GW astronomy in the coming decades.

Why ORCAS? Existing measurements with 8-10 m class telescopes and AO are insufficient to remove the AGN light which dominates the light from the innermost stars. VLT-MAVIS is being designed for operation with Strehl ratio $\sim$ 15%, which will not be sufficient for these observations.(24)

2.1.4 Outflows and star formation in AGN

The accretion disk is the primary source of power for the central engine of an AGN, which not only emits huge radiation, but also particle outflows at very high speed, both in terms of jets and non-collimated winds. The particle outflows (non-collimated winds) are one of the most powerful mechanisms by which the central engine transfers matter and energy out into the host galaxy and beyond. The most crucial evidences of these outflows impacting the SMBH surroundings and the host galaxy are : 1) The M-sigma relation, which states that mass of the SMBH and the mass of the galactic bulge are closely connected, 2) Suppression of star formation and AGN activity for massive galaxies with relic AGN, 3) The mystery of the cooling flow problem in the intra-cluster medium (ICM), which states that the ICM are bright enough to cool down rapidly (millions of years), but something is pumping them with energy and keeping them hot for longer timescales (billions of year).

The outflows in AGN are detected both in absorption and emission in the infrared, optical, UV and X-ray wavelength bands, the most vital diagnostics of the outflowing plasma. The features arise out of transitions from different ionic states of astronomically abundant elements such as H, He, O, N, C, Ne and Fe, when the central AGN light filters through the plasma. Although we have made immense progress in understanding the nature of these outflows and AGN central engine in the last three decades after the advent of HST, XMM-Newton, Chandra, Keck+AO and other high spectral resolution telescopes, some of the most fundamental questions still elude us: (1) What is the exact geometry of the central engines?, (2) How matter loses 99.999% of its angular momentum from the kpc scale and falls into the SMBH. (3) How and why are the powerful outflows generated and how do the infall of matter and outflow work together? and (4) How does the particle outflow couple with the host galaxy gas, which is an important factor determining the energy budget and impact of the outflows. In recent years, there have been improvements in spatially resolved spectroscopy in UV and IR, yet clearly they are too inadequate to resolve the dynamical neighborhood of the SMBHs (see Fig 6). Our ability to answer these fundamental questions rests on our capacity to spatially resolve the inner parsec scales of AGN to directly trace the multi-ionized and multi-phase (density, temperature) gas, in inflow or outflows. Currently, VLT-GRAVITY, using near infra-red interferometry has the capability to resolve down to a few parsecs near super massive black holes at the centres of nearby AGN. However, the best spatial resolution that can be currently achieved in the optical, for nearby AGNs is $\sim$ 10s of pc using GMOS-IFU or Keck-AO. **Keck+ORCAS** will provide us with the unique view of $<$pc scale distribution of the multi-phase gas for the first time. In particular, trace the inflow and outflow of matter using prominent/bright optical emission lines such as O III. Most importantly, in addition to attaining the spatial resolution, ORCAS assisted AO will have enough sensitivity and spectral resolution to carry out spatially resolved spectroscopy.

2.2 Exploring Dark Energy with Supernovae

Cosmological Measurements

Science Objectives: Measuring the dark energy equation of state by enhancing Roman Space Telescope and Rubin Observatory LSST supernova programs. Separate out the different supernova types, using the SN Ia for cosmology. Double the accuracy and dramatically reduce systematic errors in the measurement of each SN using new standardization techniques, such as "Twins Embedding," that use spectroscopy.

Observable and Measurements: Spectra of Type Ia supernovae out to redshift 1.7 in rest-frame visible wavelengths in order to classify them and implement Twins Embedding. Roman and/or Rubin will find these SNe in specific fields, to which ORCAS can return each orbit.

Key Functional Requirements: New Keck spectrograph covering wavelengths 0.5–2.0 μm to capture the same spectral features for all high redshift SNe all in one exposure. High-throughput over 3 octaves requires prism disperser. Maximal sky suppression requires a minimum 0.10 arcsec spatial sampling and 0.5×0.5 arcsec minimum FoV. Concept of operations will include input from new Rubin and Roman target lists. Minimum of 100 such SNe Ia to check for systematics within larger Rubin and Roman supernova surveys.

ORCAS Uniqueness: The limiting factor in measuring cosmological supernovae is the brightness of the sky and high efficiency. The AO with Keck+ORCAS will dramatically reduce the sky brightness under the PSF, leading to much higher SNR in a given time. The high Strehl ratio will pack more of the available light into that PSF, leading to much higher efficiency than with Strehl ratios from laser guide stars. The improvement will be dramatic at both visible and infrared wavelengths.

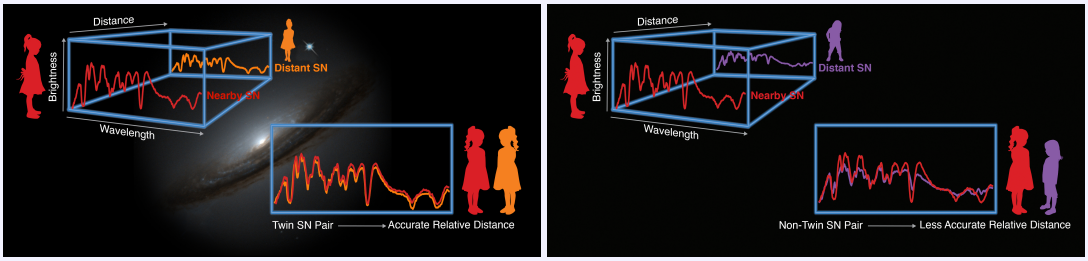

Twins Embedding: Shown are pairs of supernovae – in each case one is nearby and one distant. The ones that line up well – twins – provide much better relative distances. Almost all SNe Ia have many close twins out there in the cosmos. (Graphic credit: Zosia Rostomian/Berkeley Lab; photo credit: NASA/ESA)

Type Ia supernovae (SNe Ia) were used to discover the accelerating expansion of the universe (25; 26), whose cause has been dubbed "dark energy." Due to the lack of viable physical models, the dark energy is studied via its equation of state, w, the ratio of its pressure, P to its energy density, ρ. w is in turn studied in terms of its value at the present epoch, w_0, and its derivative with time, w_a, with

the specific form $w(z) = w_0 + w_a z/(1+z)$ being a solution to the Klein-Gordon relativistic wave equation. The quest of modern cosmology is to measure w_0, w_a, and two new major telescope facilities, NGRST and the Vera Rubin Observatory's (VRO) Legacy Survey of Space and Time (LSST), have this as one of their key projects. Currently w_0 is known to approximately $\sim 8\%$ when combining SNe Ia, CMB, and BAO, and w_a — whether the dark energy is changing — is known only $\sim 25\%$ (27).

While Rubin's LSST, and NGRST supernova survey, will discover a few tens of thousands of SNe Ia in their deep fields over the nominal course of their missions, with current plans, spectroscopy will be quite limited for SNe with redshifts $z > 0.5$, whereas the SNe Ia discoveries will extend well beyond $z \sim 1$. SN Ia cosmology measurements have important sources of systematic uncertainty that must be dealt with, but the limited availability of high-quality spectroscopy in the current plans will only make that situation even more challenging; supernova types (Ia/II/Ibc/etc) will be uncertain, and the redshifts will be uncertain, and control of drift with redshift in the population parameters will be limited. Both NGRST and LSST are taking on greater systematics risks due to their limited spectroscopy. Simulations by LSST-DESC have shown that even the powerful machine learning methods of classifying transients based on their light curves require a training data set that includes examples with high redshift (29). Similar results will apply for NGRST.

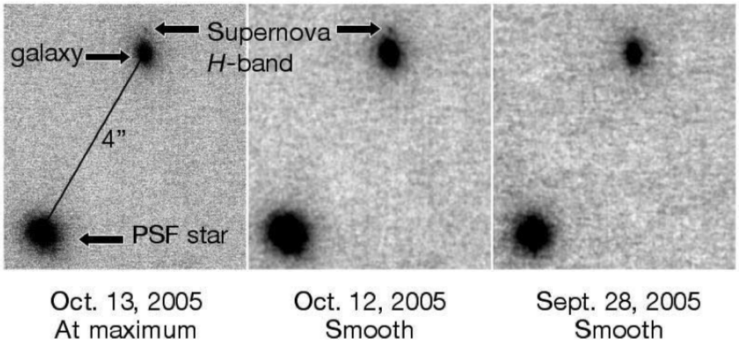

Fig 9 Keck LGS AO images obtained with NIRC2 of the redshift 1.3 Type Ia supernova SN SCP05D6 discovered using HST (28). The left image is a 1 hr exposure showing the SN near peak, with H=23.9 mag, a PSF FWHM of 0.053 arcsec, and Strehl ~ 0.3. The middle image is smoothed with a Gaussian kernel of 0.0600 to enhance the contrast. The right shows the SN 2 weeks before peak (also smoothed). The right image has half the exposure time of the left image (30 minutes vs. 1 hr). North is up, and east is to the left. To our knowledge these are the only AO observations of a high redshift SN ever obtained. ORCAS' higher Strehl would pack about $3\times$ more light into the Airy disk, effectively increasing the SNR by the same amount.

Besides the need for spectroscopy for robust classification and redshift determination, it has been demonstrated that spectroscopy is able to measure SN Ia distances to 3% — twice the accuracy of conventional light-curve-fitting methods — using only a single rest-frame visible spectrum taken at maximum light (30; 31; 32). This method is illustrated in Figure 10 and an example of bias in the light curve standardization approach is illustrated in the left panel of Figure 11. Just as important in terms of controlling systematic errors, spectroscopy has also been shown to significantly reduce the dependence of distance residuals on the SN host galaxy environment, as shown in the right panel of Figure 11. Since galaxy properties evolve with redshift, this dependence present in the conventional light-curve-based standardization (33; 34; 35) could lead to one of the dominant systematic errors (36; 37; 38). Due to these advantages, a sample of ~ 1000 SNe Ia, each with a spectrum taken at maximum light, would be able to measure the dark energy equation of state as well as all the LSST and NGRST SNe Ia light curves combined.

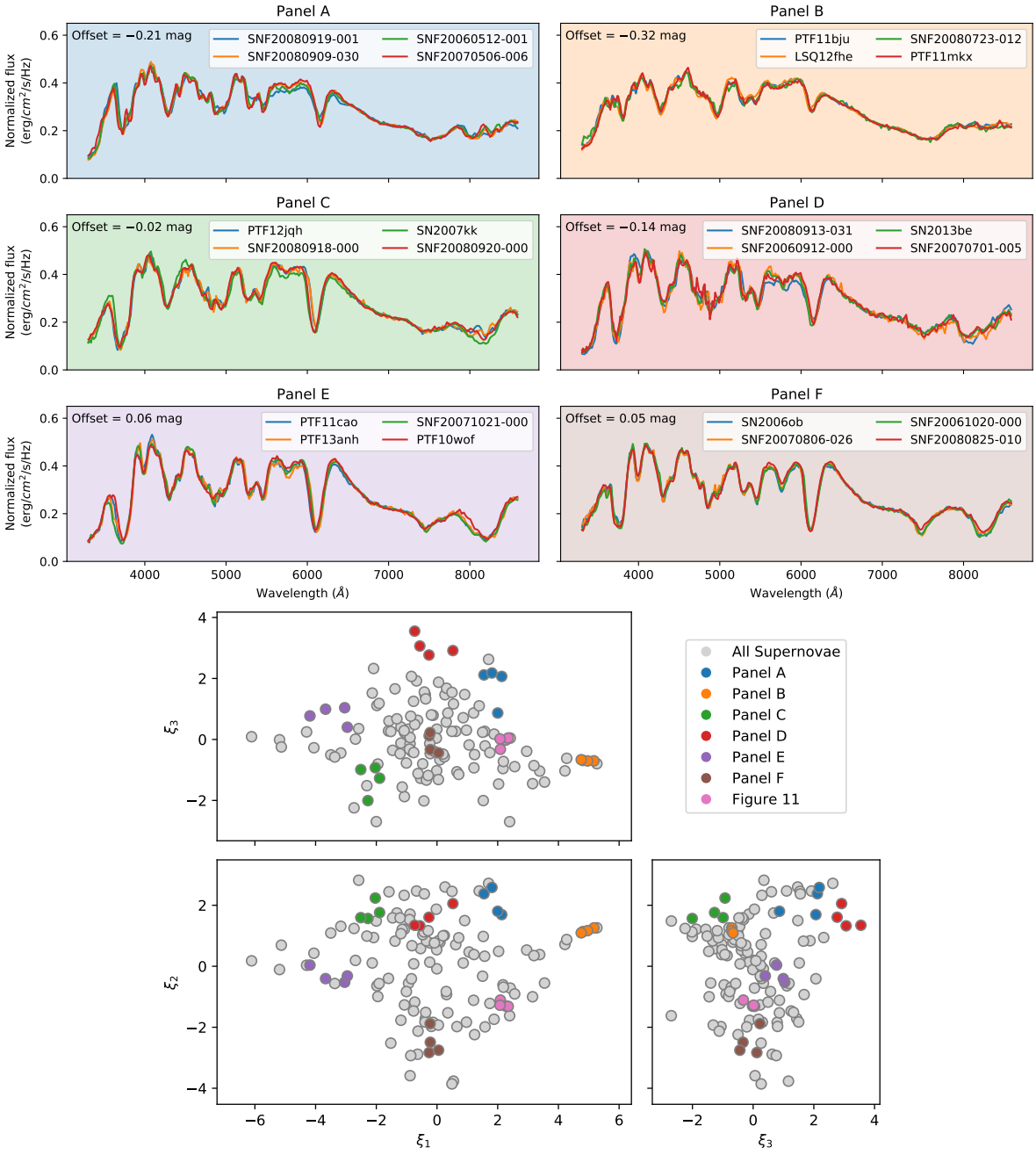

Fig 10 Examples of the spectra of groups of SNe Ia with similar Twins Embedding coordinates. In the bottom plot, we show the locations of each group in different colors. In the top plot we show the estimated spectra at maximum light of four SNe Ia from each group binned to 1000 km/s and with the "read-between-the-lines" (RBTL) brightness and color removed. In the top left corner of each panel, we show the estimated offset in brightness for SNe Ia in each group from RBTL + Twins Embedding standardization. The colors of the panels in the top plot correspond to the markers with the same colors in the bottom plot. We find that the spectra are remarkably similar within each of the groups. From (32).

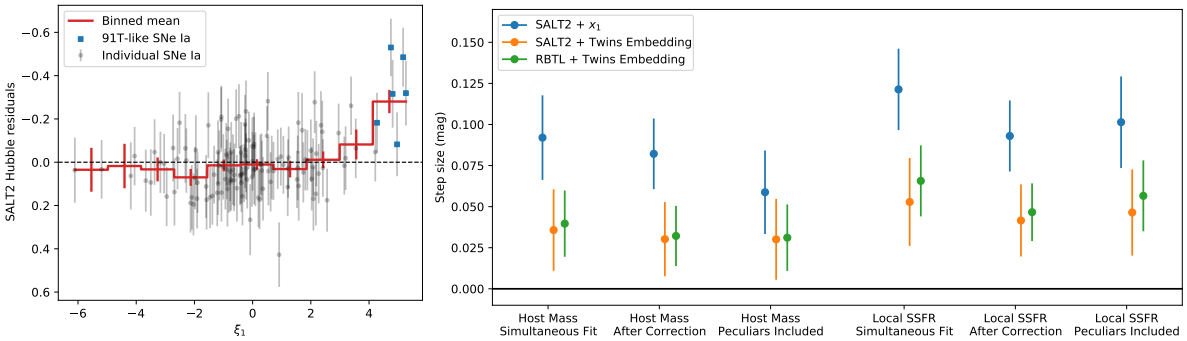

Fig 11 Plots showing biases in light-curve-based standardization that can be removed using spectrophotometry. Left: Light curve corrected magnitude residuals as a function of the first component of the Twins Embedding ξ_1 coordinate. The light curve standardization residuals are shown for individual supernovae as gray points with their associated uncertainties. We calculate the mean magnitude bias and its uncertainty in evenly-spaced bins of this component. The results of that procedures are shown with red lines. We find that light curve standardization residuals show a strong bias for large values of ξ_1. Extreme values of this component are SN1991T-like SNe Ia, as labeled with blue squares on the plot. Right: Summary of the standardization systematic error correlated with host-galaxy properties for the different for different ways of standardizing SNe Ia. For each of three methods, we show the recovered bias in different colors. Note that the uncertainties in the step sizes between different standardization methods are highly correlated: the *decrease* in host-galaxy correlation when using spectrophotometry is significant at the $\sim 3.5\,\sigma$ level, and overall bias is within $< 2\,\sigma$ of zero. From (32).

While ORCAS will not have 1000 passes through the LSST or NGRST deep fields available, there would be sufficient passes to assemble a sample of $\sim$ 100 SNe Ia with AO-assisted spectra. These could be used to examine standardization biases in the LSST and NGRST SN datasets. NGRST will be able to perform such a cross-check with its slitless prism spectroscopy, but as it will be much less sensitive on a per-SN basis and there is not yet a solid commitment to perform such observations, a sample from ORCAS would serve as a valuable cross-check on the LSST and NGRST SN Ia programs. Accordingly, we advocate as science goals obtaining precise distances to distant supernovae found by NGRST and LSST, and the ability to characterize rare transients at very high redshift or at especially early or late phases, when they are faint.

With an integral field spectrograph (IFS), ORCAS will also be able to study the host galaxy environments of high redshift SNe. As Figure 11 shows, the strongest correlation of host-galaxy biases is with the local specific star-formation rate (lSSFR), defined as the ratio of star-formation as indicated by Hα to the local stellar mass as indicated by (spectro)photometry within a region of 1 kpc surrounding each SN Ia. Keck NIR instruments can detect Hα out to $z \sim 2$ and with AO can resolve regions as small as 0.4 kpc. But ORCAS very high Strehl is also necessary, for ensuring that such measurements are not contaminated by other regions of the host galaxy. This will allow a check on whether standardization biases correlated with host-galaxy properties remain, or have been eliminated for high redshift SNe Ia, e.g., using Twins Embedding.

Among SNe, there will be a handful of cases of strong gravitational lensing. Cases of both weakly and strongly lensed SNe have already been detected (39; 40; 41; 42; 43; 44), and recently the DESI Legacy survey has identified over 1200 strong galaxy-galaxy lenses that could host a SN in the future (45). The time delay between images of a SN occurring in a lensed galaxy can be used to improve the measurement of the Hubble constant, without recourse to the local distance ladder. Because the brightnesses of SNe Ia can be standardized, they can help break the mass-sheet degeneracy in lensing mass models. Because SNe are so much more compact than QSOs, they suffer less from microlens-

ing. And finally, because the SNe fade away, it is possible to measure the profile of the lensing galaxy without contamination by light from the lensed object. Thus, while rarer, such lenses will be very valuable if a SN occurs in the lensed galaxy, and LSST will be searching for these cases. The high spatial resolution afforded by Keck+ORCAS can separate the lens components, and with spectrophotometry, can use the Twins Embedding method to produce better mass-sheet measurements and detect or remove microlensing, and significantly improve the mass model of the lensing galaxy. The main challenge for ORCAS in observing such lensed SNe will be that their timing and locations (other than the likelihood one will occur in one of the known galaxy-galaxy lensing systems found by DESI and DES) cannot be predicted. Even so, the possibility exists.

How is it that ORCAS can reach such high-redshift SNe Ia? Figure 12 shows that by tighting the SN PSF, the amount of photon noise from the night sky is strong suppressed. So rather than resolving the target itself, ORCAS resolves the terrestial sky brightness so that it does not overwhelm the SN signal.

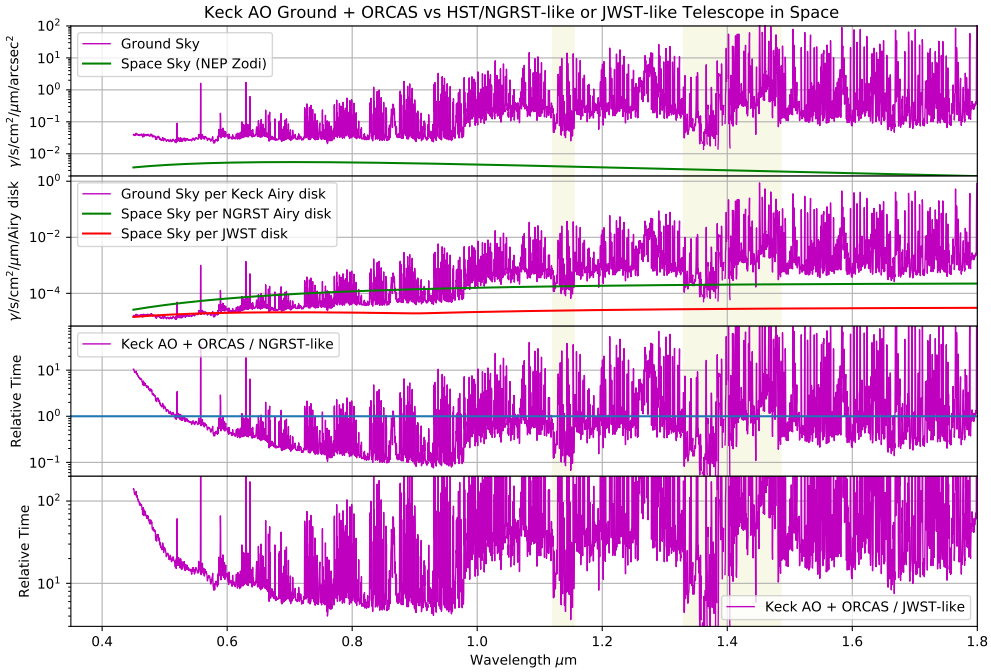

Fig 12 ORCAS plus Keck leads to lower sky photon noise relative to photon noise from a very faint science target, resulting in performance better than that of NGRST and within shouting distance of JWST at visible and NIR wavelengths. The upper panel plots the lowest natural sky background, for ground at airmass of 1 and for space at the north ecliptic pole, respectively. The second panel plots the sky brightness under the Airy disk for Keck, NGRST and JWST. (Below 0.6 μm JWST is no longer diffraction-limit so we use the actual PSF FWHM. Also, JWST has gold mirrors and filters, cutting off response to $\lambda < 0.6$ μm). The third panel uses the sky background, the Airy disk, and the Strehl ratio to estimate the relative time for an observation of the SN light in each wavelength interval collected to the same SNR by Keck or NGRST *before it enters any instrument*. Since NGRST only has slitless grism and prism spectrographs, which mixes the background light across wavelengths, it will require much longer exposure times to reach the same SNR. The final panel compares Keck+ORCAS with JWST in the same way. Note that these are not comparisons of instruments, only raw potential. Note that these plots assume performance that is sky-limited, rather than readout-noise-limited, appropriate for SN spectroscopy. The light yellow bands mark regions of strong atmospheric water absorption; Keck spectra will not be useful at these wavelengths.

2.3 Flux Calibration

Enabling Precision Cosmology and Exoplanetology

Science Objectives: Provide SI-traceable flux calibration to ground-based telescopes to dramatically reduce systematic errors on the measurement of dark energy and to characterize the stars hosting exoplanets.

Observable and Measurements: Observe calibrated beam from ORCAS from any ground-based telescope, especially Rubin Observatory, telescopes on Maunakea, and possibly the Hubble Space Telescope. Calibrated beams in chosen monochromatic wavelengths, singly for imaging, or several at a time for spectroscopy.

Key Functional Requirements: Monochromatic wavelengths centered on Rubin Observatory LSST and Roman Space Telescope WFI filters. Fluxes levels detectable by 1-10-m class telescopes for exposures of 10 min or less.

ORCAS Uniqueness: The calibrated beam from ORCAS will appear just like a star, thereby tracing the exact same path through telescope and instrument as science targets and removing one of the main sources of flux calibration uncertainty. Used in parallel with AO observations, the PSF will sample similar atmospheric turbulence and wavefront correction errors – invaluable for accurate analysis of AO science targets.

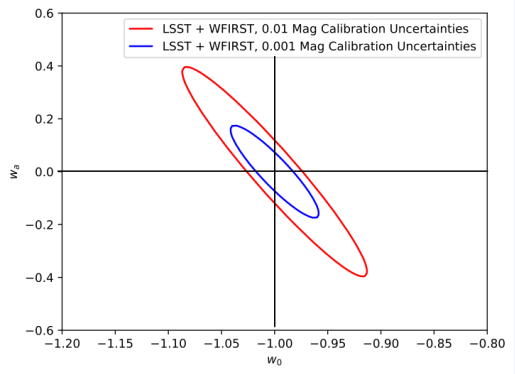

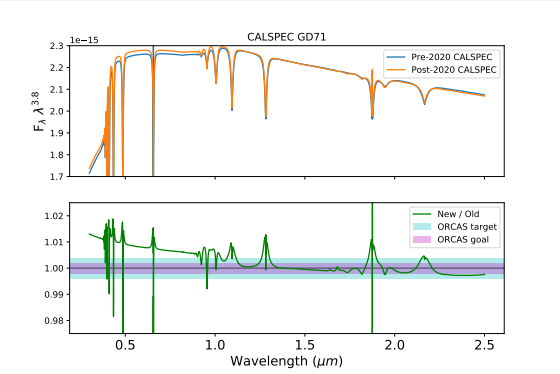

One does not necessarily think of flux calibration as "science" per se, but it enables so much science that it is itself a key discipline. Currently the fundamental flux calibration reference system, based on white dwarf atmospheric models and used for astronomy, astrophysics and cosmology, is only accurate to $\sim 1\%$. This level of accuracy is insufficient for Stage-IV cosmology experiments like LSST (Rubin) and NGRST since an error on the flux calibration translates to an error on the dark energy equation of state that is 2–3$\times$ larger. Indeed, those experiments require wavelength-relative flux references accurate to better than 0.4%, with a goal of 0.2%, in order to be able to accurately compare fluxes in the rest-frame wavelengths between science targets at high and low redshifts. Figure 13, left, shows that our calibration requirement of 0.4% will improve the measurement of dark energy by about $1.9\times$ – nearly doubling the accuracy that these multi-billion dollar investments can achieve. For our calibration goal of 0.2% the improvement is even more dramatic, reaching $3.6\times$ what otherwise

would be achieved. Figure 13, right, shows that most of the improvement is along the direction of the w_a parameter that constrains how much dark energy may vary over the history of the universe. This direction is what these experiments most desire to measure.

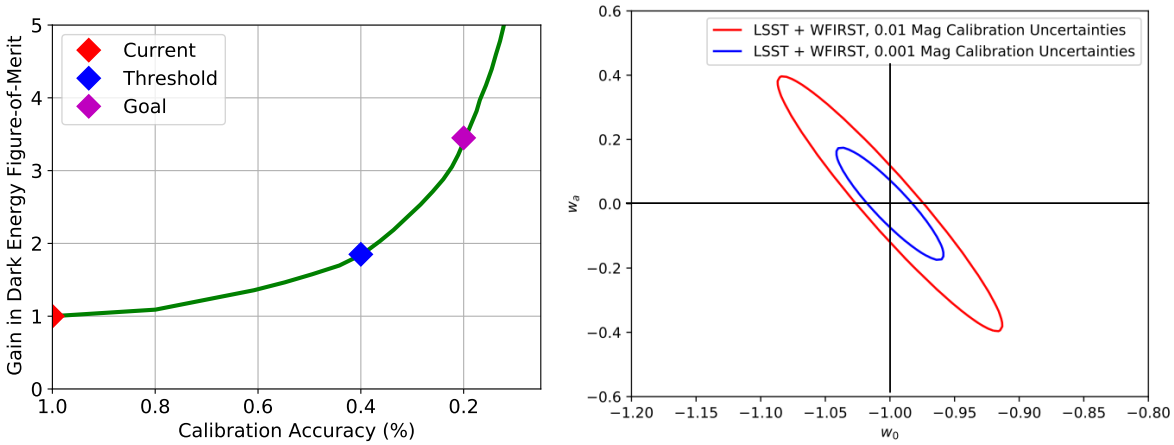

Fig 13 Left: The gain in the figure of merit (FoM) in measuring the dark energy parameters w_0 and w_a as the calibration improves. At a calibration accuracy of 0.4% the FoM will improve by $1.9\times$, and for our goal of 0.2%, by $3.6\times$. Right: The joint confidence intervals on w_0 and w_a when combining *all* LSST and NGRST SNe Ia and assuming zero curvature (essentially the CMB constraints). Two cases are shown, one in which the systematic uncertainty on the relative flux calibration is 1% and the other when the systematic uncertainty is 0.1%; the tremendous potenital for improvement is apparent. The central value is set to that of a ΛCDM universe for computational purposes only, as our goal is to determine the true values. (Left plot is derived from work by Francois Hazenberg. Right plot is courtesy of David Rubin.)

Two general approaches to establishing fundamental flux calibration exist. One is to reference stars whose stellar atmospheres can be modeled accurately; this is the approach taken for the CALSPEC system established with the Hubble Space Telescope (HST) using hot DA white dwarfs (46; 47). This approach has now reached the limits of the models, as Figure 14 demonstrates. The second method is to use an artificial star or projector system to inject calibrated light into the telescope to establish its throughput versus wavelength. In this approach, modern methods use NIST-traceable photodiodes or electrical substitution radiometers to calibrate the light being injected.

Several ground-based artificial star and projector system are under development[1]. No projector systems has yet been built that is able to fully illuminate the telescope pupil. Artificial star systems require a line of sight over ground that is subject to extinction that can be unlike that experienced by celestial sources, and is more time-variable (e.g., due to blowing dust, pollen, etc.). For all of these ground-based systems, removal of the horizontal extinction is entirely different than the removal of atmospheric extinction for celestial objects. While none of these factors demonstrably preclude reaching a calibration accuracy of 0.4%, much less 0.2%, they are serious challenges.

ORCAS could provide an artificial star with SI-traceable brightness in the sky outside the atmosphere. Such an instrument would take spectra of ORCAS and then spectra of standard stars, thereby transferring the SI calibration to the standard stars. In this mode, the ground-based telescope would remove the component due to Earth's atmosphere by observing stars and ORCAS at a range of airmasses, and then employing the Beer-Lambert law. In principle, it would even be possible to

[1]Notably, almost all involve ORCAS team members

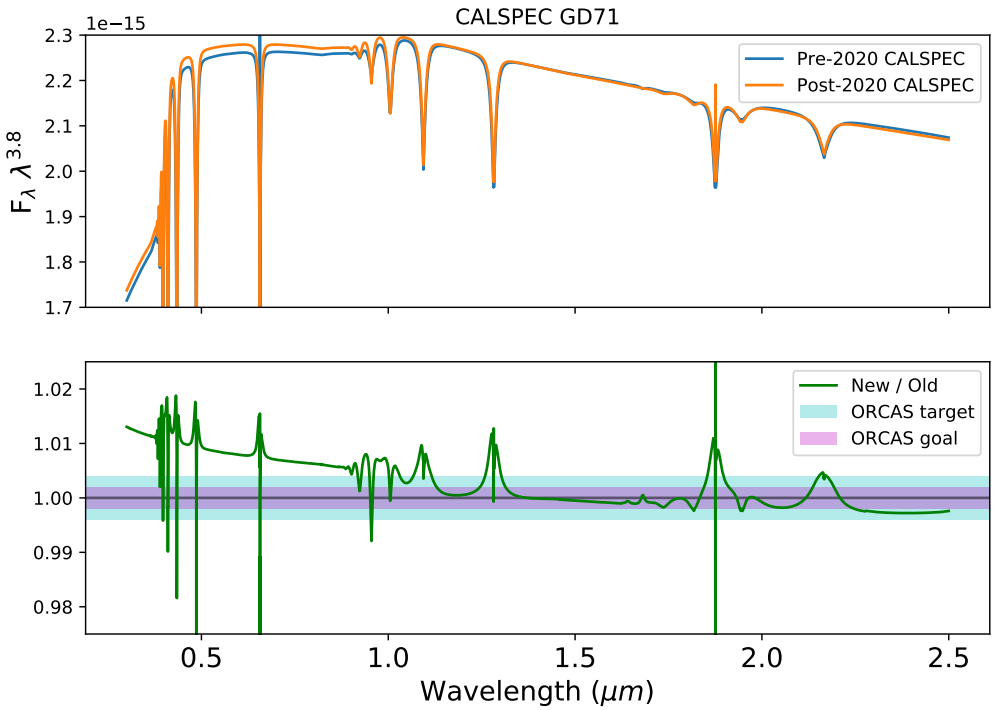

Fig 14 Demonstration that calibration based on stellar atmospheres models are too uncertain. The upper panel shows the spectrum of the CALSPEC primary calibrating white dwarf GD71, before and after being recalibrated in March 2020 with respect to different stellar models. In both cases the stellar models were believed by practitioners to be correct. The lower panel shows the ratio of the fluxes before and after — the run-out (even ignoring the regions around the absorption lines) is very large. The cyan and magenta bands show the flux calibration accuracy target of 0.4% and goal of 0.2% we have set for ORCAS. Note that in the upper panel the flux, F_λ, is multiplied by $\lambda^{3.8}$ merely for display purposes.

steer ORCAS near a series of stable stars, to which the ORCAS calibration could be transferred differentially. This would remove essentially all differences in the optical path of the light; the telescope pupil would be fully illuminated and the atmospheric extinction would essentially cancel out. For wavelengths that are difficult from the ground (UV/NIR), HST could potentially observe ORCAS and standard stars to effect transfer of SI calibration. In yet another mode, ORCAS could streak across the field of a wide-field camera on the ground or in space, potentially providing a means of calibrating several detectors at once. Once the ORCAS calibration is transferred to enough (several dozen) stable stars, 0.4%, and perhaps even 0.2%, flux calibration would be accessible to any observatory — on the ground or in space —- through those stars, long after ORCAS departs the sky.

Cosmological measurements have advanced dramatically over the past two decades, but now fundamental flux calibration has become a limiting systematic. NGRST will not fly a suitable projector systems and will therefore rely on the fundamental calibration accuracy of standard stars. LSST will deploy a projector system, but its accuracy has yet to be demonstrated. These flagship cosmology projects need to know they will have accurate fundamental calibration stars on which they can rely.

In addition to the supernova cosmology case for high-accuracy flux calibration, there may be future science cases that we cannot yet envision that will want to use archival data from NASA missions such as HST. By recalibrating standard stars that were observed by such spacecraft, such archival data can

be recalibrated, thereby enhancing the value of these valuable datasets.

2.4 High Redshift Universe

Unlocking the High Redshift Universe

Science Objectives: Constrain the number densities of faintest Star Forming clumps and constrain their physical size. Follow up with ORCAS on caustic transits of individual stars in star forming clumps detected by HST and JWST.

Observable and Measurements: A minimum of 10 ORCAS fields to formulate a census for ∼100 of these faint star forming clumps.

Key Functional Requirements: A 5" x 5" FOV with a minimum wavelength coverage of 0.5-1.2 μm. Deep images to AB $\leq$ 29 mag (10 σ) for point sources in a few hours, or 31 mag using notch filters for the spectral regions with the brightest night sky-line. Spatial resolution of ∼0.01"-0.02" FWHM with good Strehl ratios.

ORCAS Uniqueness: ORCAS can provide strong sensitivity at shorter wavelengths.

In the last three decades, major progress has been made in studies of galaxy assembly with the Hubble Space Telescope (HST) and through targeted programs using Adaptive Optics (AO) on the world's best ground-based facilities. It is not possible to review all these efforts here; we refer the reader to more detailed reviews (48), (49), (50), (51). In (52), we reviewed the advantages of high resolution science on high redshift galaxies from the ground as compared to from space. In short, diffraction limited space-based imaging provides much darker sky over a wider FOV, more stable PSF's, better dynamic range, and therefore superior sensitivity, including in the vacuum-UV. But ground-based multi-conjugate AO (MCAO) on 8-10 meter telescopes is *complementary* to space-based imaging, as it can provide much higher spatial resolution — and spectral resolution — than what space-based telescopes can currently do.

One of the early discoveries by HST was that the numerous faint blue galaxies are in majority late-type (*e.g.*, 53, and references therein), (54), (55), (56) and small see Fig.16 here (57), (58), (59) star-forming objects. These are the building blocks of the giant galaxies seen today (*e.g.*, 60). By measuring their distribution over rest-frame type (61) versus redshift, HST has shown that galaxies of all Hubble types formed over a wide range of cosmic time, but with a notable transition around redshifts z≃0.5–1.0 (54; 55; 62, *e.g.*,). This was done through HST programs like the Medium-Deep Survey (63), the Hubble Deep Field (HDF 64), GOODS (65), GEMS (66), the Hubble UltraDeep Field (HUDF 67), COSMOS (68), and CANDELS (69; 70). Coupled with models of galaxy formation, these observations suggest that subgalactic units rapidly merged from the end of reionization (71; 72) to grow bigger units at lower redshifts (*e.g.*, 60). Merger products start to settle as galaxies with giant bulges or large disks around redshifts z≃1 (*e.g.*, 73; 74). These have evolved mostly passively since then, resulting in giant galaxies today (*e.g.*, 55; 58).

Star-forming clumps have also been studied at high resolution in lower redshift turbulent galactic disks (*e.g.*, 75; 76). The size evolution of star-forming galaxies has been studied out to z $\sim$ 7 (*e.g.*, 77; 78), where galaxy half-light or effective radii $r_{\rm e}$ approximately decrease with redshift as r_e(z)$\propto r_e(0)\cdot$(1+z)$^{-s}$ with s≃0.9–1.2. This strong size evolution reflects the hierarchical formation of

galaxies, where sub-galactic clumps and smaller galaxies merge over time to form the larger/massive galaxies that we see today (*e.g.*, 79). It was the reason that HST was so successful after its refurbishment in December 1993 at identifying faint compact star-forming galaxies that form hierarchically at z$\simeq$1–7 in the ΛCDM universe. The compact object sizes thereby helped to mitigate the enormous $(1+z)^4$ cosmological SB-dimming that would quickly render large extended objects undetectable at higher redshifts (*e.g.*, 52).

The combination of multiple ORCAS or CubeSat laser MCAO beacons with ground-based 8–39 meter telescopes has the great potential to provide nearly diffraction limited imaging over wider FOV's than possible with AO alone. For instance, ORCAS combined with the 10 meter Keck telescope can provide PSF FWHM values $\lesssim$0.″01–0.″02 (10–20 mas) at 0.5–1.25 μm wavelength, and still provide a sufficient FOV ($5\times5''$–$10\times10''$) to detect a significant number of objects to very faint fluxes (AB$\lesssim$31 mag). In the visible–near-IR, ORCAS+Keck can thus compete with space-based imaging in terms of increased spatial resolution, low sky-brightness in its very small pixels, and therefore increased point source sensitivity. In the thermal infrared ($\lambda\gtrsim2\mu$m), for which JWST was designed and optimized (51), space-based imaging will remain superior in terms of PSF-stability, sky-brightness, depth, and FOV.

2.4.1 The Surface Density of Faint Star-Forming Clumps to AB$\lesssim$29 mag for ORCAS

For the success of ORCAS galaxy science, we need to be able to accurately estimate the expected number density of faint compact star-forming objects out to z$\lesssim$7 and AB$\lesssim$31 mag. To interpret the currently available lensed samples of SF clumps, we also need to make an estimate of the *intrinsic* object counts anticipated to AB$\lesssim$35-36 mag. The deepest available data to date are summarized in Fig 15a-15b for the HST ACS/WFC F606W (wide V-band) and WFC/IR F125W (J-band) filters or their ground-based equivalents. These data came from the panchromatic ground-based GAMA survey (which covers AB$\lesssim$18 mag; 80), the panchromatic HST WFC ERS survey (17$\lesssim$AB$\lesssim$26.5 mag; 81), and the panchromatic HUDF (22$\lesssim$AB$\lesssim$30 mag; 67; 82), and references therein. The HUDF/XDF limits are indicated by the green labels in the top right corner of Fig 15a-15b. Orange labels indicate the anticipated JWST Webb Medium Deep Field (WMDF) and UltraDeep Field (WUDF) survey limits, while red indicates a Webb UltraDeep Frontier Field (WUDFF) survey limit if pointed at a gravitationally lensing Frontier Field cluster. The 5σ point source detection limits for each of these surveys are indicated in Fig. 16, and for both HST and JWST assume an effective PSF width of 0.″08 FWHM (52). Blue labels indicate the anticipated 5σ point source sensitivity limit of AB$\lesssim$31 mag of unlensed objects for ORCAS+Keck with an image PSF with 0.″01–0.″02 FWHM at 0.5–1.2 μm wavelength. If ORCAS were to frequently monitor the best gravitational lensing clusters, we may detect compact sources intrinsically as faint as AB$\lesssim$35–36 mag when lensed. For an HST and JWST PSF with FWHM$\lesssim$0.″08, the depth increase from WUDF to WUDFF is about 2–3 mag, given the larger unlensed SF-object sizes ($\sim$0.″005–0.″080) sampled, while for ORCAS these magnifications could be $\sim$3–4 mag for the anticipated *smaller* unlensed SF-clump sizes ($\sim$0.″001–0.″080) that it may sample (see Fig. 16).

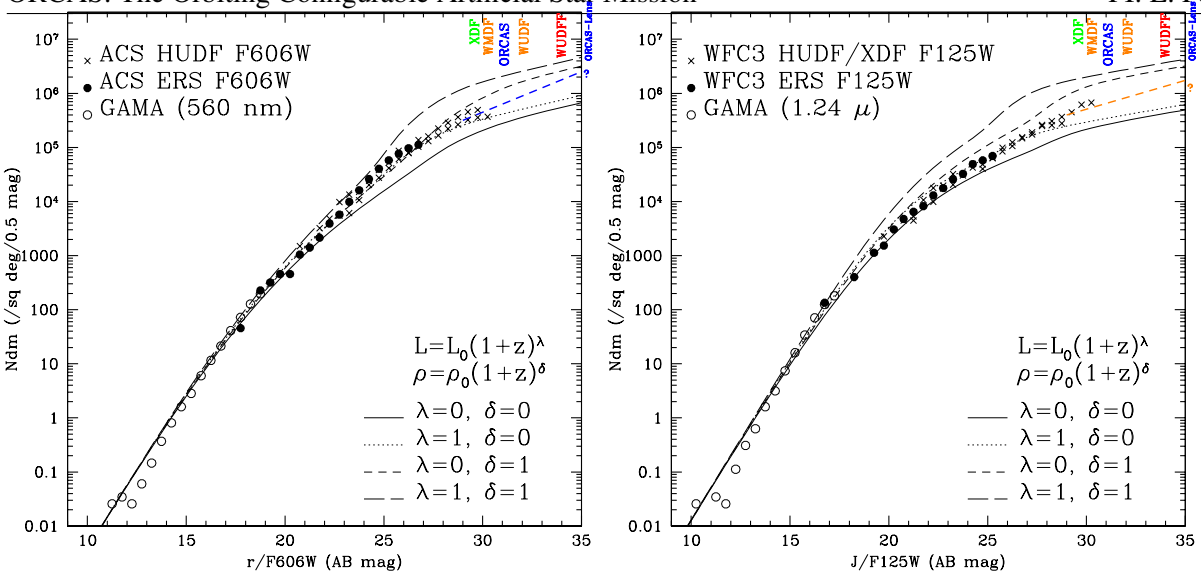

Fig 15 (a) [Left]: Differential galaxy counts in the V-band or F606W filter. Data are from the ground-based GAMA survey and the HST ACS/WFC surveys in the WFC3 ERS and HUDF fields. Combined ground-based + HST-surveys cover $10 \lesssim$AB$\lesssim 30$ mag (81; 82). Simple luminosity+density evolution models are shown and extrapolated to AB$\lesssim$35 mag (see § 2.4.1 for details). **(b) [Right]:** As Fig. 15a, but in the J-band or HST WFC3/IR F125W filter. The colored labels indicate the various HUDF/XDF, Webb and ORCAS detection limits without and with lensing. To AB$\lesssim$31 mag in both filters, ORCAS will yield about 5×10^6 faint star-forming (SF) clumps per square degree, or $\sim$0.4 per arcsec^2, or one in every box of $1.6\times1.6''$.

The observed panchromatic (0.2–1.6 μm) galaxy counts attain a converging slope ($\alpha < 0.40$) for the general flux range of AB$\simeq$17–25 mag (81; 82). These counts were fit with models that include luminosity + density evolution, as indicated by the four curves in Fig 15a-15b. Some of these models fit the panchromatic counts remarkably well for $10 \lesssim$AB$\lesssim 30$ mag. We use the differential count slope as a function of wavelength (81) to extrapolate the observed counts to the $31 \lesssim$AB$\lesssim 35$ mag range. At brighter fluxes, the 0.60–1.25 μm count-slopes are 0.30–0.26 mag/dex, respectively, but for AB$\gtrsim$30 mag we adopt extrapolations with count slopes of approximately 0.15–0.10 dex/mag, as indicated by the blue and orange dashed lines in the upper-right corners of Fig 15a-15b. The justification for this extrapolation is that the faint-end slope of the galaxy counts is dominated by galaxies at the median redshift, which in ultradeep redshift surveys approaches the peak in the cosmic star-formation diagram at z$\simeq$1.9 (83). At this redshift, the best fit faint-end slope of the Schechter LF is $\alpha \simeq 1.4$ in linear flux units (84; 85), so when converted to a magnitude count-slope, the faint-end slope of the galaxy counts is $\gamma \simeq (1.4–1)/2.5 \simeq 0.16$ dex/mag. It is possible that for fluxes fainter than AB$\sim$31 mag the LF at z$\gtrsim$2 — and therefore the observed counts — may turn over with a slope flatter than observed at brighter levels, but there are arguments against this too for a discussion, see *e.g.*, §2.3 of (86). The adopted extrapolated slopes in Fig 15a-15b are in line with the trend of the very faint-end of the plotted galaxy counts models. In both the 0.60 and 1.25 μm filters, the counts integrate to 5.0×10^6 faint star-forming (SF) clumps per square degree to AB$\lesssim$31 mag. (To go from differential to integral counts in Fig 15a-15b, one needs to multiply the differential surface density at AB=31 mag by 2$\times$ to get the counts per 1.0-mag bin, and by $\sim$3.5$\times$ to get the total integral counts over all magnitude bins.) This surface density corresponds to $\sim$0.4 SF-object per arcsec^2 to AB$\lesssim$31 mag, or on average one object in every box of $1.6\times1.6''$. A $\gtrsim 5\times5''$ FOV of the ORCAS IFU may therefore provide just enough compact SF clumps to do *relative* m.a.s.-astrometry as needed in, *e.g.*, § 2.4.3. **[Reviewers: Please enlarge the PDF figure as needed to display the full dynamic range of these data].**

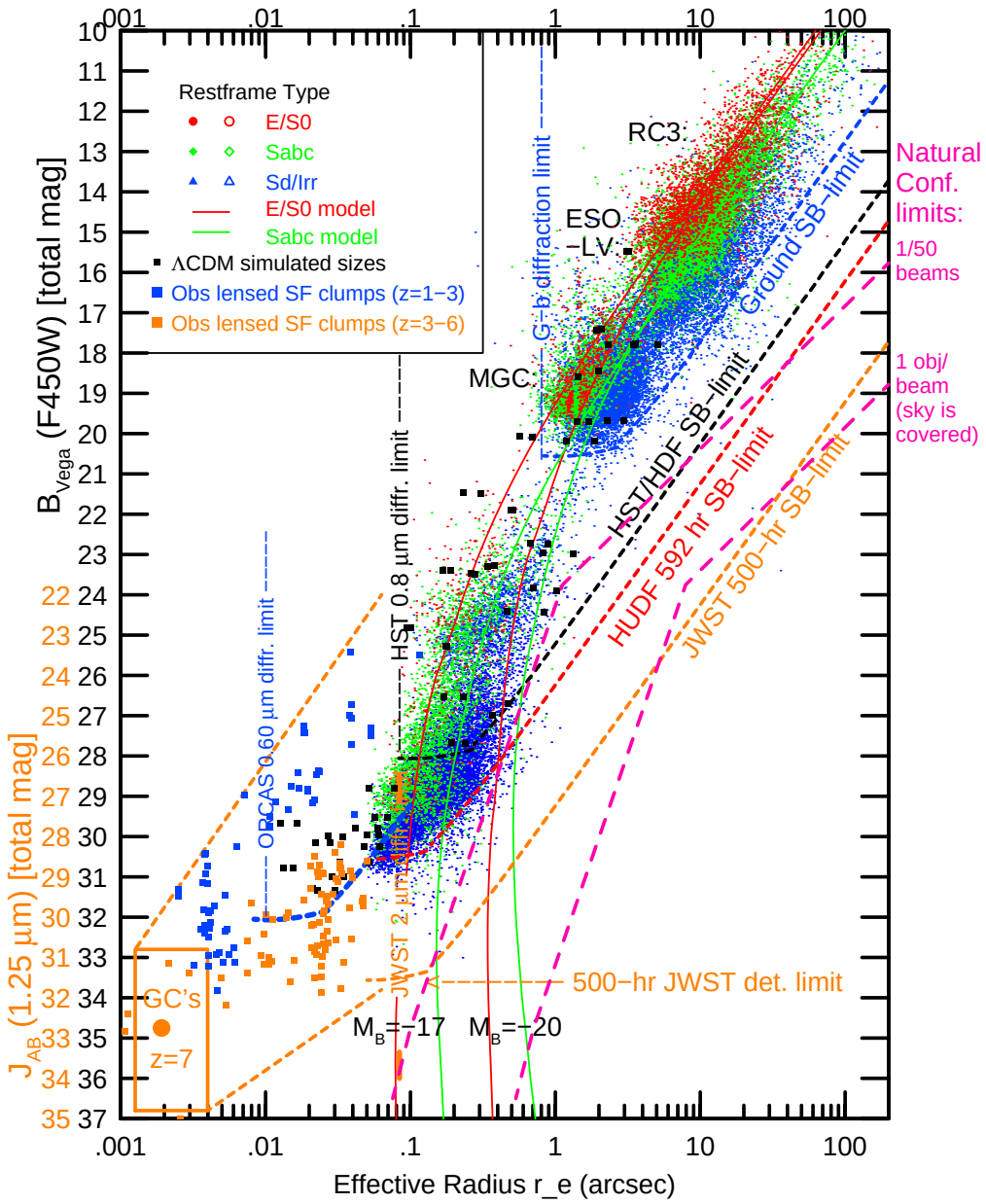

Fig 16 Galaxy sizes $r_{\rm e}$ vs. $B_{\rm Vega}$ or J_{AB} -magnitude from the RC3 to the HUDF limit. Short dashed lines indicate survey-limit wedges for the HDF (black), HUDF (red; in $i_{\rm AB}$), and JWST (orange): diffraction limits are vertical, point-source sensitivity limits horizontal, and SB-sensitivity limits have slanted slopes = +5 mag/dex. Broken long-dashed pink lines indicate the natural confusion limit (at the level of 1 detected object per 50 "beams" or object area), to the right of which objects would begin to statistically overlap due to their own sizes and surface densities. Red and green lines indicate the expected *non-evolving* sizes for RC3 elliptical and spiral galaxies at the listed $M_{\rm AB}$-values, respectively. Blue and orange squares indicate SF-clumps from gravitational lensing samples with intrinsic physical sizes converted to $r_{\rm e}$ ($''$), and unmagnified absolute UV-magnitudes converted to B-mag for z=1–3 or J_{AB} for z=3–6 (the J_{AB} -scale is shown approximately offset in orange for z$\gtrsim$3; the $i_{\rm AB}$-scale is between B and J_{AB}). Black squares indicate galaxy sizes from hierarchical simulations. The orange box shows where Globular Clusters at z=7 are expected. For details, see § 2.4.2. Most galaxies at J_{AB} $\gtrsim$27–28 mag are expected to be smaller than the HST and JWST diffraction limits (*i.e.*, $r_{hl}\lesssim 0\farcs08$). About half the faint SF-clumps to AB$\lesssim$31 mag are expected to be (barely) resolved at the ORCAS resolution of 0.01"–0.02" FWHM. [Figure adapted from (52)].

2.4.2 The Size Distribution of Faint Star-Forming Clumps to $r_{\rm e}$ $\gtrsim$0.01" for ORCAS

The median sizes of faint galaxies decline steadily towards higher redshifts and also towards fainter magnitudes, as shown in Fig. 16. Red, green, and blue dots show early-type, spiral, and irregular/SF galaxies respectively (*e.g.*, 57; 58). Galaxy structural classification needs to be as much as possible done at rest-frame wavelengths longwards of the Balmer break at high redshifts too avoid caveats from the morphological K-correction (*e.g.*, 61; 87; 88; 89). Red and green lines show the best fit regression for local galaxies and its extrapolation at fixed $M_{\rm AB}$-values to fainter magnitudes.

The HST/WFCP2 Hubble Deep Field (64) and the HST/ACS Hubble Ultra Deep Field (67) showed that high redshift galaxies are intrinsically very small with typical sizes of $r_{\rm hl} \simeq 0\farcs12$ or 0.7–0.9 kpc at z$\simeq$4–6, and sample correspondingly fainter absolute AB-magnitudes. The unique combination of these ground-based and HST surveys shows that the apparent galaxy sizes decline steadily from the RC3 to the HUDF limits (52, and Fig. 16 here). Most galaxies at $J_{AB} \gtrsim$28 mag are thus likely unresolved at $r_{hl}\lesssim0\farcs1$ FWHM, as suggested by galaxy sizes from hierarchical simulations (black squares in Fig. 16; 90).

SB and other selection effects in these surveys are significant. For each survey, the diffraction limit for point sources is shown as vertical dashed line with the survey indicated, while the nearly horizontal line of the same color indicates for each survey the corresponding $\sim5\sigma$ point-source sensitivity, and the slanted dashed line (with a of slope 5 mag/dex) indicates that survey's corresponding SB-sensitivity. That is, each survey cannot detect objects outside this wedge-shaped area. The pink lines indicate the natural confusion limit discussed in (52), that were derived from the (assumed broken power-law) counts in Fig. 15a–15b. As opposed to the instrumental confusion limit, which is determined by the FWHM of the PSF in each survey, the natural confusion lines indicate the region where galaxies would be large enough that their effective area, $\pi {r_{\rm e}}^2$ or "the galaxy beam", would occupy more than 1/50 of the total survey area, thereby limiting the ability of source detection and deblending algorithms to provide complete catalogs of overlapping objects. This is primarily visible for galaxies in the HDF and HUDF for 24$\lesssim$B$\lesssim$28 mag and $0\farcs4\lesssim r_{\rm e} \lesssim0\farcs8$, where samples become incomplete as they are no longer bunching up against the SB-selection lines. Natural confusion is expected to become more significant for JWST surveys when they are pushed to fainter than AB$\simeq$30–31 mag.

Extensive recent studies with HST of several of the best lensing clusters have resulted in many SF clumps at z$\simeq$1–6.6 that are observed close to the critical curves, where they appear highly gravitationally stretched and highly magnified in their total flux (*e.g.*, 91; 92; 93; 94). Of particularly importance are the VLT MUSE spectra and redshifts that have been obtained for many of these SF clumps (94; 95), which are shown in Fig. 16 as the blue (z$\simeq$1–3) and orange (z$\simeq$3–6.6) squares at their *intrinsic* (*i.e.*, unlensed) physical sizes and *unmagnified* absolute magnitudes (*i.e.*, their observed $M_{\rm AB}$-values after dividing by their lensing magnification). In Fig. 16 their unlensed physical sizes were converted to $r_{\rm e}$ in arcsec, and their unmagnified $M_{\rm UV}$ -values were converted to B- or J_{AB} -magnitudes at the corresponding redshifts in ΛCDM cosmology. Volume completeness is always hard to estimate even for these best available gravitational lensing surveys with faint object spectroscopy, but at least these objects show up in significant numbers in these surveys, and they populate the *unmagnified flux range* of 24$\lesssim$AB$\lesssim$34 mag, and the *intrinsic, unlensed size range* of $0\farcs001\lesssim r_{\rm e} \lesssim0\farcs08$ in Fig. 16. About half of these SF clumps are expected to be visible down to the ORCAS diffraction limit, while the other half will be slightly resolved, but still mostly above the ORCAS SB-limits. A $\gtrsim5\times5''$ ORCAS FOV may therefore provide just enough compact SF clumps to do relative (sub-)m.a.s.-astrometry, depending on the S/R-ratio achieved, which is needed in § 2.4.3.

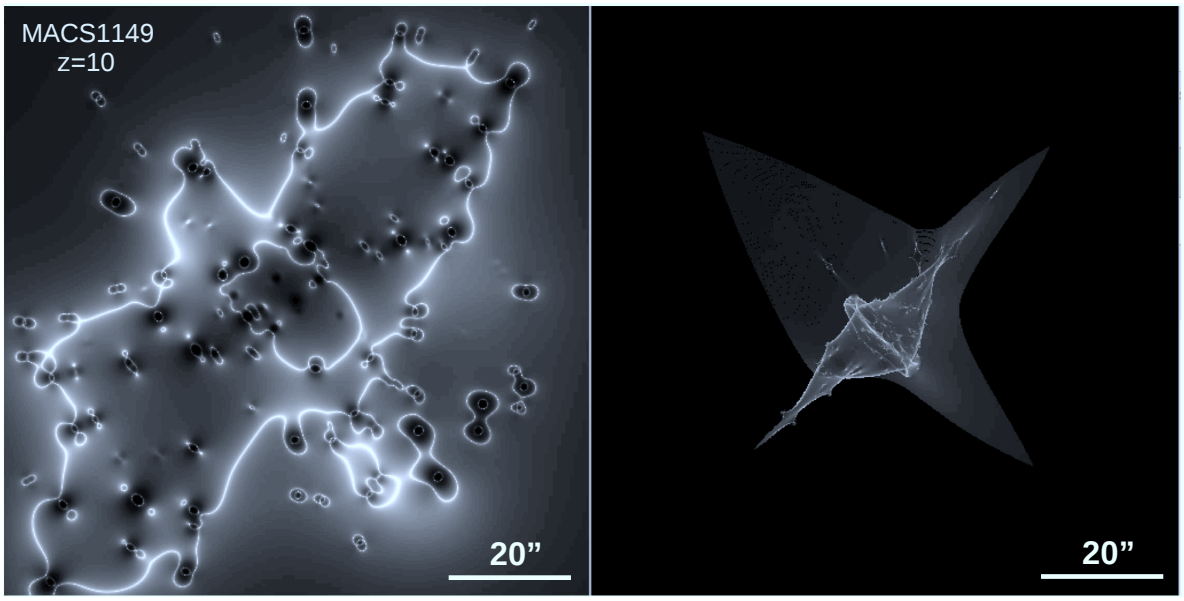

Fig 17 [LEFT] Example of the lensing magnification map for galaxy cluster MACS J1149.5+2223 at z≃0.54 and a background source at z=10 (*e.g.*, 91, and references therein). Light from the cluster galaxies is not shown to avoid overcrowding, but can be found in those papers. The white areas mark the critical curves, where maximum lensing magnification is observed from this cluster for a background source with half-light radius $r_{\rm hl}$ $\lesssim$0.″5 at z=10. The lightest regions have the highest magnification ($\mu\gtrsim$10–20), while the darkest regions are areas of low magnification ($\mu\simeq$1 or even $\mu\lesssim$1) around the cluster member galaxies. [RIGHT] Caustic map produced by the cluster mass model for a background source at z=10. This is the location where a point source at z=10 produces maximum magnification. The total length of the cluster caustics is L≃100″when estimating caustic transit probabilities (for details, see § 2.4.3 and **? ?**)windhorst$_2$018.

Natural confusion is expected to be less important for ORCAS+Keck, since the sampled unlensed SF-clump sizes from the HST gravitational lensing samples are much smaller than the HST diffraction limit. Yet is it possible that a number of larger SF clumps will fall below the ORCAS SB-limits, and only more hierarchical simulations (black squares) and deeper ORCAS observations will be able to assess this more precisely.

2.4.3 Monitoring Caustic Transits of Early Stars with ORCAS

Cluster caustic transits can occur when a compact restframe UV source transits a caustic due to the transverse cluster motion in the sky, or perhaps due to significant velocity substructure in the cluster, and have the great potential of magnifying such compact objects temporarily by factors of $\mu\simeq10^3$–10^5 (*e.g.*, 96). This is because: (1) the clusters and their substructures may have transverse motions as high as $v_T\lesssim$1000 km s^{-1}, (2) stars at z≃1–7 (including population III stars at z$\gtrsim$7) have radii R≃1–10 R$_\odot$, and (3) in the source plane the main caustic magnification goes as: $\mu\simeq10\cdot(\mathrm{d}_{caustic}/'')^{-1/2}$, where $\mathrm{d}_{caustic}$ is the distance of the star to the cluster caustic in arcsec.

This is illustrated in Fig. 17 as reproduced from (86). Since stars at z$\gtrsim$7, including Pop III stars, are of order $\sim10^{-11}$ arcsec across at z≃1–17, such caustic transits could temporarily boost the brightness of a very compact object by $\mu\simeq$7.5–12.5 mag, which may render it observable by JWST (*e.g.*, 86) and also ORCAS+Keck. The best lensing clusters are typically at z≃0.3–0.5, and are by selection the most massive, largely virialized clusters. Lensing clusters with some significant velocity substructure

are preferred, since they tend to have more significant transverse motions that increase the likelihood of caustic transits.

In the absence of microlensing by faint stars in the cluster IntraCluster Light (ICL), these caustic transits may boost the apparent magnitude of these stars by $\mu \simeq$7.5–12.5 mag for several months. This has been observed with HST for a number of hot (OB-type) stars at z$\simeq$1–1.5 (97), (98), (99), (100), (101), (102). (86) calculated the frequency of such events from both MESA models for Pop III stars and multicolor accretion disks for stellar mass black holes at z$\simeq$7–17. Both will have roughly the same radii (R$\simeq$1–100 R$_\odot$) and effective temperatures ($T_{\rm eff}\sim$50,000–100,000 K), since they will radiate close to the Eddington limit, and therefore they will have similar rest-frame UV SB. (The only difference is that Pop III stars never get much hotter than 105,000 K, while stellar mass black hole accretion disks will also radiate in X-rays when fed from lower mass companion stars in their AGB stage). Microlensing by faint foreground stars in the cluster ICL would dilute the macrolensed signal across the main caustic somewhat, but could also spread it out over more peaks over a longer period of time (98). The resulting expectation is that JWST may observe such events at the rate of up to $\sim$0.3 per cluster per year if the best lensing clusters are monitored a few times each year with JWST NIRCam (86).

While the ORCAS FOV is too small for a blind survey of caustic transits at z$\gtrsim$1, it is of particular interest to follow up with ORCAS on caustic transits of individual stars in SF clumps at z$\gtrsim$1–2 that have been detected with HST, and on caustic transits that may be detected with JWST at z$\simeq$6–17 at extreme magnifications ($\mu\gtrsim10^3$–10^5) for the first stars and their stellar mass black hole accretion disks. The ability for ORCAS to monitor such objects for decades across the (micro-)caustics provides a unique opportunity to obtain a statistical census of individual stars at cosmological distances. For instance, one could use different ORCAS epochs to precisely estimate the centroid position of a lensed star that is very close to a caustic. Assuming the two counter images of the star would form an unresolved duplet with a separation of less than the ORCAS resolution, microlensing in each of the two counter images could make the centroid of the observed image shift from epoch to epoch (*e.g.*, 103), which ORCAS could monitor at high precision. This then would add a powerful time-domain constraint to gravitational lensing models, in addition to the constraints provided by very deep high-resolution imaging.

2.5 Exoplanets

Awaiting team lead revised version

Science Objectives: Directly image exoplanets and disks around nearby stars.

Observable and Measurements: Determine the presence of and characterize exoplanets and disks orbiting nearby stars through high-contrast adaptive optics imaging and low-resolution integral field spectroscopy.

Key Functional Requirements: Visible (0.5-1.0 μm) and Near-Infrared (1-2.5 μm) imagers and integral field spectrographs (R$\sim$50) with high-order deformable mirror (HODM) adaptive optics, illuminated by the ORCAS laser guide star.

ORCAS Uniqueness: ORCAS will enable flux contrast improvements not obtainable for most nearby stars. For nearby bright stars of approximately fifth magnitude at visual wavelengths, ORCAS will provide approximately a one magnitude sensitivity improvement with HODM by providing more photons for adaptive optics corrections than available from the host star, equivalent to a zeroth magnitude guide star. For nearby stars fainter than fifth magnitude, ORCAS will enable imaging with the equivalent of a zeroth magnitude natural guide star adaptive optics (NGSAO), offering superior sensitivity compared to LGSAO by several orders of magnitude.

ORCAS will enable four key exoplanet science cases. First, ORCAS will characterize approximately eight known exoplanets from radial velocities (RVs), astrometry, ground-based direct-imaging, and other techniques. The RV technique has revealed hundreds of long-period Jovian planets through their indirect gravitational effects on their host stars (104), and GAIA will soon detect thousands of Jovian exoplanets orbiting at large semi-major axes through the indirect astrometric wobble of their host stars (105). Both techniques provide only a mass and orbital period, or lower limit to the mass of the exoplanet in the case of the RV method. The atmospheres, composition, temperature and density of these exoplanets remain unknown due to the indirect methods by which they have been discovered. ORCAS will be able to image and characterize some of these Jovian planets by measuring their spectral energy distributions directly, as well as search for additional planets in the systems. To date, the sensitivity of the direct imaging of exoplanets with ground-based adaptive optics systems has been limited to more massive brown dwarfs orbiting at large semi-major axes, such as with the TRENDS program (106), young self-luminous exoplanets orbiting massive A-type stars such as the massive Jovian planets in the HR 8799 system (107), and searching for massive exoplanets orbiting stars brighter than approximately fifth magnitude with sufficient photons for NGSAO. ORCAS will improve the number of photons available for adaptive optics corrections with next-generation HODM, improving the obtainable flux contrast by at least one magnitude at visual wavelengths (Fig 18). This improved flux contrast sensitivity will enable searches for and characterization of exoplanets that are less massive, orbit closer to their host stars, and orbit stars that are fainter than can currently be surveyed with NGSAO, for which LGSAO does not provide as accurate corrections to the wavefront. Additionally for known planetary systems that have been imaging from the ground, such as HR8799, 51 Eri and other young exoplanets, ORCAS will enable higher SNR characterization of their atmospheres with adaptive optics integral field spectroscopy.

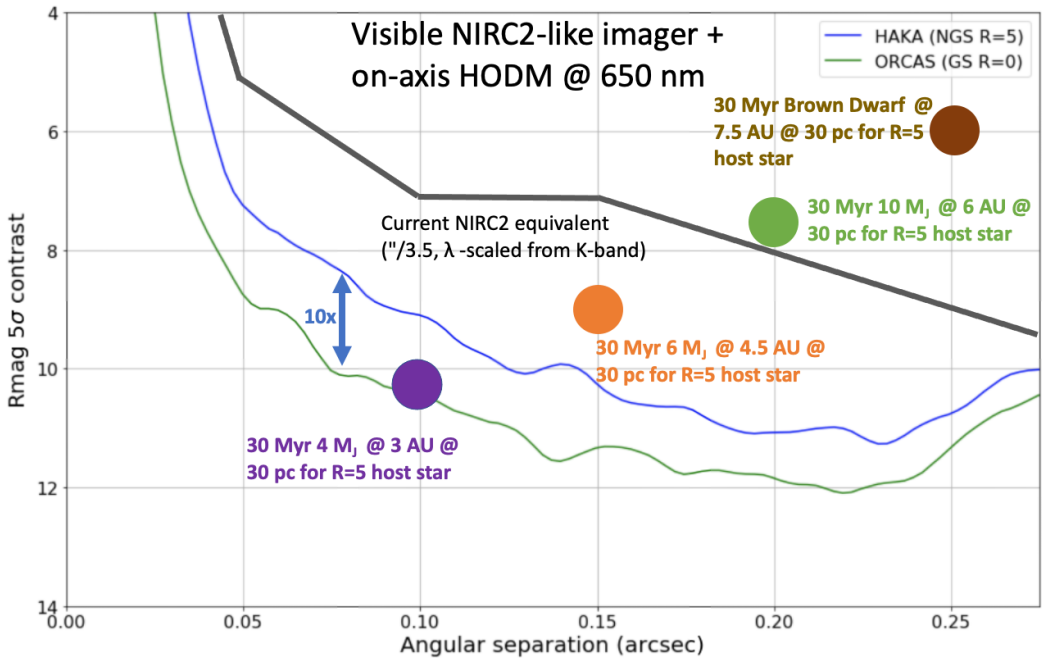

Fig 18 Simulated 650 nm R-band sensitivity contrast curves with ORCAS (green curve) and without ORCAS (HAKA concept, blue curve). HAKA is a conceptual visible imager coupled with a HODM natural guide star adaptive optics system on Keck Observatory. A wavelength-scaled approximate sensitivity from the current Keck Observatory NGSAO performance with NIRC2 at K-band is shown as the black segmented line. Shown in circles are approximate contrasts for Jovian planets orbiting a 30 Myr fifth magnitude host star. Contrast curves for MAVIS, planned for commissioning in 2027, would be intermediate between the projected performance of HAKA and a visible NIRC2-like imager.

Second, ORCAS will enable a deeper sensitivity to the zodi levels of approximately eight nearby stars and search for exoplanets around these stars as important precursor studies for a future flagship direct imaging mission such as HabEx or LUVOIR, including the "Deep Dive" HabEx targets (108; 109). These future mission concepts aim to detect Earth-size exoplanets in reflected light orbiting in the Habitable Zones of Sun-like stars. One of the complicating factors in the detection of terrestrial planets orbiting Sun-like stars is the presence of dusty debris produced by the collisions of small asteroid and cometary parent-bodies in the system, resulting in diffuse micron-sized debris scattering star-light on the same scale and brightness contrast as the exoplanets these missions will attempt to image (110; 111). Ground-based interferometric surveys have placed upper-limits to the surface brightness of these debris disks to multiples of the scattered light brightness of the dusty debris in our Solar System, or "zodis" for short (where one zodi is the surface brightness of the debris scattered light in our Solar System). ORCAS will be able to survey nearby stars to place better constraints of $<$10 zodi on the zodi levels in these systems, which will help rule out systems for which the zodi levels are too high and preclude the ability to directly image an Earth-sized planet in reflected light, thus optimizing the target list for a future NASA flagship direct imaging mission. Additionally, ORCAS may discover Jovian planets in the Habitable Zones of (or exterior to) these stars, which orbit 5-10% of Sun-like stars. Such Habitable Zone Jovian planets could dynamically preclude the presence of Earth-mass planets in the Habitable Zone, but could however possess habitable exo-moons; ORCAS would give us a better dynamical picture of these exoplanet systems prior to the launch of HabEx or LUVOIR.

Third, ORCAS will uncover the planet formation process in disks around approximately eight young, nearby stars. Many debris disks are imaged in scattered visible and near-infrared light at large semi-major axes from the ground and in space (e.g. >5–200 au), and imaged in thermal emission at sub-mm wavelengths with ALMA. Well-known examples include TW Hya, AU Mic, Vega, Beta Pic, Eps Eri, HR 4796 and Fomalhaut, where transitory features have also been observed and in the case of AU Mic move with non-Keplerian motion (112; 113; 114). ORCAS will enable unprecedented visible and near-infrared imaging and characterization of these and other disks at smaller orbital separations of <5 au not accessible with Hubble, probing the disk dynamics at Habitable Zone locations interior to the snow line. Also ORCAS will enable flux contrast sensitivity not accessible with current ground-based AO, at both visible and near-infrared wavelengths. Many known debris disk system host stars are simply too faint for natural guide star adaptive optics, and angular resolution is impacted by the wavefront error using faint LGSAO. ORCAS will provide an artificial zeroth magnitude natural guide star to achieve higher Strehl, and one that could be positioned closer to the disk features of interest than the host star itself, as some disks can extend several arc-seconds on the sky.

Fourth, ORCAS will help us constrain the occurrence rates of cool sub-Jovian and super-Neptune exoplanets orbiting approximately a half-dozen nearby cool stars and brown dwarfs, as a precursor to the TMT/ELT era of imaging Habitable Zone M dwarf terrestrial exoplanets (115; 116). Current direct imaging of exoplanets around M dwarfs are limited by the intrinsic faintness of M dwarfs and rely on LGSAO currently and will continue to rely on LGSAO even in the era of MAVIS – there are only 4 M dwarfs later than M4 in spectral type brighter than an apparent magnitude V=12. ORCAS will provide an artificial guide star of zeroth magnitude to achieve unprecedented flux contrast in visible and near-infrared wavelengths at smaller angular separations than currently possible with LGSAO for these stars. This will enable the search for cool sub-Jovian and super-Neptune exoplanets orbiting these stars and brown dwarfs (Jovian planets are rare orbiting M dwarfs relative to Sun-like stars). Finally, all four of these science cases are limited only by the number of visits that can be obtained during the primary ORCAS mission, and an extended mission would enable more stars in the above stellar samples of exoplanet and disk host stars to be surveyed.

2.6 Solar System

Viewing the Solar System in a new light through ORCAS

Science Objectives: Understand the origins and evolution of small bodies, investigate Satellites, rings, Mars, moons, and ice giants.

Observable and Measurements: Determine surface properties and architecture of small bodies. Determine the volatile composition of small bodies in the outer solar system. Understand the processes involved in the formation of our Solar System, and map clouds and trace gases of Uranus and Neptune.

Key Functional Requirements: A NIR imaging spectrometer with a wavelength coverage of 2.5 to 5.0 μm, spectral resolution $\geq$ 20,000 and pixel scale $\leq$ 50 mas.

ORCAS Uniqueness: ORCAS will have the potential to resolve rings and binaries that have not yet been achieved with direct imaging. The unprecedented resolution can help determine heterogous composition of icy bodies. Bright extended objects are not possible with current AO, unless a star or satellite is within 30"

ORCAS provides two key capabilities for Solar System research: performing AO observations on extended sources, and on faint and diffuse objects (e.g., comets, distant TNOs, small near-earth-objects NEOs / asteroids). AO observations of giant planets in our Solar System, like Jupiter and Saturn, are currently only possible when employing bright near-by satellites as tip-tilt/DM references, and even then is particularly challenging and particular coordination is required. AO observations on many planets in our Solar System (e.g., Mars, Venus, Mercury) have been tried unsuccessfully, since these extended objects do not provide an accurate correction reference frame.

Even though there is much to learn about the large planets in our Solar System at the outstanding diffraction limits of E-ELT (0.02 arcsec at 3 μm), TMT (0.03 arcsec at 3 μm) and even Keck (0.07 arcsec at 3 μm), performing AO without ORCAS on an extended source is particularly challenging. Although corrections of 0.1 arcsec have been obtained on Jupiter by using the Galilean satellites for wavefront sensing (e.g., 117), the best spatial resolutions achieved on Mars are not better than 0.4 arcsec, as demonstrated with attempts to lock the adaptive optics systems of VLT and Keck on Mars (see Villanueva et al., 2010). By combining the spatial resolution improvements provided with ORCAS with the spectral resolution provided by powerful ground-based spectrometers, we will be able to address key science goals (e.g., mapping of organic/water reservoirs and their isotopic signatures) with unprecedented accuracy and sensitivity. Similarly, performing AO on most bodies in the solar system is not possible, since they are naturally too faint (i.e., most KBOs and NEOs) or naturally non-point-sources/diffuse and faint (e.g., comets).

Visible AO. AO at visible wavelengths is still in its infancy, and ORCAS may help bring this to a mature state. One example where visible-light AO would be advantageous is observations of Neptune's dark spots (e.g., 118). Dark spots on Neptune are quite rare; only a handful have been seen since the Great dark Spot discovery by Voyager in 1989. Such spots can only be seen at blue wavelengths ($\sim$460 nm), have a typical lifetime of order 1-3 years, and are usually relatively small in extent ($\sim$100 mas). At present, only HST can observe these spots. With ORCAS on Keck they would

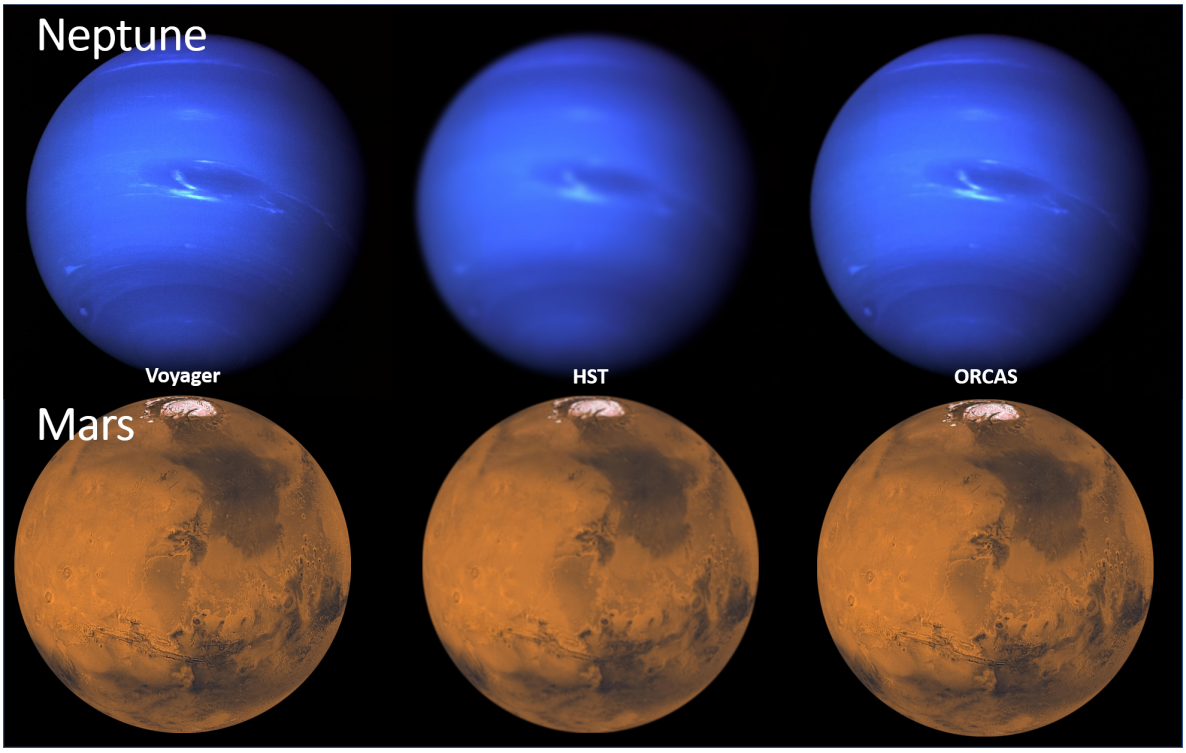

Fig 19 Images of Neptune and Mars as observed by Voyager (∼1 km/pixel), HST (at 28 au and 1 au, respectively), and PSG simulations at 500 nm with ORCAS.

be detectable at ∼460 nm. Ideally, we would be able to track the evolution of a dark spot until its demise, a process that is yet unknown.

ORCAS would enable high spatial resolution observations at visible and IR wavelengths; though at visible wavelengths HST has superb spatial resolution, in the infrared HST's spatial resolution is quite limited. JWST will provide superb resolution (at >600 nm), but not as high as can be obtained with Keck, due to the size of the telescope, and the size of the JWST pixels. However, AO on large planets can only be obtained using its natural satellites as guidestars, which limits the areal coverage over which high resolution can be obtained (isoplanatic angle), and the guidestar has to be within 30" of the source, which is only possible for limited amounts of time. High spatial resolution is in particularly important to image storm systems and impacts, ideally using an IFU (IFS) to obtain image data cubes.

Satellites and rings. Although the larger satellites of the giant planets can be observed with Keck using the satellites themselves as guidestars, small satellites and rings require the use of ORCAS. In particular observations of planetary rings would be unique, as they may reveal small embedded bodies and the evolution of wave structures within rings. But even larger satellites when observed in eclipse require ORCAS, since during those times they are too faint for NGS observations. One example of such an observation that would benefit from ORCAS would be to observe SO emission bands on Io during an eclipse. During this time the satellite's light is not overwhelmed by Io's reflected sunlight, and faint emissions become visible. Such observations have been obtained with Keck, but opportunities are rare (need another satellite nearby and not in eclipse for wavefront sensing). The origin of these emissions remain unexplained.

3 Science Traceability Matrix

3.1 Active Galactic Nuclei

ORCAS will advance AGN science with both infrared and visible waveband observations. Infrared observations would be achieved with existing ground-based instrumentation at the W.M. Keck Observatory, notably including the OSIRIS integral field spectrograph. Using existing ground-based instrumentation offers a low-risk path to key science objectives. Conceived visible waveband observations would accomplish far-reaching science and technology goals and contribute an important, missing capability for U.S astronomy

The science traceability matrix (STM) for AGN is shown in Tables 2 and 3. These tables illustrate a flow-down from key, signature science cases to specific science objectives, the physical parameters and observables associated with the science objectives, and the ground-based, W.M. Keck Observatory instrument requirements to make the necessary observations. These in turn lead to projected performance and mission requirements. These tables also provide a succinct summary of specific enabling feature of ORCAS, in the 'Why ORCAS?' column.

The instrument requirements refer to existing, planned and conceived instruments at W.M. Keck Observatory. Notably, the existing OSIRIS near-IR sensitive, integral field spectrograph can be used for some science cases. Other science cases require the planned, next generation LIGER, near-IR sensitive integral field spectrograph that is currently in development. Although existing and planned instruments observe in the near IR wavebands, there is great scientific need and potential for extending observations into the visible waveband. Requirements for conceived visible waveband observations are included where appropriate in the STM. Such instrumentation would accomplish ORCAS science objectives and contribute an important durable asset that will enhance U.S. astronomy beyond the ORCAS mission lifetime.

Table 2 Active Galactic Nuclei STM(a)

Signature Science Case	Science Objective	Physical Parameters	Observables	Instrument Requirements	Projected Performance	Mission Reqs	Why ORCAS?
Search for Dual & Triple AGN in Mergers	Use EHT-obtained estimate the mass of black hole M87 and test for the presence of a companion black hole at some point in its history. Analyze the stellar dynamics close to the black hole. Test prediction of cusp in stellar distribution (Bahcall & Wolfe 1976) (stellar cusp, which has never been observed)	Measure the velocity profile of stars near the central AGN, for comparison with theoretical models of the central region of the galaxy kinematics	CO Band head at 2.3μm	(Existing) OSIRIS Integral Field Spectrograph; IR waveband sensitive (1-2.5 micron); spectral resolution: R=3800; spatial scale: 20-100 mas/spaxel; FOV: 3.2" x 6.4" (Kn5 Filter)	One Science target (M87); R=3800; 10-20 hours integration time; Strehl ratio $>$ 0.50 (WAG, with ORCAS laser. Strehl $\approx$ 0.20 with existing LGS); SNR=50 / resolution element (100 km/s spectral, 0.09" spatial; must confirm for Keck at 2.3μm)	One Science Target (M87); R $>$ 3000; integration time 10-20 hours; Strehl $>$ 0.50 (WAG); SNR=50 / resolution element (100 km/s) spectral, 0.09" spatial; must confirm for Keck at 2.3μm)	Existing measurements with 8-10m class telescopes and AO are insufficient to remove the AGN light which dominates the light from the innermost stars
Study Outflows and star formation in AGN host galaxies	Measure acceleration of individual stars near the black hole M87* (first observation for an extragalactic source)	Individual velocity of brightest stars; traced over time using multi-epoch observations. Stars are detected spectrally via their large doppler shift due to close-in orbit near the black hole.	CO band head at 2.3μm.	(Planned) LIGER Integral Field Spectrograph; NIR waveband sensitive (0.84 - 2.4 micron); R=4000,8000; spatial scale: 14-150 mas/spaxel; FOV: 3.9" x 3.9" (lenslets)	One Science target (M87) with repeated observations; R=8000; FOV 3.9" x 3.9" (lenslets); Integration Time $\leq$ 10 hours; Strehl Ratio $>$ 0.50 (WAG, with ORCAS Laser); 1 observation per year.	One Science Target (M87) with repeated observations (1 obs per year); R $>$ 10,000 (WAG); FOV $>$ 1" x 1"; pixel size $<$ 0.03"; integration time $<$ 10 hours; Strehl $>$ 0.50 (WAG)	Existing measurements with 8-10m class telescopes and AO are insufficient to remove the AGN light which dominates the light from the innermost stars
Search for Intermediate Mass Black Holes in nearby globular clusters and dwarf galaxies	Indentify and measure mass estimate of intermediate mass black holes in globular clusters ($\sim$ 6 GCs visible from WMKO, esp M15)	Velocities of individual stars (with $\sim$ 1 km/s accuracy = 20 km/s spectral resolution)	Ca Triplet at 0.8μm.	(Planned) LIGER Integral Field Spectrograph; NIR waveband sensitive (0.84 - 2.4 micron); R=4000,8000; spatial scale: 14-150 mas/spaxel; FOV: 3.9" x 3.9" (lenslets)	$\sim$6 Science Targets visible from WMKO; spectral resolution R = 8,000; pixel size: 0.05"; FOV: 3.9" x 3.9"; integration time: $\sim$hours; Strehl $>$ 0.20 (WAG)	$\sim$6 Science Targets visible from WMKO; spectral resolution R $>$ 10,000 (WAG); pixel size $<$ 0.05"; FOV $>$ 2" x 2"; integration time: $\sim$ hours; Strehl $>$ 0.20 (WAG)	Existing measurements with 8-10 m class telescopes have insufficient Strehl Ratio to resolve individual stars

Table 3 Active Galactic Nuclei STM(b)

Signature Science Case	Science Objective	Physical Parameters	Observables	Instrument Requirements	Projected Performance	Mission Reqs	Why ORCAS?
Search for Dual & Triple AGN Mergers	Discover & study Dual, Triple, and offset AGN at close physical separation	Measure the physical separtion, kinematics & physical environments of Dual, Triple, offset AGN in nearby galaxy mergers	[OIII] 50006.843; [FeVII] 5158A, [FeXIV] 5303A, [CaV]5309A, [FeVI]5335A, [FeVII]5720A, [FeVII]6085A*, [Fe X]6374A, [FeXI]7892A, Hydrogen recombination lines: (Hα, Hβ, Hγ) 6600, 4800, 4350, [NII]6548.05, [SII]6716.44	Spatial resolution: tens of mas can identify duals of close to "final parsec" out to a few Mpc; spatial resolution: tens of mas can identify duals with d$<$ 1kpc out to a z 2; Visible and Near-IR imaging + spectroscopy (R 4000); BPT, broad coronal line detection, molecular gas tracers, outflows, stellar kinematics (higher spectral resolution best for stellar kinematics). 3' x 3' FOV		Min of 40 minutes time on target. Observe min of 10 targets over mission lifetime.	Sky coverage + extreme AO not possible with current facilities with high strehl (e.g. MUSE). (MAVIS should change this to some degree, offering something like a factor of 10-20 better sky coverage than MUSE LTAO, but is not without its challenges. The quality of the delivered correction depends on significantly on the available NGS constellation, and can vary significantly over the FOV. For extended sources this makes any study of detailed structural properties difficult)
Search for Intermediate Mass Black Holes in nearby globular clusters and dwarf Galaxies	Discover intermediate mass black holes in nearby dwarf galaxies	High sensitivity spectroscopy of local volume legacy survey galaxies		Sensitive near-diffraction limited imaging spectroscopy is crucial to probe the smallest pair separations, detect signatures of accretion, and make progress in this field			Detecting IMBHs through resolved kinematics is currently unfreasible since the sphere of influence of even a $10^5 M_\odot$ at 10 Mpc is only $\sim$ 0.01". High Spatial resolution spectroscopy is crucial in order to push the frontier down into a regime in black hole mass never before been discovered. Diffraction limited high sensitivity spectroscopy with future ELTs will enable dynamical searches for IMBHs down to $10^4 M_\odot$ out to 5 Mpc, science that cannot be achieved through JWST. Current AO capabilities will not be able to carry out this science. Of the 258 galaxies in the Local Volume Legacy Survey, a complete survey of nearby galaxies out to 11Mpc (Lee et al. 2007), not one has a bright guide star within 45' with Magnitude within the limits for use with LGS AO.
Study Outflows & Star Formation in AGN Host Galaxies	Characterize inflows & outflows at parsec scales in local Seyfert galaxies as test of dynamical torus models; Mbh modeling via gas &/or stellar dynamical modeling.	Measure the kinematics of stellar component & multiple gas phases undergoing rotation, inflow &/or outflow in the nucleus regions of local AGN.	Several emission lines throughout visible and NIR, molecular gas tracers in NIR, stellar absorption lines in visible and NIR.	Sensitive near-diffraction limited imaging spectroscopy in the NIR & visible is crucial to probe the gas & stellar dynamics on the smallest spatial scales to make progress in this field. A spatial scale of tens of mas is necessary in order to reach scales of a few parsecs out to a distance of 60Mpc. A spectral resolution of R $>$ 3000 will enable kinematic studies of inflow & outflows with both molecular & ionized gas tracers, stellar kinematics, & BPT studies. Key spectral features require minimal λ coverage of 0.5-2.4μm.			High spatial resolution spectroscopy is crucial in order to trace the kinematics of the gas & stars within the central 100pc of local Seyfert galaxies to characterize gas dynamics (inflows outflows) & constrain black hole masses. Diffraction limited high sensitivity spectroscopy will bridge the gap in spatial resolution between ALMA studies of the cold gas phases currently limited to scales of 10-100pc. using available NIR & visible tracers of these gas phases, as well as the stars, will enable meaningful comparison with current AGN inflow & outflow models, as well as calibration of multiple direct techniques for constraining black hole mass (e.g. gas & stellar dynamical modeling, reverberation mapping)

3.2 Exploring Dark Energy with Supernovae

Table 4 Supernovae STM

Signature Science Case	Science Objective	Physical Parameters	Observables	Instrument Requirements	Projected Performance	Mission Reqs	Why ORCAS?
Constrain the nature of Dark Energy	Enable discrimination between time-varying dark energy and a cosmological constant by limiting systematic errors on the standardized luminosities of Type Ia supernova from redshifts ranging out to redshift 1.7	Supernova type, and for those that are Type Ia, S/N and spectral resolution adequate to determine the SN location in the 3D Twins Embedding space	100 Type Ia supernova photometric spectra taken within 3 restframe days of maximum light, spanning a restframe wavelength range of 0.33-0.75 micron. Long term goal would be such spectra for 1000	AO-fed integral field spectrograph resolution $R > 100$. Simultaneous wavelength range of 0.5-2.3 microns. Nyquist sampling of Keck 10m Airy disk. Mag AB 20-26 SNR > 75 integrated over supernova spectrum Redshift coverage of $0.5 <$ redshift < 1.7	Twins Embedding measures distances to 3.5%. 100 supernova will test mean to 0.35% (k=1). Dependence on host galaxy mass will be measured to 1% (k=1)	Must accomodate target of opportunity with 5 day lead time. From external sources, SN position will be known with $\pm$ 3 degrees several weeks in advance, and known to $<$ 1" by 5 days in advance. Observation with Keck AO system and a simultaneous visible+NIR spectrograph, lasting up to 4 hrs. Baselined target fields are equatorial (COSMOS and XMM-LSS fields)	ORCAS AO with an approximate spectrograph can rival JWST and surpass NGRST for obtaining spectra of Type Ia supernova found by NGRST and LSST. The large Keck aperture collects more photons and has a smaller Airy disk, while the high strehl of ORCAS + AO packs most of the light into that disk. Indeed, the Airy disk is so small that the background sky and host galaxy light are strongly suppressed relative to the SN. That is, the usable signal goes up, and the background noise plummets.

ORCAS will enable spectroscopy of high redshift NGRST and LSST (Rubin) supernovae from the ground. ORCAS offers high Strehl in both the visible and NIR, leading to a compact PSF for these point sources. This suppresses the sky background and host-galaxy noise within the noise-equivalent area of the PSF to below levels attained in space. That is, while AO will not resolve the primary targets, it will make them observable from the ground with a sensitivity that competes with or exceeds existing and planned capabilities in space. This will allow spectroscopy that otherwise could not be practically achieved.

High redshift SNe Ia are especially attractive targets for ORCAS because there are enough targets within range of the ORCAS orbit maneuvers, with minimal fuel consumption. Deep SN searches take place in a small number of selected regions of several square degrees each. For example, LSST will observe its Deep Drilling Fields, each with a 7 sq. deg. footprint, with a cadence designed to find and follow SNe and other transients. Two of these, the COSMOS and XMM-LSS fields, are equatorial and readily observable at low airmass with Keck. In addition, the ORCAS orbits provide maximum observing time for equatorial fields. NGRST will also have deep fields, and there may be one observable from Keck. These will be the premier sources of transients over the coming decade. Target locations will be known days in advance for most SNe, and due to time-dilation, for many other transients of opportunity. Each field will generate ~ 4 new good targets near maximum light per night; the most suitable for each ORCAS orbit would be chosen from among these.

Exposure times are estimated to be 1-2 hrs per SN. This is well below the $\sim$ 4 hr observing window for the COSMOS and XMM-LSS fields as seen from Keck.

Assuming only one SN per night, these short exposures would require using only a fraction of a night on Keck. If there were other spectroscopic targets (e.g., field galaxies of interest or another SN), more of the full ~ 4 hr visibility window might be usable.

Assuming one ORCAS pass every 5 nights, one SN per pass, and rough 6 months of visibility, roughly 35 SNe Ia could be observed per year. This would use 45-90 hours of Keck time per year,

which is within the range we usually obtainable even now. Over the 3 year ORCAS lifetime this would yield a total of ~ 100 SNe Ia with 3% distances.

Newer techniques using spectroscopy are able to measure SN Ia distances to 3% using only a single spectrum taken at maximum light. Measurements of lightcurves must include points that are $\sim 10\times$ fainter than peak, requiring exposures $\sim 100\times$ longer, for the sky-limited case. Thus, this new technique can easily out-perform the lightcurve-based technique on a per-SN basis. But potentially more important, this technique leaves much less variation between SNe Ia, which is expected to significantly reduce the chance for bias to creep into the measurements. Since its statistical weight is 3-4$\times$ better, and the systematics are smaller, the spectroscopic standardization technique would need only ~ 1000 SNe Ia to match or exceed LSST or NGRST light curve analyses.

The need for spectroscopy is widely recognized among SN cosmologists. Implementation of a cost cap on NGRST precluded the 100M USD needed for an on-board integral field spectrograph. NGRST will have a slitless prism, but it will have only moderate sensitivity since each pixel collects the full zodiacal light spectrum over the bandpass. AO-assisted spectroscopy of NGRST supernovae would be almost as good (possibly better at some wavelengths) if sufficient numbers could be observed in this way.

Instrumentation for High-Strehl AO at Keck: There is no analogue to the multiplex of LSST or NGRST for SN spectroscopy (even for the Dark Energy Spectroscopic Instrument (DESI) or the Subaru Prime Focus Spectrograph (PFS) the multiplex is very low for SNe Ia at maximum); spectroscopy must be done one object at a time. But this means that SNe Ia spectroscopy can benefit greatly with high-Strehl AO. Fast spectroscopy can benefit a wide range of other faint point sources. Ideally the entire visible plus non-thermal IR would be observable in one shot since SNe and other transients will occur at a wide range of redshifts and will have key/interesting features at a number of restframe wavelengths. One shot coverage is also significantly more efficient and suffers no calibration discontinuities. This would require a prism (low resolution) or several channels (one for each octave in wavelength). There are a number of reasons for an AO spectrograph to have an integral field unit (IFU), observing spectra of many pixels in a contiguous field simultaneously. An IFU enables spectrophotometry, and the high contrast with the host galaxy eases the need for a second "final reference" observation for subtracting host-galaxy light from the original SN spectrum, eases acquisition overhead and guiding-instrument cross-stability requirements, and broadens the science case to include compact resolvable sources.

Presently on Keck LRIS is the workhorse visible spectrograph for supernovae and other transients. It is a slit spectrograph/imager that spans the full visible window with two spectrograph channels. The scales at the slit and detector are designed for natural seeing. The narrowest slit is 0.7 arcsec and the scale at the detector is 0.135 arcsec/pixel. The KCWI integral field spectrograph, once the red-arm upgrade is completed, would also span the full visible window with an IFU. The finest slice width is 0.35 arcsec and the scale at the detector is 0.15 arcsec/pixel. In the infrared the only instrument able to cover the full NIR is NIRES. (OSIRIS, MOSFIRE, NIRC2 and NIRSPEC cover only a fraction of the NIR in one setting, so have limited value for transient work.) The NIRES slit width is 0.55 arcsec and the scale at the detector is 0.15 arcsec/pixel.

Currently at Keck, AO can feed only NIRSC, OSIRIS and NIRSPEC, making the set of instruments suitable for AO and for transients disjoint. This is because most transient work has concentrated on visible wavelengths, where heretofore AO Strehl ratios have been too low to offer a benefit. As an example, the I-band sky is $\sim 15\times$ brighter from the ground versus space and the more compact PSF of HST or NGRST decreases the sky under the PSF by another $\sim 50\times$ relative to ground-based seeing. For a source dominated by sky noise on HST or NGRST, and for the case of natural seeing,

the larger aperture of Keck wins back about $15\times$, still leaving Keck $\sim 50\times$ behind HST or NGRST given similar instrumentation.

However, high-Strehl AO in the visible would be a game changer. It would lead to a compact PSF with most of the light in the core, leading to much higher S/N. But the large difference in spatial scale, and the desire to cover the visible and NIR all at once, would require new instrumentation. The appropriate instrumentation would be an integral field spectrograph spanning a wavelength range of roughly 0.5 -– 1.7 microns in a single shot. Spectral resolution in the range 100–500 is sufficient; higher resolution is fine as long as the full wavelength range is covered at once and the S/N summed over a 1 nm bin remains high across all wavelengths. A field of roughly 1×1 arcsec or larger would enable characterization and accurate subtraction of the SN host galaxy. Currently Keck lacks a suitable instrument. SNAP/JDEM built and tested a compact visible-NIR, one-shot IFU spectrograph; a design for a similar instrument was also produced for NGRST. Such designs could be adapted to Keck AO quite readily. Additional discussion on the type of Keck instrument we would like is provided in § 7.2.1.

High Strehl is required in order to concentrate as much light as possible into the Airy disk. Once most of the light is concentrated within a radius of $\sim$0.02 arcsec, there are no additional requirements on, e.g., contrast.

3.3 Flux Calibration

As discussed in § 4.3.2, the conceptual design for an ORCAS flux calibration module is still being studied. But essentially the light exiting the ORCAS flux calibration light source would be monitored by one or more SI-traceable detectors. A light concentrator may be needed to project sufficient light from ORCAS to receiving telescopes. A wheel might be needed to swap different detectors into a fixed exit beam location for monitoring the effects of outgassing. Shutters and careful baffling will be required.

Initially ORCAS should be used to recalibrate the existing CALSPEC stars, since they have been in heavy use for several decades. A list of their coordinates is available at **STScI link**. LSST and NGRST will require some additional faint stars since their detectors will saturate for the brightest 2/3 of CALSPEC stars.

The transfer from ORCAS to standard stars can be accomplished at visible wavelengths using the SuperNova Integral Field Spectrograph (SNIFS) on the UH88 telescope on Maunakea. This telescope is equipped with the SNIFS CALbration Apparatus (SCALA) projector system, allowing an intercomparison of the ORCAS, projector, and WD-based CALSPEC flux calibration systems. Transfer would also be possible using the LSST Auxiliary Telescope (AuxTel) slitless prism spectrograph. It would even be possible for these two telescopes to observe ORCAS simultaneously for some configurations if the exit beam is wide enough. Intercomparison between artificial star and projector systems, and between telescopes, can be invaluable for finding issues that can crop up when doing precision flux calibration and for establishing an external flux calibration covariance matrix.

Narrow-field instruments can only usefully observe ORCAS when its angular rate on the sky, ω, is low enough that ORCAS can be tracked with closed-loop guiding ($\omega < 0.1$ arcsec/sec). Some instruments could obtain useful observations running the telescope with open-loop tracking ($0.1 < \omega < 2$ arcsec/sec). For wide-field imagers, ORCAS could be observed as a streak across the field ($\omega > 2$ arcsec/sec). An example of the angular rate of ORCAS for a 5-day, equatorial HEO is shown in Figure 53 in Appendix B, with the range of rates for different tracking regimes shaded.

For a HEO orbit, ORCAS is moving slowly enough to be observed for several hours each apogee, and at several other periods of very slow angular motion, with narrow-field instruments (e.g., SNIFS or HST+STIS). For the purpose of transferring SI calibration to standard stars via ORCAS, ground-based observation for at least 20 astrostationary opportunities would be required in order to obtain a robust average over atmospheric seeing and extinction. For instance, SNIFS would observe ORCAS and a dozen or more standard stars in one night, and would try to do this at least 6 times spread over the course of a year in order to knit together all the standard stars across right ascension and beat down statistical errors. Non-photometric nights would interfere with this effort at a rate of roughly 50% (only knowable after the fact – i.e., at the end of the night, in half of those cases). With HST, ORCAS could be observed near apogee, with preceding or subsequent orbits used to observe standard stars.

Exposure Times: Exposure times would be 10s of minutes, depending on the brightness of the ORCAS calibration light (a combination of ORCAS distance and its light output) and the number of wavelengths observed. It might prove useful to chop several times between ORCAS and the star to be calibrated, but ORCAS could move between these chops. ORCAS could streak across the field of a wide-field telescope. In this case the exposure time per pixel would equal the pixel scale divided by the angular rate of motion. Consulting Figure 53, this could be as short as 1 msec when ORCAS is at perigee.

Note that only for closed-loop tracking mode would the motion of ORCAS be potentially slow enough for use with the Keck AO system. Therefore, flux calibration will be in competition for viewing time only during the astro-stationary periods, i.e, a few hours for each of three times per orbit.

Requirements:

Star-like: ORCAS should appear as an artificial star to ground- and space-based telescopes, at least during the astro-stationary portion of its orbit. This requires a minimum apogee distance of ~ 4000 km from a ground-based telescope and ~ 27000 km from a space telescope. Otherwise the telescope will need to be refocused between viewing of ORCAS and science targets or standards, or ORCAS will appear out of focus. Either of these might be an issue for measuring ORCAS and standard stars self-consistently. The baseline ORCAS orbit meets this requirement.

SI-traceability: The relative flux at several different wavelengths emitted by ORCAS in the direction towards a receiving telescope should be knowable to better than 0.4%, with a goal of 0.2%. This typically would be done by monitoring the light output on-board using a NIST-traceable photodiode and/or an electrical substitution radiometer, ensuring that the exit beam profile is known at each wavelength (preferably being the same at all wavelengths), and ensuring the distance is known to (much) better than 0.05%.

Exit beam profile: The primary requirement is that the exit beam of the flux calibration unit be sufficiently smooth and stable such that the ratios of fluxes between wavelengths be essentially the same at the entrance pupil of the receiving telescope as at the SI-traceable flux monitor(s) on-board ORCAS.

Depending on the final design, the exit beam might have a Lambertian spread from the direct exit port of an integrating sphere, or the much narrower (1-10 mrad) beam exiting a light concentrator, or an even narrower beam from a focused device (arcseconds, tens of microrad). The beam profile can be studied by monitoring with the receiving telescope as the spacecraft orientation is adjusted in pitch and yaw. This may be time-consuming, so it is desirable for any non-smoothness in the beam to be stable.

In normal operation, the portion of the beam intercepted by the flux calibration monitor will not reach the receiving telescope and so cannot be studied in this way. Obtaining this portion of the beam profile may rely on pre-flight lab measurements and/or the use of an x-y scanning stage on ORCAS.

The combination of chromatic beam non-uniformity and spacecraft orientation knowledge will need to be included in the uncertainty budget; a beam that is achromatic or chromatically smooth will allow relaxed knowledge of the spacecraft orientation.

We have not placed an independent constraint on the beam profile. Rather, all differences in the wavelength-relative fluxes, when combined with other uncertainties, should be below 0.4%. This issue is discussed further in Appendix B.7.

Wavelengths: The ORCAS source should emit light at isolated wavelengths so that calibration versus wavelength can be determined. A bare minimum of three wavelengths spread fairly evenly across the 0.35–2.3 μm range is required in order to compare the calibration slope from ORCAS with calibration from calibrated projector systems and WD stellar atmospheres. A more robust calibration would provide ORCAS output at the central wavelengths of the four filters used by LSST and the six filters used by NGRST. These overlap, leading to the desire to cover eight wavelengths. The wavelengths, including a Table 33 of those we considered, is in Appendix B.2.

Some NASA missions could also benefit from UV calibration for purposes other than the supernova cosmology science case. These wavelengths are not accessible from the ground, requiring direct observation from NASA facilities. For instance, if orbital configurations allow HST STIS to observe ORCAS, it could transfer the UV calibration from ORCAS to spectrophotometric standard stars, including those observed by past missions. Note that the nominal 5-day ORCAS orbit would not be visible to JWST or Roman, due to Sun angle constraints.

For spectrographs observing ORCAS, all wavelengths could in principle be observed at once in a single exposure. For imagers like LSST, it would be best to only emit the wavelength matched to the LSST filter being used at the time. The overall flux level, i.e., the achromatic component set by geometric factors such as the exit beam solid angle or the distance from the telescope to ORCAS need be known to only a few percent for most purposes, but better than 1% knowledge may be useful for some science applications.

Light sources: Potential light sources are lasers, laser diodes, LEDs or a properly crafted continuum source. A laser source can have speckles in its beam profile, but this can be managed if anticipated. A smooth continuum source would need to be calibrated with an on-board spectrograph, adding complexity. Observation of this source would be primarily useful to telescopes equipped with spectrographs. A continuum source with sufficient output and spectral smoothness at all wavelengths will prove difficult, so monochromatic sources are more likely to be used. Note that the spectrum of the Sun is not a sufficiently smooth source. We intend the brightnesses to be tunable.

Monitoring detectors: Monitoring detectors might be photodiodes, an electrical substitution radiometer, light traps, and/or a calibrated pyroelectric device. These will require lab testing to check for non-linearity, hysteresis, etc. These will then require NIST-traceability, preferably performed directly at NIST. More discussion can be found in Appendix B.5.

Satellite background removal: ORCAS will be illuminated by the Sun and Earth and Moon, so this illumination will need to be subtracted. This requires a pair of observations with the light turned on then off within a period of time short enough such that the background subtraction error is well below 0.4% of the light brightness. In streaking mode, the light could be turned on and off along the streak for this purpose. For stability, it may be preferable to use a shutter rather than change the power to the light source. This requires detailed modeling, but an initial examination of this issues is provided in Appendix B.6

Observed brightnesses: The appropriate brightness has a wide range. The upper limit would be that ORCAS not saturate SNIFS or AuxTel in a 10 sec exposure; this leads to an upper limit of roughly 10^5 photons/m^2/sec in a monochromatic line. A minimum flux would be roughly 10 photons/m^2/sec in a monochromatic line., i.e., for 8-m class telescopes. These brightness ranges would need to be satisfied for whatever distances allow ORCAS to appear astro-stationary for at least $\sim$ 10 min. Note that for streaking mode the effective exposures are a few msec per pixel, so photon rates up to $\sim 10^7$ photons/m^2/sec could be tolerated.

Emitted brightnesses: ORCAS will span a large range of distances from potential telescopes, and different telescopes can accommodate different flux ranges (see above) and observe ORCAS for different rates of motion on the sky. In addition, for sufficient emitted power, the use of an electrical substitution radiometer – capable of providing more fundamental calibration – can be considered. A preliminary engineering study is required to find the ranges of emitted power required to match the combined observed brightness and distances parameters. Further discussion can be found in Appendix B.3.

Downstream Instrumentation: ORCAS would be observed with existing ground-based instruments and probably HST. Since ORCAS will have periods when it is astro-stationary over Maunakea, SNIFS could observe ORCAS and then transfer the ORCAS calibration to standard stars. These stars could then be observed with NGRST and LSST. This would cover visible wavelengths only. Since NGRST will be unable to observe ORCAS in HEO directly, in the NIR other instrumentation would be needed to observe ORCAS and transfer that calibration to standard stars. It may be necessary to construct such an instrument; it would not be necessary to site that instrument at Keck Observatory.

Some non-requirements: The primary flux calibration goal of ORCAS is to provide SI-traceable flux calibration. There is no requirement to enable measurements of pixel-to-pixel flat fields, crosstalk, non-linearity, reciprocity failure, persistence, charge transfer inefficiency, ghosting, etc. Correcting and modeling of these effects is done by instrument teams using lab and on-sky measurements with their specific instruments. This is beyond the scope of ORCAS.

It may be the case that ORCAS can in some way help with some of these issues incidental to its primary mission. An example would be testing in-situ linearity by exploiting the precise knowledge ORCAS will have of its flux over a large range in observed brightness (i.e., versus observing distance or via internal adjustment).

Table 5 Flux Calibration STM (a)

Signature Science Case	Science Objective	Physical Parameters	Observables	Instrument Requirements	Projected Performance	Mission Reqs	Why ORCAS?
Provide flux calibration to advance cosmology and astrophysics	Wavelength-relative (color) flux calibration to 0.4%, with a goal of 0.2%, for instance as required for cosmology with Type Ia supernovae. Overall scale to 1%, for instance as required to determine stellar parameters when combined with GAIA parallax.	Star-like light source with brightness traceable to SI system	This source would either be observed directly with dark energy instruments (e.g., Vera Rubin Observatory, SNIFS). This source would be observed and used to transfer calibration to standard stars.	Quasi-monochromatic light at a minimum of 3 wavelengths and a goal of 8 wavelengths spaced fiarly evenly over the range 0.35-2.3 microns (nominally in the ugriz and NGRST bands). The output should be monitored by an SI-calibrated detector (photodiode and/or light trap and/or electrical substitution radiometer). More than one monitoring detector is desired. Detector SI-traceability changes due to outgassing should be controlled and monitored. Observed brightness on the ground should be equivalent to a star of AB 8-18 mag. Exit beam illumination profile should achromatic to better than 0.4% at any angle, and uniform to better than 1%. Requires ability to subtract sunlight and earthlight reflected off satellite in the direction of the beam. An on-board calibrated broadband source would enable some operation efficiencies for some use cases.	The overall slope of the flux uncertainty will be less than 0.4% over this wavelength range. The relative RMS will be less than 0.3% per 0.1 micron wavelength interval. The absolute scale (achromatic factor) will be established to better than 5%, with 1% desired.	Satellite must point the flux calibration beam towards the receiving telescope while minimizing reflected sunlight and the variation in reflected sunlight. When using spectrographs on the receiving telescope, the flux calibration should be able to cycle through all wavelengths at a rate up to 0.1 Hz. The satellite and ground station will need to coordinate exposure start/stop times, wavelength selection, background observations; this likely will need communication with a resolution around 0.1 Hz. Observations will occur at sky locations set by other science programs. Access to flux calibration unit for closed loop tracking ($\omega <$ 0.1 arcsec/s) at least once per month to knit together standard star system and have enough clear nights for ground based telescopes.	ORCAS provides a star-like source about the atmosphere using the full telescope aperture without the need for refocusing the view telescope; this best mimics the stars being calibrated. Existing systems on the ground consist of projectors (SCALA, VRO's CBP) or light sources at a distance overland (StarDice, NistStars). Projectors create "artificial planets" not stars, and subsample the telescope aperture, whereas over-land light sources require refocusing and have high atmospheric extinction. Moreover, ORCAS could provide UV calibration, and could calibrate HST directly, which is not possible from the ground. Finally, cosmology analyses require an external error estimate, so more than one method of calibration would be ideal.

Table 6 Flux Calibration STM (b)

Signature Science Case	Science Objective	Physical Parameters	Observables	Instrument Requirements	Projected Performance	Mission Reqs	Why ORCAS?
Measuring the absolute fluxes of exoplanet host stars	Host star characterization: with GAIA, the absolute flux calibration is now the limiting uncertainty term in determining host stellar radii, which have implications for planet radii, HZ location, and planet irradiance	Stellar absolute flux; star-like light sources with brightness traceable to the SI system	Multi-band imaging in vis (e.g. Vera Rubin Observatory) and NIR, wide field of view (>5 arc-minutes up to the order of a degree]	Ground instrument: Standard Multi-band CCD and NIR imaging cameras, deep well (16 bit or deeper); low read-noise and dark-current; preferably minmal field curvature; SNR>1000 photon+detector noise; typical stellar brightness we are calibrating against would be V 10 mag; Payload Instrument: The output should be monitored by an SI-calibrated detector (photodiode and/or light trap and/or electrical substitution radiometer). Quasi-monochromatic light at a minimum of 4 wavelengths spaced fairly evenly over the range 0.35 – 2.3 micron. More than one monitoring detector is desired. Detector SI-tracability changes due to outgassing should be controlled and monitored. Observed brightnesses on the ground should be equivalent to a star of AB 8–18 magnitude. Exit beam illumination profile should be achromatic to better than 0.4% at any angle, and uniform to better than 1%. Requires ability to subtract sunlight and earthlight reflected off satellite in the direction of the beam. An on-board calibrated broadband source would enable some operation efficiencies for some use cases, particularly spectroscopy.	RMS of 0.4% in absolute flux calibration in each wavelength range.	$> 10^6$ photo-electrons per exposure across multiple sub-exposures; tracking times <1 hr. Satellite must point the flux calibration beam towards the receiving telescope while minimizing reflected sunlight and the variation in reflected sunlight. When using spectrographs on the receiving telescope, the flux calibration should be able to cycle through all wavelengths at a rate up to 0.1 Hz. The satellite and ground station will need to coordinate exposure start/stop times, wavelength selection, background observations; this likely will need communication with a resolution around 0.1 Hz. Observations will occur at sky locations set by other science programs. Access to flux calibration unit for closed loop tracking ($w <$ 0.1 arcsec/s) at least once per month to knit together standard star system and have enough clear nights for ground-based telescopes.	Ground- based absolute flux calibration limited to 1% accuracy after 40+ years of CCDs on telescopes, and is tied to synthetic SED models of white dwarfs. ORCAS provides a star-like source above the atmosphere using the full telescope aperture without the need for refocusing the view telescope; this best mimics the stars being calibrated. Existing systems on the ground consist of projectors (SCALA, VRO's CBP) or light sources at a distance overland (StarDice, NistStars). Projectors create "artificial planets" not stars, and subsample the telescope aperture, whereas over-land light sources require refocusing and have high atmospheric extinction.

3.4 High Redshift Universe

Imaging with low R spectroscopy, since sources are faint.

Summary of Science Goals and ORCAS Requirements

Here we summarize the ORCAS science goals on faint SF-clumps and their implications for the ORCAS Requirements Matrix as following. Note that Science Goal 1+2 may be achieved from other random ORCAS imaging of very faint foreground targets, such as solar system KBO's:

Science Goal 1: Constrain the number densities of the faintest SF-clumps at z$\simeq$1–7. ORCAS will address how galaxies assemble from smaller clumps to stable disks by measuring ages, metallicities, and gradients of clumps within galaxies.

Requirements 1:

• Deep images to AB$\lesssim$31 mag for point sources in a few hours, necessary to sample SF-clumps with a surface density of 5.0×10^6 per square degree.

• An $\gtrsim5\times5''$ FOV (that includes IFU capabilities), which at 5.0×10^6 objects per square degree will contain $\sim$10 faint SF clumps. This is a minimum needed to do *relative* (sub-)m.a.s.-astrometry, depending on the S/R-ratio achieved, and anticipating that most objects will be compact enough to auto-correlate their images to get the best possible relative astrometric positions.

• Wavelength coverage ideally at 0.3–2.2 μm, but at minimum 0.5–1.2 μm. Standard ugriz+YJHK filter set with potential modifications suggested below and in Fig. 20, to get photometric redshift estimates before IFU spectroscopy is attempted. IFU follow-up on selected targets will be needed.

• At minimum 10 ORCAS fields would be needed to start a census for $\sim$100 of these faint SF clumps. A long term goal should be to get at least 100 ORCAS fields to get a more accurate assessment of the redshift, luminosity and size distribution from $\sim$1000 SF clumps.

Science Goal 2: Constrain the physical sizes of the faintest SF-clumps at z$\simeq$1–7. Anticipated typical angular sizes at z$\simeq$1–7 are $r_{\rm e}\simeq$1–80 m.a.s. to AB$\lesssim$31 mag. About half of these SF clumps will be below the ORCAS diffraction limit, and the other half will be slightly resolved, but still mostly above the ORCAS surface brightness (SB) limits.

Requirements 2:

• Spatial resolution of $\sim0\farcs01$–$0\farcs02$ FWHM, with good Strehl ratios.

• If SB-sensitivity for the larger SF-clumps becomes an issue, ORCAS should consider some "notch-filters", as shown in Fig. 20.

Science Goal 3: Follow up with ORCAS on caustic transits of individual stars in SF clumps at z$\gtrsim$1–2 that have been detected with HST, and those that may be detected with JWST at z$\simeq$6–17 at extreme magnifications ($\mu\gtrsim10^3$–10^5) for the first stars and their stellar mass black hole accretion disks.

Requirements 3:

• Deep images to AB$\lesssim$31 mag for point sources. Unmagnified magnitudes (*i.e.*, their observed lensed fluxes after dividing by their lensing magnification) may be as faint as AB$\lesssim$35–36 mag.

• Spatial resolution of $\sim0\farcs01$–$0\farcs02$ FWHM. Unlensed sizes may be smaller than 1–10 m.a.s. when searching with ORCAS around the critical curves of the best lensing galaxy clusters imaged with HST and JWST.

• *Relative* (sub-)m.a.s.-astrometry will be needed to monitor potential parity changes of lensed sources when they go across a caustic, and therefore may change shape or apparent position at high redshift (Note: this is not a true proper

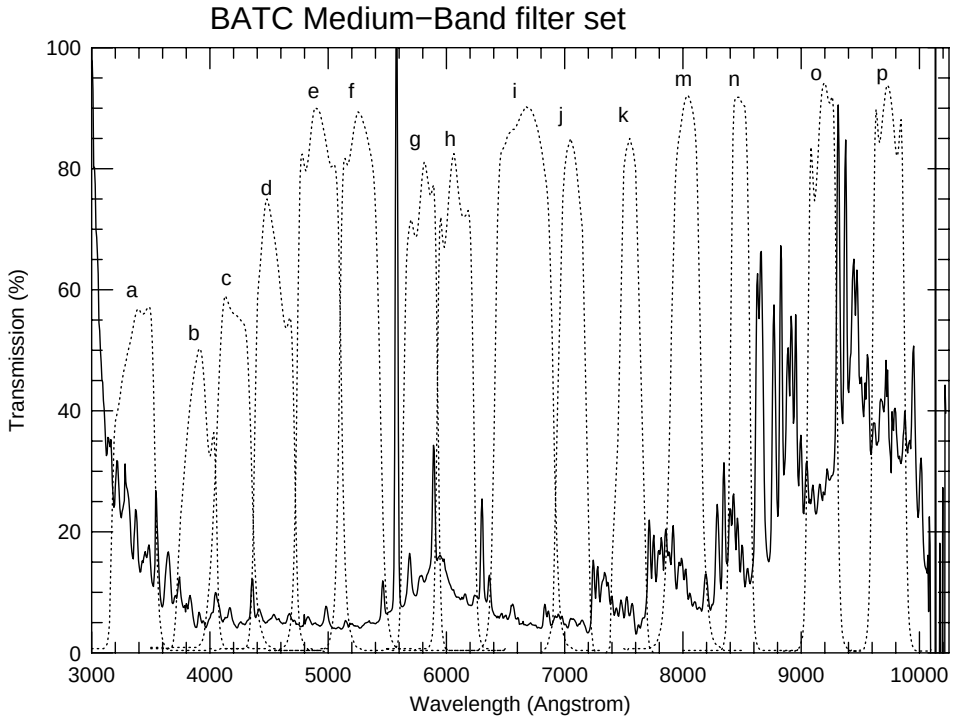

Fig 20 An example of medium-band filters that avoid most of the brightest night-skylines affecting ground-based observations (119). ORCAS will likely mostly target very faint objects, possibly in a standard broad-band filter set like ugriz+YJHK. More than half of these objects may be slightly resolved at ORCAS' spatial resolution of 0.″01–0.″02 FWHM (Fig.16). Hence, to maximize the SB-sensitivity for the very faintest slightly resolved objects, ORCAS could consider replacing some of the broad-band filters that include the brightest night-sky lines with "notch-filters" that essentially suppress these lines. E.g., one could replace the V-band or F606W filter with a notch-filter that consist of filter f+g or g+h here. This would permit imaging to lower SB-levels (*e.g.*, 120).

motion, but a light-path change of the lensed source in the gravitational landscape of the lensing cluster when the source goes across a caustic.

• Monitor caustic-transiting stars for decades across the (micro-)caustics to obtain a statistical census of individual stars at cosmological distances, and the microlensing stellar population in the foreground galaxy cluster ICL.

• Preimaging with HST or follow-up imaging with JWST of ORCAS targets may be needed to identify the best possible candidates for caustic transits.

Table 7 High Redshift Universe STM

Signature Science Case	Science Objective	Physical Parameters	Observables	Instrument Requirements	Projected Performance	Mission Reqs	Why ORCAS?
Constrain the Number Densities of Faintest SF-clumps at z $\sim$1-7.	Constrain the Number Densities of Faintest SF-clumps at z $\sim$1-7. (UPDATE)	Star Formation Clumps with a surface density of 5.0 x 10^6 per square degree.	λ Coverage ideally set to sim 0.3-2.2 μm, but at a minimum of 0.5-1.2 μm.	FOV: 5" x 5"; Deep Images to AB $\leq$ 31 Mag for point sources in a few hours; λ coverage of 0.3-2.2 μm; Standard ugriz + YJHK filter set with potential modifications to get photometric redshift estimates before IFU spectroscopy is attempted.		Integration time of a few hours; A minimum of 10 ORCAS fields needed to star a census for $\sim$ 100 of these faint SF clumps. Long term goal of 100 ORCAS fields	ORCAS will address how galaxies assemble from smaller clumps to stable disks by measuring clumps to stable disks by measuring ages, metallicities, and gradients of clumps within galaxies
Caustic Transits of Individual stars in SF clumps at z $\geq$ 1-2.	Follow up with ORCAS on Caustic Transits of Individual stars in SF clumps at z $\geq$ 1-2 that have been detected with HST, and those that may be detected with JWST at z $\sim$ 6-17 at extreme magnifications ($\mu > 10^3 - 10^5$) for the first stars and their stellar mass .	Monitor caustic-transiting stars for decades across the (micro-)caustics to obtain a statistical census of individual stars at cosmological distances, and the microlensing stellar population int he foreground galaxy cluster ICL.	Deep Images to AB $\leq$ 31 mag for point sources. Unmagnified magnitudes may be as faint as AB $\leq$ 35-36 mag; Caustic-transiting Stars.	Spatial resolution of $\sim$ 0.01" x 0.01" FWHM; Unlensed sizes may be smaller than 1-10 mas; sub-mas astrometry will be needed to monitor potential parity changes across a caustic; Deep Images to AB $\leq$ 31 Mag.		Preimaging with HST or follow-up imaging with JWST of ORCAS targets may be needed to identify the best possible candidates for caustic transits.	
Constrain the Physical Sizes of the faintest SF-clumps at z $\sim$ 1-7.	Constrain the Physical Sizes of the faintest SF-clumps at z $\sim$ 1-7.	Star forming Clumps	Anticipated angular sizes are $r_e \sim$ 1-80 mas to AB $\sim$ 31 mag.	Spatial resolution of $\sim$ 0.01" x 0.01" FWHM; Good Strehl ratio		About half of the SF clumps will be below the ORCAS diffraction limit, and other half will be slightly resolved, but still mostly above the ORCAS surface brightness.	

3.5 Exoplanets

ORCAS will expand the field of ground based high contrast direct imaging. In particular, ORCAS will characterize the atmospheric composition of known planets from previous RV studies and astrometry. In addition to characterization, orbital inclination, and planet radius. Previously found planets through direct imaging methods will be enhanced with high SNR. The properties of exozodiacal dust disks is still an ever-expanding field with many unanswered questions that ORCAS hopes to address. ORCAS will caculate the Zodi levels of nearby stars currently on the target list for both HabEx and LUVOIR by measuring the surface brightness of the exozodiacal dust disk. This will provide the necessary system parameters for identifying planetary signals.

Continuing with exozodiacal dust, ORCAS will uncover the planet formation process within the dust disks of young stars. This can place constraints on the time-scales involving planetary formation, can better inform models, and improve planet cooling curves.

Future surveys of M dwarf stars habitable zones will be conducted with TMT in search for sub-Jovian and super Neptune exoplanets . ORCAS can kick-start this search almost a decade earlier. This will require a high contrast imager in both NIR and Visible and the ability to locate point source and confirm proper motion with a minimum of 1 year return visit.

Many of these science goals can be summarized with similar engineering requirements. For all exoplanet science cases, the minimum required Inner Working Angle (IWA) of 100 milli-arcseconds with a contrast between 10^{-6} and 10^{-8}. Further details relating to the Exoplanet science requirements can be seen in Tables 8 and 9.

Table 8 Exoplanets STM (a)

Signature Science Case	Science Objective	Physical Parameters	Observables	Instrument Requirements	Projected Performance	Mission Reqs	Why ORCAS?
Characterizing Known Planets from RVs, Astrometry, Ground-Based Direct-Imaging, and other Techniques	Confirming the planets found by other techniques; determining the orbital inclination in the case of RV planets; determining planet radius through modeling; measuring atmospheric composition of planet; for systems already imaged from the ground, ORCAS will enable higher fidelity SNR spectra of those systems.	Point source location and brightness; Spectra of planet emission; confirming common proper motion with a minimum repeat visit 1 year later	High Contrast Imaging (NIR/VIS); moderate resolution (R<100) spectra in NIR/VIS; contrast curve as a function of angular separation	<100 mas iwa; match or exceed Keck iwa performance with KPIC/HISPEC (PI: Mawet); Exposure time requirement: case study: V=9 star; V=24-29 mag planet at SNR 10 w/ 10^{-6} to 10^{-8} contrast	80 mas iwa, 10^{-8} flux contrast	93 total, V=4-10, iwa>80 mas; known exoplanets; msini>0.1 MJup to have sufficient flux contrast for potential detection; 18 have been previously directly imaged; Few mas position stability of the beacon; ability to feedback a pointing offset from the ground-telescope to the beacon; Exposure times: >1 hr tracking/sequence for imaging, spectroscopy will take longer; mult-wavelength laser to get atmospheric chromaticity	Complements NGRST direct imaging with additional and fainter targets due to larger ground-telescope apertures; and achieved smaller iwa (<100 vs <200 mas) with Vector Vortex Coronagraph, and observations at visible wavelengths to complement NGRST NIR imaging. Depending on launch timeline, may also provide additional targets for NGRST
Understanding the Zodi Levels of Nearby Stars AND Searching for Exoplanets around HabEx / LUVOIR targets	Measure the surface brightness of Zodis for nearby stars down to some delta magnitude; Identify and Jovian planets in the HZs of these systems	Surface brightness as a function of angular separation and azimuth	High Contrast Imaging (NIR/VIS), contrast curve as a function of angular separation	<100 mas iwa; match or exceed Keck iwa performance with KPIC/HISPEC (PI: Mawet); Flux contrast requirement < 10^{-7}; Exposure time requirement: case study: what is surface brightness of a few zodis? Exposure time requirement: case study: V=6 star; V=21-26 mag planet/zodi at SNR 10 w/ 10^{-6} to 10^{-8} contrast.	80 mas iwa, 10^{-8} flux contrast	HabEx / WFIRST / LUVOIR target list V=4-10, the top prioritized targets are the deep dive 8 HabEx targets + maybe a few from the WFIRST target list; Few mas position stability of the beacon; ability to feedback a pointing offset from the ground-telescope to the beacon; Exposure times: >1 hr tracking/sequence for imaging; mult-wavelength laser to get atmospheric chromaticity	Key precursor knowledge for a future NASA flagship direct imaging mission that will optimize the yield of HabEx / LUVOIR; complements NGRST direct imaging with additional and fainter host stars due to larger ground-telescope apertures; and achieved smaller iwa (<100 vs <200 mas) with Vector Vortex Coronagraph, and observations at visible wavelengths to complement NGRST NIR imaging. Depending on launch timeline, may also provide additional targets for NGRST

Table 9 Exoplanets STM (b)

Signature Science Case	Science Objective	Physical Parameters	Observables	Instrument Requirements	Projected Performance	Mission Reqs	Why ORCAS?
Uncovering the Planet Formation Process in Disks Around Young Stars	Place constraints on planet formation time-scales, planet formation dynamical models, and planet cooling curves	Surface brightness as a function of angular separation and azimuth (aka structure, gaps, rings for disks); and locating point sources in disk	Imaging and IFS at low-resolution in the NIR and VIS reflected light, surface brightness maps	<100 mas iwa; match or exceed Keck iwa performance with KPIC/HISPEC (PI: Mawet);Exposure time requirement: case study: what is surface brightness of a few zodis? Exposure time requirement: case study: V=6-9 star; V=21-24 mag planet/zodi at SNR 10 w/ 10^{-6} contrast	80 mas iwa, 10^{-6} flux contrast	gather disk targets: Eps Eri, AU Mic, Fomalhaut; Few mas position stability of the beacon; ability to feedback a pointing offset from the ground-telescope to the beacon; Exposure times: >1 hr tracking/sequence for imaging; mult-wavelength laser to get atmospheric chromaticity	Complements NGRST direct imaging with additional and fainter targets due to larger ground-telescope apertures; and achieved smaller iwa (<100 vs <200 mas) with Vector Vortex Coronagraph, and observations at visible wavelengths to complement NGRST NIR imaging. Depending on launch timeline, may also provide additional targets for NGRST
Understanding the Occurrence Rate of Cool Sub-Jovian and Super-Neptune Exoplanets Orbiting Nearby Cool Stars and Brown Dwarfs as a precursor to TMT era of HZ M dwarf searches	Search for Neptune-mass planets outside the iwa, and in some cases, terrestrial planets such as Prox Cen c	Point source location and brightness; confirming common proper motion with a minimum repeat visit 1 year later	High Contrast Imaging (NIR/VIS), contrast curve as a function of angular separation	<100 mas iwa; match or exceed Keck iwa performance with KPIC/HISPEC (PI: Mawet); Flux contrast requirement < 10^{-7}; Exposure time requirement: case study: Barnard's Star V=10, V=25-30 planet at SNR 10 broadband detection; we are targeting planets in the $10^-6 - 10^-8$ contrast regime, which are sub-Jovian; Neptune analogs at 10^{-9} are not feasible. Note, Jovian planets around M dwarfs are expected to be rare ¡5% of M dwarfs have one; so the yield of this survey will be low	80 mas iwa, 10^{-8} flux contrast	34 targets, 1-2 visits; list of M dwarfs b/t V=4-10 mag - GAIA search, V=4-10 mag, Teff<4000, and R¡1 solar radius to get rid of giants; late M and BD targets < 10 pc: Luhman 16AB, Wolf 359, Lalande 21185, Luyten 726-8, Ross 154; Few mas position stability of the beacon; ability to feedback a pointing offset from the ground-telescope to the beacon; Exposure times: ¿1 hr tracking/sequence for imaging; mult-wavelength laser to get atmospheric chromaticity	There are only 4 M dwarfs later than M4 in spectral type brighter than V of 12, and none bright enough for NGSAO. Thus these targets are limited to LGSAO contrast curves in the NIR and visible. Only ORCAS can push the flux contrast and iwa beyond current ground-capabilities

3.6 Solar System

As described in Figure 14 (Solar system STM), ORCAS will lead to an increase of an order of magnitude in our ability to study small and faint (often icy) bodies with AO and ground-based observations. Similarly, we will be able to achieve spatial resolutions on Mars and other extended bodies rivaling orbital spacecraft. This is particularly relevant, since mapping and the characterization of the atmospheres of e.g., Mars, Jupiter and Saturn is best done employing high-resolution spectroscopy, which is often too complex/bulky for an orbiter. In that sense, observations from the ground with AO+ORCAS will permit to map the full observable disk of these planets and other extended and faint/diffuse objects in a short period of time, thanks to the large collecting area of ground-based observatories and the AO capabilities provided by ORCAS.

Table 10 Solar System STM

Signature Science Case	Science Objective	Physical Parameters	Observables	Instrument Requirements	Projected Performance	Mission Reqs	Why ORCAS?
Understand the Origins and Evolution of small bodies in the solar system.	Determine surface properties and architecture of small bodies and their systems.	Map chemical and physical properties across asteroids, comets, satellites, Pluto, and Kuiper belt objects	Map distribution of surface (composition/ice), resolve rings and/or binary/tertiary systems.	UV/Vis/NIR IFU; Medium spectral resolution (R>3000); Continuous wavelength coverage from 0.5 to 5 μm	Increase by an order of magnitude our ability to study small and faint icy bodies with AO and ground-based observations	Critical timing of bodies to resolve rings/systems. Likely follow-up observations from occultations. Mapping across larger objects need to consider time on source vs rotation rates.	Potential to resolve rings/binaries that have not been achieved with direct imaging – only through occultations.
Understand the origins and preservation of volatiles in the solar system.	Determine the volatile composition of small bodies in the outer solar system and origin of Earth's ocean.	Map heterogenous composition in the diffuse atmosphere/comae of comets/centaurs	Measure/Map volatiles: D/H ratios in water, Organic composition, Ice, CO/CO2 in multiple comets (JFCs, Oort Cloud, ISOs?) and Centaurs.	NIR imaging spectrometer - Wavelength coverage: 2.5 to 5.0 important for water, D/H, organics and ices (0.5 to 2.5 um also good for ices); Spectral resolution: >20,000; Pixel scale (mas/pix): <50 mas would be good to maximize AO advantages (25 mas range is ideal); FOV (for IFU or slit length): >10 arcsec length / IFU wide for extended sources (comets) - The larger the better; Dynamic range: 0 up to 12th mag	Increase by an order of magnitude our ability to study small and faint icy bodies with AO and ground-based observations	High-resolution spectroscopy (>20,000) and fine pixel scales (<50 mas/pixel)	Determine at unprecedent spatial resolutions jets and possible heterogenous composition and properties of icy bodies. ORCAS will provide access to fainter targets that AO cannot be done on target itself.
Satellites and Rings	Understand the processes involved in the formation of our solar system and of giant planets and their moons	Map chemical and physical properties across satellite surfaces and atmospheres.	Surface and atmosphere composition	UV/Vis/NIR IFU; Medium spectral resolution (R>3000); Continuous wavelength coverage from 0.5 to 5 μm; high spectra resolution (>25,000) for atmospheres (Io).	Observations with ORCAS will permit to image faint moons and rings with AO, image both bright and faint moons in the visible, and moons in shadow to surpass JWST in the visible.	Bright ORCAS laser (¡mag=1) to surpass scattered lightt from nearby bright giants. Modest spectral resolution for surfaces (R<3000) and high for atmospheres (R>25000)	Images in the visible would surpass HST by a factor of 4, and JWST by almost a factor of 2, which should result in superb images of moons and rings – such as resolving lava flows on Io, and image ring arcs and waves in rings.
Mars and Moons	Understand the evolution of terrestrial planets and volatiles in potentially habitable atmospheres in our Solar system. Were Phobos/Deimos captured? How did they impact the volatile reservoirs of Mars?	Map the whole disk of Mars and its composition (e.g., trace gases, isotopes) at spatial resolutions permitting to resolve detailed climatological processes. Map the surface composition, and evolution of Phobos and Deimos	Surface and atmosphere composition	NIR imaging spectrometer - Wavelength coverage: 2.5 to 5.0 important for water, D/H, organics and ices (0.5 to 2.5 um also good for ices); Spectral resolution: ¿20,000; Pixel scale (mas/pix): ¡50 mas would be good to maximize AO advantages (25 mas range is ideal); FOV (for IFU or slit length): ¿10 arcsec length / IFU wide for extended sources (comets) - The larger the better; Dynamic range: 0 up to 12th mag	Observations with ORCAS will permit to image the atmosphere of the whole visible disk of Mars in one snapshot at high-spatial resolutions, something not possible from low orbit. Broad and sensitive spectroscopy of the moons will permit detailed monitoring.	Bright ORCAS laser (¡mag=1) to surpass scattered light from nearby bright Mars. Modest spectral resolution for surfaces (R¡3000) and high for atmospheres (R¿25000)	Bright extended objects are not possible with current AO, unless there is a star or satellite within 30". LGS was attempted with Jupiter and Mars on Keck. On Jupiter the laser got swamped when getting to 5" from the limb; on Mars one got closer to planet (up to 1") before losing AO. Likely need capability for ORCAS of brighter than 3 mag
Ice Giants	Map clouds and trace gases of Uranus and Neptune; in particular during the development of large storm system and dark spots.	3D distribution of clouds/aerosols and trace gases	Map the spectral and spatial distribution of gases and clouds	UV/Vis IFU; Wavelength coverage: down to 450nm; FOV or slit length – 5".	Observations with ORCAS will permit to map the ice giants in the visible down to 450 nm at high-spatial resolutions.	Bright ORCAS laser (¡mag=1) to surpass scattered light from the ice giants. Spectral resolution similar to HIRES on keck.	Bright extended objects are not possible with current AO, unless there is a star or satellite within 30". LGS was attempted with Jupiter and Mars on Keck. On Jupiter the laser got swamped when getting to 5" from the limb; on Mars one got closer to planet (up to 1") before losing AO. Likely need capability for ORCAS of brighter than 3 mag

4 Science Implementation

Key Findings

- We establish the engineering requirement traceability matrix summarizing all major requirements for all science cases for the ORCAS mission and its major subsystems in Section 4.1.
- We share the Spacecraft designs including the mass and power budgets as outlined in Section 4.2.
- We present a High TRL design for the laser system in Section 4.3. Additionally, a preliminary recommendation for a flux calibrator design is proposed in Section 4.3.2.
- We establish the ground telescope system requirements and present the proposed upgrades to the W. M. Keck Observatory which will allow it to meet those requirements in Section 4.4. The current and future Keck instruments are also described.
- Section 4.5 discusses how the ground station and spacecraft will work together to achieve the observation requirements for ORCAS.

This section establishes engineering requirements that will meet the scientific goals of the mission and shows how the spacecraft, payloads, and ground system can meet these requirements. In Section 4.1, we establish the engineering requirements for each of the mission sub-systems and trace them to the original scientific requirements. Section 4.2 and 4.3 shows the spacecraft, laser, and flux calibrator design and how each one meets these engineering requirements and enables the science goals. In Section 4.4, the current state of the telescope's instrument suites and adaptive optics are summarized, and we discuss the requirements to meet the science goals and the proposed upgrades. Finally, we present the data approach and ground system in Section 4.5.

4.1 Engineering Requirements and Mission Traceability

Key Findings

- We establish major engineering mission requirements for six individual science cases identified by the ORCAS science teams. Five major subsystems are defined with individual requirements for each. Requirements cover both the AO and flux calibration observation modes.
- Table 11 provides a high-level traceability matrix of all engineering requirements. Requirements are indexed by science case, source of requirement, and subsystem.
- The table and indexing system will allow us to trace all mission requirements and ensure they are met.

The mission engineering requirements have been defined by the science teams to ensure ORCAS is able to meet the goals for each science case. These requirements are outlined in Table 11. Each requirement is labeled for traceability. The first number in the prefix corresponds to the science case, where the science cases are **1)** Exoplanets, **2)** Solar System, **3)** Supernovae, **4)** Active Galactic Nuclei,

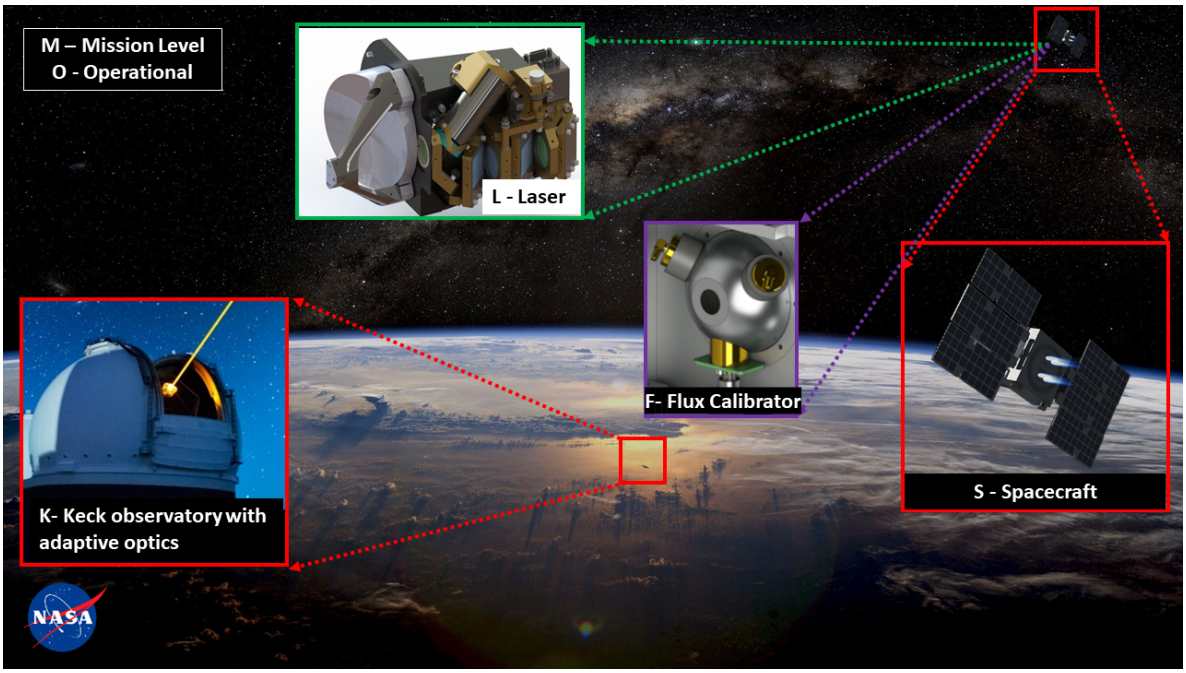

Fig 21 The major ORCAS mission components. Labels for each component corresponds to the engineering requirements traceability matrix seen in Table 11.

5) High Redshift Universe, and **6)** Flux Calibration. The letter corresponds to the requirement component as defined in Figure 21, where the components are **M)** Mission level, **O)** Operational, **L)** Laser, **K)** Keck Observatory, **F)** Flux Calibrator, **S)** Spacecraft. Finally, the last number indicates the identifying number of the requirement. For example, requirement 1.M.1 identifies itself as a requirement for the Exoplanet science case defined by the Mission Level, and it is the first such requirement.

The ORCAS mission is composed of two major elements, the Keck Observatory and a spacecraft. At observation, the spacecraft is positioned on the line of sight to the target, and provides the required calibration signal to enable near diffraction limited performances, thus enabling us to conduct observations with unprecedented capabilities. Figure 21 provides an identification of major mission subsystems and labels them for convenience so that the engineering requirements associated with each one can be easily traced.

To accomplish the science goals for the ORCAS mission, we must meet the scientific observational and mission requirements provided by the ORCAS Science Team. These requirements are composed of six distinct science cases: **1)** Exoplanets, **2)** Solar System, **3)** Supernovae, **4)** Active Galactic Nuclei, **5)** High Redshift Universe, and **6)** Flux Calibration. Each group has formulated a Science Traceability Matrix (STM) for their respective science cases.

Table 11 Engineering Requirement Traceability Matrix. Each bold numeral in the prefix corresponds to its respective ORCAS Science Case. If multiple science cases have an identical requirement, a single row will be filled. The letter corresponds to the mission component as defined in Figure 21. Note that the guide star laser power need not be continuous; it can be the time average of a pulsed laser, if the pulse rate is enough larger than the few KHz adaptive optics sample rate.

Requirement Traceability Matrix			
Prefix	Parameter	Requirement	Expected Performance
1.M.1	Observations	30 Targets, 2 observations	300 observations
2.M.1	Observations	10 Targets, 2 observations	
3.M.1	Observations	100 Targets, 1 observation	
4.M.1	Observations	7 Targets, 2-4 observations	
5.M.1	Observations	7 Targets, 2-4 observations	
6.M.1	Observations	Observe when able	
1-6.M.2	Mission Lifetime	3 Years	3-5 Years
1-6.K.1	Laser Reference Beam	100 fW/cm^2	850 pW/cm^2
1-6.K.2	Reference Laser Divergence	$\leq$ 1’	14”
1-6.K.3	Reference Laser Pointing Accuracy	7”	2”
1-6.K.4	Reference Laser Power	0.5 - 15 W	0.5 - 15 W
1.K.5	Instrument	KPIC/HISPEC	
2.K.5	Instrument	UV/VIS/NIR IFU	
3.K.5	Instrument	UV/NIR	
4.K.5	Instrument	VIS/NIR Spectrograph	
5.K.5	Instrument	VIS/NIR Spectrograph	
6.K.5	Instrument	OSIRIS/LIGER	
1-6.K.6	Time to Acquire ORCAS Laser	$\leq$ 3 Hours	15 Minutes
1-6.K.7	Wavefront Error Input (Zenith Angle $\leq$ [30°, 50°])	$\leq$ [150nm, 160nm]	
1-6.K.8	Tip-Tilt Error (Zenith Angle $\leq$ [30°, 50°])	$\leq$ [5mas, 7mas]	
1,3-5.L.1	AO Source Brightness	5 Magnitude	0-5 Magnitude
2.L.1	AO Source Brightness		1 Magnitude
1-5.L.2	Payload Used	Laser 532 nm or 1064 nm	532 / 1064 nm
6.L.2	Payload Used	Flux Calibrator	
1-6.L.3	Laser FOV	4’ x 4’	8’ x 16’
1-6.L.4	Laser Volume	$\leq$ 6U	4U
1-6.L.5	Laser Mass	$\leq$ 6kg	4kg
1-6.L.6	Laser Power	$\leq$ 150W	75 - 130W
1-6.L.7	Laser Pointing	$\leq$2”	0.2”
6.F.1	Flux Calibrator	0.35-2.3μm	
6.F.2	Flux Calibrator Brightness	8-15 Mag	
5.F.3	Flux Calibrator Flux Knowledge	Monitor exit flux — vs wavelength slope to between than 0.4%, with a goal of 0.4%, RMS between wavelengths to 0.3%, absolute to 0.3% all wrt NIST over 0.35–2.3 μm	
5.F.4	Flux Calibrator Appearance	$\leq$ 0.5 arcsec FWHM	
5.F.5	Flux Calibrator Output Scan	1° scan range; 2m resolution at receiver	
1-5.F.6	Flux Calibrator Volume	$\leq$ 12U	12U
1-5.F.7	Flux Calibrator Mass	$\leq$ 25kg	20kg
1-5.F.8	Flux Calibrator Power	$\leq$ 250W	200W
1-4.S.1	Absolute Position Knowledge (GPS)	$\leq$ 100 mas	50 mas at 3σ
1-4.S.2	Trajectory Knowledge (GPS)	$\leq$ 5 mas	3 mas at 3σ
1-5.S.3	Spacecraft Body Pointing	3’	7”
1-5.S.4	Delta-V (m/s)	$\geq$ 4000	4200-4700
1-5.S.5	Thrust	$\geq$ 60 mN	100 mN
1-5.S.6	Projected Thrust Lifetime	$\geq$ 1000 kN-s	1200 kN-s
1-5.S.7	Power	$\geq$ 1600W	2300W

4.2 Flight System Design

Key Findings

- We establish a viable flight system design that fulfills all mission engineering requirements as detailed in Table 11.
- We provide for the flight system: 1) the functional block diagram, 2) power and mass budgets and 3) the major equipment list (MEL).
- The spacecraft complies with the 2019 ESPA Grande Rideshare Users Guide (RUG).

As part of the ORCAS study, an RFI was released asking for viable spacecraft designs that can meet mission engineering requirements. In response we were provided with three viable space craft configurations. Following a trade study conducted by our team, we decided to showcase in this chapter the solution proposed by Blue Canyon Technologies (BCT). The selected spacecraft is expected to be launched for a DOD customer within the coming year, bringing it to a TRL-9. The spacecraft design put forward by BCT was examined and vetted at the ORCAS mission planning Lab (MPL) and was found to meet major ORCAS mission requirements with minor modifications. A schematic of the spacecraft is displayed in Figure 22.

To provide specific spacecraft characteristics, the ESPA Grande bus platform features an attitude determination and control system (ADCS). It consists of a star tracker and reaction wheels enabling a 7.2 arcsec 1σ in the tracker frame, and it has a slew rate of 1 deg/s. The spacecraft is in compliance with GSFC-STD-7000 thermal margins. The propulsion system is powered by 4 Xenon thrusters. Each has 25 mN of thrust and an expected lifetime of 300 kN-s. Each thruster utilizes 400 W, and has a specific impulse of 1,400 s. The propulsion system will enable more than 4,000 m/s Delta V, which satisfies requirement S.4. To understand how all individual spacecraft components operate and work together, see Figure 23 for the BCT ESPA Grande system architecture block diagram of the entire spacecraft.

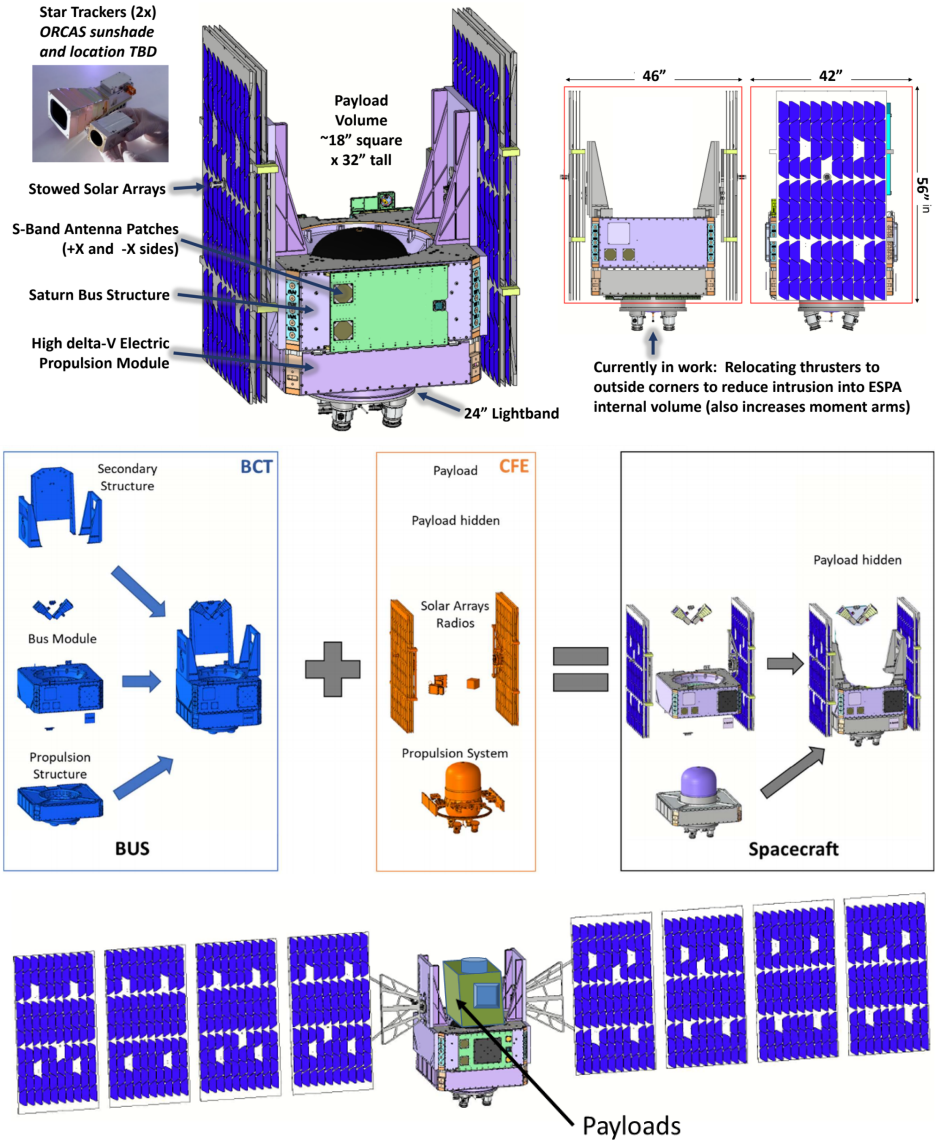

Fig 22 The ESPA Grande bus design for the ORCAS mission. The top image shows the stowed spacecraft with different components such as the S-Band Antenna Patch, the electric propulsion module, and the two Star Trackers. The middle image shows the breakdown of the ESPA Grande bus; the left image shows each major component of the bus, the middle image presents all major components of the core flight system, and the bottom image shows the spacecraft fully deployed.

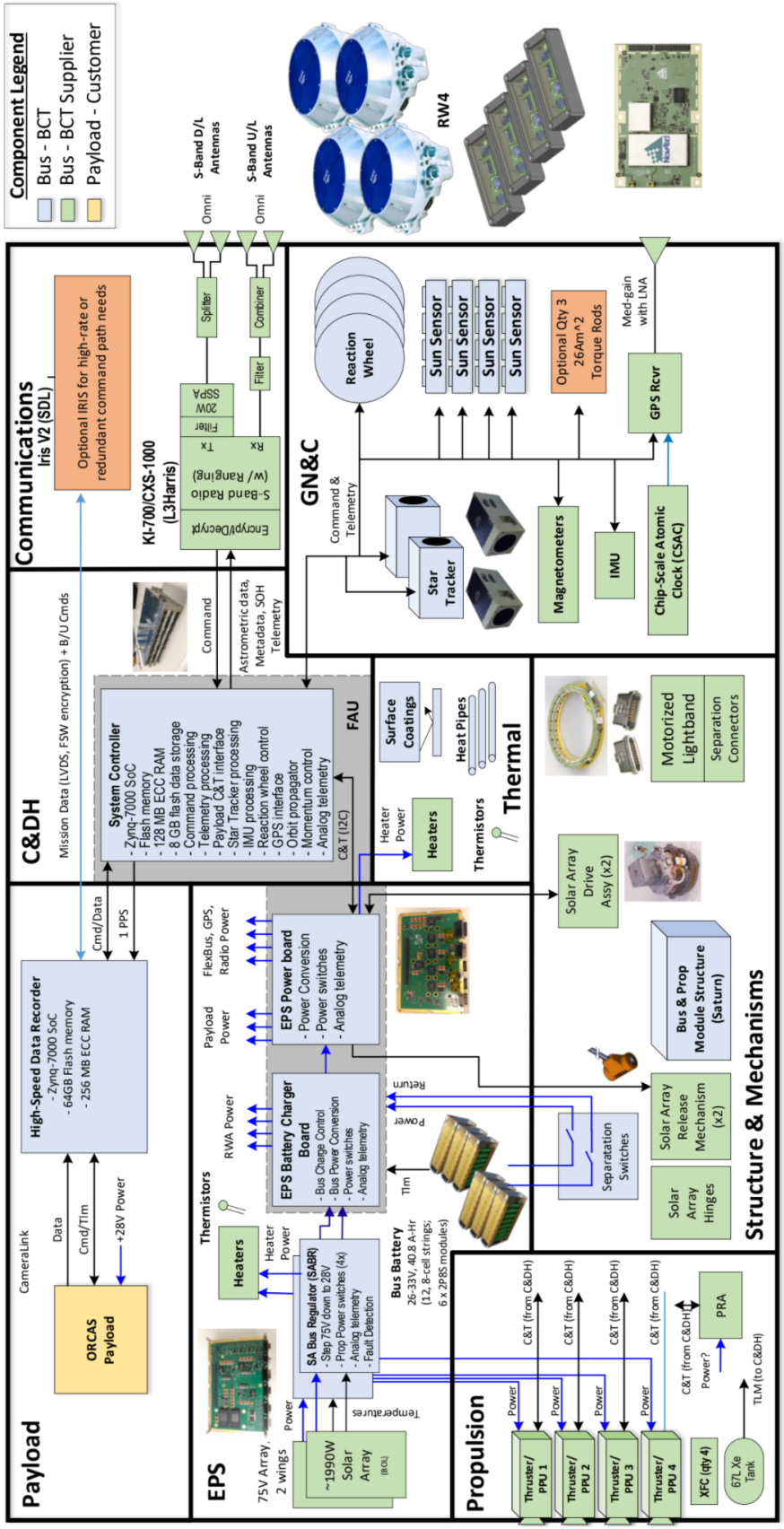

Fig 23 The system functional block diagram of the ORCAS spacecraft.

One key result from the Mission Planning Lab was quantifying the spacecraft mass and power budgets. A breakdown of all components and mass margins is showcased in Table 12. The specific fuel mass required for specific maneuvers both at the beginning of the mission and end of mission can be found in Table 31. The current best estimate for the laser and flux calibrator mass meets requirement L.5 and F.7 respectively. A full breakdown of the spacecraft power margins can be summarized in Table 13, and it demonstrates that both systems pass requirement L.6 and F.8. For both power and mass margins, we apply the GSFC GOLD Rules that recommend 25% for the margin plus the additional reserves. These can be seen at the bottom of Tables 12 and 13.

Table 12 ORCAS Spacecraft mass margins

Subsystem	**Mass CBE (kg)**	**Contingency (%)**	**Mass w/ Contingency (kg)**
Spacecraft Bus Total	236.8	5%	248.6
Laser Payload	4.8	20%	5.7
Flux Calibrator Payload	19.3	20%	23.1
Payload Structure	10	30%	13.0
Payload Radiator	3.3	30%	4.3
Heaters, Thermistors, Coatings	1.1	30%	4.3
Ultra Stable Oscillator (USD)	0.1	5%	0.1
NavCube Mini 3.0	2.0	25%	2.5
Mechanical Housing	1.2		
SpaceCube v3.0	0.15		
GNSS RF Card	0.11		
Power Card	0.11		
Black Plane	0.1		
Coax. Cables	0.1		
LNA	0.12		
Custom GPS Antenna	0.12		
Observatory Total (Dry)	**279.4**		**303.6**
Propellant (Xenon)	112		115
Observatory Total (Wet)	**391.4**		**418.6**
		Max ESPA Grande	450.0
		GOLD Rule Dry Mass (% margin)	41.1
		SALMON AO Dry Mass (% margin)	29.1
		GOLD Rule Wet Mass (% margin)	3.7
		SALMON AO Wet Mass (% margin)	3.6

Table 13 ORCAS Power Modes. Green cells indicate components that meet requirements. The Laser Payload was set to the maximum power value from the two designs from the RFI response.

		Power (W)	Contingency (%)	Power (W) w/ Contingency	Checkout		Delta-V		RF Comm		Science 1 Laser		Science 2 Flux Cal		Safe	
					Duty Cycle	Pwr	Duty Cycle	Pwr	Duty Cycle	Pwr	Duty Cycle	Pwr	Duty Cycle	Pwr	Duty Cycle	Pwr
Payload 1	Laser Payload ON	130	25%	156.3	0%	0	0%	0	0%	0	100%	156.3	0%	0	0%	0
	Standby Active	19.7	25%	24.6	0%	0	0%	0	100%	68.75	0%	0	100%	68.75	0%	0
Payload 2	Flux Cal ON	130	25%	162.5	0%	0	0%	0	0%	0	0%	0	100%	162.5	0%	0
	Flux Cal OFF	50	25%	62.5	0%	0	0%	0	100%	81.25	100%	81.3	0%	0	0%	0
High Alt	NavCube 3.0	15	15%	17.3	0%	0	0%	0	100%	17.25	100%	17.3	100%	17.25	0%	0
	Ultra Stable Oscillator	5	8%	5.4	0%	0	0%	0	100%	5.375	100%	5.4	100%	5.375	0%	0
C&DH/EPS	FlexBus	14.5	0%	14.5	100%	14.5	100%	14.5	100%	14.5	100%	14.5	100%	14.5	100%	14.5
	SABR	20	0%	20.0	100%	20	200%	40	100%	20	100%	20	100%	20	50%	10
	Data Recorder	3.1	0%	3.1	0%	0	0%	0	0%	0	100%	3.1	100%	3.1	0%	0
	DC-DC Converter Inefficiency					0.9		0.9		0.9		1.2		1.2		0.6
SADA	Solar Array Drive	6.5	0%	6.5	0%	0	10%	0.65	10%	0.65	0%	0	0%	0	0%	0
RF Comm	Star Trackers x2	6	0%	6.5	0%	0	10%	0.65	10%	0.65	0%	0	0%	0	0%	0
	Tx Only	80	0%	80.0	0%	0	0%	0	0%	0	0%	0	0%	0	0%	0
	RX + TX	86	0%	86.0	10%	8.6	0%	0	100%	86	10%	8.6	0%	0	2%	1.72
	Encryptor/Decryptor	4.2	0%	4.2	100%	4.2	100%	4.2	100%	4.2	100%	4.2	100%	4.2	100%	4.2
GN&C	Star Trackers x2	3	0%	3.0	100%	3	100%	3	100%	3	100%	3	100%	3	0%	0
	GPS + CSAC	2	0%	2.0	100%	2	100%	2	100%	2	0%	0	0%	0	100%	2
	Torque Rods	0	0%	0.0	0%	0	0%	0	0%	0	0%	0	0%	0	0%	0
	Reaction Wheels (Quies)	24	0%	24.0	100%	24	100%	24	100%	24	100%	24	100%	24	100%	24
	Reaction Wheels (Max)	84.9	0%	84.9	0%	0	0%	0	0%	0	0%	0	0%	0	0%	0
Thermal	Bus Internal Heaters	33.1	0%	33.1	0%	0	100%	33.1	100%	33.1	50%	16.6	100%	33.1	100%	33.1
	External Component Heaters	46.5	0%	46.5	20%	9.3	100%	46.5	100%	46.5	50%	23.3	100%	46.5	100%	46.5
	Payload Heaters	53	30%	68.9	0%	0	50%	34.5	0%	0	0%	0	0%	0	100%	68.9
Prop	Prop Module	10	0%	10.0	100%	10	100%	10	0%	0	0%	0	0%	0	0%	0
	Propulsion	30	0%	30.0	20%	6	50%	15	100%	30	100%	30	100%	30	100%	30
	PPU Heaters	21.2	0%	21.2	20%	4.24	20%	4.24	100%	21.2	100%	21.2	100%	21.2	100%	21.2
				973.1		**112.1**		**238.5**		**458.7**		**435.1**		**460.7**		**262.6**
				Solar Array Power Avail (2164W - 1600W)		564.0		564.0		564.0		524.5		564.0		564.0
				With Modifications to FPGA		964.0		964.0		964.0		924.5		964.0		964.0
				Battery Reserves (3 hour, 50% DoD)						252.0		252.0		252.0		
				GOLD Rule (% margin)		402.9		136.4		77.9		78.5		77.1		114.8
				SALMON AO (% margin)		80.1		57.7		43.8		44.0		43.5		53.4

As can be seen from Tables 12 and 13, the spacecraft will have a total mass with contingency of 418.6 kg and a total power with contingency of 973.1 W. Both the mass and power pass the SALMON AO margins. For the total power allocated to the Laser payload, we list 130 W, as that is the largest power value from the two designs, to avoid underestimating. To understand how all individual spacecraft components operate and work together, see Figure 23 for the BCT ESPA Grande system architecture block diagram of the entire spacecraft. For more information on each spacecraft design, see Appendix.

4.3 Payload Design

Key Findings

- We present two high TRL laser designs that meet the wavelength, divergence, mass, and power requirements for the Laser payload in Section 4.3.1. Each design has a mass $<$ 5 kg, a power $<$ 130 W, and a volume $<$ than 4U
- Section 4.3.2 discusses the requirements for the flux calibrator system. A preliminary design has not yet converged for this subsystem, but we recommend flying several approaches together to meet the requirements.

4.3.1 Laser

As outlined in the engineering requirements section (Table 11), the ORCAS laser beacon needs to meet an array of requirements to enable mission science goals. At the ground-based observatory, the ORCAS laser beacon is required to provide the flux equivalent of a 0th magnitude star in its high brightness mode and must be able to reduce the flux provided to the equivalent of a 5th magnitude star in low brightness mode. The beacon needs to be able to do this at two different wavelengths, one in the visible, and one in the near-IR, and be able to transmit either wavelength alone, or both together. In order for ORCAS to point its beacon laser at the observatory, the observatory would need to provide a ground-based beacon to ORCAS that the ORCAS laser system can track on. For this ground-based beacon we plan to leverage the existing Sodium Laser Guide Star lasers (wavelength 589nm) already present at most large observatories.

At a wavelength of 532 nm a photon flux equivalent to a 0th magnitude star is approximately 1.2 million photons per square centimeter per second. ORCAS needs to provide this flux at the observatory from a range of 200,000 km. This requires only a modest laser power to be transmitted by the ORCAS laser instrument. A Gaussian beam with a total power of 1W and $1/e^2$ divergence radius of 66 micro-radians will create a spot at a distance of 200,000 km with a maximum photon flux of 1.2 million photons per square centimeter per second. The $1/e^2$ radius of this spot would be 11.9 km.

The required photon flux could be achieved with lower laser power, but at the cost of a smaller beam divergence, which would require increased beam pointing precision and lower pointing jitter. Neither the laser power or divergence in this hypothetical example are particularly challenging in comparison with laser systems already flown in space by NASA and commercial entities. Most of the functions required by the ORCAS laser system (acquiring a beacon, pointing a laser back at the ground-based beacon and tracking it) are functions already included in laser communications terminals, thus it was natural to leverage technologies previously demonstrated for laser communications to meet the needs of the ORCAS mission.

In order to keep the electrical power consumption less than 200W (requirement 1-6.L.6) the ORCAS laser needs to be efficient. The need for a compact and efficient laser source, and the need for excellent beam quality naturally suggests a fiber laser source for ORCAS. An ytterbium laser source at approximately 1064 nm would be an efficient way to generate the 1064 nm beacon required for ORCAS. The use of a nonlinear frequency doubling crystal would allow the 1064 nm output to be doubled to provide the 532 nm visible wavelength also required. Filters could be used to determine

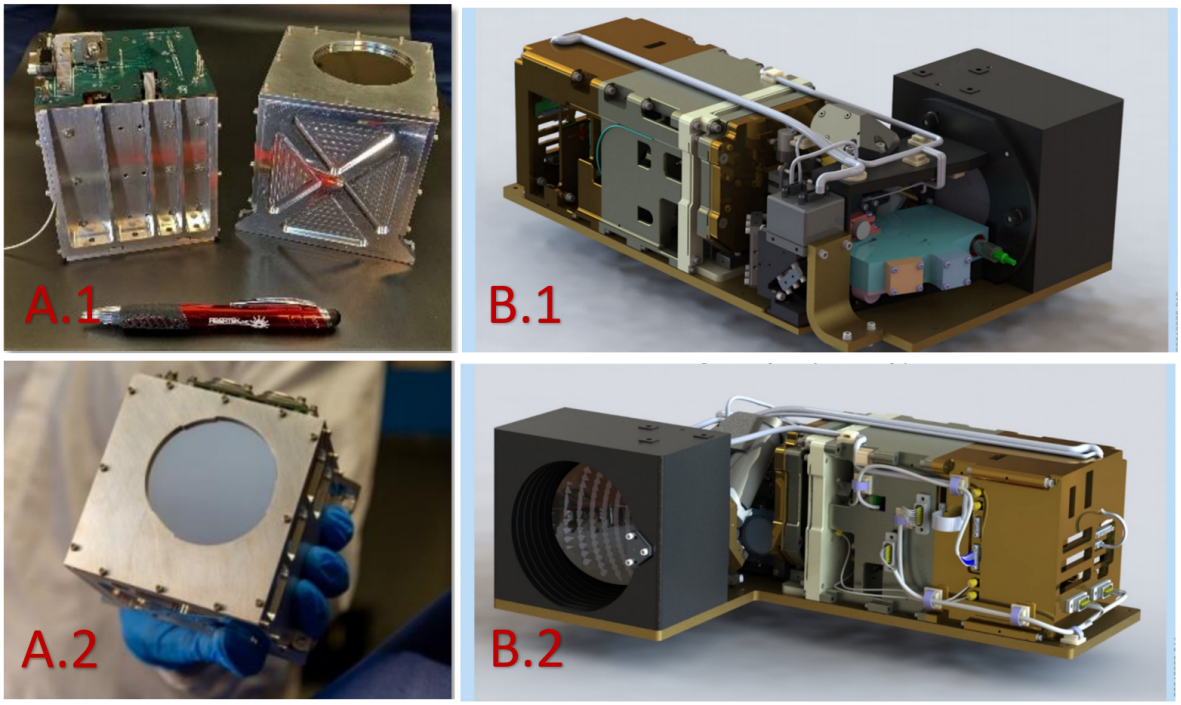

Fig 24 (A) Images of the Fibertek Oracle 2U terminal, similar to what the ORCAS payload would look like; (B) Rendering of the General Atomics ORCAS payload from different angles, showcasing the combined Laser Electronics Assembly (LEA) and Laser Telescope Assembly (LTA)

if 1064 nm, 532 nm or both wavelengths together are transmitted. The photon flux of the ORCAS beacon at the observatory can be adjusted by changing the fiber laser output power and/or the beam divergence.

The laser divergence will set the pointing requirements of the ORCAS optical beam director. In order to ensure that the fluctuation in intensity seen by the observatory is less than approximately 10%, the pointing wander of the ORCAS beacon should be kept to less than 20% of the beam divergence. In the above example with a beam divergence of 66 micro-radians this means that the pointing jitter of the ORCAS laser be kept less than 13micro-radians. Existing commercial laser communications space terminals are able to keep pointing jitter well under this amount.

In response to an RFI for the ORCAS laser instrument, Fibertek (FT) and General Atomics (GA), the two companies deemed most suitable, provided very mature conceptual designs based on their existing laser communications space terminals, featured in figures 24. Both companies have laser communications terminals that operate at a wavelength of 1550 nm using an erbium fiber laser. Both proposed to change the erbium fiber to ytterbium fiber and add a frequency doubling crystal to provide the 532 nm output. Both of the existing systems had optical beam directors that would easily meet pointing requirements. Both respondents proposed designs that used well under 150W spacecraft power and had a mass and volume that fit within the ORCAS requirements of 6 kg (1-6.L.5) and 6U (1-6.L.4). We provide a block diagram for each design that details all major components as shown in figure 25.

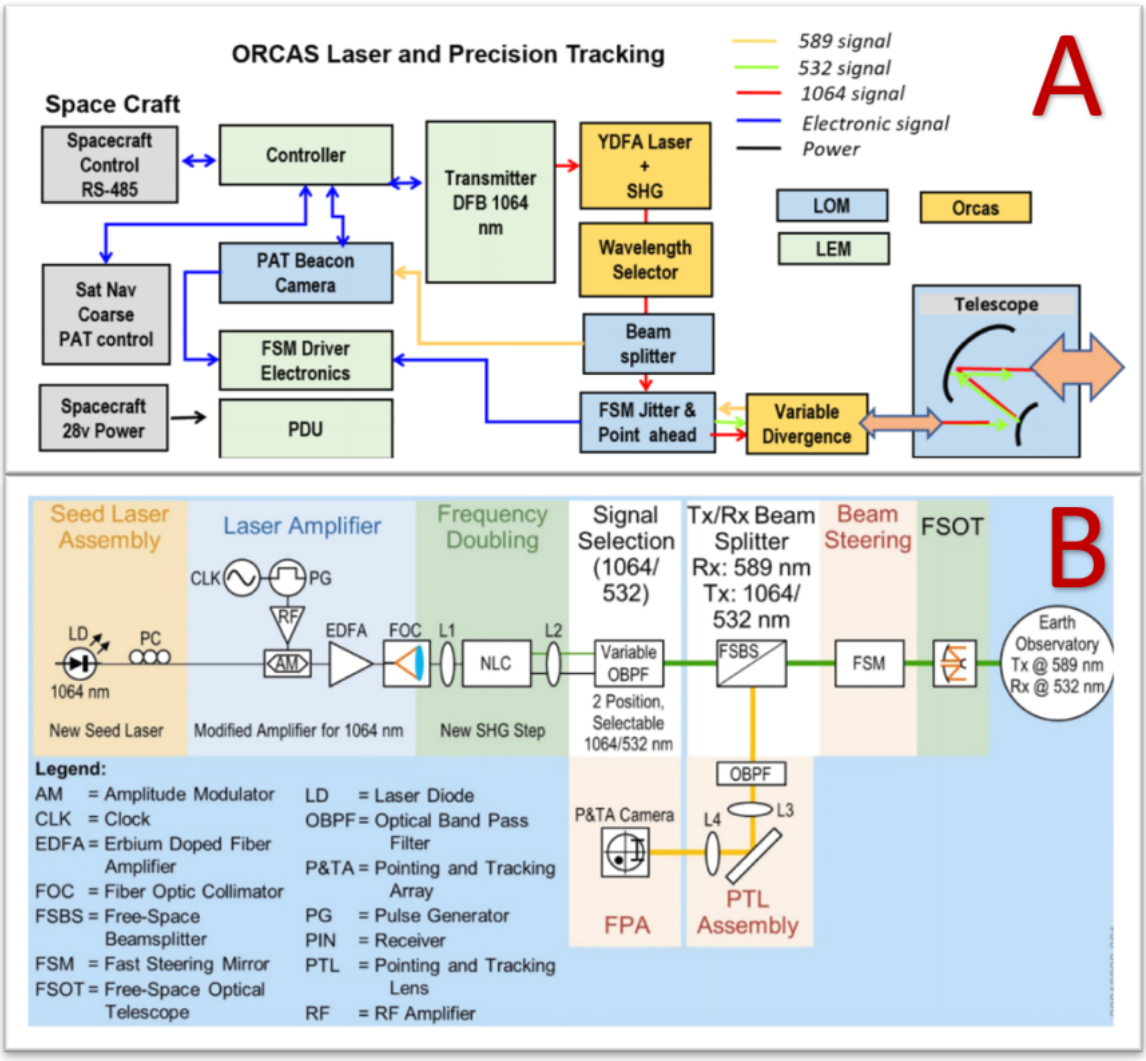

Fig 25 Fibertek (A) and General Atomics (B) block diagrams showcasing the laser beacon design based on existing laser communications terminals

In both proposed laser systems one of the largest departures from existing design was the addition of the frequency doubling crystal, and both companies proposed a path to mitigate this risk. On-orbit performance data for both company's existing laser communication terminals is likely to be available by the end of this year.

4.3.2 Flux Calibrator

A preliminary design for the flux calibration module has not yet converged. A central benefit of ORCAS — the astrostationary viewing opportunities afforded in part by its large apogee distance — presents a challenge in terms of projecting a sufficiently bright beam from ORCAS. Methods that lead to a brighter beam also lead to less certainty on the beam shape. The studies carried out so far are detailed in the Appendix.

Our study has concluded that several approaches should, and likely can be, flown together. One approach would have an integrating sphere (IS) fed by monochromatic light sources, having one bare exit port and one exit port facing having an optical concentrator. In addition, for a smaller set of 3–5 wavelengths, the payload would include lasers injected into single-mode fibers. Each wavelength would have its own laser and custom fiber core size. To mitigate the risk of contamination of a fiber end, for each given wavelength the laser would be able to feed any of three alternative fibers. Each output beam would be monitored regularly by a calibrated photodiode (PD), with cross-calibration checks performed with an electrical substitution radiometer (ESR).

Figures 26 and 27 show the conceptual layout for one of these components – an integrating sphere, with input light sources, an SI-traceable flux monitor, and the exit port that would be observed by a receiving telescope.

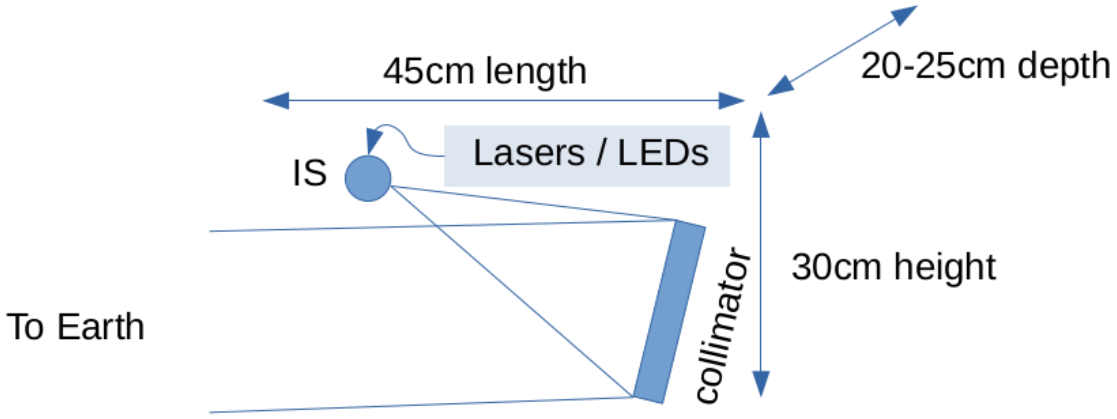

Fig 26 Rough conceptual design for a flux calibration module consisting of an IS and a collimator to concentrate the output beam.

As stated, Figures 26 and 27 show the conceptual layout for an integrating sphere, with input light sources, an SI-traceable flux monitor, and the exit port that would be observed by a receiving telescope.

A concept for an alternative, or rather complementary, light source for flux calibration that would be based on single-mode optical fibers is shown in Figure 28 below.

Power: Power must be sufficient to provide the emitted brightness, the SI-traceable monitoring system, one or more shutters, the DAQ, potentially a mechanism to move the flux reference detector, and any bus maneuvers that may be necessary to reduce contamination by reflected sunlight. Since we cannot yet rule out the need for high-powered lasers, 200 W should be reserved for light sources until there is a preliminary design.

Mass: The mass will consist of several light sources, their heat sinks and power and control electronics, an integrating sphere, several photodiodes and their readout electronics, an electrical substitution radiometer, which may require cooling, and its electronics, baffling, an optical concentrator, a detector motion mechanism, and the support super structure. A mass estimate requires a preliminary design, but a ROM might be a few $\times$ 10 kg.

Volume: The flux calibration device probably will fit 3U, unless a concentrator is needed, in which it may require up to 6U in order to allow the concentrator to have an appropriate focal length and to

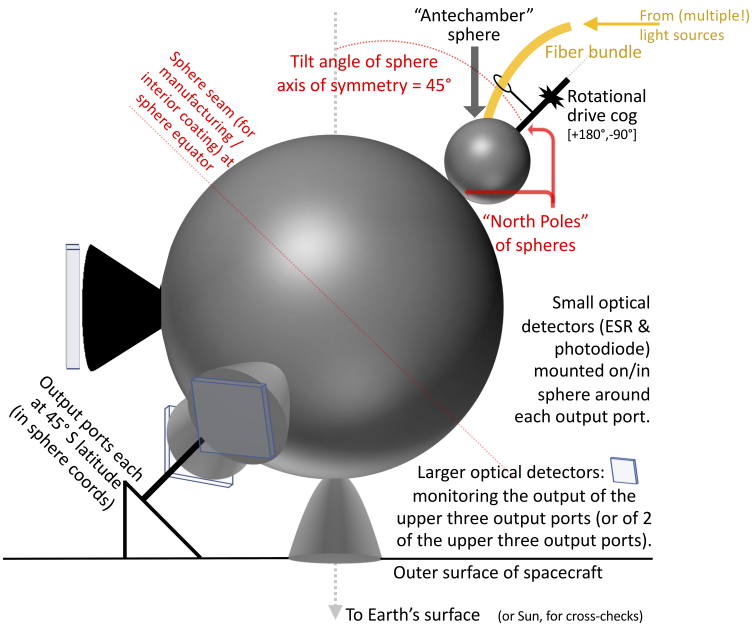

Fig 27 Similar to the figure above, a conceptual design for an IS-based flux calibration module; however here the optical output collimators are mounted onto the IS itself.

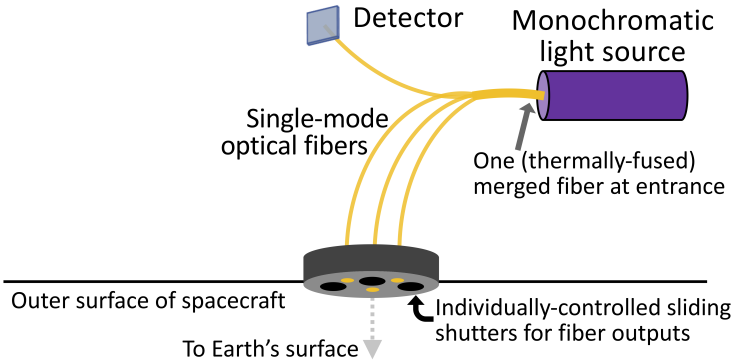

Fig 28 A conceptual view of a single mode fiber-based flux calibration module. (Multiple optical modes could and would propagate within the fused entrance end of the fiber bundle; however the individual output fibers would each be single-mode and identical.)

allow clearance for the exit beam. There is the possibility that the addition of baffling could exceed 3U.

Communications: Some ORCAS observations will require tight coordination with the telescope(s) observing it. The ability to upload new wavelength, on/off, and potentially brightness-tuning sequences at least several times per minute is desirable in order to maximize the efficient use of ORCAS and the telescopes being calibrated. Likewise, time-stamped data on lamp states, bus position and orientation, and flux monitor will need to be downloaded. Ideally this would be near-realtime, i.e, around 1 Hz, so that the spacecraft state can be used to drive the receiving telescope observing sequence (i.e., exposure time, tracking, filter selection, etc.)

Outgassing and other surface contamination: Surface contamination could alter the reflection and

absorption properties of the ORCAS light or flux monitors, both relative to pre-flight testing as well as over the mission lifetime. The light exiting ORCAS will be monitored, so up-stream of the monitor the concern would be changes that significantly reduce the output flux. An example would be deposits that reduce the reflection efficiency of the integrating sphere walls.

Deposits on the flux monitors are a more serious concern. Monitoring during the mission lifetime may be possible by having several detectors, each with differing controlled exposure to outgassing. For instance, one could have several hermetically-sealed photodiodes, and then open a new one every few months in order to re-establish the SI zero-point for previously-used photodiodes.

Radiation tolerances: Light source electronics, flux-monitoring detectors and their electronics must be rated for the expected mission lifetime. The flux-monitoring detectors and electronics also must not change their sensitivity due to radiation damage. Some flux-monitoring detectors, such as photodiodes and light traps, will also detect radiation hits. Their net impact needs to be at least $2\times$ below 0.4%, and preferably 0.2%. If the flux detected at the monitor detector is large, radiation hits may make only an insignificant contribution. If radiation hits are detectable in the data stream, it may be possible to remove their contamination of the flux monitoring measurement.

Cost: A ROM cost is 10 M USD. Most of the cost will be in the form of personnel for engineering and lab testing. We expect that even space-qualified components will total less than \$0.5M as many are COTS. If a concentrator is needed, it may require a free-form optics surface profile, adding design and fab costs relative to a COTS optic. If a mechanism is needed to move detectors in/out of the exit beam, then the "\$1M per moving part" rule may apply. Engineering personnel will be needed for all stages of the design process. Engineering and lab scientist personnel for establishing the calibration of the monitoring detectors, for end-to-end testing, and for assembly will be needed. (Experience shows that lab testing is essential for finding detector anomalies and/or parasitic light paths, and to provide sufficient pre-flight characterization to interpret in-flight data.) Engineering for the DAQ (light control, shutter control, detector control and readout, and possibly a mechanism) will be needed, as this system should be flexible enough to work with a range of wavelength/exposure/brightness sequences for different receiving telescopes.

Risk: No detailed risk assessment is possible without a preliminary design. We consider component risk to be low. But because astronomical flux calibration has improved only slowly compared to lab SI flux accuracy, despite numerous on-going efforts, it is wise to assume that there may be significant risk in achieving 0.4% flux knowledge from (the first) ORCAS. For instance, detection of unexpected parasitic light in lab tests might require some redesign, which has cost and schedule implications. (In fact, it should probably be assumed that several design/test iterations will be required for the flux calibration unit.) Some of this unquantifiable risk may be reduced or retired once results from ORCASsat or ground-based efforts such as SCALA, StarDice, and NISTstars become available over the next ~ 2 yrs.

4.4 Telescope System Design

Key Findings

- The ground telescope system requirements are identified and detailed in Section 4.4.1.
- We outline the proposed upgrades such that the W. M. Keck Observatory could meet its requirements. Block diagrams of the proposed updates to Keck Observatory to meet the given telescope system requirements are given in Section 4.4.2. The section has figures showing the proposed updates and also gives a list of required updates to meet the stated requirements.
- A table of the current and future Keck instruments is given in Section 4.4.3.

The W. M. Keck Observatory has two telescope systems, Keck I and Keck II, which are pictured in Figure 29 (left). Each telescope has a 10 m primary aperture mirror. Both telescopes use adaptive optics (AO) systems to remove atmospheric distortion from images. The projected lasers for the Keck AO system can also be seen in Figure 29 (right). A number of science instruments are fed by the AO systems.

Fig 29 (Left) The Keck I and Keck II telescopes. (Right) The lasers used fro AO correction being projected from the telescopes.

In this section, the specific requirements for the Keck telescope system are given. Based on the given requirements, the proposed updated AO system plan is then presented. The current Keck instruments, both in use and proposed projects, are briefly described.

4.4.1 Requirements and Interfaces

This section outlines the engineering requirements for the telescope system design. High level requirements were given in Table 11 in Section 4.1. More in-depth requirements are given in Table 14 below.

Table 14 Telescope system requirements matrix.

Category	Requirement
Telescope observational wavelengths	Keck I & II: Observations from λ = 0.4 to 5 μm
Wavefront Sensing	λ = 532 nm and/or 1064 nm
Time to acquire ORCAS laser	$\leq$ 15 minutes
Time to perform dither	$\leq$ 10 seconds
Time lost during observation window	$\leq 1\%$ of available observing time
Observing non-sidereal Orbits	Observe up to rates of $1''$/s
Use ORCAS location and orbital information	Within 5 mas (24 nrad)
Provide beacon for ORCAS	100 fW/cm^2 brightness
Time lost to Maunakea laser traffic control	None
Pointing and tracking accuracy	$2''$
Keck Laser Divergence	$\geq 14''$ diameter
Keck laser	Detune from sodium line during observation
ORCAS interface	Provide time-stamped location & orbit information

4.4.2 Optical System Upgrade

In order to meet the given requirements for the ORCAS mission, several Keck systems will need upgrades. Figure 30 shows the AO bench which is where most of the hardware upgrades will be needed, and the location of the current AO science instruments. The primary hardware change will be to replace the deformable mirror (DM) labelled as item 3 in Figure 30, and corresponding changes to the Shack-Hartmann wavefront sensor optics (item 15) and field steering mirrors (item 14), as well as the infrared wavefront sensors located to the right of item 10.

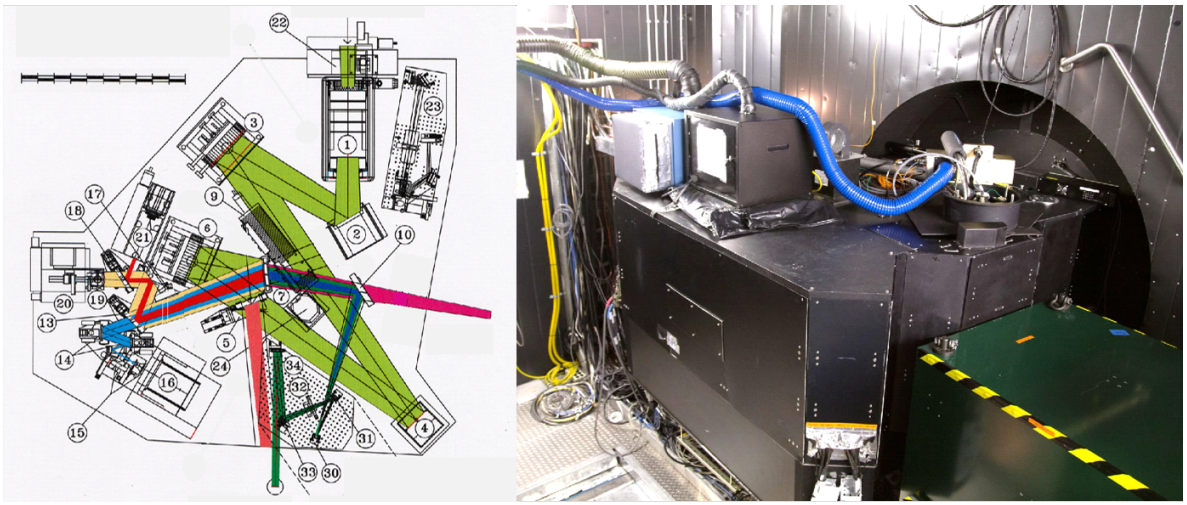

Fig 30 (Left) Keck II AO bench layout. Rotator (item 1), tip-tilt mirror (2), off-axis parabolas (3, 6), DM (4), dichroic beamsplitter (7), field steering mirrors (14), Shack-Hartmann wavefront sensor camera (16), low bandwidth wavefront sensor (19), tip-tilt sensor (20), acquisition camera (21). (Right) Keck I AO bench and OSIRIS science instrument. This image corresponds to (22) in the AO bench layout on the left.

The upgrades required for this proposed system are highlighted in the list below. Each item gives the overall upgrade as well as the steps required to upgrade the system.

1. **Reduce atmospheric and static primary mirror fitting errors in Keck II.** The high order deformable mirror (HODM) needs to be updated to provide 20 cm subapertures on the Keck primary mirror. The visible Shack-Hartmann wavefront sensor lenslet array and reducer optics will need to be updated to match the HODM actuator spacing. The infrared pyramid WFS pupil relay optics will need to be updated to properly sample the HODM actuator spacing. The real-time controller algorithms and processor speed will need to support the increased number of WFS subapertures and HODM actuators for both the visible and infrared WFS modes. The daytime simulation and calibration tools will need to be upgraded to support integration and optimization.

2. **Improve reliability and efficiency.** This includes the motion control system, supervisory control system, and operations software.

3. **Improve pointing control.** This would include laser pointing and focus control, the visible Shack-Hartmann WFS field tracking, and the infrared pyramid WFS field tracking.

4. **Optimize performance.** This includes tip-tilt performance, primary mirror phasing, non-common path aberrations, speckle nulling, and optimized gains.

5. **Upgrade observing and operations support tools.** This step includes the proposals and scheduling as well as observation planning. The ORCAS communication and control interfaces will need to be created. The acquisition and observing sequence, the PSF-reconstruction, and the laser projection changes will need updates.

6. **Develop a fast visible camera.** Develop and implement a simple visible imager which will be located next to the AO acquisition camera. No changes are needed for the science dichroic.

7. **Improve visible science instrument infrastructure.** This will include updating the dichroic beamsplitter to transmit visible wavelengths wavelength to the science instrument. The dichroic changer will need to swap between the existing science dichroic and the visible science dichroic. A visible atmospheric dispersion corrector will need to be acquired.

8. **Modify OSIRIS for operation to 800 nm if required.** Modify dichroic beamsplitter and changer to meet requirements. Modify filters, control software, and data reduction pipeline to work with ORCAS team. Note that these modifications could be applied to Liger instead of OSIRIS if it is implemented in time.

4.4.3 Keck Instruments

A table of the current and proposed Keck instrumentation can be seen in Table 15. As shown, several upgrades to the observatory have already been proposed or are in development. ORCAS would leverage these proposed projects to ensure that all mission requirements can be met. These instruments all operate at different wavelengths, which are summarized in Figure 31.

Table 15 Major current and future AO and instrument capabilities at Keck.

Category	Instrument	Telescope	Current/Future
AO Systems	Deformable Mirrors	Keck I & II	Current
	Lasers	Keck I & II	
	Shack-Hartmann Wavefront Sensors	Keck I & II	
	NGS Tip-Tilt and Low Bandwidth Wavefront Sensors	Keck I & II	
	Near-Infrared Tip-Tilt Sensor	Keck I	
	Pyramid Wavefront Sensor (PyWFS)	Keck II	
	Real-Time Controllers	Keck I & II	In Development
	NIRSPEC MEMS Deformable Mirror	Keck II	
AO Science Instrument	OSIRIS IFS and Imager	Keck I	Current
	NIRC2 Camera	Keck II	
	NIRSPEC Spectrograph	Keck II	
	Liger IFS and Imager	Keck I	Future
	SCALES IFS	Keck I & II	
	HISPEC Spectrograph	Keck II	
	Visible Science Instrument	Keck I & II	

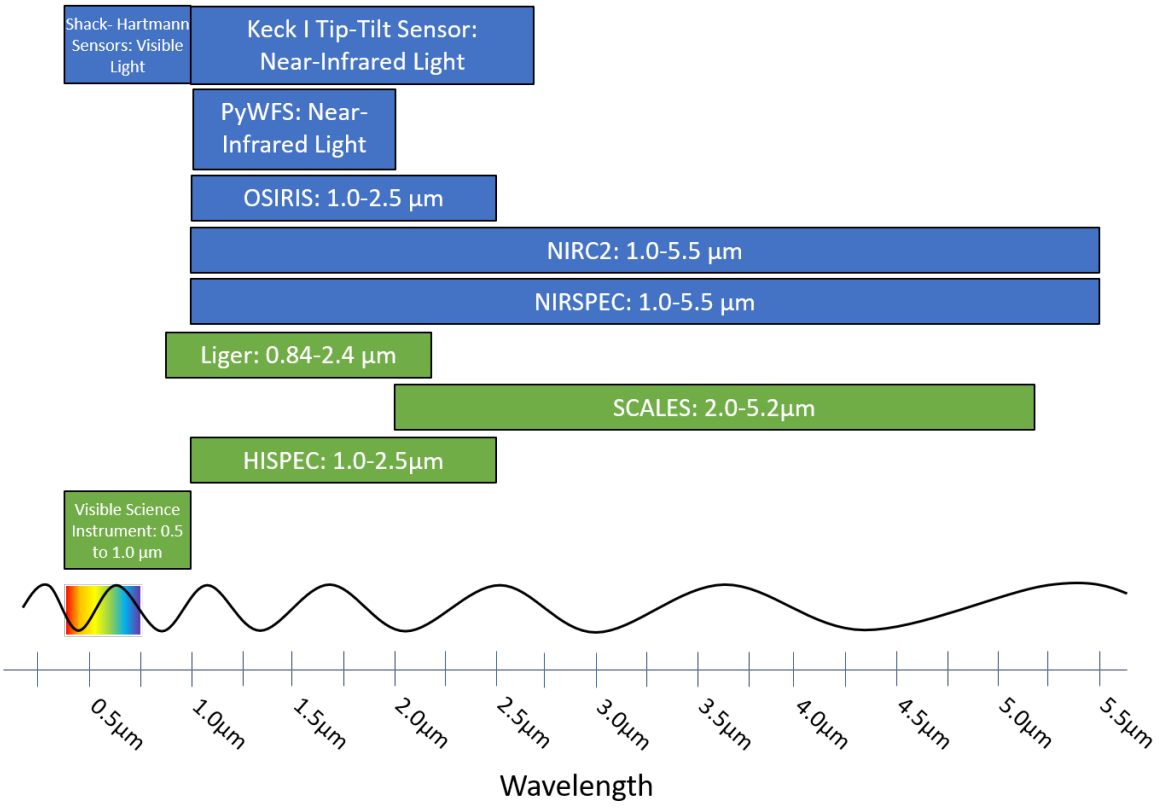

Fig 31 The wavelengths that the current (blue) and future (green) Keck instruments operate at.

4.5 Data Approach and Ground System

Key Findings

- The ground station and spacecraft can work together to achieve observation requirements for ORCAS.

Figure 32 gives a visualization of how all the mission components and systems of ORCAS work together. The science teams for each of the science cases will give information on their desired next target stars, the schedule for when observations should occur, and the Keck instrument which would be needed to make the observation. This information will be sent to the Mission and Science Operations Centers (MOC/SOC), who will send it on to the Flight Dynamics Facility (FDF) and the W. M. Keck Observatory. The FDF will take the desired targets and schedule and will use their mission planning tool to determine the optimal order of targets and the orbits required to view them.

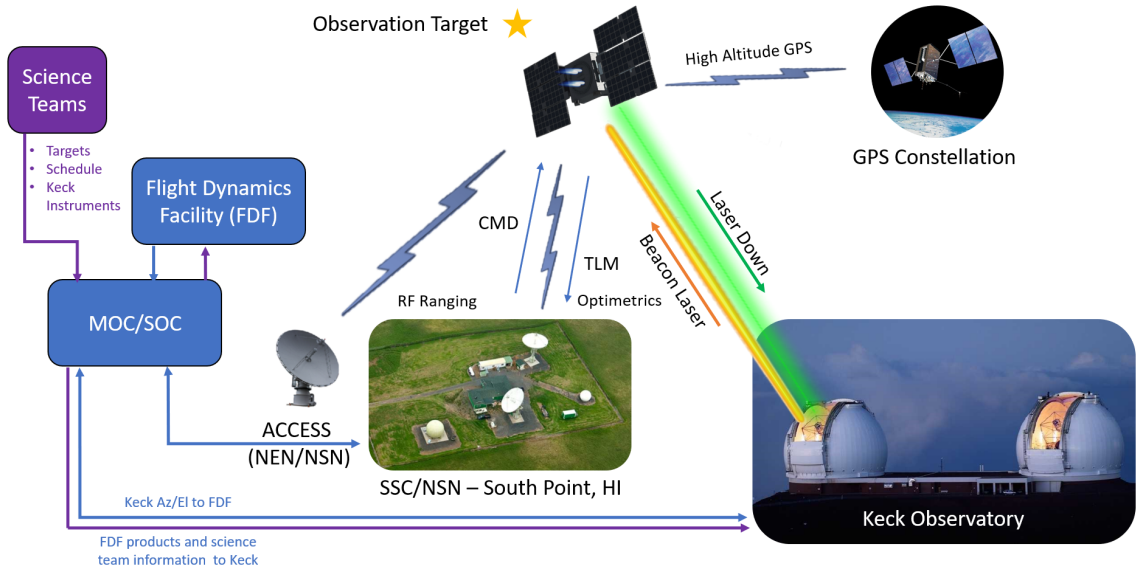

Fig 32 A visualization of all mission components and systems working together

The orbital data will then be sent back to the MOC/SOC, who will send it on to Keck Observatory and the SSC Near Space Network station in South Point, Hawaii. The Near Space Network (NSN) will be used to send the spacecraft command information and receive telemetry data. The South Point station, along with ACCESS, will send the command data up to the spacecraft via RF ranging and optimetrics, and will receive the spacecraft telemetry. The High Altitude GPS constellation will be used to determine the spacecraft's position. It is estimated that the housekeeping data, including overhead, from the spacecraft will be 24.5 Mb per day (reference the MPL docs? Or add appendix?). A High Speed Data Recorder (HSDR) will be used to store data. The HSDR provides 64 GB of flash memory, which is more than one month's worth of storage data. The data collection rate for housekeeping data will be 0.237 kbps.

The W. M. Keck Observatory will receive information on the target stars to be viewed, the schedule of when observations will occur, and the science instruments to be used for each observation from the

Table 16 A breakdown of the RF link budget for ORCAS.

	Distance (km)	Data Rate (kbps)	Margin (dB)	Data Rate (kbps)	Margin (dB)
		Downlink		Uplink	
Initial RF Contact	36,000	64	11	8	21
NSN at Perigee	7,000	512	13	64	23
NSN at Apogee	200,000	16	3	2	13
NSN at Max Range	1,200,000	4	0.6	2	7.7

MOC/SOC. The observatory will send up a beacon laser to the ORCAS spacecraft, and the spacecraft will send down a laser beam to be used for AO.

5 Mission Operations

Key Findings

- We show that AO and flux calibration observations can take place with a family of highly elliptical orbits we have developed which are described in Section 5.1.1.
- This orbit family allows for up to 3 AO observations of up to a few hours, depending on target star declination and observable wavelength, per orbit.
- Detailed operation sequences for both AO and flux calibration modes are given in Section 5.1.2. Less than three hours of observatory preparation time is required for each observation.
- We have developed a robust and flexible mission optimization algorithm for mission planning which is described in Section 5.2. The tool accounts for weather events and low visibility by updating the mission schedule after each observation. It outputs solutions which perform up to 300 observations within the time and fuel budget, twice the stated requirement for the mission.

In this section, we describe how the ORCAS mission will achieve its scientific goals. The engineering requirements traceability matrix given in Table 11 defines our requirements for this section. We begin by discussing the mission operations concept in Section 5.1. This includes the orbit design in Section 5.1.1, in which we have developed a highly elliptical orbit which allows for up to 3 AO observations of up to 2.5 hours for a field of view radius of 7.3 arcseconds and also allows for flux calibration observations. The maximum duration depends on the isoplanatic patch angle, which in turn depends on wavelength, seeing, declination, and zenith angle. Detailed operations sequences for both AO and flux calibration operation modes can be found in in Section 5.1.2. Finally, Section 5.2 goes through development of the mission planning tool which can be used to optimize the order of target stars viewed.

5.1 Mission Operations Concept

Key Findings

- We develop a highly elliptical orbit which can meet all mission requirements for ORCAS, which is described in detail in Section 5.1.1. The orbit can make AO observations of target stars of up to 2.5 hours for a field of view radius of 7.3 arcseconds without maneuvers, depending on target star declination. Up to 3 such observations can be made during one orbit period.
- In section 5.1.2, detailed operations concepts for both AO and flux calibrator observations are given. The total required time for observation preparations is less than 3 hours.

5.1.1 Orbital Configurations

We have developed a family of orbits that can meet the ORCAS mission requirements. These are five-day, highly elliptical orbits, and AO observations can be made at up to three locations near apogee.

The orbit path around Earth in the ECI frame for an example target star with a declination of 20° and a right ascension of 0° can be seen in Figure 33A.

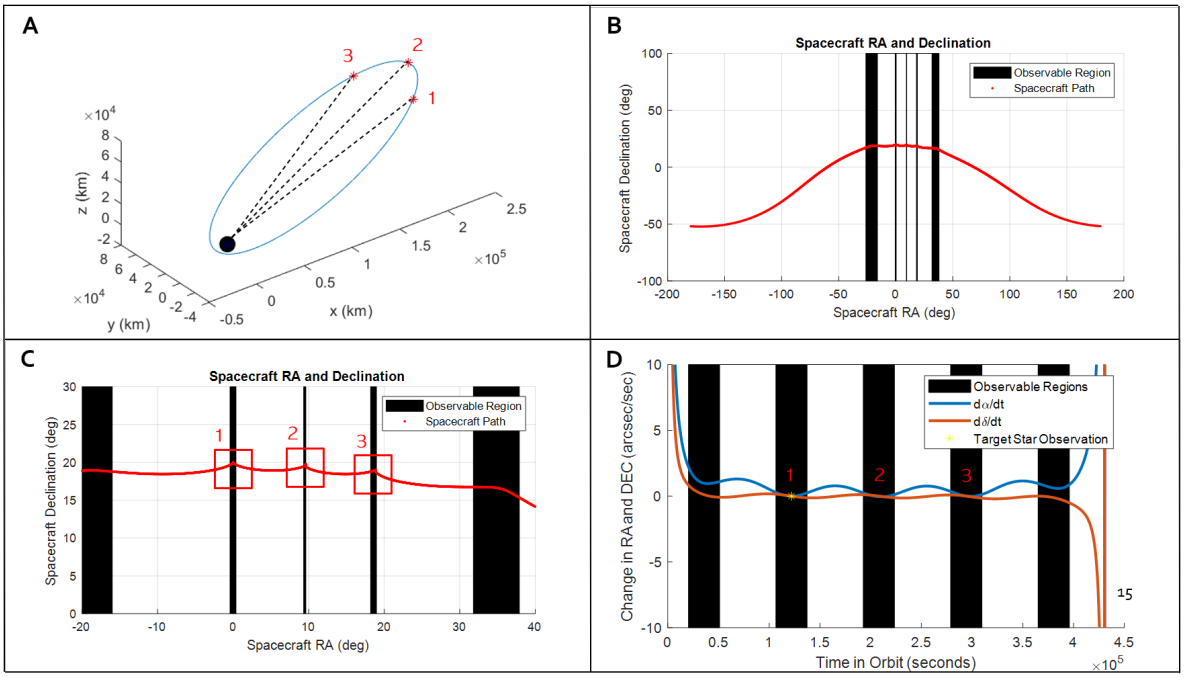

Fig 33 (A) Example orbit in ECI frame with a target star declination of 20° with dotted lines showing the line of sight to the locations in the orbit where AO observations can be made. (B) ORCAS spacecraft right ascension and declination over one orbit with observable regions where observation angle requirements are met in black. (C) ORCAS spacecraft RA and DEC showing the three AO observation points. (D) The change in right ascension and declination of the spacecraft over one orbit period with observable regions shown in black and the three AO observation points labeled.

Figure 33B shows the orbit trace on the right ascension and declination plane as seen from the ground telescope over one orbit period of five days. The black sections on the plot show the observable regions where the angle between the sun and the observatory zenith is greater than 110° and the angle between the observatory zenith and the line of sight vector to the target star is less than 60°. As shown in the figure, the orbit passes through the target star location in an observable region. In addition to being able to view the desired target star, there are two other points on the orbit where observations longer than 10 minutes can be made. These regions of interest can be seen in more detail in Figure 33C. Finally, the rate of change for right ascension and declination can be seen in Figure 33D. As shown, at the points where observation is occurring, the rate of change for both values is nearly zero, so the observation times will be longest there.

Figure 34 shows what the spacecraft trajectory would look like from the Keck Observatory when observing Teegarden's Star for one possible, but non-optimal, orbital solution.

The highly elliptical orbit was developed using two main guidelines for observation. The first is that the spacecraft must be on the line of sight from the observatory to the target star within a certain tolerance corresponding to the telescope field of view. The second is that the velocity of the spacecraft perpendicular to the line of sight should closely match the velocity of the observatory. The observation time can be increased by matching a slightly slower velocity at observation than that of the observatory, allowing a loop to appear in the field of view. Figure 35 shows the optimal orbital

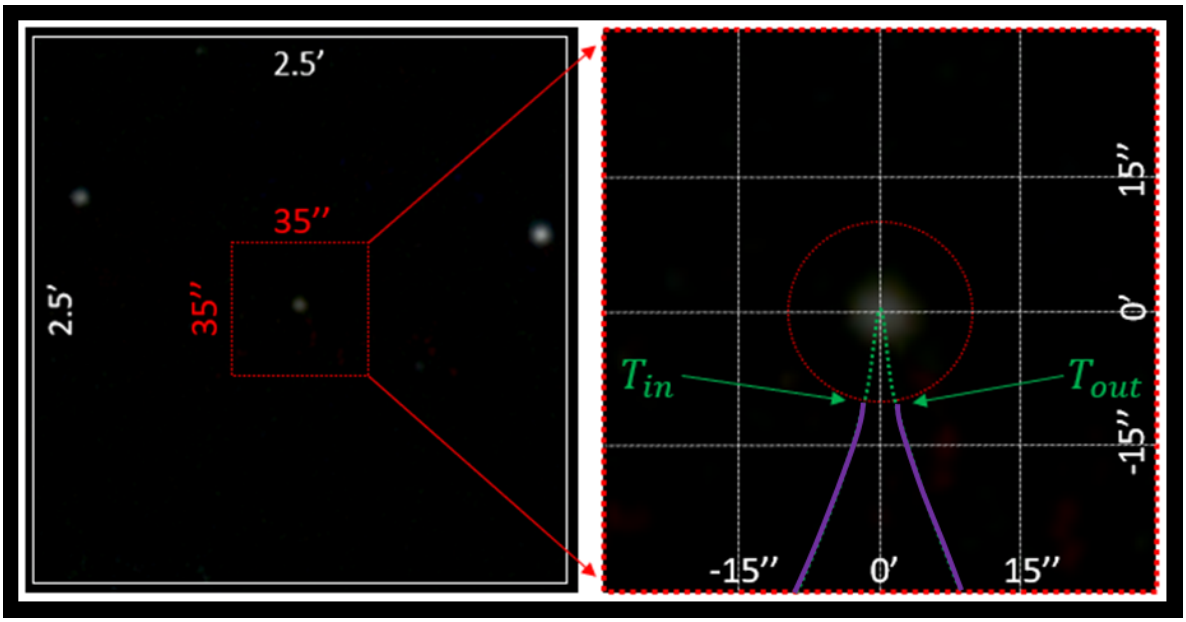

Fig 34 Spacecraft trajectory in the isoplanatic frame for a non-optimal orbit, during a one-hour observation of "Teegarden's Star", from W. M. Keck Observatory on the night of Dec 3rd, 2025. Left) Teegarden's Star as seen from Maunakea, white frame indicates 2.5 arcminutes field of view, while the red frame indicates 1 arcminute field of view. RA 43.2542 degrees Dec 16.8814 degrees. Right) An enlarged image of the red zone marked, red dashed circle indicated the FOI size, green dashed line indicates the natural spacecraft trajectory as seen from Maunakea, total time on target (within the FOI) is 3300 sec without using thrusters.

solution's observation times where the ORCAS spacecraft is within a 7.3 arcsecond field of view.

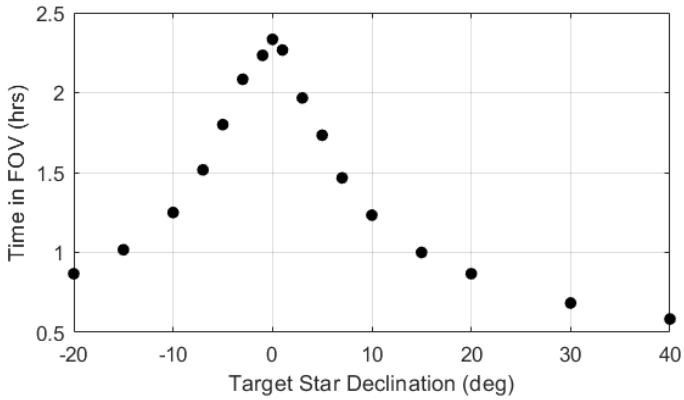

Fig 35 The amount of time in hours the ORCAS spacecraft will remain in a 7.3 arcsecond radius field of view as a function of target star declination. This data is for orbits which have been tuned for the optimal time in field of view.

Based on these results, for each orbit there are three points which can have observation times of at least ten minutes ranging to up to 2.5 hours based on the target star declination. Additionally, in the highly elliptical orbit, the majority of time is spent near apoapsis. This means that for about 3.5 days, the spacecraft is moving very slowly with respect to the observatory. In this time region, flux calibration observations could be made. Due to the orbit path, these will be at roughly the same declination

as the target star the orbit was designed for, but will be along a wide range of right ascensions.

5.1.2 AO and Flux Calibration Operations Concepts

ORCAS provides two observation modes in support of its mission science goals, AO and flux calibration, provided by the laser and the flux calibrator payloads respectively. In this section we discuss the established operation sequences, which describe the chronological order of all operational steps to be taken to enable each observational mode. An illustration of the operations sequence from T-2.5 days to T-12 hours for AO observations is shown in Figure 36.

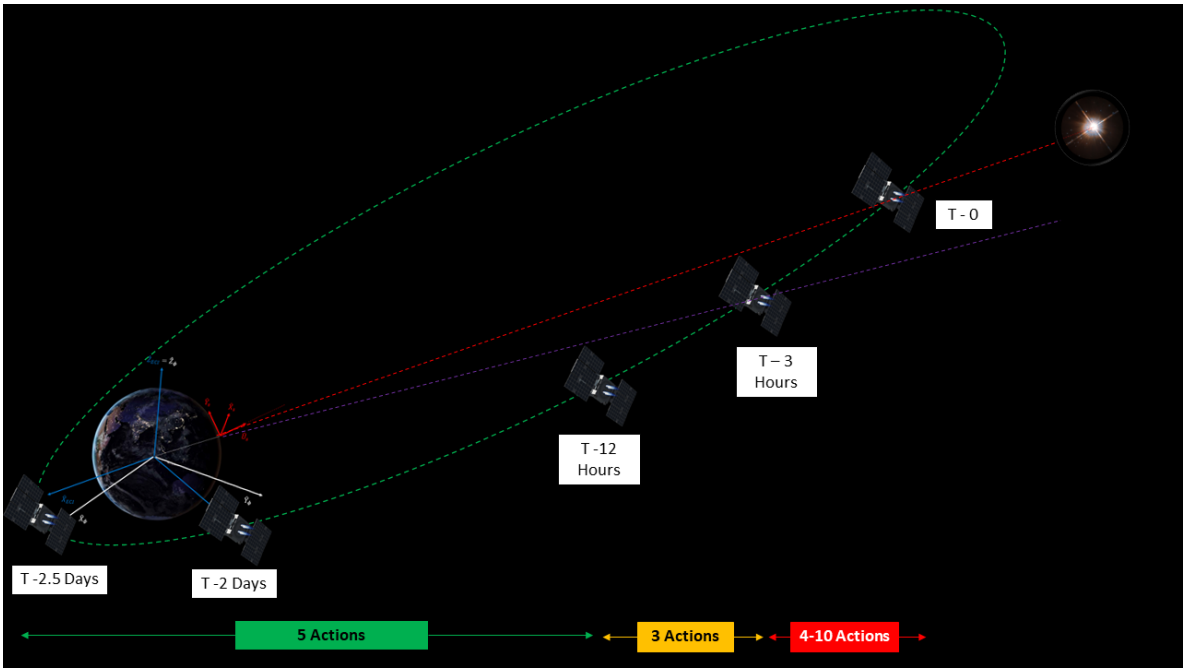

Fig 36 An illustration of the AO observation sequence.

Both observation modes share basic observational preparation activities as described in Table 17 that begin as the ORCAS spacecraft is near perigee. Note that this table lists optional sequences which can be done if enough time is available but are not required for every observation. For either case, orbit determination will take about 3 hours. The mission can verify the target scheduling sequence with Keck observatory up to 2.5 days prior to observation. Tests of the payload system and the go/nogo decision window can be 12 hours before observation. The total preparation time required for the observatory is about 3 hours, although because of the design of the orbit at least 2.5 days will be available for preparation. Note that many of the steps may occur in parallel, and not all these steps are required for every orbit. The time listed in the tables gives a rough estimate for when the events should take place. Note that the Keck telescopes are doing other observations during most of the preparations.

In Table 18, we detail the AO mode operations sequence. For a given observation, the ORCAS observing time, science target, AO science instrument and modes to be used, science ADC, and AO wavefront sensor would be prescheduled. The target list would be loaded for that night. The Keck telescope would slew to ORCAS at a pre-determined time in advance of ORCAS being within a prescribed distance from the science target. The AO system would be configured for an NGS AO observation with either the visible or infrared wavefront sensor prior to the end of the slew. The

Table 17 The chronological sequence of actions ORCAS can perform in preparation for either observation mode and the time at which the actions can be done.

Operational Actions	Time
Orbit Determination	T-2.5 Days
GPS Sampling rate 1Hz (near perigee sub meter accuracy)	T-2.5 Days
Mission Verify targets scheduling sequence, send to Keck	T-2.5 Days
Adaptive Optics Observation / Flux Calibration Prep	T-2 Days
Small Maneuver Corrections 1 Day Window	T-2 Days
Establish Keck observation configuration (EOC), including instrument Wavefront Sensor, (visible/IR), LGS power and divergence	T-1 Day
RF Ranging - S&X Band Sampling at 1Hz	T-12 Hours
Test Payload System Readiness	T-12 Hours
Go/Nogo Decision Window	T-12 Hours

detuned Keck laser would be projected with the prescribed power and maximum divergence. ORCAS would lock on the Keck laser and project either both ORCAS laser wavelengths, or the 532 nm laser wavelength only if the visible wavefront sensor is to be used, toward the Keck telescope. The ORCAS 532 nm laser would be detected and positioned on the science camera using the AO acquisition camera. The appropriate AO wavefront sensor would be positioned to acquire the laser at the detected location on the AO acquisition camera. The AO loops would be closed on the ORCAS laser.

The AO wavefront sensor would remain fixed. ORCAS position changes would be absorbed by the AO tip-tilt mirror which would be periodically offloaded to the Keck telescope pointing. If the AO infrared wavefront sensor is to be used the ORCAS 532 nm laser should be shuttered at this time. If a science instrument ADC is being used it should be set for the science filter in use. Science exposures can now be taken. The Keck laser power could potentially be reduced to the level needed to maintain ORCAS tracking to the observatory.

If dithering of ORCAS (and hence the science object) on the science instrument is required this should be able to be carried out in an automated sequence commanded from the science instrument: send move request to telescope, open AO loops, move telescope, close AO loops, start science exposure.

Table 19 covers the operations sequence required for observations using ORCAS for flux calibration. When the flux calibration payload is used near an astrostationary point, the spacecraft operations timeline needed by any Keck AO observations will first be established (see Table 18). Several steps can take place at T-12 hours, but these are not required for every observation. A test of the payload system readiness, the decision window, and beginning the internal calibrations can all begin all that point. ORCAS will provide the expected on-sky trajectory to the ground observatory. The ground observatory can select a usable guide star if tracking is being done.

The required steps for an observation begin at T-30 minutes. ORCAS will provide updates with the current location and anticipated trajectory during observation to the observatory thirty minutes prior to the star of observation. The ORCAS flux calibration payload exit beam will point towards the ground-based telescope twenty minutes before observation, and at the same time ORCAS will prepare the requested light sources.

An observation will be scripted according to the needs of the ground-based telescope being used. This could be the selection of a single wavelength, e.g., when flying over a wide-field telescope with a monolithic broadband filter, or cycling through multiple wavelengths quickly, e.g., to properly av-

Table 18 Time stamped adaptive optics operations sequence. Red items are for the spacecraft and blue items are for the observatory.

AO Observation Sequence	Time
Projected vs. Measured Trajectory comparison (MOC/SOC) ground	T-3 Hours
Keck System Configuration (AO, WFS, instrument)	T-3 Hours
Fine Maneuver corrections (1 Hour window)	T-3 Hours
ORCAS establishes communication with MOC to sync ops with Keck	T-3 Hours
MOC/SOC provide location to Keck update	T-2 Hours
Keck acquires science field location and centers (point telescope to ORCAS)	T-1.8 Hours
Keck - Detuned Laser Guide Star (LGS) (ground) projected toward science target	T-1.7 Hours
ORCAS body points laser payload FOV to the beam (LGS)	T-1.6 Hours
ORCAS Laser Payload Acquire LGS (Point to target, search pattern if not seen)	T-1.3 Hours
ORCAS Laser Payload locks and provides to required beam (based upon EOC)	T-1.2 Hours
Safety Gap (Second attempt to acquire if req.)	T-1.2-0.5 Hours
Keck AO system sets predetermined ORCAS power and wavelength, closes Keck AO loops and tracks ORCAS Source	T-0.5 Hours
Flight Dynamics provides Keck, MOC/SOC an updated ORCAS trajectory estimate (GPS + Optimetrics)	T-0.25 Hours
Begin Adaptive Optics Observation #1	T
End Adaptive Optics Observation #1	T + Δ T (minutes - hours)
Total Time	2-3 Hours

Table 19 Time stamped operations sequence for flux calibration. Red items are for the spacecraft and blue items are for the observatory.

Flux Calibration Observation Sequence	**Time**
ORCAS updates with current location and anticipated trajectory to ground-based telescope	T -30 minutes
ORCAS body points the flux calibration payload exit beam towards ground-based telescope	T -20 minutes
ORCAS prepares requested light sources	T -20 minutes
ORCAS activates one wavelength to ground-based telescope can confirm tracking & guiding (if desired)	T -10 minutes
Begin observation	T minutes
End observation	T + Δ T minutes
Total Time	30 minutes

erage over atmospheric seeing when observing multiple wavelengths during an exposure with a spectrograph.

The flux calibration payload will likely need to execute internal calibrations. These may include, for example, cross-calibrating photodiodes versus electrical substitution radiometers, and scanning the exit beam. If there is an on-board spectrometer for use with either an on-board broadband source or the Sun, it will require cross calibration as well. If light from the Sun is to be fed into ORCAS, movement of a gimballed mirror or a spacecraft maneuver will be required. Some internal testing will be requested when ORCAS has "set" as seen from ground-based telescopes.

It may be possible to coordinate observations of the ORCAS flux calibration payload with the Hubble Space Telescope or other LEO spacecraft. Many of the steps will follow those in Table 19, but there will be some differences; for instance, the decision window will not need to account for weather or day/night constraints.

5.2 Observation Schedule Optimization

Key Findings

- A sample mission sequence which outlines the proposed mission timeline is given in Table 20 in Section 5.2.1. The sequence outlines the maneuvers needed to get to the science orbit, the observation timeline and science lifetime, and de-orbiting at the end of the mission.
- The spacecraft will take 6.5 months from launch to reach its science mode orbit. It will then be active for up to 3 years, completing around 100 observation orbit cycles. At the end of its lifetime, it will de-orbit over 4 months.
- In Sections 5.2.2-5.2.4, we detail the development of a robust and flexible schedule optimization algorithm which can successfully perform 300 AO observations, double the stated 150 observation requirement, across the 3 year mission lifetime with the given fuel budget.
- The algorithm has the ability to be altered in real time during the mission if new targets are chosen, or in the event that low visibility or weather events interfere with an observation and it needs to be repeated.

5.2.1 Mission Lifetime

A sample mission sequence which outlines the proposed mission timeline is given in Table 20. The mission starts out with release from the Artemis spacecraft at about 36,000 km. The spacecraft then goes through a series of maneuvers to get it into the proposed orbit, which was detailed in Section 5.1.1. The spacecraft will be in position about 6.5 months after launch. At that point, observations can begin. Orbit determination will take 2.5 days, and the AO observation preparation will take an additional 40 hours. Then, a series of observations, each taking about 3 hours, will begin, with 21 hours between observations. Once observations are completed, the spacecraft will transfer to the next science orbit, which depending on the orbit will take five to thirty days. The total observation sequence therefore is on average about 15 days, and this sequence will be repeated about 100 times to allow for observations of as many target stars as possible. Once the mission is finished, de-orbit will take 120 days.

5.2.2 Optimization Requirements and Guidelines

In this section we detail the requirements for the mission planning tool developed which optimizes the order in which the target stars are viewed. We would like to conduct observations at night, reasonably close to zenith, and with minimal spacecraft glare. Following observatory standards, we allow observations at times when the sun is more than than 18 degrees below the horizon, and require observations to occur within 60 degrees of the observatory zenith to reduce the mass of air being observed through. We mitigate reflection by allowing the significant reflecting surfaces of the spacecraft to be deflected up to 40º from the spacecraft-observatory LOS to the point where the sun is behind its earth-facing surfaces. These imply requirements on the spacecraft configuration. For a detailed analysis on how the observable sky is built, see (121).

Table 20 Mission Timeline

Sample Mission Sequence		
Commissioning	Release spacecraft Maneuver to science orbit	6.5 Months
Science (Single Observation Orbit)	Orbit Determination, Verify target schedule at Keck Adaptive Optics Observation Prep	2.5 Days 3 Hours
	Observation #1 - Imaging Drift to next observation point	3 Hours 21 Hours
	Observation #2 - IFU Drift to next observation point	3 Hours 21 Hours
	Observation #3 - Imaging Flux Calibration	3 Hours 3 Hours
	Transfer to next science orbit - will be done about every 2 orbits to allow repeat observations	5-20 Days
	Total time for 1 observation sequence	10 Days
Total Science Lifetime	Repeat 10-day observation sequence (3 AO observations each) up to 110 times	3 years
End-of-Life	De-Orbit and Disposal	120 Days

These constraints determine the times of night that each given target may be observed on a desired observation date. We pre-compute each star's maximum achievable observation duration, times and expected zenith angle range for each day of the year. The map of maximum observation time can be seen in Figure 37. The contoured region corresponds to the integrated area under a spherical sector rotating around the Earth over night with a region of forbidden spacecraft positions removed.

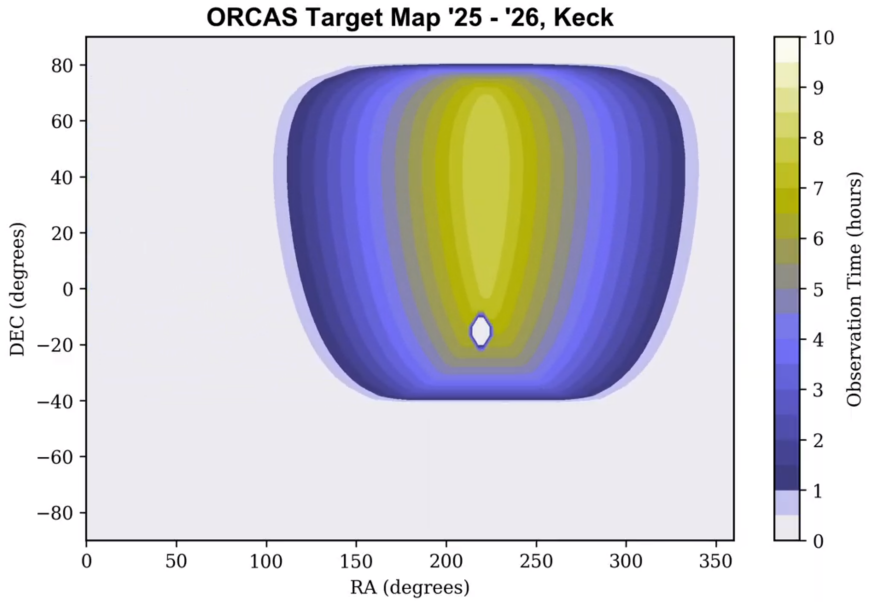

Fig 37 The Observable Sky for ORCAS working with Keck on a night in June, contoured according to available observation time for each possible celestial coordinate. Each location in this map requires a different orbit choice to achieve the astro-stationary condition.

Transferring between targets is, at a basic level, the process of re-configuring to a new orbit in

the ORCAS HEO family which is designed for the desired target star. As informed by collocation-optimized low thrust orbital reconfiguration simulations, we find that the propellant cost of inter-target transfers can be upper-bounded in direct proportion to the angular distance between targets, approximately 30 m/sec/deg, and approximately extended to large transfers by dividing it into the smallest achievable number of intermediate orbits. With estimates of each possible target's value, conditions of observation and the costs of traversing between them in hand, it is possible to optimize the mission profile for maximum delivered value within its required operational constraints (lifetime and propellant).

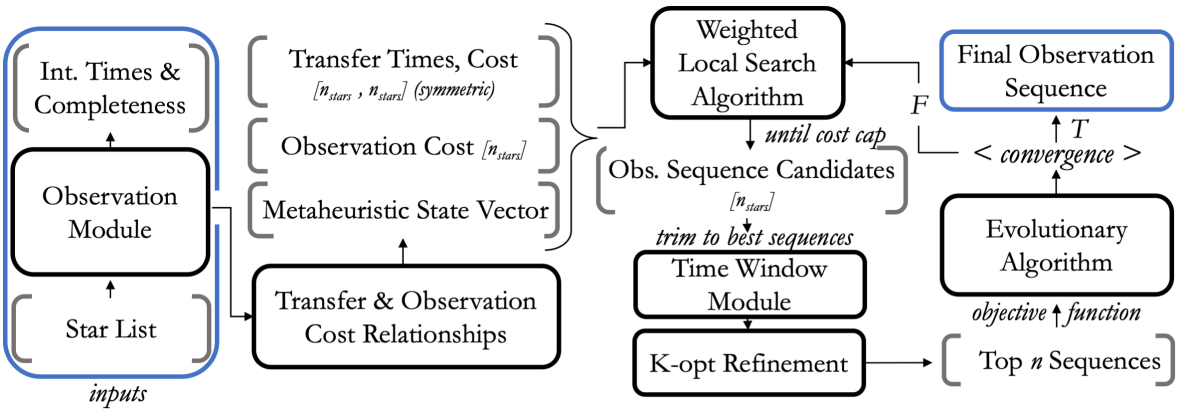

Fig 38 Sequence-Optimizing algorithm flowchart.

We have developed a metaheuristic (genetic) algorithm to explore and optimize this very high dimensional time dependent travelling salesman problem— over a range of future and current scientific objectives and engineering constraints. An overview of this optimization method is provided in Figure 38, and a detailed presentation in (122), (123).

5.2.3 Mission Parameters

For the optimized results presented in this report, we used baseline value of 4000 m/s ΔV less 700 m/s of propellant consumption during cislunar drop-down, a 3 year mission starting December 1st, 2025, and one intermediate 'buffer' orbit between each reconfiguration and subsequent observations. To prioritize interesting targets, we scale their relative value — on top of their observability and, in the case of exoplanets, expected completeness— by a combined weight of uniqueness in the target list data-set and a heuristic 'desirability' factor informed by mission science cases. For instance, M87 is considered valuable. Regions such as the HDF or XMM-LSS are modelled by a discrete set of between 6-10 observation 'targets' over their surface. We do not include solar system bodies at this stage, but work is ongoing to include them- we expect many observation opportunities for targets near the ecliptic.

5.2.4 Science Yield from Schedule

Two unique sequences using our schedule optimization code have been generated for two scientific target priority scenarios, as presented below. Figure 39 illustrates the motion of ORCAS across the sky as it performs observations throughout the mission lifetime.

Each target identified within Figure 39 is only the primary target observed near apogee. Each is allocated two observation orbits. For each orbit there is an opportunity for two additional observations

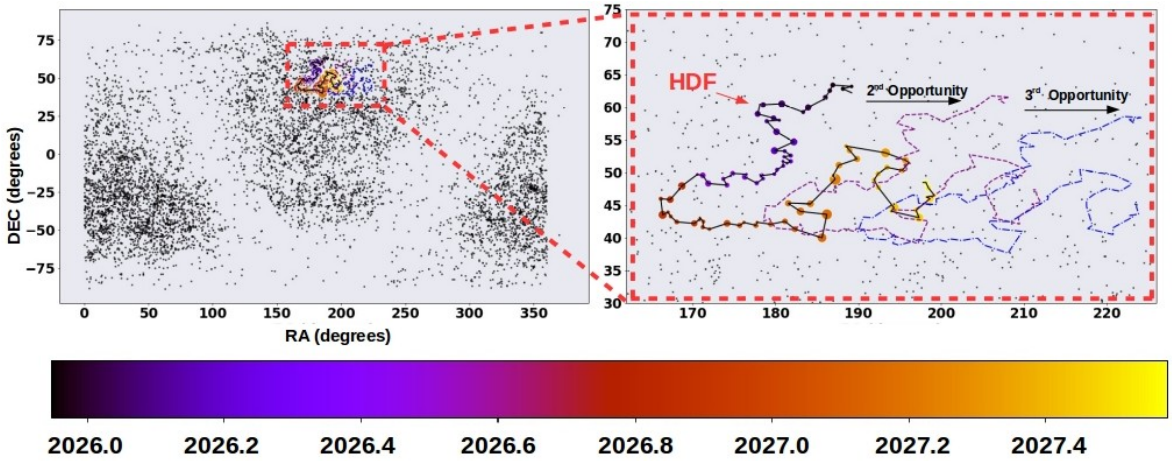

Fig 39 Targets with ORCAS across a 3-year mission lifetime. The size of each observation corresponds to the total cost to observe, and the color corresponds to the time (in years) that has already passed. There are 285 AO observations in this sequence containing the Hubble Deep Field (HDF), and are spread across 2 additional observing opportunities as seen in the purple and blue curves. This sequence serves only as an example and not as a final mission observing schedule.

on the nights at and following apogee across a stretch of sky approximately +- 10 degrees RA. Work is ongoing to identify the fraction of these secondary observation opportunities which can be made on targets in our list. In general we find that more heterogeneous target priorities reduce the total number of optimal target list observations, as they produce a mission profile that stretches over a larger range of sky in reaching 'desirable' targets. To understand how sensitive our schedule optimization is to different orbits and fuel cost, please refer to the Appendix A.9.1. Currently, the existing tool can meet all mission requirements, but improving the method of viewing three targets per orbit could increase the science yield of the mission.

6 Mission Development Approach

Key Findings

- We present the ORCAS science team, including each member's role and contribution, in Section 6.1.
- Section 6.2 provides an estimated cost breakdown. The overall estimated mission cost for ORCAS is **$71.8M** including a space contingency of 30% and a ground contingency of 15%.
- A risk matrix for the project is presented in Section 6.3. The project overall is low risk. The medium and high identified risks are detailed in Table 25 along with their mitigation approaches.
- The mission development schedule is presented in Section 6.4. If work on the ORCAS mission begins in January of 2022, ORCAS will be ready for a March 2026 launch date.
- The ORCAS project plan is currently at a high TRL and a low hardware risk. Section 6.5 outlines the TRL of all ORCAS subcomponents.

6.1 Science Team

The ORCAS team has multiple roles and responsibilities, according to mission phase. The team is currently developing the scientific objectives, simulating and planning observations, and analyzing the necessary instrument and AO capabilities to meet the mission objectives. They are also working with W.M. Keck observatories and hardware development communities to develop a consensus view of hardware plans and operational processes and policies, bearing in mind the many possibilities for obtaining support from NSF, NASA, and partner organizations. The ORCAS team will also be responsible for writing the scientific objectives and observing plans for a NASA flight mission proposal. During the design and construction of the ORCAS system, the science team would participate in design trade studies affecting scientific results and would review the implementation to confirm that the original objectives will be met. If that proposal calls for a specific observing program that is already approved by the Keck Observatory, and it is approved and funded by NASA, then the ORCAS science team would be funded to analyze the observations.

It is also envisioned that the ORCAS/Keck system will be available to all US astronomers, through the NASA share of the Keck observing time, currently at approximately 1/6th of the total time available, and/or through collaboration with other Keck partners. NASA's share of the Keck observing time is allocated by a proposal process, which may need to be modified to allow for the additional NASA contribution to Keck, for the original scientific program to be submitted to NASA, and additional observing time requests to support ORCAS. A key issue will be the interaction between the scientific team proposing to NASA, and the larger user community. Keck community advice will be sought.

The ORCAS Science Team is presented in Table 22. The science team is composed of highly experienced interdisciplinary scientists and engineers from several research institutions. Principal Investigator Eliad Peretz leads the ORCAS mission and is the Lead Researcher for New Space Missions at NASA Goddard Space Flight Center. Project Scientist John Mather is the Senior Project Scientist for the James Webb Space Telescope. Co-I Stefanie Milam serves as the Deputy Project Scientist

for Planetary Science for JWST to evaluate science and operation decisions to assist with the telescope's capability to observe the solar system. Joining Co-I Milam is Imke de Pater; she has extensive experience within planetary science, specifically her work on Jupiter's Synchrotron radiation.

Co-I's Shobita Satyapal and Peter Kurczynski will lead the Active Galactic Nuclei science. Satyapal is an observational astrophysicist with a deep interest in understanding how AGN operate as well as conditions required to form super-massive black holes. Kurcyznski currently serves as the Chief Scientist of NASA's Cosmic Origins Program. Sibasish Laha is a mult-wavelength astronomer at NASA GSFC focusing on the properties of supermassive black holes and will be working alongside Satyapal and Kurczynski. Co-I Peter Plavchan will lead the Exoplanet science case; he will bring his experience as an observation exoplanet astronomer serving as the PI for NASA Probe Mission concept EarthFinder and serving on the Executive Committee for ExoPAG. Additionally, Co-I Max Millar-Blanchaer will be working on the Exoplanets science case; Max has experience performing high contrast imaging to observe exoplanets and focuses on polarimetry to assist with characterization.

The supernovae science case will be led by Co-I Greg Aldering. Aldering co-discovered dark energy using supernovae and served as a co-investigator of the Supernova/Acceleration Probe (SNAP). Aldering will also be leading the Flux Calibration science case alongside Co-I Justin Albert. Albert directed the ALTAIR/STARCal project producing calibrated light sources flown on high altitude balloons to calibrate ground observatories. Co-I Rogier Windhorst will lead the High Redshift Universe science case. Rogier has contributed significantly to better understand the formation and evolution of distant galaxies; he is also one of the Interdisciplinary Scientists for JWST. Co-I John O'Meara will also be a part of the High Redshift science case; he serves as the Chief Scientist at the Keck Observatory.

Table 21 ORCAS Science Team Members

Name	Affiliation	Role	Contribution
Eliad Peretz	NASA/GSFC	Principal Investigator	PI
John Mather	NASA/GSFC	Co-Investigator	Project Scientist
Justin Albert	UVic	Co-Investigator	Flux Calibration
Greg Aldering	LBL	Co-Investigator	Flux Calibration & Supernovae
Peter Kurczynski	NASA/GSFC	Co-Investigator	AGN
Robert Lafon	NASA/GSFC	Co-Investigator	Laser System
Stefanie Milam	NASA/GSFC	Co-Investigator	Solar System
John O'Meara	W.M. Keck Observatories	Co-Investigator	High Redshift
Imke de Pater	UC Berkeley	Co-Investigator	Solar System
Saul Perlmutter	UC Berkeley	Co-Investigator	Flux Calibration & Supernovae
Peter Plavchan	GMU	Co-Investigator	Exoplanets
Shobita Satyapal	GMU	Co-Investigator	AGN
Rogier Windhorst	ASU	Co-Investigator	High Redshift
Peter Wizinowich	W.M. Keck Observatories	Co-Investigator	Ground Observatory
Aaron Barth	UC Irvine	Collaborator	AGN
Randall Campbell	W.M. Keck Observatories	Collaborator	Ground Observatory
Gabriela Canalizo	UC Riverside	Collaborator	——-
Matt Cristina	General Atomics	Collaborator	Laser
Gianluca Di Rico	INAF	Collaborator	——-
Josh Duncan	BCT	Collaborator	Spacecraft
Aaron Freeman	General Atomics	Collaborator	Laser
Karl Gebhart	University of Texas	Collaborator	——-
Kelsey Gilchrist	University of Chicago	Collaborator	Study
Eric Golliher	NASA/GSFC	Collaborator	Propulsion
Kevin Hall	University of Maryland	Collaborator	Study
Christine Hamilton	Stanford University	Collaborator	Study
Erin Hicks	University of Alaska, Anchorage	Collaborator	——-
Douglas Hyland	General Atomics	Collaborator	——-
Stephanie Juneau	NOAO	Collaborator	——-
Marc Kassis	WMKO	Collaborator	——-
Mike Koss	Eureka Scientific	Collaborator	——-
Daniel Küsters	UC Berkeley/DESY	Collaborator	Flux Calibrator
Sibasish Laha	UMBC	Collaborator	AGN
Jessica Lu	UC Berkeley	Collaborator	High Redshift
Matthew Malkan	UCLA	Collaborator	——-
Claire Max	UC Santa Cruz	Collaborator	——-
Kyle McCormick	General Atomics	Collaborator	Laser
Adam Michaels	NASA/GSFC	Collaborator	Navigation
David Michelson	UBC	Collaborator	Flux Calibrator
Max Millar-Blanchaer	UCSB	Collaborator	Exoplanets
Ellouise Moehring	Purdue University	Collaborator	Study

Table 22 ORCAS Science Team Members

Name	Affiliation	Role	Contribution
Francisco Mueller Sanchez	University of Memphis	Collaborator	——-
Rebecca Oppenheimer	AMNH	Collaborator	Exoplanets
Lucas Pabarcius	NASA/GSFC	Collaborator	Study
Piotr Pachowicz	GMU	Collaborator	Outreach
Elisa Portaluri	GMU	Collaborator	——-
Robert Pritchett	NASA/GSFC	Collaborator	Navigation
Joe Rice	NIST	Collaborator	Flux Calibrator
Barry Rothenberg	LBT	Collaborator	——-
Sara Seager	MIT	Collaborator	Exoplanets
Richard Slonaker	NASA/GSFC	Collaborator	Study
Mark Stephen	NASA/GSFC	Collaborator	Laser
Mark Storm	Fibertek	Collaborator	——-
Geronimo Villanueva	NASA/GSFC	Collaborator	Planetary Sciences
Vivian U	UC Irvine	Collaborator	——-
Wayne Yu	NASA/GSFC	Collaborator	Navigation

6.2 ORCAS Cost Estimates

Key Findings

- ORCAS estimated mission cost is **$71.5M** including a ground-based contingency of 15% and a space-based contingency of 30%.
- We provide a phased spending plan for the mission as well as an estimated cost breakdown structure for the space, ground, payload, and mission operation expenses.

During the ORCAS Concept Study, cost estimates were gathered for each component of the mission: ground systems, spacecraft, payload, and mission operations. A Request For Information (RFI) cost estimate (in the fiscal year 2021 dollars (FY21$)) was requested for all effort to implement the proposed approach for the hardware unit quantities. The cost estimates were broken down into design and development, including all effort to design, develop, build, and test, including development units and ground test sets.

The team conducted grassroots cost estimates to accurately determine the total cost of the mission. The collaborative effort of many organizations results in cost estimations specific to each. In February 2021, ORCAS produced a RFI for the ORCAS laser, photometric calibration, spacecraft, partnership, and advice:

1. Concepts and designs for the development of the Adaptive Optics (AO) Laser source
2. Concepts and designs for the development of the Flux calibration source
3. Concepts and designs for the spacecraft bus
4. Scientific advice for the adaptive optics systems and photometric calibration systems
5. US and international partnerships, capable of providing access to other observatories and instrument systems

For this RFI, a quantity of one full source payload complement was assumed when developing plans and cost estimates. To enable assessment of cost estimates and trades involving other quantities of systems, the cost estimate to develop the first unit, four units, and each additional unit was requested. After reviewing the responses received, ORCAS selected those which most favorably met the mission requirements and formulated a baseline mission cost (Table 23).

Costs include full system integration, test, launch, and commissioning activities, including all effort to integrate the hardware, perform full system performance and environmental test, launch site activities, and commissioning as requested per the **RFI**. Each system utilizes a different portion of the budget as the project progresses to each phase. The cost breakdown per scheduled project phase (see ORCAS schedule, Figure 42) is demonstrated via Figure 40.

Table 23 Mission Cost Estimate

ORCAS Mission Cost Estimation		
WBS	**System**	**Mission Expenses (FY21$)**
1	W.M. Keck Ground Adaptive Optics System*	$8,311,500**
2	W.M. Keck Visible Science Instrument	$9,500,000**
3	Spacecraft Bus Design and Development	$20,050,000
4	Payload - Laser Source	$6,400,000
5	Payload - Flux Calibrator	$ 9,000,000
6	Operation (GSFC)	$4,250,000
	Ground-Based Contingency(15%)	$3,009,225
	Space-Based Contingency(30%)	$10,635,000
	Total	**$71,455,725**

*operations on ground system operations are included in WBS 1
**proposed upgrades may be approved in the coming year and result in lower mission costs, including savings of up to $\tilde{\$}$1.5 million dollar for WBS 1, and up to $\tilde{\$}$3.5 million dollar for WBS 2.

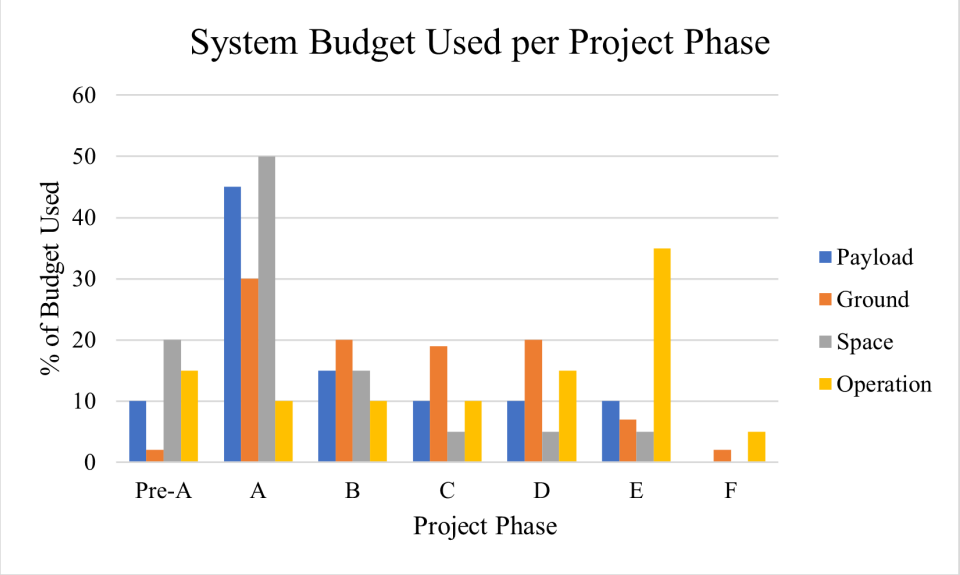

Fig 40 Budget used per scheduled project phase.

Table 24 Work Breakdown Structure of ORCAS mission

WBS (Work Breakdown Structure)		
WBS	**Task**	**Cost (with inflation)**
W.M. Keck Ground Adaptive Optics System		
1.1	Direct Labor Cost	$4,165,000
1.2	Procurement	$3,344,000
1.3	Travel	$52,500
1.4	Indirect Costs	$750,000
	WBS 1 Total	$8,311,500
Spacecraft Bus Design and Development		
3.1	Labor, Recurring Engineering	$2,253,616
3.2	Material	$6,308,565
3.3	Supplier Material	$10,476,449
3.4	Container and Shipping	$116,595
4.5	Full System Integration, Test, Launch, and Commissioning Support Activities	$850,000
	WBS 3 Total	$20,005,225
Payload Laser Source		
4.1	NRE for Design, Integration, Test	$5,460,000
4.2	Material Cost	$345,000
4.3	Manufacturing Engineering & Oversight	$445,000
4.4	Program Management, Travel & Oversight	$150,000
	WBS 4 Total	$6,400,000

The AO ground systems procurement budget by work breakdown structure is estimated to be **$8.3M**. This AO budget would be reduced by $2M if the NSF MRI HAKA proposal was funded to implement a high order DM for the Keck II AO system. The ORCAS RFI responses produced a

total of four spacecraft designs to be considered (see appendix). The estimated cost of the selected spacecraft is **$20M**, including design, full system integration, test, launch, and commissioning support activities. The payload laser system is estimated to cost **$6.4M**. These expenses includes design, integration, testing, management, and oversight by the selected organization. More information and specific details of cost breakdown can be found in Appendix. The ORCAS mission operations will be conducted largely by NASA GSFC. The cost of labor by civil servants, contractors, subawards, and other expenses are included in the GSFC operations cost.

6.3 Risk Assessment and Mitigation Plans

Risk assessment is a key step for any NASA mission. We used NASA's risk management process to identify project risks. The overall hardware risk for the project is low, and ORCAS has a high technology readiness level. There are several commercial options available for the ORCAS spacecraft. The AO system required can be developed and tested based on natural guide stars before ORCAS launches. Precise orbit management was established for the Magnetospheric Multiscale Mission (MMS) using high altitude GPS and the same system is the baseline for ORCAS. Orbit optimization is already available with established tools.

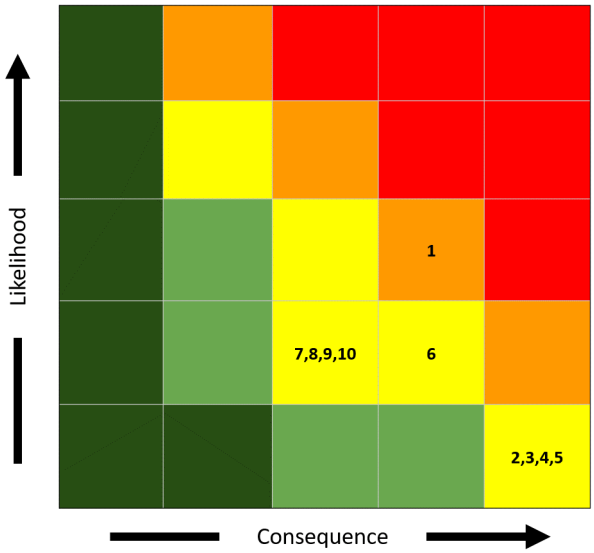

Fig 41 The risk matrix for the ORCAS mission.

The risk matrix for the ORCAS mission is shown in Figure 41. The medium and high category risks are identified in Table 25, which describes each risk and its likelihood, consequence, and resulting impact. The approach for risk mitigation for each item is also described.

Table 25 A table of the high and medium category risks for the ORCAS mission and their associated approach for risk reduction.

ID#	Risk	Likelihood	Consequence	Impact	Mitigation Approach
1	Schedule Slip due to Funding or Late Delivery of Key Ground Components	3	4	High	4.2 years have been allocated to mission development to enable schedule flexibility.
2	Laser System Failure	1	5	Medium	The laser is built to provide both 532 and 1064nm wavelengths so the system is redundant. The laser uses high TRL components.
3	Propulsion System Failure	1	5	Medium	The propulsion system has four separate engines. We have baselined usage to the TRL 9-tested performance of the thruster.
4	Time in Umbra Leads to Bus Cooling	1	5	Medium	Minimize or avoid umbra crossings. Reduce the size of bus radiators to slow cooling time.
5	Thruster Plumes Contaminate Receiver Optics	1	5	Medium	Design the location of thrusters and the ejection nozzle direction to minimize interference. An optional baffle could be added if needed.
6	Relative Orbit Path Not Known to 5mas	2	4	Medium	The mission is designed to exceed this requirement to 3mas. There is redundancy in our measurement systems (NSN, GPS, ground telescope).
7	Single Thruster Failure	2	3	Medium	Four thrusters are baselined to support mission objectives.
8	Access to Keck Observing Time	2	3	Medium	Integrate the Keck and Goddard teams to ensure both are invested in making ORCAS observations.
9	Ground System does not Achieve Required Performance	2	3	Medium	The mission is designed for threshold requirements that are lower than the expected performance of the ground system.
10	Non-Optimal Propulsion Maneuvers Required	2	3	Medium	Include umbra calculations in optimization software to ensure this is accounted for in mission planning.

6.4 Mission Development Approach

Key Findings

- The schedule for the mission is summarized and outlined in Figure 42.
- If work on the ORCAS mission begins in January of 2022, ORCAS will be ready for a March 2026 launch date.

6.4.1 Development Schedule

Based on the design work outlined in this chapter, the mission development schedule was created and can be seen in Figure 42. If ORCAS is approved to go forward, pre-phase A would begin in January of 2022. At that point, design and fabrication of both the ground segment and the payload would begin. The payload would include both the laser and the flux calibrator systems. For the ground segment, design would take a total of 26 months, and then fabrication would take an additional 12 months and integration and testing would take another 12 months. Design and fabrication of the payload would also take 26 months, and assembly, integration, and test would take 12 months.

The mission would be ready to launch in March of 2026 and would have a lifetime of 3-5 years. At the end of the mission, it would take 4 months to de-orbit and safely dispose of the ORCAS spacecraft.

Space Segment	**Pre-Phase A**	**Phase A**	**Phase B**	**Phase C**	**Phase D**	**Phase E**	**Phase F**
	Concept Studies	**Concept & Technology Development**	**Preliminary Design & Technology Completion**	**Final Design & Fabrication**	**System Assembly, Integration, Test & Launch**	**Operations & Sustainment**	**Closeout**
	Feasible Concept	**Top-Level Architecture**	**Functional Baseline**	**Allocated Baseline**	**Product Baseline**	**As-Deployed Baseline**	
Duration (months)	6	10	10	12	12	36-60	4
Start Date	1/1/2022	7/1/2022	5/1/2023	3/1/2024	3/1/2025	3/1/2026	
Ground Segment	**Design, Fabrication, Integration & Testing**					**Operations & Sustainment**	**Closeout**
	System Design	**Preliminary Design**	**Detailed Design**	**Fabrication**	**I&T**	**Science**	
Duration (months)	6	10	10	12	12	36-60	4
Start Date	1/1/2022			3/1/2024		3/1/2026	
Payloads	**Design and Fabrication**			**System Assembly, Integration, Test**		**Operations & Sustainment**	**Closeout**
Duration (months)	26 (Laser Payload)			+12 (Flux Calibrator)		36-60	4
Start Date	1/1/2022			3/1/2024		3/1/2026	

Fig 42 The ORCAS mission development schedule.

6.5 Technology Readiness Level Assessment

The ORCAS project plan is currently currently at a high TRL and has a low hardware risk. The TRL for each subsystem of ORCAS is outlined in Table 26.

Table 26 Table outlining the technology readiness level of ORCAS subsystems.

ID#	Payload	TRL	Notes
Space Payload			
1	Spacecraft	9	The three proposed spacecraft designs would achieve TRL 9 by 2021.
2	Laser System	6	Two companies have provided mature conceptual designs based on their existing laser communications space terminals. On-orbit performance data for both company's existing laser communications terminals likely to be available by end of year.
3	Flux Calibrator	3-4	Preliminary design has not yet converged. Many approaches that have previously been used could be used together for the design. May be significan risk in achieving 0.4% flux knowledge on the first ORCAS spacecraft.
Ground-Based System			
4	Adaptive Optics	8	Three major AO upgrades are currently under development at Keck. All can be tested on natural guide stars prior to launch of ORCAS.
5	Keck Instruments	8	Both existing instruments at Keck and instruments in development will be used.
6	ORCAS Ground Systems	8	Updates can begin once project is approved, low risk because systems can be tested on natural guide stars prior to launch of ORCAS.

As shown, the only high risk item is proving the desired 0.4%, or better, accuracy of a photometric calibrator. This is needed for flux calibration observations. The current plan for this gap can be seen in more detail in Section 4.3.2. The team currently has concepts for how to get this accuracy, but no preliminary design has been created yet. However, since flux calibration observations are a bonus giving extra observations this risk is not mission critical. AO observations would not be affected.

7 Technology Challenges and Future Trade Studies

Key Findings

- Section 7.1 discusses potential future trade studies, including different science cases, using other observatories, and using multiple spacecraft.
- Details on the future technology required for ORCAS to be successful, including the Keck Spectrometer, optical interferometers, and compatibility with other observatories, are presented in Section 7.2.

7.1 Future Trade Studies

The initial plan for ORCAS has been presented in this report, but several future trade studies can be conducted to provide additional options regarding cost and science cases.

Currently, ORCAS is aimed at multiple science cases. One trade study which could be conducted is whether we want to be a multi-science case mission or a single science case mission with some ancillary observations. Since the AGN science case is the strongest so far, one option is that we focus only on AGN observations and not include flux calibration observations. Alternatively, we could have the mission only do flux calibration observations. In that case, fewer ground system updates would be needed, so the cost of the mission would be much lower, but the science achieved would also be lower.

Another possibility is the type and number of observatories that can work with ORCAS. Right now, ORCAS will work with the W. M. Keck Observatory, but if it was able to support additional observatories at different times of night, ORCAS could become a global service. We could also look at working with different instruments, such as interferometers, and expand the science cases we are able to support.

The current proposal is for a single spacecraft, but a trade study could be done looking at using a constellation of spacecraft. This could allow for longer observation times as multiple spacecraft pass through a telescope's field of view. Alternatively, different spacecraft could be used to do completely different observations on the same night, increasing the science yield. Different ORCAS spacecraft could pair with different observatories on different nights, since it is most fuel efficient to look at one section of sky with a single ORCAS satellite. This could significantly increase science yield, but would also increase costs.

7.2 Future Technology

7.2.1 Keck Spectrometer

In order to fully exploit ORCAS, Keck will need a new spectroscopic instrument. Currently Keck has no visible instruments with the required spatial resolution. Keck's NIR instruments OSIRIS, MOSFIRE, NIRC2 and NIRSPEC can obtain spectra in one band at a time, requiring 4–7 set-ups. Thus, while suitable for single emission/absorption line complexes at known wavelength (i.e., known redshift for extragalactic targets), but is inefficient for broad wavelength coverage and/or for targets with unknown redshift. Keck's NIRES slit spectrograph does provide continuous NIR coverage in an Echelle mode, but it's throughput is low, both at the blaze peaks and further when accounting for the blaze function for each order. For the high-spatial resolution that ORCAS will provide, telescope pointing for faint targets is challenging to say the least; an integral field spectrograph (IFS) alleviates this challenge.

From this we conclude that to fully exploit ORCAS for our key science casees we require an IFS, with high spectral resolution at selected visible wavelengths for AGN spectroscopy, and with broad-band simultaneous visible plus NIR coverage for spectroscopy of faint cosmological supernovae.

In order to implement the SN Ia twinning method (Section 2.2), ideally the restframe 0.33–75 μm should be covered, as indicated in Table 4. For SNe Ia $0.5 < z < 1.7$ this translates to wavelength coverage $0.5 < \lambda < 2.0$ μm. The only dispersing element able to cover this broad wavelength range with high throughput is a prism. Prisms are usually used in low resolution of 100-200, and indeed low resolution is needed in order to pack the spectra onto a single detector, such as a 4k×4k H4RG. Fortunately, SN classification and use of the twinning method for SNe Ia is able to work at low resolution since SN line widths are of order 10^4 km/s, e.g., requiring a minimum $\mathcal{R} > 30$. The line positions can move around by several thousand km/s, so measuring those changes push towards $\mathcal{R} \sim 200$ or so.

One can write the wavelength at pixel i along a spectrum as:

$$\lambda_i = \lambda_{\rm min}\ (1 + 1/\mathcal{R})^i \tag{1}$$

from which one can determine the value of $i_{\rm max}$ that gives $\lambda_{\rm max} = 2.0$ μm given $\lambda_{\rm min} = 0.5$ μm as

$$i_{\rm max} = \frac{\log_{10}(\lambda_{\rm max}) - \log_{10}(\lambda_{\rm min})}{\log_{10}(1 + 1/\mathcal{R})} \tag{2}$$

Rounding up to the nearest integer gives $i_{\rm max} = 139$ for $\mathcal{R} = 100$ and 278 for $\mathcal{R} = 200$. Since the resolution is defined such that each resolution element is sampled by two pixels on the detector, the length of our spectra will be 278 or 556 pixels, for $\mathcal{R} = 100$ or 200, respectively. Packing these spectra onto a H4RG with a microlens type IFS allows for 56×60 or 44×52 spatial elements, over the visible plus NIR wavelength range (see Figure 43). The microlens IFS would have 3360 or 2288 spatial resolution elements. An image-slicer type IFS would fit a field with 14 or 7 pseudo-slits, respectively, possibly laid out as 17 or 24 physical slices per pseudo-slit. The net number of spatial resolution elements for such an image-slicer would be about 57344 or 28672.

For the AGN case, specific wavelengths need to be covered, and high resolution is needed. In the NIR, the existing Keck AO instruments can be used. In the visible, if it is possible to implement an observing mode that swaps a grating for the prism, and windows the spectra to fit within the same length as for the prism mode, it would be possible to pack the high resolution spectra onto a H4RG using the same image segmentation (microlens or slicer) optics. For example, Eq. 2 indicates that wavelength windows of 1.4% or 2.8% for $\mathcal{R} = 10000$ would fit in the same footprint on the detector. Around Hα this would be a wavelength window of 92 Å or 185 Å. This would require a custom filter centered around each spectral region of interest. For optimal performance for different AGN lines, probably a couple of gratings would be desirable.

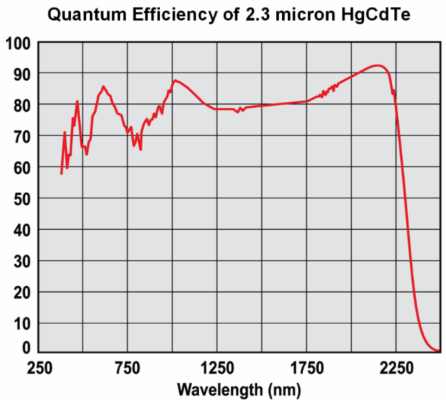

Fig 43 QE curve for a COTS detector from Teledyne. Note that both the visible and NIR can be covered with this one type of detector.

In the same spirit of mulit-purposing as many of the optics and the detector as possible, the foreoptics could be used to select a few discrete angular scales on which the

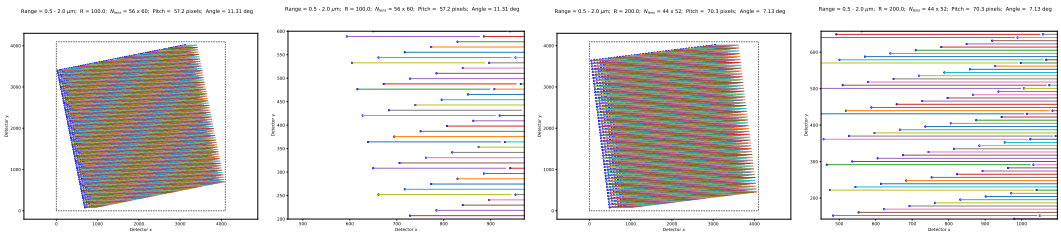

Fig 44 Example layouts of IFS spectra for a microlens array dispersed onto a H4RG detector. The left two plots are for $\mathcal{R} = 100$ and the right two are for $\mathcal{R} = 200$. Each pair shows the full field and a zoomed field, respectively.

image segmentation optics would sample the telescope fo-
cal plane. The observer could trade FoV for spatial resolution, or even perform a series of observations at different scales.

Of course these are simply notional; exact values, including whether the optics can provide low aberration over the full detector, would be required for a true preliminary design. Even so, these minimal geometry can help determine whether all the spectrograph requirements can be met. In particular, the SN/faint-object science case will want to take full advantage of the sky suppression by Nyquist-sampling the PSF. A field magnifier that sets the scale at 10 mas per spatial resolution element would provide a field of 0.56×0.60 arcsec for $\mathcal{R} = 100$ and 0.44×0.52 for $\mathcal{R} = 200$ for a microlens IFS. This satisfies the FoV requirements for the SN/faint-object science case. The AGN science cases require a range of FoV and spatial samplings; the dual/triple AGN cases requires a 3×3 arcsec FoV, which for the 56×60 microlens IFS could be covered with sampling of around 50 mas per spatial element. An image slicer would provide about $4\times$ finer spatial sampling.

7.2.2 Optical Interferometers

One particularly unique technological capability of ORCAS is in its use with ground-based long baseline optical (visible, NIR, MIR) interferometers (LBOI). Current US ground-based LBOI operational facilities are the CHARA Array on Mount Wilson, and the NPOI facility near Flagstaff, AZ; additionally ESO operates the VLTI on Paranal in Chile. Individual apertures in a LBOI benefit from adaptive optics - both NGS and LGS - but unfortunately the equivalent of a laser guide star does not exist for LBOIs: the 10-100 micron pathlength variations in the Earth's atmosphere that corrupt signal coherence (at the 10nm level) in such a system are not sampled by LGS or any similar system. However, an ORCAS beacon within the on-sky coherence angle (1-2 arcseconds) of a target of interest could be used to phase an array. As a result, the system coherence time could be extended from the atmospheric limit of milliseconds, to many tens of seconds or longer, dramatically improving the sensitivity of these high-angular resolution systems. The current limits of CHARA at 8th magnitude and NPOI at 5th magnitude would then scale upwards, linearly with improved coherence time, by factors of 100 to 1,000 or more.

With a limiting magnitude improvement of 5 to 7 magnitudes, what new science vistas await milli- to microarcsecond-class LBOI imaging? Techniques already applied for surface imaging of bright stars (e.g. see images of zet And from Roettenbacher et al. 2016, Nature 533, 217) can easily be applied to whole new classes of objects. Two of the many examples are as follows: first, direct imaging the inner parsec of active galactic nuclei will give new insights into the nature of galactic core phenomena such as torus morphology, feedback, dust sublimation, and core binarity (M. Kishimoto et al 2019). Second, interferometric images of young stellar objects LBOI would allow characterization of the terrestrial planet-forming disks surrounding their host stars. Similar ALMA images of the outer,

icy planet regions have already amazed the astronomical community; operations at LBOI wavelengths provide the sensitivity to warmer thermal emission and scattered light observations, along with the necessary angular resolution for probing terrestrial planet formation (Monnier et al 2019).

7.2.3 Compatibility with Other Observatories

The ORCAS mission would potentially be compatible with many other observatories, including DKIST, Subaru, Gemini N/S, LBT, GMT, TMT, VLT, and ELT. All these observatories could update their AO systems to use the ORCAS beacon wavelengths. They all have the capability to send up a 589 nm reference beam to help the ORCAS point at the observatory. This reference beam would not have to be bright. All the listed observatories could use the photometric calibrator without special target alignment.

Appendices

A Further Mission Details and Studies

A.1 Master Equipment List

In this appendix, the Master Equipment List (MEL) is given (Table 27). The block diagrams and additional details about individual components can be found in Section 4.

Table 27 Master Equipment List

Level	Name (Mission or Payload Name)	TRL	Level	Name (Mission or Payload Name)	TRL
1	Spacecraft Bus	9	1	Laser Payload	6
2	Electrical Subsystem	9	2	Laser Electronics Assembly	6
3	Solar Arrays	9	3	Seed Laser Assembly	6
3	EPS Battery Charger Board	9	3	Laser Amplifier	6
3	EPS Power Board	9	3	Frequency Doubling	6
3	Bus Battery	9	3	Beam Splitter	6
2	Attitude Control Subsystem	9	3	Beam Steering	6
3	Star Trackers	9	2	Laser Telescope Assembly	6
3	Magnetometers	9	3	Pointing and Tracking Lens	6
3	IMU	9	3	Pointing & Tracking Array Camera	6
3	Chip-Scale Atomic Clock	9	3	Free-Space Optical Telescope	6
3	GPS Receiver	9	1	Flux Calibration Payload	3-4
3	Reaction Wheel	9	3	Large & Small Optical Detectors	3-4
3	Sun Sensors	9	3	Optical Fiber Bundle	3-4
2	Propulsion Subsystem	9	3	Detector	3-4
3	Electric Propulsion Module	9	1	Observatory	8
3	Thrusters	9	2	AO Systems	8
3	XFC	9	3	Deformable Mirrors	8
3	Propellant Tank	9	3	Lasers	8
3	Xenon Propellant	9	3	Shack-Hartmann WFS	8
2	Command & Data Handling Subsystem	9	3	NGS Tip-Tilt Sensors	8
3	System Controller	9	3	Low Bandwidth WFS	8
2	Communications Subsystem	9	3	Pyramid Wavefront Sensor	8
3	Iris V2 (SDL)	9	3	Real-Time Controllers	8
3	KI-700/CXS-1000 (L3Harris)	9	3	NIRSPEC MEMS DM	8
3	S-Band D/L and U/L Antennas	9	3	Near-Infrared Tip-Tilt Sensor	8
2	Thermal Subsystem	9	2	AO Science Instrument	8
3	Heaters	9	3	OSIRIS IFS and Imager	8
3	Surface Coatings	9	3	NIRC2 Camera	8
3	Heat Pipes	9	3	NIRSPEC Camera	8
3	Thermistors	9	3	Liger IFS and Imager	8
2	Mechanical Subsystem	9	3	SCALES IFS	8
3	Solar array Hinges	9	3	HISPEC Spectrograph	8
3	Separation Switches	9	3	Visible Science Instrument	8
3	Solar Array Release Mechanism	9			
3	Bus and Prop Module Structure (Saturn)	9			
3	Solar Array Drive	9			
3	Motorized Lightband	9			
3	Separation Connectors	9			

A.2 Acronyms and Abbreviations

Table 28 A list of all acronyms and abbreviations included within this report

Acronyms & Abbreviations	
ACS	Attitude Control System
ADCS	Attitude Determination and Control Systems
AGN	Active Galactive Nuclei
ALMA	Atacama Large Millimeter/submillimeter Array
ALTAIR	Airborne Laser for Telescope Atmospheric Interference Reduction
AO	Adaptive Optics
AS3	Astrophysics Science SmallSat Studies
BAO	Baryon Acoustic Oscillations
BATC	Beijing Arizona Taiwan Connecticut Sky Survey
BCT	Blue Canyon Technologies
BDRF	Bidirectional Reflectance Distribution Function
BLR	Broad Line Regime
CANDELS	Cosmic Assembly Near Infrared Deep Extragalactic Legacy Survey
CCD	Charge Coupled Device
ΛCDM	Lambda Cold Dark Matter
CDRL	Contract Data Requirements List
CHARA	Center for High Angular Resolution Astronomy
CMB	Cosmic Microwave Background
COSMOS	Cosmological Evolution Survey
COTS	Commercial Off The Shelf
CPFF	Cost Plus Fixed Fee
CSIM	Compact Solar Irradiance Monitor
DAQ	Data Acquisition System
DEC	Declination
DESI	Dark Energy Spectroscopic Instrument
DKIST	Daniel K. Inouye Solar Telescope
DM	Deformable Mirror
Dragonfly	NASA Helicopter to fly on Titan
ECI	Earth Centered Inertial
ELT	Extremely Large Telescope
EMCCD	Electron Multiplying Charge Coupled Device
ESA	European Space Agency
ESPA	EELV Secondary Payload Adapter
ESR	Electrical Substitution Radiometer
Europa Clipper	NASA Mission to Orbit Europa
EVM	Earned Value Management
FDF	Flight Dynamics Facility
FOV	Field of View
FT	Fibertek
FWHM	Full Width Half Max

Acronyms & Abbreviations	
FY21$	Fiscal Year 2021 Dollars
GA-EMS	General Atomics Electromagnetic Systems
GEMS	Galaxy Evolution from Morphologies and SEDs
GMOS-IFU	Gemini Multi Object Spectrographs-Integral Field Unit
GMT	Giant Magellan Telescope
GOODS	Great Observatories Origins Deep Survey
GPS	Global Positioning System
GRS	Gamma Ray Spectrometer
GSFC	Goddard Space Flight Center
GW	Gravitational Waves
H4RG	Hawaii 4RG
HDF	Hubble Deep Field
HEO	Highly Elliptical Orbit
HISPEC	High Resolution Infrared Spectrograph for Exoplanet Characterization
HODM	High Order Deformable Mirror
HSDR	High Speed Data Recorder
HST	Hubble Space Telescope
HUDF	Hubble UltraDeepField
I&T	Integration and Technology
ICM	Intra-Cluster Medium
IFS	Integral Field Spectrograph, AKA IFU
IMBH	Intermediate Mass Black Hole
INAF	Instituto Nazionale Di Astrofisica
IR	Infrared
JDEM	Joint Dark Energy Mission
JWST	James Webb Space Telescope
KBO	Kuiper Belt Object
KCWI	Keck Cosmic Web Imager
KPIC	Keck Cosmic Web Imager Integral Field Spectrograph
LBOI	Long Baseline Optical/Infrared
LBT	Large Binocular Telescope
LEO	Low Earth Orbit
LGS	Laser Guide Stars
LISA	Laser Interferometer Space Antenna
LOS	Line of Sight
LRIS	Low Resolution Imaging Spectrograph
LSST	Legacy Survey of Space and Time
LTAO	Laster Tomography Adaptive Optics
LUVOIR	Large UV/Optical/IR Surveyor
MAS	Milliarcseconds
MAVIS	MCAO Assisted Visible Imager and Spectrograph

Acronyms & Abbreviations	
MCAO	Multi Conjugate Adaptive Optics
MEL	Major Equipment List
MEMS	Micro-Electro-Mechanical
MIR	Mid-Infrared
MMS	Magnetospheric Multiscale
MOC	Mission Operations Center
MOSFIRE	Multi Object Spectrometer for Infrared Exploration
MPL	Mission Planning Lab
NEO	Near Earth Object
NGRST	Nancy Grace Roman Space Telescope
NGS	Natural Guide Star
NgVLA	Next Generation Very Large Array
NIR	Near Infrared
NIRC2	Near Infrared Camera 2
NIRCAM	Near Infrared Camera
NIRES	Near Infrared Echellette Spectrometer
NIRSPEC	Near Infrared Spectrometer
NIST	National Institute of Standards and Technology
NOAO	National Optical Astronomy Observatory
NPOI	Navy Precision Optical Interferometer
NSF MRI	National Science Foundation Major Research Instrumentation
HAKA	High order All sky Keck Adaptive optics
NSN	Near Space Network
OD	Orbit Determination
ORCAS	Orbiting Configurable Artificial Star
OSIRIS	OH Suppressing Infrared Integral Field Spectrograph
PD	Photodiode
PSF	Point Spread Function
PTA	Pulsar Timing Arrays
PTFE	Polytetrafluorethylene
PyWFS	Pyramid Wavefront Sensor
RA	Right Ascension
RBTL	Read Between the Lines
RFI	Request for Information
ROM	Rough Order of Magnitude
Roman	Nancy Grace Roman Space Telescope (AKA WFIRST)
RUG	Rideshare Users Guide
SCALA	SNIFS Calibration Apparatus
SDL	Space Dynamics Laboratory
SDSS	Sloan Digital Sky Survey
SED	Sciences and Exploration Directorate

Acronyms & Abbreviations	
SEP	Solar Electric Propulsion
SF	Star Forming
SMBH	Supermassive Black Holes
SN (SNe)	Supernova (Supernovae)
SNAP	Supernova Acceleration Probe
SNIFS	Supernova Integral Field Spectrograph
SNR	Signal-to-Noise Ratio
SOC	Science Operation Center
SRP	Solar Radiation Pressure
STM	Science Traceability Matrix
TMT	Thirty Meter Telescope
TRL	Technology Readiness Level
USO	Ultra Stable Oscillator
UV	Ultraviolet
VLT	Very Large Telescope
VRO	Vera Rubin Observatory
WAG	Wild Guess
WBS	Work Breakdown Structure
WFI	Wide Field Interferometer
WFIRST	Wide Field Infrared Space Telescope (AKA Roman)
WFS	Wavefront Sensor
WMKO	W. M. Keck Observatory
WUDF	Webb UltraDeep Field

A.3 Mission Architecture

In this section, we compare the current mission architecture with both upscope and downscope options.

A.3.1 Mission Architecture A

The proposed mission architecture given in this report has a cost of $71.8M and would include a spacecraft with both flux calibrator and AO laser observation capabilities. This would enable up to 300 AO mode observations of active galactic nuclei, supernovae, the high redshift universe, exoplanets, and the solar system, and up to 1,500 flux calibration observations.

A.3.2 Mission Architecture B: Downscopes

Downscope I: Flux Calibrator Only

One downscope option for ORCAS is to only use it for flux calibration observations. This would result in a much more limited science case and therefore fewer requirements. For this science case, useful observations can be made by 1-10 m class telescopes for exposures of ten minutes or less.

In this case, no ground observatory updates would be needed, since WMKO already has these capabilities. Therefore all costs relating to observatory upgrades would be removed from the project budget. The spacecraft itself would also be redesigned as it would no longer need to have a laser payload. All development work for the laser beacon would no longer be needed. Only development relating to the flux calibrator would be needed at this point. The cost of the spacecraft itself would go down significantly since only a flux calibrator is needed as a payload. The current cost estimate for a spacecraft is $20M. The laser design for ORCAS is less than 5kg mass, less than 130W power, and less than 4U volume. With only the flux calibrator, much less mass, power, and volume would be required, so the corresponding materials and development costs would be lower. Of the $20M current cost estimate, about $16M goes into materials and $2M goes into labor. For a spacecraft with less required materials and labor, we estimate the cost of both these categories would be reduced by about 30%, so the new total spacecraft cost would be $14M. The cost to develop the flux calibrator would be approximately $10M for a total mission cost of $24M. A 30% space contingency would be added to the cost estimate, leading to a total budget of about $32M, less than half the cost of the current mission architecture.

Downscope II: AO Laser Only

A second downscope option for ORCAS would be to only have the mission do AO laser observations. In this case, fewer updgrades to the WMKO would be needed. Currently, approximately $17M of the ORCAS budget is allotted for upgrades to the WMKO AO system and visible science instrument. Of the science cases, AGN and SNe both require wavelengths of 0.5 to 2μm, the high redshift universe requires wavelengths of 0.5 to 1.2μm, exoplanets require wavelengths of 0.5 to 2.5μm, and the solar system requires wavelengths of 2.5 to 5μm. If instead of upgrading both the visible light and near infrared spectrums of WMKO only the AO system was upgraded, the total project cost would be reduced by $9.5M plus a 15% ground systems contingency.

Additionally, in this case the flux calibrator would not be needed, reducing the ORCAS mission cost by $9M plus the space contingency. The spacecraft bus design and development would also be decreased. The decrease would be less since the majority of the mass and power budget currently goes to the laser, but the budget would be reduced by $3M. Additionally, in this case the ground segment costs could be reduced by $2.5M and the operation costs could be reduced by $1M. This leads to a total overall budget of $40M.

A.3.3 Mission Architecture C: Upscope

An upscope option for ORCAS is to launch multiple spacecraft like the one proposed in this report, which would greatly increase the science yield. Having multiple spacecraft would allow for either significantly longer observation times as a constellation of spacecraft moved in and out of the field of view, or better sky coverage if the spacecraft were in significantly different orbits. The main option discussed in this section is the second one, which would result in a significantly wider variety of observations with large fuel savings. The estimated cost of changing the target star location for an orbit 1° in either right ascension or declination is 30m/s. Therefore, with a limited budget of fuel for each spacecraft for the mission, it makes sense to focus on one section of the sky to get the largest number of observations. However, if multiple spacecraft were launched, each would be able to target a particular section of the sky, allowing for much greater coverage. This can be seen in Figure 45. Additionally, the orbits could be planned so that they would reach apogee at different times, allowing for observations to be made nearly every night.

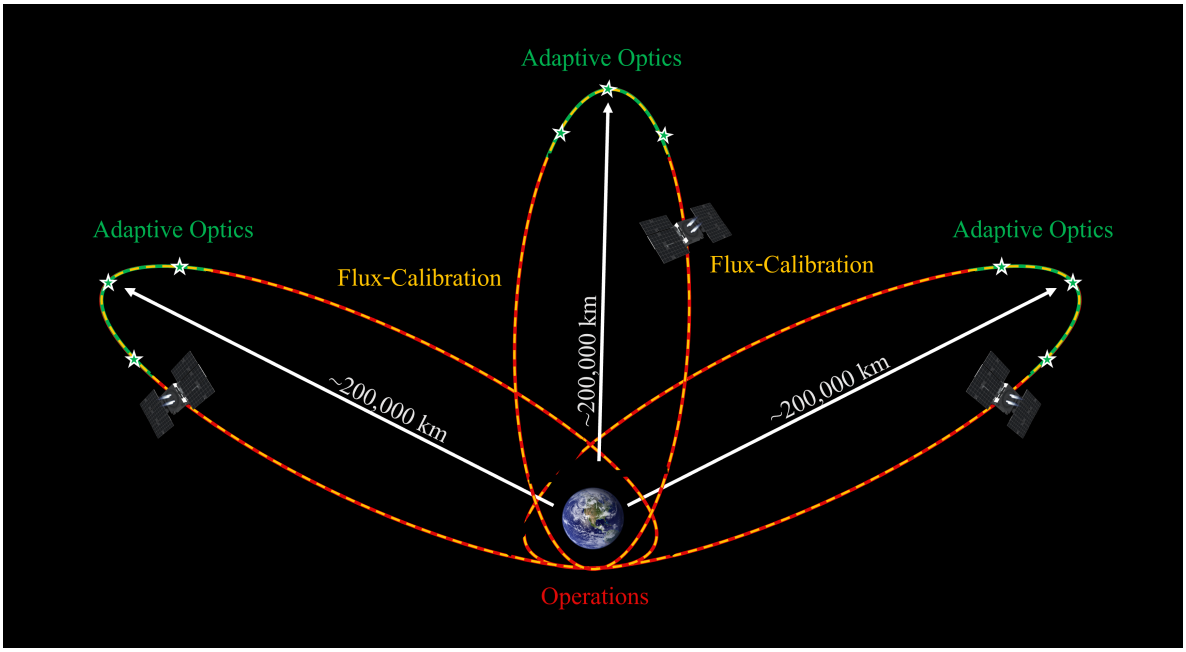

Fig 45 Proposed upscope mission architecture.

Increased upgrades to the ORCAS mission could classify it as a SMEX mission level with an increased budget of $120M. Each additional spacecraft would cost approximately $18M plus a 30% space contingency, for a total cost of $23.4M. The current mission cost is $71.5M, so we would be able to add two additional spacecraft, for a total mission cost of $118.3M, to ORCAS if it was a SMEX level mission. This additional cost would allow us to triple the total science yield.

A.4 Radiation Effects on Subcomponent Level

Radiation effects that should be considered for instrument and spacecraft design fall roughly into three categories: degradation from total ionizing dose (TID), degradation from non-ionizing energy loss (NIEL), and single event effects (SEE). Total ionizing dose in electronics is a cumulative, long-term degradation mechanism due to ionizing radiation-mainly primary protons and electrons and secondary

particles arising from interactions between these primary particles and spacecraft materials. It causes threshold shifts, leakage current, and timing skews. The effect first appears as parametric degradation of the device and ultimately results in functional failure. It is possible to reduce TID with shielding material that absorbs most electrons and lower energy protons. As shielding is increased, shielding effectiveness decreases because of the difficulty in slowing down the higher energy protons.

Table 29 Radiation Mission Dose Depth

Inclination	Al Absorber Thickness (mm)	Total Mission Dose (rad)
0°	1	4.50E5
	2	1.23E5
	5	5.83E3
30°	1	1.94E5
	2	5.27E4
	5	3.20E3
60°	1	5.90E4
	2	1.74E4
	5	1.96E3

Total ionizing dose is primarily caused by protons and electrons trapped in the Van Allen belts and solar event protons. As electrons are slowed down, their interactions with orbital electrons of the shielding material produce a secondary photon radiation known as bremsstrahlung. Generally, the dose due to galactic cosmic ray ions and proton secondaries and bremsstrahlung is small compared to other sources in modern spacecraft having typical shielding. For surface degradation, it is also important to include the effects of very low energy particles.

Table 29 shows the total mission dosage in rads for different Al thicknesses and at different orbit inclinations. The values given are for a 75% model.

A.5 Navigation Requirement

The requirements imposed by the ORCAS mission's science observation modes filter down to navigation requirements that dictate the accuracy with which the spacecraft's state must be known before, during, and after each observation. Proper understanding of the navigation requirements depends upon familiarity with three different reference frames used to represent the motion of the ORCAS spacecraft. The first of these frames is the common J2000 Earth-centered inertial (ECI) reference frame which is used to propagate the motion of the ORCAS spacecraft. The J2000 term denotes that this frame is defined at the beginning of the Julian year 2000. The second frame, the radial-intrack-crosstrack (RIC) reference frame, is also Earth-centered; however, its axes are defined by the orbit of the ORCAS spacecraft making this frame useful for understanding motion relative to the nominal orbit of a spacecraft. The $\hat{R}$-axis is aligned with the radial vector from the Earth to the spacecraft, the $\hat{C}$-axis is parallel to the angular momentum vector of the orbit, and the $\hat{I}$ axis is defined to complete the orthonormal set. The final frame is the camera frame which depicts the motion of the spacecraft relative to the line-of-sight (LOS) of a ground observatory, in this case, Keck. The z-axis of the camera frame is parallel to the LOS from the ground observatory to the target star, thus the inertial direction of this axis changes along with the rotation of the Earth. Motion projected in the x-y plane of the camera frame displays how the path of the ORCAS spacecraft will appear when viewed from the ground observatory. Furthermore, positions in this plane are typically represented in arcseconds to correspond with the units employed for astronomical observations. Conveniently, at the 200,000

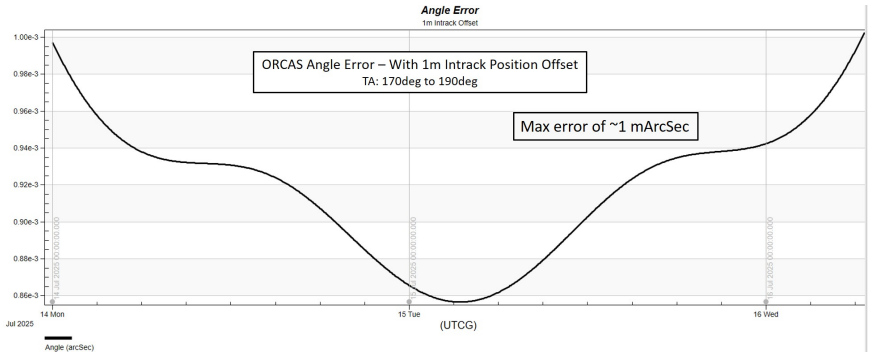

Fig 46 Spacecraft position error mapped to angle error for a science orbit with 5 day period and an approximate observatory to spacecraft distance of 200,000 km.

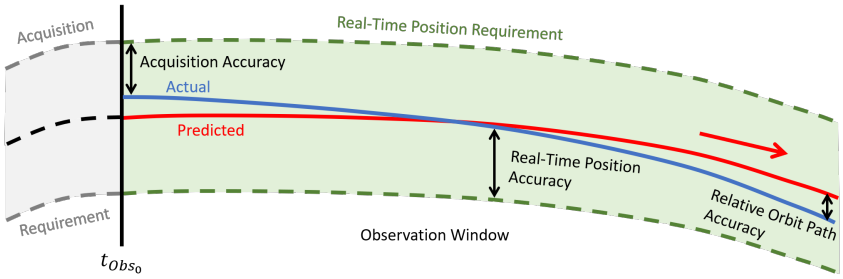

Fig 47 Sketch of the three different navigation requirements imposed on the ORCAS spacecraft during the observation window. The predicted trajectory (red) is the expected path of the spacecraft and is delivered to the ground observatory prior to the observation window. The actual trajectory (blue) is the observed path of the spacecraft through the observation window, i.e., the path that the spacecraft actually takes.

km apoapse altitude of the highly elliptical Earth-centered science orbit, an approximately one-to-one relationship exists between arcseconds and kilometers. This relationship is demonstrated in Figure 46 which shows that over the roughly three day period that the ORCAS spacecraft lingers near apoapsis an intrack position offset of 1 meter corresponds to approximately a 1 milliarcsecond (mas) offset in the camera frame. This close correspondence simplifies the translation of the spacecraft navigation requirements from their definition in arcseconds in the camera frame to a representation in kilometers in the RIC frame.

Three types of navigation requirements are placed on the ORCAS spacecraft: an acquisition requirement, a real-time position requirement, and a relative orbit path requirement. Each of these requirements is initially defined in the camera frame and then translated to the RIC frame. A schematic depicting how these requirements relate to one another is displayed in Figure 47. The acquisition requirement states that the absolute position of the spacecraft at the start of the observation window must be within 1 arcsecond, i.e., 1 km in the RIC frame, of the predicted trajectory through the observation window. This requirement ensures that the spacecraft is close enough to its intended path that it can be acquired by Keck at the start of the observation window. The second navigation requirement is similar to the first and states that ORCAS must remain within this 1 arcsecond envelope of the predicted trajectory throughout the observation window. Because this requirement is imposed during the observation window it is termed the real-time position requirement. The acquisition and real-time position requirements appear as grey and green bands, respectively, centered around the predicted trajectory in Figure 47. In reality, these requirements define a cylinder in position space, centered around

the predicted trajectory, which the actual trajectory must remain within.

The third navigation requirement, the relative orbit path requirement, dictates the relative position error permitted between the predicted and actual trajectory of the ORCAS spacecraft during the observation window. While initial offsets between the predicted and actual trajectories can be accounted for at the start of an observation window, if these trajectories evolve in significantly different ways this could prevent the ground observatory from accurately tracking the spacecraft through the observation window and reduce the quality of the collected scientific data. The relative orbit path requirement is imposed to prevent this scenario and requires that the deviation between the predicted and actual trajectories must remain within 3 milliarcseconds. Meeting this requirement will ensure that discrepancies between the predicted and actual paths of the spacecraft do not significantly degrade the scientific data.

A.5.1 Relative Orbit Path Requirement Analysis

Errors in force modeling at the beginning of the observation window will result in a deviation from the expected orbit as the spacecraft propagates through the observation window. The most prominent errors sources are the orbit determination (OD) process – namely the estimation of the state and solar radiation pressure (SRP) acceleration knowledge. The mismodeling of acceleration due to drag, gravity harmonics, or any additional unknown accelerations may also cause a deviation from the expected orbit. However, due to the high altitude at which the observations will occur, the error contributions from these factors will be insignificant relative to the more prominent errors mentioned.

An analysis was conducted to ensure that the relative orbit path requirement could be met. After the first measurement is received during operations, the actual position of the spacecraft will be known. The initial point of the predicted trajectory can then be corrected such that this point is aligned with the first measurement point in the camera frame. However, due to the errors from OD and SRP coefficient modeling, this predictive ephemeris will continuously drift from the measurement points.

For this analysis, a Monte-Carlo strategy was employed which generated a set of potential mission trajectories modeling realistic errors and compared these versus the "actual" trajectory. This requirement would be considered satisfied if the relative position remains within 3 mas in the camera frame throughout the duration of the observation window.

The "actual" trajectory was generated by propagating the ORCAS satellite over the span of the observation window without adding any errors to the spacecraft configuration or initial state. This ephemeris maps the path of the true measurement points over the course of the observation window. The potential mission trajectories were generated by perturbing the initial state and SRP Cr value and propagating the satellite over the course of the observation window.A cannonball model was used to model the effect of SRP on the spacecraft during the propagation in this analysis. In this spacecraft model a coefficient of reflectivity - often referred to as Cr - was used to compute the acceleration due to SRP. Although the correction to the nominal Cr value is estimated during the OD process, an error will inevitably exist in this estimated value.This Cr estimation error will be a contributing factor in the deviation of the predicted from the true trajectory. To ensure a statistically significant number of potential trajectories, 2000 combinations of OD and SRP errors were applied.

The initial state errors for each perturbed trajectory were computed by sampling from a normal distribution in each component. These values were determined from the uncertainties expected at the observation window start time and calculated from independent OD analyses where GPS and radiometric tracking were used to estimate the orbit. The values used in this study are shown in Table 30 in the RIC coordinate system.

	Radial	Intrack	Crosstrack
Position [m]	50	30	20
Velocity [mm/s]	0.4	0.4	0.3

Table 30 RIC 3σ position and velocity values used as sampling distribution boundaries

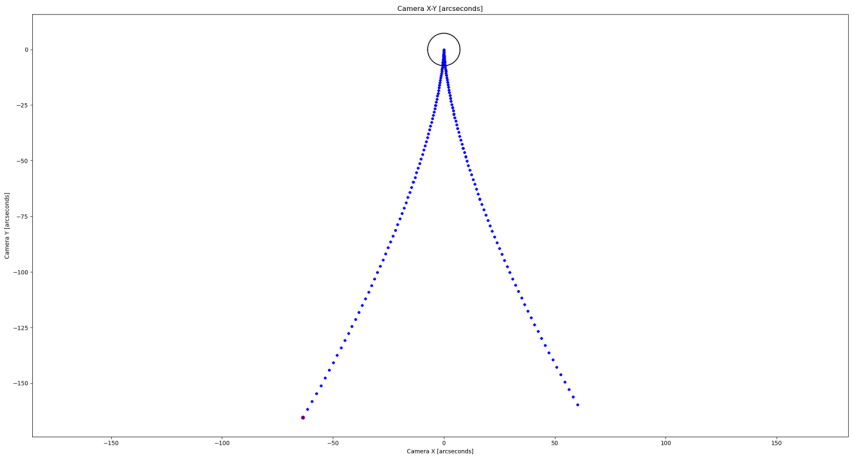

Fig 48 All trajectories (nominal and perturbed) transformed to the camera frame. Individual dots show the 1-minute step size of the trajectory. Circle represents the observatory line-of-sight view.

During the prior OD analysis it was shown the Cr coefficient could be estimated to within approximately 0.01 3σ of the nominal value. To ensure the most conservative situation was evaluated, this value was scaled by 10 and a potential error of 0.1 3σ was used as the boundary of the normal distribution in this analysis.

Figure 48 shows the potential mission trajectories converted to the camera frame. Figure 48 also verifies that, under the current assumptions, the acquisition and real-time accuracy requirements of 1 arcsecond (navigation requirements 1 and 2) can be satisfied with significant margin. The difference between the actual and predicted trajectories - referred to here as residuals - for all 2000 cases are plotted for both camera X and Y axes in 49. The maximum error for each case was extracted and the distributions in both camera X and Y axes are plotted in 50. These figures show that after approximately 2 hours, the error in the X and Y camera frame will exceed the 3 mas requirement.

It was determined that the ability to meet this requirement is largely driven by the initial velocity error between the predicted and actual trajectory at the start of the observation window, at t_0 in Figure 47. Larger errors in initial velocity lead to more significant deviations between the predicted and actual orbital paths. This trend is highlighted in Figure 51 which shows how position errors at the end of the observation window are driven by the velocity errors present at the start of the window. The estimates for initial velocity error considered in this analysis are presented in Table 30. It would be advantageous to improve these relative orbit path errors to ensure the relative orbit path requirement could can be met in all cases. Figure 51 shows that by halving the initial velocity error the resulting relative orbit path errors can be halved as well ensuring that the relative orbit path error remains well within the required bound.

This improvement in velocity knowledge can potentially be achieved with upgrades to the software or hardware used for navigation on-board the ORCAS spacecraft and on the ground. Additionally, rather than modeling the reflectivity properties using a cannonball method, an N-plate model could be

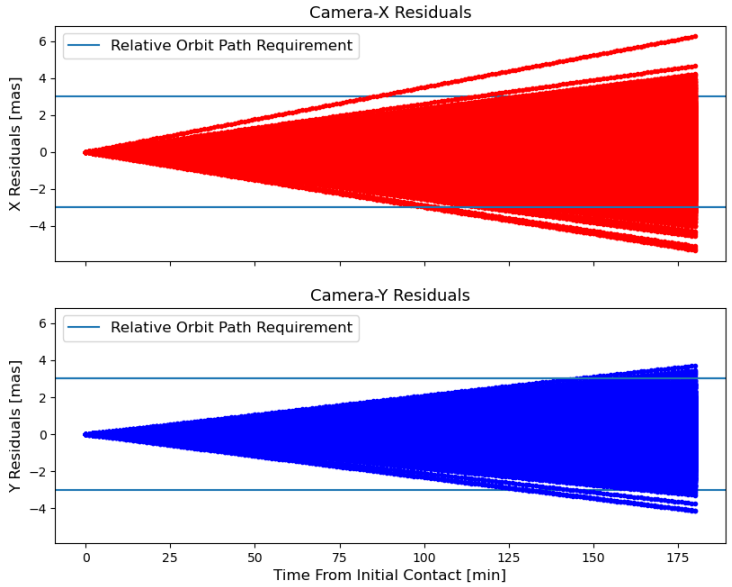

Fig 49 Residuals throughout the observation arc in both X and Y coordinates in the camera frame.

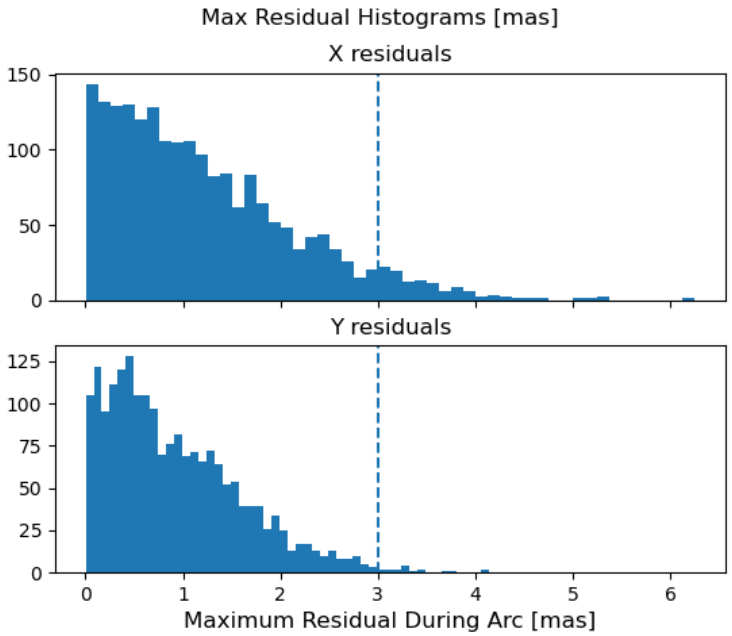

Fig 50 Maximum Residual extracted from the observation arc in both X and Y coordinates in the camera frame.

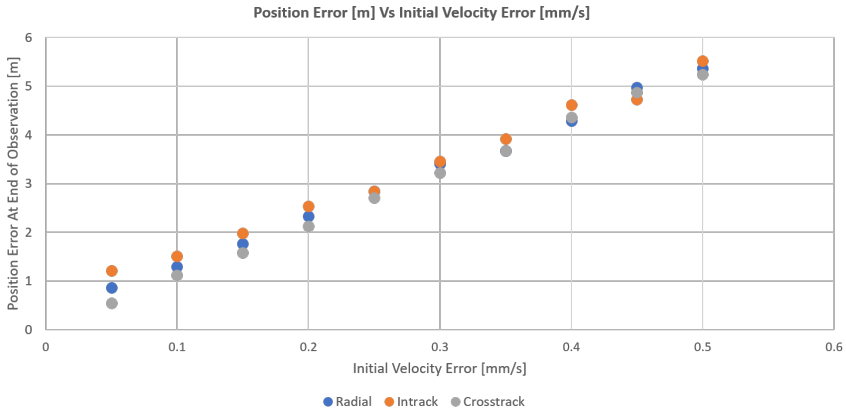

Fig 51 Relationship between velocity errors at the beginning of an observation window and the resulting position errors at the end of the observation window where these errors are at a maximum.

used. This will inevitably improve the extent to which the effect of SRP on the spacecraft could be estimated and thereby improving the quality of the observations. Future flight dynamics work could focus on investigating these advanced navigation strategies and exploring the benefits they offer to improving the quality of the observations made using ORCAS.

A.6 Orbit Families

The ORCAS concept places a beacon between the target and the telescope to serve as an artificial star for adaptive optics, a phase reference for interferometers, or for photometric calibration. There is a special case where the beacon appears to stop moving relative to the target, which we can generically describe as target-stationary, where the target can be moving in an arbitrary way. Useful examples for observatories on the ground include astro-stationary, for stars; helio-stationary, for studying the Sun; geostationary, for targets orbiting the Earth once per day. There are cases for moving, accelerating, and rotating solar system objects. There are parallel cases for space observatories like Hubble, JWST, Roman, HabEx, or LUVOIR. In all cases, the accelerations of the observatory and beacon are different, leading to a limit on the useful period of accurate alignment (without station-keeping thrust on the beacon).

Angular tolerances range from tens of milliarcseconds (for placing a beacon exactly in front of an exoplanet host star for extreme adaptive optics), to a fraction of an arcsecond (for placing the beacon in the diffraction limited central pixel of an interferometer telescope image), to several arcseconds (for placing the beacon in the isoplanatic patch for adaptive optics), to tens of arcseconds (for serving as a phase reference for an interferometer), or arcminutes (for serving as a tip-tilt guide star for sodium-layer AO systems).

The target-stationary requirement is that the beacon is on the line of sight, and the transverse velocity (perpendicular to the line of sight) of the beacon matches that of the moving observatory and possibly moving target. The orbit choices still span a multi-dimensional parameter space: given a target and an observatory, we must choose three numbers: 1. The moment of observation, 2. The distance from observatory to the beacon at that time, and 3. The radial velocity of the beacon then. The choice of distance and radial velocity is equivalent to a choice of orbit period and perigee height, or apogee and perigee, or other pairs of parameters. In the case of the restricted 3-body problem, including the gravity of the Sun or Moon, quasi-periodic orbits can be found around the Lagrange points.

Here we survey examples, give some useful numbers, and consider orbits that enable multiple use cases in a single orbit. The examples are: 1. a long elliptical orbit, 2. an orbit around Sun-Earth L1, for solar observations, 3. an orbit around L2, for targets near the ecliptic, 4. high inclination orbit near the distance to L2, 5. radial orbit for repeat observations of a special target, 6. lower orbits for observations of Earth satellites, e.g. geosynchronous or geostationary, 7. Hubble observatory, 8. L2 telescopes like JWST, HabEx, or LUVOIR. In all cases position measurement and propulsion are required to achieve precise alignment, the propulsion ΔV capability controls the total distance between the targets, and the maximum acceleration governs the time necessary to maneuver from one target to another. Also, the inclination of the Earth's spin axis to the ecliptic plane is important for observing astronomical targets.

A.6.1 Long elliptical orbit

This is the nominal case for ORCAS. According to the conservation of angular momentum, the transverse velocity of the beacon (as seen from the center of the Earth) is inversely proportional to the distance from the center of the Earth. The minimum orbit period is obtained when the transverse velocity of the observatory is maximum (observing on the meridian) and the perigee is the minimum safe value. It is convenient for the period to be an integer number of days. If the apogee is large enough, there can be multiple observing opportunities on each orbit, since the time of observation controls the transverse velocity of the observatory and enables a match to the orbit. However, the ability to maneuver the orbit and choose the observing time so that each opportunity aligns with a scientifically valuable target is governed by the available acceleration. A 5-day orbit yields one excellent astro-stationary moment and two others. It may be possible for two of them to be exactly astro-stationary, for different targets. Non-integer orbit periods can also be useful in spreading out the observable locations, or in providing access to different observatories at different longitudes.

The duration of each event depends on the angular tolerance, and the relative velocity and acceleration at the observing time. If the relative velocity is zero at the middle of the event, then the duration is governed by the projected acceleration of the observatory. The east-west acceleration is zero if the target is on the meridian, and the north-south acceleration is zero if the target and the observatory are on the equator. Since the acceleration of the observatory is a rotating vector, it is possible to optimize the observing period by having the velocity of the spacecraft at observation be slightly less than that of the observatory, allowing for a loop shape of the beacon in the field of view. Far from Earth, the transverse acceleration of the beacon is negligible by comparison to that of the observatory.

Calculated observing times within the isoplanatic patch vary from a few hours on the equator to about 30-40 minutes at higher declinations, depending on wavelength. Away from the equator, the duration scales as the square root of the product of the beacon distance and the angular tolerance. The isoplanatic patch size scales as the 6/5 power of the wavelength.

A similar calculation enables a helio-stationary moment once per orbit as well. There can also be two other approximately helio-stationary moments on each orbit, but only one can be placed near the Sun.

There are also two nearly geo-stationary moments per orbit, when the radial distance is a little less than the geo-stationary satellite altitude. An observatory like Keck could take a nearly instantaneous image, and an interferometer like NPOI could obtain one set of visibility fringe measurements very quickly. Whether these are sufficient depends on the question being asked.

Geostationary moments also mark the boundary at which the telescope tracking motors stop moving and reverse direction. These moments can also be useful for photometric calibration, since we

know that the telescope can track fast enough to keep the beacon in an instrument field of view. On the other hand, the stars move rapidly through the field of view at the rate of 360°/day = 15 arcsec/sec. Whether this matters to a photometric calibration depends on details.

Maneuvering costs to re-orient the orbit are approximately L/b, where L is the specific angular momentum and b is the semi-minor axis of the orbit. For the 5-day elliptical orbit this number is about 30 m/s/degree. Given this approximation, or using higher-fidelity orbit tools, we have algorithms to optimize a trajectory connecting a selected list of high-priority targets.

A.6.2 Sun-Earth L1 orbits

An orbit around the L1 point at 1.5 mkm makes the beacon hover near the line to the Sun, and this could be useful for observing the Solar corona with DKIST. The rate of motion of the Sun is about 1°/day or 0.041 arcsec/sec against the background stars. Relative to the Sun, the beacon appears to move in an ellipse every day as the Earth carries the observatory around. The long axis of the ellipse in the E-W direction is about the size of Earth as seen from L1, about ½°. The maximum angular rate relative to the Sun is about 400 m/s (the transverse observatory velocity on the meridian) divided by the distance to L1, or 0.053 arcsec/sec. It roughly matches the solar rate at an angle off meridian of acos(.041/.053) = 39°. In other words, every day there are also two nearly astrostationary moments.

The beacon appears to move relative to the Sun, so a particular coronal feature would stay within the isoplanatic patch for a short time. Assuming the isoplanatic diameter is say 4 arcsec (smaller than at night), we could observe a particular feature for (4/0.053) = 75 sec. If the total observable trajectory is 1/3°, then there would be (20 arcmin/4 arcsec) = 300 independent images every day. We need to determine what science can be done in this mode. For comparison, the nominal long elliptical orbit gives exposure times up to a few hours for a single isoplanatic patch, but does not scan nearly as far.

The minor axis is smaller in proportion to the sine of the declination of the Sun. The L1 orbit is unstable in the radial direction so some station-keeping thrust may be needed. Orbits around L1 are called halo orbits and can be approximated with epicycles with an apparent period of 1/2 year. Active orbit management would be required to place the beacon at the right place relative to the solar disk for a particular observation.

A.6.3 Sun-Earth L2 halo orbits

These are similar to L1 orbits except that they are overhead at midnight instead of noon. Also, we are interested in a range of orbits much farther from the L2 point. Halo orbits explored for use with JWST and other observatories have radii up to 300,000 km around the L2 point, and in the rotating coordinate system the beacon orbits the L2 point twice per year. From the Earth the beacon still sweeps out a roughly great circle trajectory around the whole sky once per year. There is also a family of orbits somewhat closer than L1 and L2 that orbit the Earth twice a year. The beacon could be observed as long as the angles between the line-of-sight, Zenith, and the Sun meet observation constraints, typically 6 to 8 hours each night. However, whether the spacecraft beacon is aligned with a section of the sky that is worth observing depends on the chosen halo orbit. Observations of a given star happens once a year for a single night. This astrostationary moment enables very long exposures. If needed the orbit can be adjusted to place a specific target exactly on the astrostationary moment for a particular observatory and angle from the meridian (time). Because of the great distance, observing windows (within the isoplanatic patch) are significantly longer than for the 5-day orbit case, approximately in proportion to the square root of the distance. (1.5 mkm / 180,000 km)$^{1/2}$ = 4.3.

Some propulsion is required to ensure that the observing window(s) each day are really astrostationary and are close to the desired targets. This orbit is well suited for surveys and observations of specific targets near the ecliptic plane, although each target can be seen only once per year. Targets on successive days are spaced approximately 1° apart. On the other hand the duty cycle can be very high, with many hours of good observations every night.

Orbit maneuvers are slow because of the great distances involved, but for the same reason the total ΔV costs can be low. Conversely, the orbital dynamics in the three-body problem are interesting and offer many options to minimize fuel consumption. We have developed a method to define a Sun/Earth L2 orbit for any given target star below a certain inclination. This type of orbit allows for significantly longer observation times and also allows for observation of other stars throughout its orbit. Additionally, maneuver costs are significantly lower than those for HEO orbits.

A.6.4 High inclination orbit at L2 distance

This is nearly unexplored territory. Given an observatory, an observing time, and a target, there are still two degrees of freedom for the orbit: e.g. radial distance and radial velocity. The observatory transverse velocity of $\approx$ 400 m/s is comparable to escape velocity at the distance of L2. Whether it leads to escape or return depends on many factors including proximity to the L1 or L2 points, or the neutral plane for the solar gravity gradient, in other words being at the same distance from the Sun as the Earth. Given sufficient ΔV capability, all astronomical targets appear to be accessible. The interesting challenge is in optimizing a trajectory given a selected list of high priority targets.

A.6.5 Radial orbit for repeat observations of a specific target

For highly variable targets or extremely important targets, it may be essential to obtain daily repeat observations. This can be accomplished with a very distant beacon. If the beacon is sufficiently far from the observatory, then the time within the isoplanatic patch can be long enough to be useful, even if the encounter is not strictly astro-stationary. Suppose we choose an orbit that appears exactly radial from the Earth's center. Then the angular rate of motion due to the observatory motion is v_T/r, where v_T = 400 m/s. Assume r = 1.5 mKm, the distance to L1 or L2. Then the angular rate is 0.053 arcsec/sec as we found for the L1 orbit case. If the isoplanatic diameter is 5.2 arcsec we can observe the target for about 100 sec, and we can do it every day. If the distance is increased, the observing time is increased proportionally. Maintaining this alignment over many days would require propulsion to deal with the gravitational forces of the Sun and Moon; the Earth's field is radial so has little effect on the transverse motion. But by construction the orbit perigee is zero, so orbit management is required to avoid eventual collision with the Earth. Similar considerations apply to repeat observations of a solar system target like a planet, comet, asteroid, etc. An observatory at the South Pole does not accelerate, so the observing time can be essentially infinite. At present there are no telescopes at the South Pole equipped with adaptive optics.

A.6.6 Lower orbits for observations of Earth satellites

Given a particular Earth satellite to be observed, there are still three parameters to choose: time, radius, and radial velocity. The closer the radius and radial velocity are to matching the subject satellite, the smaller the relative acceleration. An exact orbital match is not required to keep the subject in view for long enough to observe it. The necessary observing time depends on target brightness. It is possible to choose an orbit that allows examination of multiple satellites in sequence. For example, if the orbit were chosen to have a period slightly different from 1 day, then it could travel all around the Earth,

aligning momentarily with each object in geostationary orbit. If the difference were chosen to make a complete circuit in 1 year, the relative angular rate would be 360°/365.25 days = 0.041 arcsec/sec. With an isoplanatic diameter of 5.2 arcsec we could observe each one for about 126 seconds. Since the subject satellites are not all exactly in the equatorial plane, and the observatory is not on the equator, some propulsion will be required to enable the series of observations.

A.6.7 Hubble observatory

This is a very interesting case because it is not impossible to find astro-stationary orbits, in which the beacon is momentarily stationary against the star field. This could be useful for photometric calibration. There are two special cases, the similar but inclined orbit and the shared orbit plane.

If the beacon is in the same orbit as the Hubble, but at a different inclination, then the line of sight from Hubble to beacon traces out a cylinder, perpendicular to the plane that bisects the angle between the orbit planes. The distance from Hubble to beacon ranges from zero (when the orbits cross) up to several thousand km (depending on the relative inclination). The orbits precess rapidly but differently because they have different inclinations. The close encounter must be avoided. In principle very long (tens of minutes) astrostationary events could be obtained with little propulsion needed. This could be of interest for a demonstration of an orbiting starshade, or for photometric calibration. A similar case was investigated for the mDOT demonstration of a starshade in both LEO and HEO.

If the beacon orbit is in the same plane as the Hubble orbit, there are possible astrostationary events ranging from very close (a few thousand km for a 5 day elliptical orbit, when the beacon is at perigee and Hubble is looking nearly straight up) to very far (hundreds of thousands of km, with Hubble looking nearly tangent to its own orbit). The Hubble accelerates very rapidly so none of the observation opportunities are long, even accounting for a several arcminute field of view of a Hubble instrument. With enough orbit control, the beacon could be made to cross the field of view of Hubble at a relatively slow rate, and this could be useful for photometric calibration. The Hubble orbit plane precesses rapidly, making a complete rotation several times per year, while the long ellipse of the beacon precesses very slowly.

A.6.8 L2 orbits for L2 space telescopes

These have been investigated for two purposes: serving as a phase reference to focus telescopes, and for placing a starshade. Similar considerations would apply to photometric calibration. All require maneuvering to align with specific targets. The total ΔV required is proportional to the spacing from telescope to beacon, and inversely proportional to the time allowed for each maneuver. Precise relative navigation may require cooperation between observatory and beacon. Raising the orbit from a 5-day high elliptical orbit to escape requires $\sim$ 157 m/s impulse at perigee.

A.7 Mission Sensitivity

As it can be seen in Figure 2, ORCAS can provide unprecedented angular resolution and sensitivity. All data provided in the curves seen in the figure come from past reports and instrument handbooks. The LUVOIR (124) and MAVIS (125) mission reports contain relevant mission performances. Additional data on the future of UVOIR astronomy (126), specifically in the performance of future missions, provides similar data that confirms with previous reports. The Roman Space Telescope angular resolution and Sensitivity within the NGRST space telescope science sheet from June 2021.

To calculate the sensitivity for Keck + AO and Keck + ORCAS, we take the responsivity (e/sec) and multiply by the proposed Strehl ratio for each band. For the curve seen in Figure 2, we utilize the

Echellette Spectrograph and Imager (ESI) instrument. We refer you to (127) for more technical details regarding the instrument. An aperture size of $(0.03 \text{ arcsec})^2$ is taken with the correct sky brightness. Additional noise components are considered, and we compute the SNR with an exposure time of 10,000 seconds. For each band, we determine the magnitude that yields and SNR ≥ 10.0.

A.8 Breakdown of Propellant Use

In this section, an estimated breakdown of the propellant use for the ORCAS mission is given. As shown, science maneuvers and the transfer from the drop off to the science orbit represent the vast majority of the fuel use for the mission.

Allocation Title	**Propellant (kg)**
Transfer from the drop off to the science orbit	18
ACS momentum dumping	2
Null tip off rates from the ESPA ring release (TBR)	1
Disposal orbit (TBR). Lower perigee and re-enter within 25 years	6
Unusable propellant remaining in tank	2
Eclipse Avoidance (TBR)	3
Orbit Maintenance (TBR)	1
Science Maneuvers	54
Extended Mission Science Maneuvers	28
Total Available Propellant	**115**

Table 31 Caption

A.9 Example Observation Sequence

As seen in Figure 39, ORCAS can perform $\sim$ 300 AO observations. Table 32 provides the coordinates of all ORCAS AO target opportunities and the dates each observation will occur. It is important to remember that Each science orbit will contain three AO observation opportunities, so consecutive targets within 24 hours will contain large jumps in Right Ascension. The table does not provide the names of each target because it is only here to serve as an example of what the mission schedule can do. In future versions, all potential targets will have a different priority value that will reflect how the schedule is built.

Table 32 The observation schedule built within the ORCAS mission schedule optimization tool as discussed in Section **??**

Observation	RA	DEC	Retargeting (m/s)	Date	Observation	RA	DEC	Retargeting (m/s)	Date	Observation	RA	DEC	Retargeting (m/s)	Date
1	189.205	62.22	0.0	2025-12-08	92	203.1798	45.3641	0.0	2026-05-19	184	198.4295	42.6033	0.0	2027-03-05
2	189.205	62.22	0.0	2025-12-13	93	176.3	49.33	40.313	2026-05-22	185	209.8117	40.9724	nan	2027-03-06
3	188.15	62.83	23.41	2025-12-18	94	189.8009	48.1839	0.0	2026-05-23	186	183.025	44.0389	70.348	2027-03-09
4	206.9664	61.1933	0.0	2025-12-19	95	202.159	46.2307	0.0	2026-05-24	187	195.3279	43.0413	0.0	2027-03-10
5	189.2	63.19	17.922	2025-12-23	96	176.5	49.73	12.617	2026-05-27	188	206.7781	41.3872	0.0	2027-03-11
6	208.2306	61.5365	0.0	2025-12-24	97	190.1056	48.5719	0.0	2026-05-28	189	181.55	45.2836	48.84	2027-03-14
7	186.93	63.41	31.303	2025-12-28	98	202.5408	46.5937	0.0	2026-05-29	190	194.106	44.2523	0.0	2027-03-15
8	206.0948	61.7461	0.0	2025-12-29	99	174.83	49.87	32.614	2026-06-01	191	205.7524	42.5329	0.0	2027-03-16
9	222.0786	58.5936	0.0	2025-12-30	100	188.4729	48.708	0.0	2026-06-02	192	181.5561	45.3337	1.57	2027-03-19
10	186.57	62.55	26.261	2026-01-02	101	200.9351	46.7204	0.0	2026-06-03	193	194.1226	44.3011	0.0	2027-03-20
11	205.2232	60.9262	0.0	2026-01-03	102	174.6	49.52	11.416	2026-06-06	194	205.7771	42.5789	0.0	2027-03-21
12	220.9259	57.8722	0.0	2026-01-04	103	188.1505	48.3685	0.0	2026-06-07	195	184.22	45.22	56.338	2027-03-24
13	186.02	61.5	32.436	2026-01-07	104	200.5447	46.4029	0.0	2026-06-08	196	196.7628	44.1902	0.0	2027-03-25
14	204.0893	59.9232	0.0	2026-01-08	105	173.7	49.03	22.939	2026-06-11	197	208.3988	42.4744	0.0	2027-03-26
15	219.4602	56.9833	0.0	2026-01-09	106	187.1235	47.8928	0.0	2026-06-12	198	187.2154	48.9671	127.956	2027-03-31
16	185.83	61.21	9.117	2026-01-12	107	199.4248	45.9579	0.0	2026-06-13	199	200.6231	47.8316	0.0	2027-04-01
17	203.7455	59.6461	0.0	2026-01-13	108	174.15	48.07	30.151	2026-06-16	200	212.9124	45.9008	0.0	2027-04-02
18	219.0262	56.7362	0.0	2026-01-14	109	187.335	46.9605	0.0	2026-06-17	201	186.9817	49.5489	18.05	2027-04-05
19	183.95	59.97	46.372	2026-01-17	110	199.4585	45.0839	0.0	2026-06-18	202	200.5397	48.3965	0.0	2027-04-06
20	201.2398	58.4582	0.0	2026-01-18	111	171.88	48.32	46.002	2026-06-21	203	212.9394	46.4295	0.0	2027-04-07
21	216.1477	55.6738	0.0	2026-01-19	112	185.1261	47.2036	0.0	2026-06-22	204	186.9	49.43	3.937	2027-04-10
22	183.35	59.27	22.893	2026-01-22	113	197.2947	45.3119	0.0	2026-06-23	205	200.4266	48.281	0.0	2027-04-11
23	200.3086	57.7865	0.0	2026-01-23	114	171.2238	49.5698	39.657	2026-06-26	206	212.804	46.3214	0.0	2027-04-12
24	215.0134	55.0696	0.0	2026-01-24	115	184.7872	48.4167	0.0	2026-06-27	207	187.6679	51.1373	53.296	2027-04-15
25	180.7646	60.522	54.07	2026-01-27	116	197.191	46.4483	0.0	2026-06-28	208	201.6607	49.9369	0.0	2027-04-16
26	198.3265	58.9873	0.0	2026-01-28	117	170.57	49.7	13.27	2026-07-01	209	214.3773	47.8668	0.0	2027-04-17
27	213.3983	56.148	0.0	2026-01-29	118	184.1677	48.5429	0.0	2026-07-02	210	189.85	52.08	49.52	2027-04-20
28	178.5183	60.3733	33.53	2026-02-01	119	196.5971	46.5665	0.0	2026-07-03	211	204.1192	50.8498	0.0	2027-04-21
29	196.0058	58.8447	0.0	2026-02-02	120	168.6859	47.936	64.695	2026-11-08	212	217.0342	48.7162	0.0	2027-04-22
30	211.033	56.0206	0.0	2026-02-03	121	168.43	47.5	14.069	2026-11-13	213	188.95	53.4	42.842	2027-04-25
31	178.13	60.42	5.905	2026-02-06	122	167.291	45.8571	54.579	2026-11-18	214	203.6315	52.1275	0.0	2027-04-26
32	195.6404	58.8894	0.0	2026-02-07	123	179.9694	44.8101	0.0	2026-11-19	215	216.8368	49.8998	0.0	2027-04-27
33	210.6822	56.0606	0.0	2026-02-08	124	166.1529	45.9853	24.056	2026-11-23	216	188.53	54.05	20.882	2027-04-30
34	177.8525	58.9884	43.149	2026-02-11	125	178.8591	44.9347	0.0	2026-11-24	217	203.426	52.7561	0.0	2027-05-01
35	194.6819	57.516	0.0	2026-02-12	126	166.3787	43.5216	74.064	2026-11-28	218	216.7811	50.4801	0.0	2027-05-02
36	209.3065	54.826	0.0	2026-02-13	127	178.5806	42.5376	0.0	2026-11-29	219	193.2996	53.02	90.46	2027-05-06
37	179.7737	58.3432	35.678	2026-02-16	128	189.9527	40.9102	0.0	2026-11-30	220	207.8592	51.7597	0.0	2027-05-07
38	196.316	56.8958	0.0	2026-02-17	129	167.02	43.93	18.522	2026-12-03	221	220.9797	49.5597	0.0	2027-05-08
39	210.7601	54.2653	0.0	2026-02-18	130	179.3015	42.9353	0.0	2026-12-04	222	195.7	51.88	55.637	2027-05-11
40	180.48	58.02	14.777	2026-02-21	131	190.7351	41.2868	0.0	2026-12-05	223	209.9091	50.6563	0.0	2027-05-12
41	196.8826	56.5848	0.0	2026-02-22	132	167.35	43.27	21.05	2026-12-08	224	222.7816	48.5362	0.0	2027-05-13
42	211.2387	53.9836	0.0	2026-02-23	133	179.5039	42.2927	0.0	2026-12-09	225	196.12	51.5	13.817	2027-05-16
43	178.95	57.87	24.77	2026-02-26	134	190.8385	40.6779	0.0	2026-12-10	226	210.2174	50.2881	0.0	2027-05-17
44	195.289	56.4406	0.0	2026-02-27	135	168.08	42.43	29.881	2026-12-13	227	223.0092	48.194	0.0	2027-05-18
45	209.6036	53.8527	0.0	2026-02-28	136	180.0778	41.4746	0.0	2026-12-14	228	195.3	50.32	38.649	2027-05-21
46	180.13	56.25	52.271	2026-03-03	137	191.2898	39.9016	0.0	2026-12-15	229	209.0643	49.1443	0.0	2027-05-22
47	195.8167	54.8803	0.0	2026-03-04	138	170.2	42.2039	47.516	2026-12-18	230	221.6152	47.1282	0.0	2027-05-23
48	209.7061	52.4308	0.0	2026-03-05	139	182.1569	41.2544	0.0	2026-12-19	231	193.48	50.8	37.554	2027-05-26
49	182.2258	54.6995	58.588	2026-03-08	140	193.3366	39.6924	0.0	2026-12-20	232	207.3774	49.61	0.0	2027-05-27
50	197.3449	53.3837	0.0	2026-03-09	141	170.85	42.83	23.65	2026-12-23	233	220.025	47.5623	0.0	2027-05-28
51	210.8523	51.0584	0.0	2026-03-10	142	182.9215	41.864	0.0	2026-12-24	234	192.4	49.82	35.953	2027-05-31
52	179.8762	53.3488	57.926	2026-03-13	143	194.1912	40.2714	0.0	2026-12-25	235	206.0296	48.6596	0.0	2027-06-01
53	194.5413	52.0781	0.0	2026-03-14	144	170.87	43.1	8.094	2026-12-28	236	218.4821	46.6752	0.0	2027-06-02
54	207.7351	49.8541	0.0	2026-03-15	145	182.9919	42.1269	0.0	2026-12-29	237	191.92	48.87	30.004	2027-06-05
55	181.12	53.28	22.38	2026-03-18	146	194.3012	40.5209	0.0	2026-12-30	238	205.3031	47.7374	0.0	2027-06-06
56	195.7626	52.0114	0.0	2026-03-19	147	171.3	42.48	20.865	2027-01-02	239	217.5737	45.8125	0.0	2027-06-07
57	208.9413	49.7924	0.0	2026-03-20	148	183.307	41.5231	0.0	2027-01-03	240	192.42	47.72	35.914	2027-06-10
58	181.85	52.6	24.296	2026-03-23	149	194.5261	39.9478	0.0	2027-01-04	241	205.5211	46.6209	0.0	2027-06-11
59	196.2778	51.3535	0.0	2026-03-24	150	171.22	41.63	25.568	2027-01-07	242	217.5812	44.7644	0.0	2027-06-12
60	209.3056	49.1832	nan	2026-03-25	151	183.0753	40.6954	0.0	2027-01-08	243	194.3202	44.6071	101.382	2027-06-16
61	181.03	52.42	15.902	2026-03-28	152	194.1742	39.1608	0.0	2027-01-09	244	206.7368	43.5942	0.0	2027-06-17
62	195.4026	51.1793	0.0	2026-03-29	153	172.03	41.33	20.317	2027-01-12	245	218.2749	41.9108	0.0	2027-06-18
63	208.3907	49.0215	0.0	2026-03-30	154	183.8332	40.403	0.0	2027-01-13	246	193.97	44.07	17.784	2027-06-21
64	181.8513	51.7143	26.032	2026-04-02	155	194.8908	38.8827	0.0	2027-01-14	247	206.2791	43.0716	0.0	2027-06-22
65	196.0116	50.4959	0.0	2026-04-03	156	174.1608	42.2097	54.489	2027-01-17	248	217.734	41.4158	0.0	2027-06-23
66	208.8485	48.3872	0.0	2026-04-04	157	186.1187	41.26	0.0	2027-01-18	249	197.3562	43.0848	79.301	2027-06-26
67	181.4	51.42	12.191	2026-04-07	158	197.2993	39.6977	0.0	2027-01-19	250	209.4753	42.1121	0.0	2027-06-27
68	195.4742	50.2108	0.0	2026-04-08	159	175.68	41.9	35.091	2027-01-22	251	220.7824	40.5069	0.0	2027-06-28
69	208.2494	48.1218	0.0	2026-04-09	160	187.5825	40.9583	0.0	2027-01-23	252	196.975	44.2167	34.95	2027-07-01
70	180.9	51.73	13.164	2026-04-12	161	198.7194	39.411	0.0	2027-01-24	253	209.3131	43.2143	0.0	2027-07-02
71	195.0649	50.511	0.0	2026-04-13	162	176.2	42.35	17.784	2027-01-27	254	220.7907	41.551	0.0	2027-07-03
72	207.905	48.4013	0.0	2026-04-14	163	188.1833	41.3967	0.0	2027-01-28	255	198.675	45.9906	64.244	2027-07-06
73	180.95	51.02	21.316	2026-04-17	164	199.3838	39.8276	0.0	2027-01-29	256	211.3823	44.9398	0.0	2027-07-07
74	194.9092	49.8229	0.0	2026-04-18	165	177.6442	41.9116	34.717	2027-02-01	257	223.144	43.1819	0.0	2027-07-08
75	207.6021	47.7611	0.0	2026-04-19	166	189.5488	40.9696	0.0	2027-02-02	258	198.23	46.25	12.104	2027-07-11
76	180.2	50.45	22.245	2026-04-22	167	200.6873	39.4217	0.0	2027-02-03	259	210.9939	45.1922	0.0	2027-07-12
77	193.9997	49.2705	0.0	2026-04-23	168	177.78	42.38	14.379	2027-02-06	260	222.7996	43.4198	0.0	2027-07-13
78	206.5772	47.2459	0.0	2026-04-24	169	189.7687	41.4259	0.0	2027-02-07	261	199.22	46.48	21.635	2027-07-16
79	179.87	49.78	21.083	2026-04-27	170	200.9736	39.8553	0.0	2027-02-08	262	212.0353	45.4158	0.0	2027-07-17
80	193.4887	48.6206	0.0	2026-04-28	171	179.4275	42.0825	37.666	2027-02-11	263	223.8794	43.6305	0.0	2027-07-18
81	205.9337	46.639	0.0	2026-04-29	172	191.3625	41.1361	0.0	2027-02-12	264	198.4872	47.6329	37.694	2027-07-21
82	178.3521	49.5192	30.505	2026-05-02	173	202.5251	39.58	0.0	2027-02-13	265	211.5673	46.5362	0.0	2027-07-22
83	191.9024	48.3677	0.0	2026-05-03	174	181.15	42.52	40.409	2027-02-16	266	223.6123	44.685	0.0	2027-07-23
84	204.2965	46.4023	0.0	2026-05-04	175	193.1643	41.562	0.0	2027-02-17	267	198.1808	48.4753	26.005	2027-07-26
85	178.1383	49.6603	5.935	2026-05-07	176	204.3892	39.9848	0.0	2027-02-18	268	211.4652	47.3542	0.0	2027-07-27
86	191.7255	48.5044	0.0	2026-05-08	177	182.345	41.328	44.61	2027-02-21	269	223.6628	45.4533	0.0	2027-07-28
87	204.1467	46.5303	0.0	2026-05-09	178	194.1478	40.4011	0.0	2027-02-22	270	197.82	48.48	7.171	2027-07-31
88	178.52	49.07	19.212	2026-05-12	179	205.2051	38.8809	0.0	2027-02-23	271	211.1055	47.3588	0.0	2027-08-01
89	191.9541	47.9318	0.0	2026-05-13	180	185.625	40.0053	84.523	2027-02-26	272	223.304	45.4576	0.0	2027-08-02

including:

- Diffraction-limited visible band imaging and integral field unit (IFU) spectroscopy with adaptive optics (AO) on the world's largest telescope, with 0.005 arcsec pixels and $16\times$ the collecting area of Hubble, capable of resolving the neighborhoods of AGN,
- Suppression of sky background by a factor of 10,000 for point source imaging and spectroscopy, by shrinking the image size, enabling the necessary sensitivity,
- Wavelength coverage including key diagnostic features O III (500.7 nm), Hα (656.3 nm), Ca II (850, 854, 866 nm), and redshifted Lyα,
- Spectral resolution of 100 (for SNe) to 10,000 (for AGN velocity fields),
- Sensitivity to 29^{th} magnitude stars in 1 hour, 10 σ,
- Flux and PSF calibration in parallel with AO observations,
- When not in use for AO, flux calibration traceable to NIST, with 0.4%or better accuracy between wavelengths, to be observed by terrestrial telescope systems, then used directly, and also transferred to spectrophotometric standard stars, to meet the SN cosmology distance scale requirements,
- Mission life of at least 3 years.

The low-risk AO and instrument package for the Keck observatory will be constructed with commercial parts: wavefront sensors, mirrors, lenses, deformable mirrors, narrow-band filters to block the laser from the science instruments, and electron-multiplying CCD (EMCCD) or HgCdTe (mercury cadmium telluride) detectors for highest sensitivity. The whole AO system and instrument package is smaller than non-AO systems, and fits on a table-top. It can be demonstrated using natural guide stars (NGS) but dark sky performance requires the laser beacon because of stray light from the star. Actual design would follow a requirements analysis with the Keck observer and hardware community.

Future studies include optimization of the Keck AO and instrument package for key science, and options such as exozodiacal dust and exoplanet detection; simultaneous operation of all AO observatories on the same mountain; design of focused photometric standards; optimization of the observation sequence for minimum fuel consumption; observations shortly after dawn, when the atmosphere is still quiet; choosing a specific class of launch opportunities; enabling observations of the fine structure of the solar corona with AO on the Daniel K. Inouye Solar Telescope (DKIST); enabling observations with optical imaging interferometers like NPOI and CHARA, to gain 100x in sensitivity along with full sky coverage for extreme angular resolution of 200 microarcsec; cooperating with the European VLTI-GRAVITY infrared interferometer to extend its coverage to more targets; cooperating with other AO facilities like Gemini N/S and the LBTI; planning for use with GMT, TMT, and ELT; and establishing a working group to enable and manage future multiple orbiting beacons with multiple telescopes and interferometers.

A.9.1 Schedule Optimization Sensitivity

To assess how these delivered target sequences are sensitive to uncertainty or may change under future revisions to either engineering or operational mission parameters, we generate optimized mission profiles with varying re-targeting cost and times by multiplying their respective cost functions by factors between 0.5 and 2.0. In terms of propellant consumption, the inverse of our cost factor effectively reflects a changed total fuel allocation e.g. 1.2 x Delta V costs corresponds to approximately 83% tank size.

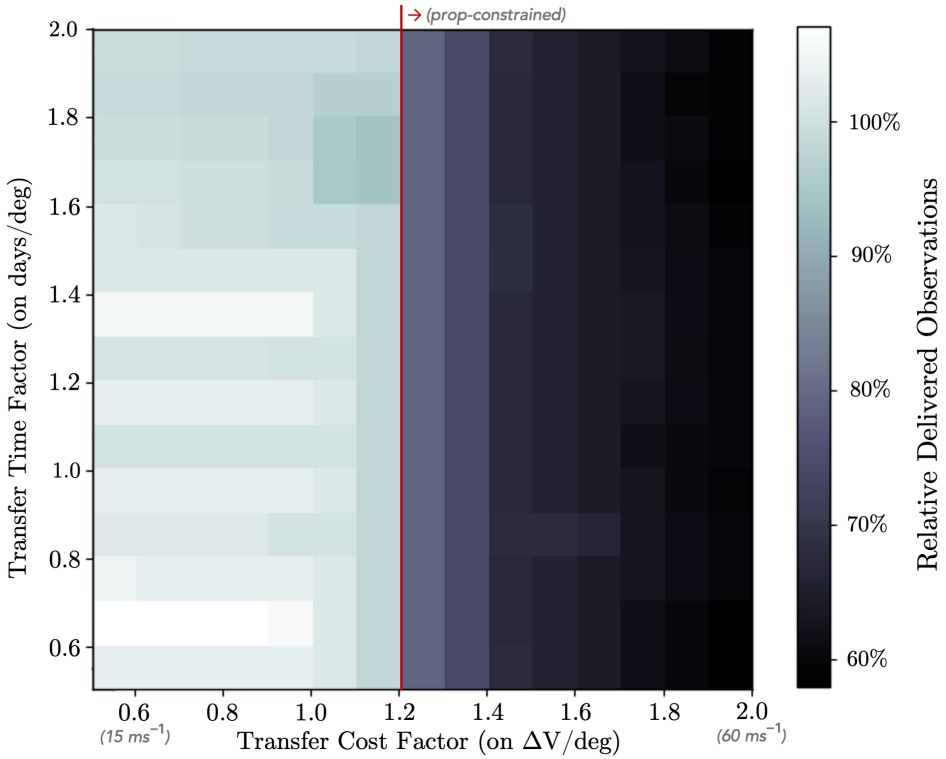

Fig 52 Sensitivity map of delivered observations to time and fuel over a mission lifetime, plotted relative to scaled transfer times and Delta V costs.

B Flux Calibration Studies

B.1 Observing Modes

Ground-based observations with different types of instruments will be more or less suitable depending on the angular rate of motion of ORCAS on the sky. Narrow-field instruments can only usefully observe ORCAS when its angular rate on the sky, ω, is low enough that ORCAS can be tracked with closed-loop guiding ($\omega < 0.1$ arcsec/sec). Some instruments could obtain useful observations running the telescope with open-loop tracking ($0.1 < \omega < 2$ arcsec/sec). For wide-field imagers, ORCAS could be observed as a streak across the field ($\omega > 2$ arcsec/sec). An example of the angular rate of ORCAS for a 5-day, equatorial HEO is shown in Figure 53, with the range of rates for different tracking regimes shaded.

Here one sees several opportunities for observations with narrow-field — generally spectroscopic — instruments. Then, ORCAS will spend a majority of its orbit in a mode suitable for open-loop tracking or for rather slow motion across the focal plane of an imager tracking at sidereal rate.

The tracking rate is important not only in terms of how stellar ORCAS will appear, but also for the length of the trails of background field stars. If the trails of the stars are too long, or if the stars are tracked and the trail of ORCAS is long, the ORCAS flux calibration signal and signal from stars will interfere with each other. The ORCAS track and the stellar tracks will not be parallel, and while ORCAS data cutting across bright stars would be clipped, there will be many more faint stars whose non-uniform background light will be hard to remove. The impact will depend on the brightness of ORCAS relative to the stars. If ORCAS flux calibration beam were $1000\times$ brighter than most stars, this would not be an issue. But as we discussed below, we don't plan to make the ORCAS flux

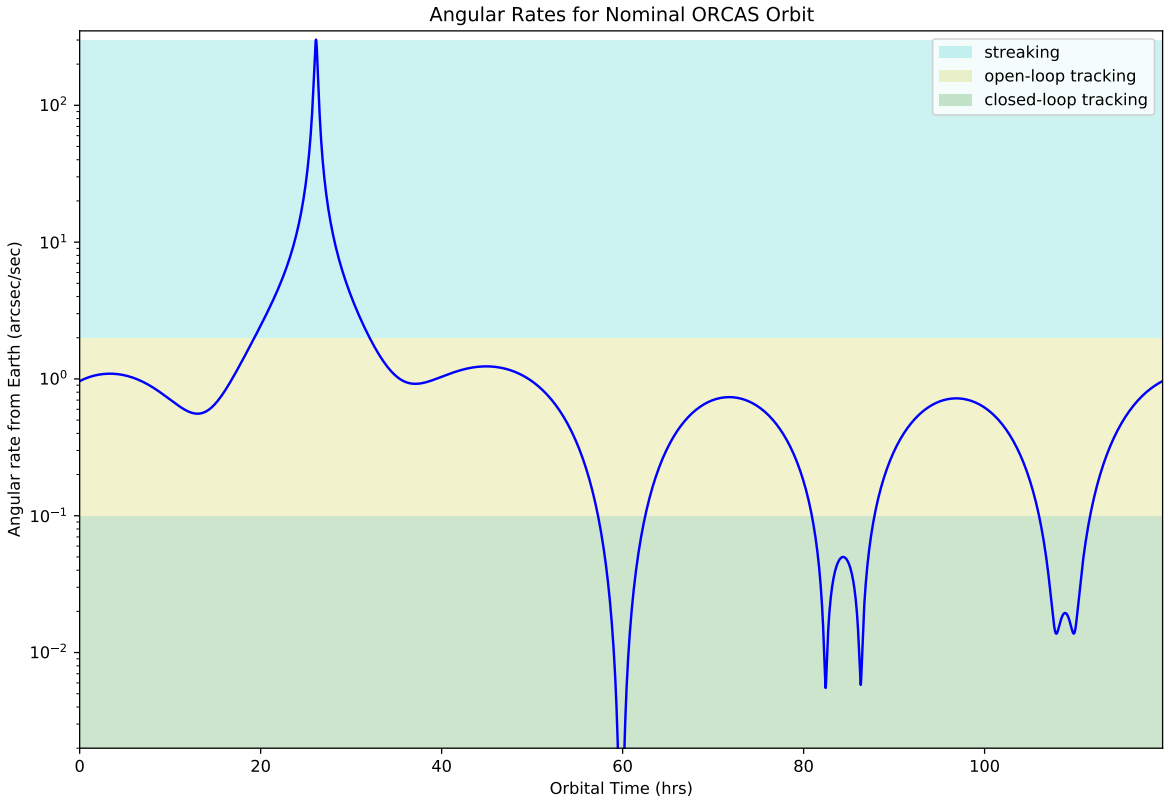

Fig 53 The angular rate of motion on the sky as seen by a ground-based telescope for the nominal ORCAS HEO orbit, in arcsec/sec, versus time along the orbit. The main astrostationary configuration is seen at 60 hrs, and other configurations presenting very slow motion on the sky.

calibration unit overwhelming bright. Given that for broadband imagers the stellar continuum will be integrated over the full filter bandpass (typically $\sim$ 100 nm), the ORCAS flux calibration beam is likely to experience occasional stellar contamination in open-loop mode, and considerable contamination in streaking mode. The impact of contamination by stars will also depend strongly on Galactic latitude. We haven't yet simulated the impact of stellar trails, but given the significant windows of time when the motion of ORCAS is slow, this issue can be left for detailed observation planning once ORCAS is flying.

Spectroscopic instruments can observe many wavelengths at once. However, the on-board monitoring detectors (PDs and ESRs) can monitor only one wavelength at a time. In order to extract the ORCAS signal using the same software as used for standard stars, ground-based observations will require statistically similar atmospheric turbulence phase screens so that all wavelengths have point-spread functions as similar as possible. Readout times for the spectrograph detectors (usually CCDs) are usually of order 60s, making very short spectroscopic exposure times very inefficient. Combining these constraints suggests that the spectroscopic observing mode would consist of ORCAS cycling through it's wavelengths many times during a single spectrographic staring observation. For example, the spectrograph could take a 600s observation of ORCAS, during which ORCAS cycles through 6 wavelengths, 10 times with 10s per wavelength. The 10 emissions of 10s each from ORCAS would sample the turbulence well and give 100s of exposure on each line, several wavelengths could be

observed in a single exposure, and the readout overhead would be modest.

Imaging observations will be different in that an imager will need to swap in a filter appropriate for a single ORCAS wavelength, observe, then readout, then perform the same sequence for the next desired filter/wavelength combination.

ORCAS will supply numerous opportunities for all tracking and observations combinations.

B.2 Wavelengths

Table 33 lists filters of upcoming major facilities for which accurate calibration – especially precise wavelength-relative calibration for studies of dark energy – would enhance the final results. Our primary focus is on the NRGST and LSST visible and NIR wavelengths for which very large samples of SNe Ia will be obtained. JWST is unlikely to obtain SN Ia samples large enough that calibration systematic errors will dominate, but doubtless accurate calibration will enhance the value of the JWST dataset. It may be impractical to also calibrate the thermal IR (i.e., beyond 2 μ m) in this mission due to the extensive use of cryogenics that would entail. UV wavelengths, again while not a driver for cosmology, could benefit from improved calibration. UV can only be observed from space, so for now we have not explored this option very deeply other than to note that it may be possible for other spacecraft to observe ORCAS under the right circumstances.

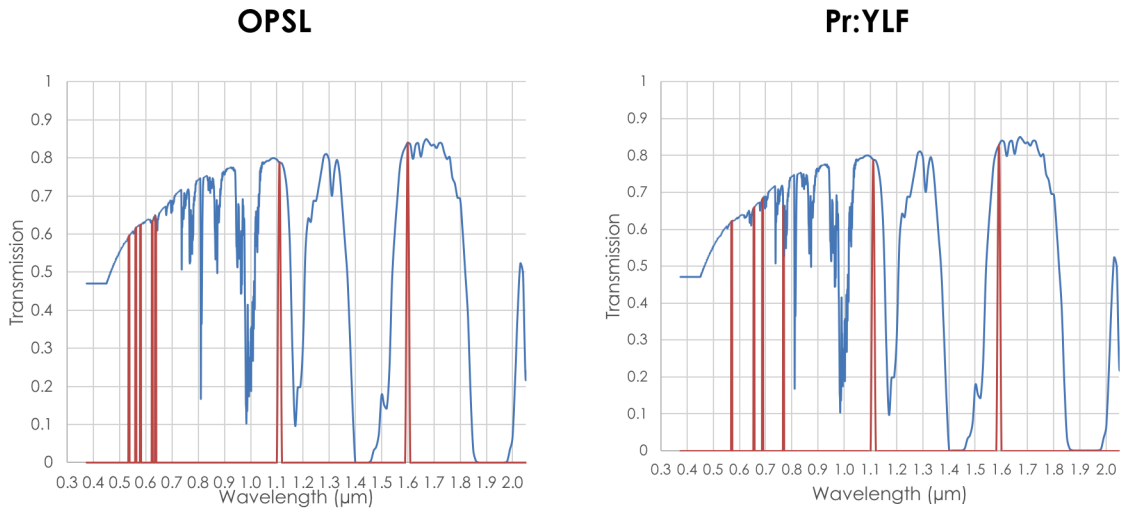

Fig 54 Example wavelengths for several possible high-power lasers, with the transmission of the Earth's atmosphere overlaid. The left panel shows lines for optically-pumped semiconductor lasers from Coherent. The right panel shows lines for laser diode pumped trivalent praseodymium crystal continuous wave lasers.

B.3 Source Types and Brightnesses

We examine various ideas for the light source that ORCAS would project to the ground.

B.3.1 Continuum versus Monochromatic Sources

Most astronomical sources, including standard stars, are continuum-dominated sources, but that does not imply that a continuum calibration source is preferred. The primary advantage to a continuum

Table 33 Filters

Telescope	Instru-ment	Filter Name	Min λ (μm)	Max λ (μm)	Mean λ (μm)	Width (μm)	Resolution ($\lambda/\Delta\lambda$
NRGST	WFI	F062	0.48	0.76	0.620	0.280	2.2
NRGST	WFI	F087	0.76	0.977	0.869	0.217	4
NRGST	WFI	F106	0.927	1.192	1.060	0.265	4
NRGST	WFI	F129	1.131	1.454	1.293	0.323	4
NRGST	WFI	F158	1.380	1.774	1.577	0.394	4
NRGST	WFI	F184	1.683	2.000	1.842	0.317	5.81
NRGST	WFI	W146	0.927	2.000	1.464	1.030	1.42
NRGST	GRS	G150	1.0	1.93	1.465	0.930	461λ (2 pix)
NRGST	PRS	P120	0.75	1.80	0.975	1.05	80–180 (2 pix)
LSST	–	u	0.3205	0.4081	0.3694	0.473	7.8
LSST	–	g	0.3873	0.5665	0.4841	0.1253	3.9
LSST	–	r	0.5376	0.7055	0.6258	0.1207	5.2
LSST	–	i	0.6765	0.8325	0.7560	0.1175	6.4
LSST	–	z	0.8035	0.9375	0.8701	0.998	8.7
LSST	–	y	0.9089	1.0897	0.9749	0.872	11.2
JWST	NIRCam	F070W	0.6048	0.7927	0.7088	0.1213	5.8
JWST	NIRCam	F090W	0.7882	1.0243	0.9083	0.1773	5.1
JWST	NIRCam	F115W	0.9976	1.3058	1.1624	0.2055	5.7
JWST	NIRCam	F140M	1.3042	1.5059	1.4074	0.1367	10.3
JWST	NIRCam	F150W	1.3041	1.6949	1.5104	0.2890	5.2
JWST	NIRCam	F162M	1.5126	1.7439	1.6297	0.1626	10.0
JWST	NIRCam	F182M	1.6960	2.0011	1.8494	0.2251	8.2
JWST	NIRCam	F200W	1.7249	2.2597	2.0028	0.4190	4.8
JWST	NIRCam	F210M	1.9619	2.2337	2.0982	0.2055	10.2
JWST	NIRCam	F250M	2.3935	2.6178	2.5049	0.1783	14.0
JWST	NIRCam	F277W	2.3673	3.2203	2.7845	0.6615	4.2
JWST	NIRCam	F300M	2.7704	3.2506	2.9940	0.3256	9.2
JWST	NIRCam	F335M	3.1203	3.6442	3.3675	0.3389	9.9
JWST	NIRCam	F356W	3.0733	4.0801	3.5935	0.7239	5.0
JWST	NIRCam	F360M	3.3260	3.9037	3.6298	0.3585	10.1
JWST	NIRCam	F410M	3.7764	4.4048	4.0887	0.4263	9.6
JWST	NIRCam	F430M	4.1228	4.4449	4.2829	0.2295	18.7
JWST	NIRCam	F444W	3.8040	5.0996	4.4394	1.0676	4.1
JWST	NIRCam	F460M	4.4653	4.8146	4.6316	0.2309	20.0
JWST	NIRCam	F480M	4.5820	5.0919	4.8213	0.3141	15.3

source is that it can calibrate many wavelengths of a spectrograph at one time, but for filtered imaging this advantage disappears.

It is import to recognize that the likely on-board brightness monitoring detectors (see § B.5) are sensitive over a very large range of wavelengths. This means that they are unable to distinguish between different spectra shapes having the same integrated intensity. In fact, the responsivity varies with wavelength sufficiently that the wavelength of the light being calibrated must be know to better than 0.1 nm in order to maintain a 0.2% calibration. For this reason, such detectors are only effective

at monitoring near-monochromatic light. Of course one could imagine using on-board monochromatic sources to transfer calibration to an on-board spectrograph, which would in turn monitor a continuous source. But this likely to add considerable complexity, and it is unclear whether the necessary on-board projector system would be any better than the projector-based calibration systems (SCALA, NISTstars, STARdice, CBP) already available on the ground.

The flux calibration issue we wish to solve also does not require that every wavelength be precisely calibrated, only that the mean run-out over hundreds of nm be small. Models of WD stars are likely to be adequate for *interpolating* the calibration between a set of discrete wavelengths.

B.3.2 Monochromatic Sources

Monochromatic sources include lasers, laser diodes and LEDs. Lasers can provide more than adequate power. Laser diodes are generally fainter, but one might consider running several at once.

Since the flux calibration system at apogee requires significant power on-board to be sufficiently bright as seen from Earth at apogee, we have first focused on TEM_{00} lasers with more than 1 W of optical power. Examples are show in Figure 54.

Conceptually attractive would be a tunable laser, which would obviate the need to fly many different light sources, and would allow wavelength choices to be optimized for whichever telescope is observing ORCAS. Examples include the EXSPLA NT242-SH-SFG in routine use at NIST, the OPOTEK Radiant X30 series QX4130, and the HUBNER Photonics C-WAVE GTR. Current tunable lasers are bulky and have a reputation as "finicky," but are improving. At any particular wavelength they also are fainter than discrete lasers. So while useful in the lab, we did not consider tunable lasers to be the best choice for ORCAS.

A challenge in using lasers will be avoiding speckle. For example, it is well known that speckle will be present across the output port of an integrating sphere illuminated with a laser.

B.3.3 Continuum Sources

While monochromatic sources are likely to be easier to work with, there might be some advantage to also having a continuum source available. Ordinary FEL lamps have spectra that are very red, and they are very hot, so we did not consider those further. Laser-driven or "supercontinuum" light sources are available over the visible and NIR. Another option is to redirect the light of the sun onto the dark side of the Earth.

B.4 System Architectures

B.4.1 Integrating Sphere

An integrating sphere (IS) is the simplest method of producing a simple and stable output beam whose shape is wavelength-independent. The output is very nearly Lambertian, going as $cos(\alpha)$ for exit angle α. The Optical and Radio Calibration Satellite (ORCAsat; https://www.orcasat.ca) will use an integrating sphere with laser diodes at 660 and 850 nm as its light sources. Initially, we envisioned a similar system for ORCAS, but with more wavelengths and more NIST-traceable detectors to monitor the output beam. However, while a bare IS is bright enough at ORCASsat's distance of 400 km, we found that obtaining a sufficiently bright IS at the distances of ORCAS is not practical.

The throughput of an IS is given by:

$$\tau_{IS} = \frac{rf}{1 - r(1 - f)} \tag{3}$$

where r is the reflectivity of the IS interior coating and f is the ratio of the area of the exit port to the area of the IS interior. For each bounce in the IS a fraction $1-r$ of the light is lost, so for N bounces, the loss is $1-r^N$. Therefore, while several bounces are needed to homogenize the angular distribution of the light, if the light does not exit the IS soon enough, the reflection loses lead to low τ_{IS}. Even a very aggressive combination of a IS 1 cm diameter IS with a 1 mm exit port only has $\tau_{IS} \sim 0.7$.

Spectralon is a typical high-quality IS coating, having a mean reflectivity of $r \sim 0.98$ for visible and NIR wavelengths. Labsphere sells a number of standard IS diameters and exit port sizes Another material often used in IS is PTFE. A 10 mm thickness ODM98 has relectivity of 98.5% at visible wavlengths, and stays above 93% over the 0.25–2.5 μm range (https://www.gigahertz-optik.com/en-us/service-and-support/knowledge-base/odm-material-specifications/).

However, even for a very small exit port, a ground-based telescope will intercept only a tiny fraction, $\epsilon_{IS} = sin^2(\alpha)$, where α is the angular extent of the ground-based telescope primary mirror as seen from ORCAS. Near apogee, when ORCAS appears astrostationary from the ground, $\alpha \sim 2.5 \times 10^{-9} D$ and so $\epsilon_{IS} \sim 2.5 \times 10^{-17}$ for a telescope diameter D. Even near perigee $\epsilon_{IS} \sim 2.5 \times 10^{-15}$. The net flux will be given by $f = I_0 \tau_{IS} \epsilon_{IS} T_{tel}$, where I_0 is the input intensity and T_{tel} is the throughput of the ground-based telescope. For 1 W of monochromatic input power at 500 nm, the expected count rates are $\sim 0.5D^2$ photons/s and $\sim 50D^2$ photon/s near apogee and perigee, respectively.

A further challenge is that for too much input optical power Spectralon will experience damage. The advertised damage threshold is $4J/cm^2$. Treatment with hexane followed by baking (128) has been shown to increase the allowed damage threshold by at least a factor of two. Cooling of the IS has helps (128), and may be necessary. PTFE has withstood up to 4.2 kW of peak power and a mean of 21 W from a pulsed laser spot of 200 μm. PTFE is also easy to clean (https://www.gigahertz-optik.com/en-us/service-and-support/knowledge-base/odm-material-specifications/). Also related to IS power limits, note that light that does not exit the IS will be absorbed and converted to heat in the IS. For instance, with an IS efficiency of 20% and a 1 W source, 0.8 W is converted to heat. PTFE itself can withstand temperatures up to 280 C, while Spectralon can withstand temperatures up to 350 C. For long duration flux calibration observations, some means to cool an IS should be considered.

B.4.2 Integrating Sphere with Concentrator

In order to boost the fraction of light intercepted from the IS exit port by a ground-based telescope, a concentrator can be used. For example, a parabolic mirror can pick-up a portion of the Lambertian exit beam and direct a nearly parallel beam to the ground. The gain when using a concentrator goes as

$$G \sim \left(\frac{D_{concentrator}}{d_{port}} \right)^2 \tag{4}$$

where d_{port} is the diameter of the IS exit port, 1 mm in our aggressive example, and $\mathrm{D}_{concentrator}$ is the diameter of the concentrator mirror. For example, a 20 cm concentrator mirror and the aggressively small 1 mm exit port diameter, $G \sim 200^2 = 4 \times 10^4$. Such a beam would have a geometric diameter ~ 500 km projected onto the Earth when ORCAS is at apogee. Wave optics would not be of material concern as the diffraction beam would be only ~ 0.6 km, which is much much less than the size of the geometric beam.

Once additional optics are introduced outside the IS, the exit beam needs to be monitored after those optics. This configuration would be similar to that employed for SCALA. The main difference is that the flux monitors on ORCAS will be placed at a tiny fraction of the total beam length. The

challenge will be in predicting the very far-field beam from measurements in the near field, or in scanning the beam from the ground by stepping ORCAS through an array of inclinations relative to the line-of-sight. For example a 500 km diameter beam footprint would require $\sim 2 \times 10^5$ samples with a 1 m ground-based telescope to fully cover the beam profile.

B.4.3 Laser Beam

Directly observing the output of a laser, as with the ORCAS AO system, would provide plenty of light even at apogee. However, the output beam of a laser can have a complex shape, including strong modulation due to speckle. The profile shape is cleanest for TEM_{00} lasers, which are available at a few wavelengths, but even then speckle would be a problem. An example is shown in (129). For this reason, we have not explored the use of a bare laser beam any further.

B.4.4 Singe-mode Optical Fiber

An ideal single-mode optical fiber fed by a laser will produce a smooth output beam, nominally characterized as a Gauss-Hermite profile. An example far-field profile scanned at NIST is shown in (130; 131). The beam width depends on the wavelength, which presents a challenge for our experiment, in which our tightest constraint is on the wavelength-relative calibration. Moreover, any non-ideal behavior, e.g., a speck of dust on the output face of the optical fiber, or speckle, will negatively impact the smoothness of the beam profile. Typical fibers have output beams of roughly F/4, so at apogee the output beam would be spread over an area larger than the Earth, making such a profile difficult to scan from the ground.

For ORCAS we would need to have a fiber for each monochromatic wavelength, and to lower the risk of contamination on the optical fiber face, for each wavelength we would like to have several different fibers; the input laser could be switched between these, so it would not be necessary to fly redundant lasers.

It would be possible to concentrate such a beam further, possibly at the cost of making the beam shape more complex and therefore making its profile on the ground less predictable.

B.5 On-board Beam Monitor

In space we would seek to implement the NIST detector-traceable system. A number of suitable detectors were explored and found to have sufficient space heritage. The simplest of these is the photodiode (PD), usually coupled to a transimpedance amplifier. PDs are know to be linear over a large range in flux and can easily respond on timescales of milliseconds. NIST supplies those with 0.1% calibration at visible wavelengths and 0.3% calibration in the NIR. More fundamental are trap detectors and electrical substitution radiometers (ESR). Si trap detectors are the most common and have flight heritage, but InGaAs trap detectors also can be obtained. Due to the high optical power needed for the ORCAS light sources, the ESR technology is viable, and has flight heritage (e.g., from the Compact Spectral Irradiance Monitor mission). An ESR responds on timescales of minutes, but its calibration by NIST is the most robust. Therefore, an ESR will be most suitable as a means of checking the calibration of fast-responding PDs.

These will respond to scattered light and particle hits. Scattered light, including reflections off the face of the detectors, will need to be carefully controlled via baffling, and tilting the detector faces. The optical power at ORCAS is likely to overwhelm the signal from particle hits, and for PDs with fast response (kHz), many such events can be filtered out of the response time series.

Our strategy will be to fly all of these technologies if possible. The detectors and electronics are sufficiently compact to allow this. This strategy allows intercomparison over the mission lifetime, as with CSIM, where it was shown that the response of their PDs changed by of order a tenth of a percent over a lifetime of around 1.5 yrs (so far). The different levels to which NIST can calibrate each type of device, and the different response timescales makes it essential to fly at minimum a PD and an ESR.

For the pure integrating sphere architecture it would be possible to mount the monitor detectors in the wall of the IS since the detectors would see light that is statistically the same as that leaving the IS exit port. For any of the laser or concentrator architectures, the monitoring detectors would need to monitor the exit beam itself. Relating this intercepted cross-section of the ORCAS exit beam with the far-field beam seen at the ground will require careful work, the details of which are not yet resolved.

B.6 Reflected Sunlight

The spectrum of the Sun has been calibrated with satellites such as the Compact Solar Irradiance Monitor (CSIM) cubesat (132). (133) has proposed use of a convex mirror to form a virtual image of the Sun that can be viewed from a wide range of angles; this concept as been patented. The primary issues that we have identified is the difficulty of calibrating the reflected light over the range of angles (the BDRF) and over the lifetime of the mission. In addition, the Sun is a continuum source and can't be turned off. Use of broadband sources requires that facilities observing ORCAS know their wavelength bandpass very well; this is not a challenge for spectrophotometry, but may be for broadband filter imaging. Since the Sun can't be turned off, a solar reflection system would require a shutter; since it would need to cover all angles, such a shutter would be as large as the reflector itself. If such a shutter is shown to not present an issue, this would be a very inexpensive light source for applications that simply need a continuum source with only modestly-accurate flux calibration.

B.7 Determining the Beam Far-Field Beam Profile

Ideally, by sampling a portion of the exit beam on-board ORCAS we can reliably predict the flux that a ground-based telescope should receive. For our primary goal of accurate wavelength-relative calibration, simple geometric factors can be dealt with. For beams whose profiles are wavelength-dependent, as with the single-mode fiber, such a prediction is even more challenging.

For a given monochromatic wavelength we want to determine a ratio, R, that will relate the on-board monitored flux to the flux predicted on the ground (minus the atmosphere).

$$R(\lambda) = \frac{\iint_{\Omega_{\mathrm{ground}}} B(\theta,\phi,\lambda) * P(\theta,\phi,\lambda)\, d\theta\, d\phi}{\iint_{\Omega_{\mathrm{ORCAS}}} B(\theta,\phi,\lambda)\, d\theta\, d\phi} \tag{5}$$

where $B(\theta,\phi)$ is the near-field beam profile, Ω_{ORCAS} is the solid angle monitored by the on-board PD, ESR or trap detector, Ω_{ground} is the solid angle monitored by the telescope on the ground, and $P(\theta,\phi)$ is the transfer function between the near-field beam and the far-field beam. $B(\theta,\phi)$ can be measured pre-flight, and an on-board scanning system could measure it in flight. But for all of the examples above, save perhaps the bare IS port, the perturbation of the beam projected onto the ground, $P(\theta,\phi)$ either needs to be predicted (from some combination of calculations, ground-based scanning, and scanning on ORCAS) or directly scanned for each wavelength and calibration campaign .

B.7.1 Scanning the Beam from the Ground

We have considered the practicality of scanning the beam from the ground as a check on the beam profile. Recall that for absolute wavelength-relative calibration we simply need to measure the ratios of $R(\lambda)$ from Eq 5 between wavelengths:

$$\mathcal{R}(\lambda_\rangle, \lambda_|) = R(\lambda_i)/R(\lambda_j) \tag{6}$$

The challenges include the number of samples required to cover the beam, the number of wavelengths needed to be covered, the photon statistics of the ORCAS source, and the impact of atmospheric scintillation. ORCAS will be brighter at perigee, and its beam footprint on Earth will be about $100\times$ more compact. However, ORCAS will be steaking across the sky, making a controlled scan of its beam profile exceedingly difficult, if not impossible. Apogee presents the complementary challenge, with a beam footprint that is $100\times$ larger and with ORCAS being $100\times$ fainter; this nominally makes scanning at apogee $\mathcal{O}(10^4)$ times harder than if ORCAS were magically stationary at perigee.

For a bare IS, the beam spans 2π sr and would be impractical to scan; fortunately this beam is the one that is most predictable. An IS with a concentrator can produce a more compact beam, but it will still be hundreds of km in diameter, requiring $\mathcal{O}(10^{11})$ samples, which is also impractical. An F/4 beam exiting a single-mode fiber would have an even larger footprint. Therefore, scans from the ground would only be useful as a sub-sampled check on the beam profile.

Atmospheric scintillation noise sets the minimum exposure time per sample. Scintillation noise was received renewed interest, as it is a limiting factor in detecting exoplanet transits from the ground. (134) show that scintillation noise is around 0.3% for major observatories, such as Maunakea and Paranal. This value is about 50% larger than that given by Young's canonical formula. A modified version of Young's formula scaled to modern data gives:

$$\sigma_Y^2 = 10^-5\, C_Y^2\, D^{-4/3}\, t^{-1}\, X^3\, e^{-2h_{obs}/H} \tag{7}$$

where σ_Y is the RMS scintillation contribution for a telescope of diameter D at an observatory at altitude h_{obs}, for exposure time t, for a target at airmass X. H is the atmospheric scale height, which is around 8 km according to (134). For Maunakea, the median value of C_Y is 1.63, with iterquartile range of 1.34–2.02. However, Young's formula does not scale well with the more complete formula given by (134):

$$\sigma_I = 17.34 D^{-7/3} X^3 \int_0^\infty h^2 C_n^2(h) dh \tag{8}$$

for short exposures and

$$\sigma_I = 10.66 D^{-4/3} t^{-1} X^{3.5} \int_0^\infty \frac{h^2 C_n^2(h)}{V(h)} dh \tag{9}$$

for long exposures. Here $C_n^2(h)$ is the vertical refractive index structure function and $V(h)$ is the wind velocity perpendicular to telescope the line of sight. The dividing line between "short" and "long" exposures itself has the dependence

$$t_{knee} = 0.62\ D\ X^{0.5\pm0.5} \int_0^\infty \frac{1}{V(h)} dh, \tag{10}$$

with the ±0.5 signifying parallel or perpendicular wind directions, respectively. t_{knee} lands right in

the tenth to hundredth second range at which we would want to scan the ORCAS beam. Similar formulae are given for telescopes with large central obstructions, such as the Vera Rubin telescope, Averaging over scintillation has added importance since it is chromatic

However, scanning the entire beam footprint isn't needed, as long as the wavelength-dependence of the portion of the beam observed from the ground is well characterized relative to the wavelength-dependence of the portion of the beam that is monitored on ORCAS.

B.7.2 Scanning the Beam in the Lab

Near-field scanning of the beam in the lab would be one of the payload validation activities. This can be done by mounting a detector on a scanning stage, or by changing the orientation of the ORCAS flux calibration payload with respect to the detector. In one of the responses to our RFI, NIST indicated that they would be capable of providing such scans. Note that careful attention to stray light is key for such measurements.

A ground-based telescope will be observing the far-field beam from ORCAS; if this could be scanned in the lab it could greatly reduce the need for scanning the beam from the ground. The far-field is a handy mathematical construct rather than a physical one, and is defined to start at the Fraunhofer distance, d_F, defined as

$$d_F \sim 2D^2/\lambda \tag{11}$$

where D is the diameter of the exit beam at ORCAS[2]. We are primarily concerned with the cases of an IS with concentrator optics, or the output of a single-mode fiber. For a 20 cm diameter concentrator measured at $\lambda = 1\,\mu$m one has $d_F \sim 2 \times 200^2/10^{-3} \sim 8 \times 10^7$ mm. This is 80 km, and therefore impossible to measure in a lab. On the other hand, for a $10\,\mu$m diameter single-mode fiber core, $d_F \sim 2 \times 10^{-2^2}/10^{-3} \sim 0.2$ mm. So in this case, measuring the far-field in the lab is definitely possible. For a bare IS exit port of 1 mm diameter $d_F \sim 2 \times 1^2/10^{-3} \sim 2 \times 10^3$ mm, or 2 m, which is also possible within the confines of a lab.

One possibility that we have begun to examine is the 40 m vacuum tunnel at Caltech, developed for LIGO (http://www.ligo.caltech.edu/news/ligo20191104). This tube has been carefully baffled using super-polished stainless steel that is coated with diamond-like carbon the strongly absorbs light. The baffles are tilted so that any light that is not absorbed is directed away from the detector. A 40 m separation would be in the far-field for an aperture up to 4.5 mm. This could help in testing predictions for the far-field beam from near-field measurements, which could then be applied to the IS plus concentrator case.

B.7.3 Scanning the On-board ORCAS

A translation stage holding a fast-response detector such as a PD could scan the ORCAS exit beam. The ability to predict the far-field beam (that the ground will see) is enhanced if the on-board scanning is performed some distance from the beam exit. The same near-field/far-field distinction as for the lab applies. So scanning the output of a single-mode fiber in the far-field would fit within ORCAS. The cases of an IS with our without a concentrator would be near-field scans.

[2]Technically D is the size of any source of diffraction.

B.8 Spacecraft Reflected Light

A complication that ORCAS will introduce is light reflected off the spacecraft while viewing the flux calibration light source. When viewing ORCAS from the ground at night, the face of the ORCAS spacecraft will be sunward. It will be possible to rotate the solar panels to minimize their reflected light. The reflections will have a combination of diffuse and specular components, with the later being very sensitive to orientation and therefore having higher temporal variation.

Our nominal plan will be to flash the ORCAS light sources on and off so that the background can be subtracted. This mode is reliant on stability in the amount of reflected light relative to the brightness and observation duration of the calibration source. For spectroscopy, it should be possible to spectrally interpolate and subtract the background. The background will have a solar spectrum, modulated by spectral properties on the ORCAS spacecraft materials. The former is known and the later should be rather smooth. For imaging in streaking mode, temporal variations in the reflected light will translate into spatial variations along the satellite streak. Therefore, spatial interpolation of the background should be possible as long as temporal variations are slow compared to the angular rate of ORCAS across the imager. Near perigee ORCAS will be crossing the sky at a rate of ~ 200 arcsec/sec, so for ground-based images of FWHM = 1 arcsec, the interpolation should be good for background variations slower than about 10 Hz.[3]

It is important to note that, while the ORCAS flux calibration beam may be monochromatic, imagers typically use filters of width ~ 100 nm, so the reflected solar spectrum will be integrated over this entire wavelength interval.

B.8.1 Astronomical magnitudes, in the AB system, of blackbody sources and of their reflections

What follows is some general information on the magnitudes of blackbody (or near-blackbody, for example the Sun) sources and of their reflections; so that we can then estimate apparent magnitudes, as observed from the Earth, of light — which predominantly will be solar light — that is reflected from surfaces of ORCAS.

We begin with some necessary formulae:

$$\underline{\textbf{Definition}}\ \textbf{of AB magnitude}^4\textbf{:} \qquad \boldsymbol{m_{\rm AB} \equiv -2.5 \log_{10} f_\nu^{\rm CGS} - 48.60,} \quad (12)$$

where $\boldsymbol{f_\nu^{\rm CGS}}$ is the spectral flux density from the light source, at the location of the observer, in the CGS units of erg s^{-1} cm^{-2} Hz^{-1};

$$\underline{\textbf{Planck's Law}}\ \textbf{of blackbody spectral radiance:} \quad \boldsymbol{B_\nu(\nu, T) = \frac{2h\nu^3}{c^2} \frac{1}{e^{\frac{h\nu}{k_B T}} - 1},} \quad (13)$$

where $\boldsymbol{h}$ ($= 6.626 \times 10^{-34}$ m^2 kg s^{-1}) is Planck's constant, $\boldsymbol{\nu}$ is the frequency, in Hz, of the output light that is under consideration; $\boldsymbol{c}$ ($= 2.998 \times 10^8$ m s^{-1}) is the speed of light; $\boldsymbol{k_B}$ ($= 1.381 \times 10^{-23}$ m^2 kg s^{-2} K^{-1}) is Boltzmann's constant; $\boldsymbol{T}$ is the temperature in Kelvin of the blackbody light source; and $\boldsymbol{B_\nu(\nu, T)}$ is the spectral radiance from the blackbody light source (in units of

[3] Collecting 99.9% of the light for a ground-based PSF requires a region of about 5 $\times$ FWHM. One can't fit the background at higher frequency than this. So, a segment of 20 arcsec contains 4 PSF-sized samples, one of which contains the ORCAS, leaving 3 degrees of freedom for fitting the background.

[4] The AB magnitude system was first defined in Ref. (135), and is the only absolute standards-based (*i.e.*, invariantly convertible, per its definition, to SI-defined units) magnitude system presently in use for optical astronomy. (The Jansky, another absolute unit, is presently used in radio and microwave astronomy.)

W m^{-2} sr^{-1} Hz^{-1});

Conversion formula from f_ν^{CGS} to f_ν^{SI}: $$f_\nu^{\mathrm{CGS}} = 1000 f_\nu^{\mathrm{SI}}, \quad (14)$$

where both f_ν^{CGS} and f_ν^{SI} are the spectral flux density from the light source at the location of the observer. f_ν^{CGS} is in CGS units of erg s^{-1} cm^{-2} Hz^{-1}, and f_ν^{SI} is in the standard SI units of W m^{-2} Hz^{-1};

Conversion formula from the spectral radiance B_ν of a spherical light source of radius R, to the spectral flux density f_ν^{SI} at a distance d from the center of the light source (where $d > R$): $$f_\nu^{\mathrm{SI}} = \frac{\pi R^2}{d^2} B_\nu, \quad (15)$$

where both R and d are in meters; and, as previously, B_ν is the spectral radiance from the light source in units of W m^{-2} sr^{-1} Hz^{-1} and f_ν^{SI} is the spectral flux density from the light source in units of W m^{-2} Hz^{-1}.

We now include some important constants here:

Definition	Symbol	Value and units	
Average radius of the solar photosphere	$R_\odot$	6.963×10^8	m
Average temperature of the solar photosphere	$T_\odot$	5778.0	K
Average Earth-Sun distance (= 1 AU)	$d_\oplus$	1.496×10^{11}	m
Planck's constant	h	6.626×10^{-34}	m^2 kg s^{-1}
Speed of light in vacuum	c	2.998×10^8	m s^{-1}
Boltzmann's constant	k_B	1.381×10^{-23}	m^2 kg s^{-2} K^{-1}

Let us now consider the case of diffuse, Lambertian solar reflection from a flat spacecraft surface of area A, where this particular spacecraft surface has a diffuse reflection coefficient C_d. (We will assume that this fraction C_d of the solar radiation incident on the surface reflects in a perfectly Lambertian way, and that the value of C_d does not depend on wavelength.)

We then will have that

$$m_{\mathrm{AB}}(\lambda) = -2.5 \log_{10} \left[\frac{C_d A \cos\theta \cos\phi}{4 l^2 \lambda^3 \left(e^{\frac{2489.5}{\lambda}} - 1 \right)} \right] - 52.442, \quad (16)$$

where λ is the wavelength (in nm) of the reflected solar light that is under consideration, θ is the angle between the surface normal and a ray from the surface to the observer, ϕ is the angle between the surface normal and a ray from the surface toward the Sun, and l is the distance (in m) of the spacecraft from the observer on the Earth's surface.

Just for example, for a specific case where $C_d = 0.5$, A = 1 m^2, $\theta = 0°$, $\phi = 60°$, λ = 532 nm, and $l = 10^8$ m (= 100,000 km), we then have that

$$m_{\mathrm{AB}} = +16.084. \quad (17)$$

B.8.2 Advanced Materials to Suppress Solar Reflections

While the above is a rough baseline example, considerable study on darkening starshades for exoplanet observations is applicable (136). Materials like Vantablack have $C_d \sim 0.00035$ at normal incidence;

if such a material could be used it would reduce the brightness to $m_{\rm AB} \sim 24$ for $\phi = 0^\circ$ and all other variables the same.

Very diffuse reflection with $C_d \sim 0.02$ can be obtain by mixing carbon black into microporous PTFE[5]. This material, in the form of 2.5 mm thin sheets, has been flown on NASA's OSIRIS-REx mission (137) [6]. This would be sufficient to dim ORCAS to $m_{\rm AB} \sim 20$ for $l = 100,000$ km.

[5]https://www.berghof-fluoroplastics.com/en/products/optopolymerr-optical-materials-and-coatings/engineered-parts
[6]https://www.berghof.com/en/magazine/article/ptfe-from-berghof-goes-into-space-with-the-osiris-rex-mission

8 Bibliography

References

[1] K. Gebhardt, J. Adams, D. Richstone, *et al.*, "The Black Hole Mass in M87 from Gemini/NIFS Adaptive Optics Observations," *The Astrophysical Journal* **729**, 119 (2011).

[2] S. Veilleux, G. Cecil, and J. Bland-Hawthorn, "Galactic Winds," ARA&A **43**, 769–826 (2005).

[3] F. Müller-Sánchez, E. K. S. Hicks, M. Malkan, *et al.*, "The Keck/OSIRIS Nearby AGN Survey (KONA). I. The Nuclear K-band Properties of Nearby AGN," ApJ **858**, 48 (2018).

[4] Gravity Collaboration, A. Amorim, M. Bauböck, *et al.*, "The central parsec of NGC 3783: a rotating broad emission line region, asymmetric hot dust structure, and compact coronal line region," A&A **648**, A117 (2021).

[5] J. E. Greene, J. Strader, and L. C. Ho, "Intermediate-Mass Black Holes," ARA&A **58**, 257–312 (2020).

[6] P. Madau and F. Haardt, "Cosmic Reionization after Planck: Could Quasars Do It All?," *The Astrophysical Journal Letters* **813**, L8 (2015).

[7] J. Kormendy and L. C. Ho, "Coevolution (Or Not) of Supermassive Black Holes and Host Galaxies," *Annual Review of Astronomy and Astrophysics* **51**, 511–653 (2013).

[8] J. C. Lee, J. Kennicutt, Robert C., S. J. J. G. Funes, *et al.*, "Dwarf Galaxy Starburst Statistics in the Local Volume," ApJ **692**, 1305–1320 (2009).

[9] J. M. Bellovary, C. E. Cleary, F. Munshi, *et al.*, "Multimessenger signatures of massive black holes in dwarf galaxies," MNRAS **482**, 2913–2923 (2019).

[10] Event Horizon Telescope Collaboration, "First M87 Event Horizon Telescope Results. VI. The Shadow and Mass of the Central Black Hole," *The Astrophysical Journal Letters* **875**, L6 (2019).

[11] J. N. Bahcall and R. A. Wolf, "Star distribution around a massive black hole in a globular cluster.," *The Astrophysical Journal* **209**, 214–232 (1976).

[12] L. Blecha, A. Loeb, and R. Narayan, "Double-peaked narrow-line signatures of dual supermassive black holes in galaxy merger simulations," MNRAS **429**, 2594–2616 (2013).

[13] H.-C. Hwang, Y. Shen, N. Zakamska, *et al.*, "Varstrometry for Off-nucleus and Dual Subkiloparsec AGN (VODKA): Methodology and Initial Results with Gaia DR2," ApJ **888**, 73 (2020).

[14] S. Satyapal, N. J. Secrest, C. Ricci, *et al.*, "Buried AGNs in Advanced Mergers: Mid-infrared Color Selection as a Dual AGN Candidate Finder," ApJ **848**, 126 (2017).

[15] R. W. Pfeifle, S. Satyapal, N. J. Secrest, *et al.*, "Buried Black Hole Growth in IR-selected Mergers: New Results from Chandra," ApJ **875**, 117 (2019).

[16] M. Koss, R. Mushotzky, S. Veilleux, *et al.*, "Host Galaxy Properties of the Swift Bat Ultra Hard X-Ray Selected Active Galactic Nucleus," ApJ **739**, 57 (2011).

[17] M. J. Koss, L. Blecha, P. Bernhard, *et al.*, "A population of luminous accreting black holes with hidden mergers," Nature **563**, 214–216 (2018).

[18] R. W. Pfeifle, S. Satyapal, C. Manzano-King, *et al.*, "A Triple AGN in a Mid-infrared Selected Late-stage Galaxy Merger," ApJ **883**, 167 (2019).

[19] C. Rodriguez, G. B. Taylor, R. T. Zavala, *et al.*, "A Compact Supermassive Binary Black Hole System," ApJ **646**, 49–60 (2006).

[20] L. Blecha, W. Brisken, S. Burke-Spolaor, *et al.*, "Detecting Offset Active Galactic Nuclei," *Astro2020: Decadal Survey on Astronomy and Astrophysics* **2020**, 318 (2019).

[21] E. Treister, G. C. Privon, L. F. Sartori, *et al.*, "Optical, Near-IR, and Sub-mm IFU Observations of the Nearby Dual Active Galactic Nuclei MRK 463," ApJ **854**, 83 (2018).

[22] S. L. Ellison, D. R. Patton, J. T. Mendel, *et al.*, "Galaxy pairs in the Sloan Digital Sky Survey - IV. Interactions trigger active galactic nuclei," MNRAS **418**, 2043–2053 (2011).

[23] S. Satyapal, S. L. Ellison, W. McAlpine, *et al.*, "Galaxy pairs in the Sloan Digital Sky Survey - IX. Merger-induced AGN activity as traced by the Wide-field Infrared Survey Explorer," MNRAS **441**, 1297–1304 (2014).

[24] F. Rigaut, R. McDermid, G. Cresci, *et al.*, "MAVIS conceptual design," in *Society of Photo-Optical Instrumentation Engineers (SPIE) Conference Series*, *Society of Photo-Optical Instrumentation Engineers (SPIE) Conference Series* **11447**, 114471R (2020).

[25] A. G. Riess, A. V. Filippenko, P. Challis, *et al.*, "Observational Evidence from Supernovae for an Accelerating Universe and a Cosmological Constant," AJ **116**, 1009–1038 (1998).

[26] S. Perlmutter, G. Aldering, G. Goldhaber, *et al.*, "Measurements of Ω and Λ from 42 High-Redshift Supernovae," ApJ **517**, 565–586 (1999).

[27] S. Alam, M. Aubert, S. Avila, *et al.*, "Completed SDSS-IV extended Baryon Oscillation Spectroscopic Survey: Cosmological implications from two decades of spectroscopic surveys at the Apache Point Observatory," Phys. Rev. D **103**, 083533 (2021).

[28] J. Melbourne, K. S. Dawson, D. C. Koo, *et al.*, "Rest-Frame R-band Light Curve of a z ~1.3 Supernova Obtained with Keck Laser Adaptive Optics," AJ **133**, 2709–2715 (2007).

[29] J. E. Carrick, I. M. Hook, E. Swann, *et al.*, "Optimising a magnitude-limited spectroscopic training sample for photometric classification of supernovae," *arXiv e-prints* , arXiv:2012.12122 (2020).

[30] H. K. Fakhouri, K. Boone, G. Aldering, *et al.*, "Improving Cosmological Distance Measurements Using Twin Type Ia Supernovae," ApJ **815**, 58 (2015).

[31] K. Boone, G. Aldering, P. Antilogus, *et al.*, "The Twins Embedding of Type Ia Supernovae. I. The Diversity of Spectra at Maximum Light," ApJ **912**, 70 (2021).

[32] K. Boone, G. Aldering, P. Antilogus, *et al.*, "The Twins Embedding of Type Ia Supernovae. II. Improving Cosmological Distance Estimates," ApJ **912**, 71 (2021).

[33] P. L. Kelly, M. Hicken, D. L. Burke, *et al.*, "Hubble Residuals of Nearby Type Ia Supernovae are Correlated with Host Galaxy Masses," ApJ **715**, 743–756 (2010).

[34] M. Sullivan, A. Conley, D. A. Howell, *et al.*, "The dependence of Type Ia Supernovae luminosities on their host galaxies," MNRAS **406**, 782–802 (2010).

[35] M. Childress, G. Aldering, P. Antilogus, *et al.*, "Host Galaxy Properties and Hubble Residuals of Type Ia Supernovae from the Nearby Supernova Factory," ApJ **770**, 108 (2013).

[36] M. J. Childress, C. Wolf, and H. J. Zahid, "Ages of Type Ia supernovae over cosmic time," MNRAS **445**, 1898–1911 (2014).

[37] M. Rigault, G. Aldering, M. Kowalski, *et al.*, "Confirmation of a Star Formation Bias in Type Ia Supernova Distances and its Effect on the Measurement of the Hubble Constant," ApJ **802**, 20 (2015).

[38] M. Rigault, V. Brinnel, G. Aldering, *et al.*, "Strong dependence of Type Ia supernova standardization on the local specific star formation rate," A&A **644**, A176 (2020).

[39] J. Nordin, D. Rubin, J. Richard, *et al.*, "Lensed Type Ia supernovae as probes of cluster mass models," MNRAS **440**, 2742–2754 (2014).

[40] R. M. Quimby, M. Oguri, A. More, *et al.*, "Detection of the Gravitational Lens Magnifying a Type Ia Supernova," *Science* **344**, 396–399 (2014).

[41] S. A. Rodney, B. Patel, D. Scolnic, *et al.*, "Illuminating a Dark Lens : A Type Ia Supernova Magnified by the Frontier Fields Galaxy Cluster Abell 2744," ApJ **811**, 70 (2015).

[42] P. L. Kelly, S. A. Rodney, T. Treu, *et al.*, "Deja Vu All Over Again: The Reappearance of Supernova Refsdal," ApJ **819**, L8 (2016).

[43] A. Goobar, R. Amanullah, S. R. Kulkarni, *et al.*, "iPTF16geu: A multiply imaged, gravitationally lensed type Ia supernova," *Science* **356**, 291–295 (2017).

[44] D. Rubin, B. Hayden, X. Huang, *et al.*, "The Discovery of a Gravitationally Lensed Supernova Ia at Redshift 2.22," ApJ **866**, 65 (2018).

[45] X. Huang, C. Storfer, A. Gu, *et al.*, "Discovering New Strong Gravitational Lenses in the DESI Legacy Imaging Surveys," ApJ **909**, 27 (2021).

[46] R. C. Bohlin, L. Colina, and D. S. Finley, "White Dwarf Standard Stars: G191-B2B, GD 71, GD 153, HZ 43," AJ **110**, 1316 (1995).

[47] R. C. Bohlin, I. Hubeny, and T. Rauch, "New Grids of Pure-hydrogen White Dwarf NLTE Model Atmospheres and the HST/STIS Flux Calibration," AJ **160**, 21 (2020).

[48] A. Renzini, C. Cesarsky, S. Cristiani, *et al.*, "Eso for goods' sake," *ESO ASTROPHYSICS SYMPOSIA* , 332–337 (2003).

[49] J. P. Gardner, J. C. Mather, M. Clampin, *et al.*, "Science with the James Webb space telescope," in *Space Telescopes and Instrumentation I: Optical, Infrared, and Millimeter*, J. C. Mather, H. A. MacEwen, and M. W. M. de Graauw, Eds., **6265**, 171 – 182, International Society for Optics and Photonics, SPIE (2006).

[50] B. L. Ellerbroek, C. Boyer, C. Bradley, *et al.*, "A conceptual design for the Thirty Meter Telescope adaptive optics systems," in *Society of Photo-Optical Instrumentation Engineers (SPIE) Conference Series*, B. L. Ellerbroek and D. Bonaccini Calia, Eds., *Society of Photo-Optical Instrumentation Engineers (SPIE) Conference Series* **6272**, 62720D (2006).

[51] J. P. Gardner, J. C. Mather, M. Clampin, *et al.*, "The james webb space telescope," *Space Science Reviews* **123**, 485–606 (2006).

[52] R. Windhorst, N. Hathi, S. Cohen, *et al.*, "High resolution science with high redshift galaxies," *Advances in Space Research* **41**, 1965 (2008).

[53] R. G. Abraham, N. R. Tanvir, B. X. Santiago, *et al.*, "Galaxy morphology to I=25 mag in the Hubble Deep Field," MNRAS **279**, L47–L52 (1996).

[54] S. P. Driver, R. A. Windhorst, E. J. Ostrander, *et al.*, "The Morphological Mix of Field Galaxies to M I = 24.25 mag (b J approximately 26 mag) from a Deep Hubble Space Telescope WFPC2 Image," ApJ **449**, L23 (1995).

[55] S. P. Driver, A. Fernández-Soto, W. J. Couch, *et al.*, "Morphological number counts and redshift distributions to [formula][f]i¡26[/f][/formula] from the hubble deep field: Implications for the evolution of ellipticals, spirals, and irregulars," *The Astrophysical Journal* **496**, L93–L96 (1998).

[56] K. Glazebrook, R. Ellis, B. Santiago, *et al.*, "The morphological identification of the rapidly evolving population of faint galaxies," MNRAS **275**, L19–L22 (1995).

[57] S. C. Odewahn, R. A. Windhorst, S. P. Driver, *et al.*, "Automated morphological classification in deep [ITAL]hubble space telescope UBVI[/ITAL] fields: Rapidly and passively evolving faint galaxy populations," *The Astrophysical Journal* **472**, L13–L16 (1996).

[58] S. H. Cohen, R. A. Windhorst, S. C. Odewahn, *et al.*, "The hubble space telescope WFPC2 b-band parallel survey: A study of galaxy morphology for magnitudes $18 \leq b \leq 27$," *The Astronomical Journal* **125**, 1762–1783 (2003).

[59] N. P. Hathi, "High redshift galaxies in the hubble ultra deep field," *Publications of the Astronomical Society of the Pacific* **120**, 1255–1257 (2008). Full publication date: 24 October 2008.

[60] S. M. Pascarelle, R. A. Windhorst, S. P. Driver, *et al.*, "The serendipitous discovery of a group or cluster of young galaxies at [ITAL]z[/ITAL] $\simeq$ 2.40 in deep [ITAL]hubble space telescope[/ITAL] WFPC2 images," *The Astrophysical Journal* **456** (1996).

[61] R. A. Windhorst, V. A. Taylor, R. A. Jansen, *et al.*, "A Hubble Space Telescope Survey of the Mid-Ultraviolet Morphology of Nearby Galaxies," ApJS **143**, 113–158 (2002).

[62] D. M. Elmegreen, B. G. Elmegreen, S. Ravindranath, *et al.*, "Resolved Galaxies in the Hubble Ultra Deep Field: Star Formation in Disks at High Redshift," ApJ **658**, 763–777 (2007).

[63] R. E. Griffiths, S. Casertano, K. U. Ratnatunga, *et al.*, "The Morphology of Faint Galaxies in Medium Deep Survey Images Using WFPC2," ApJ **435**, L19 (1994).

[64] R. E. Williams, B. Blacker, M. Dickinson, *et al.*, "The Hubble Deep Field: Observations, Data Reduction, and Galaxy Photometry," AJ **112**, 1335 (1996).

[65] M. Giavalisco, H. C. Ferguson, A. M. Koekemoer, *et al.*, "The Great Observatories Origins Deep Survey: Initial Results from Optical and Near-Infrared Imaging," ApJ **600**, L93–L98 (2004).

[66] H.-W. Rix, M. Barden, S. V. W. Beckwith, *et al.*, "GEMS: Galaxy Evolution from Morphologies and SEDs," ApJS **152**, 163–173 (2004).

[67] S. V. W. Beckwith, M. Stiavelli, A. M. Koekemoer, *et al.*, "The Hubble Ultra Deep Field," AJ **132**, 1729–1755 (2006).

[68] N. Scoville, H. Aussel, M. Brusa, *et al.*, "The Cosmic Evolution Survey (COSMOS): Overview," ApJS **172**, 1–8 (2007).

[69] N. A. Grogin, D. D. Kocevski, S. M. Faber, *et al.*, "CANDELS: The Cosmic Assembly Near-infrared Deep Extragalactic Legacy Survey," ApJS **197**, 35 (2011).

[70] A. M. Koekemoer, S. M. Faber, H. C. Ferguson, *et al.*, "CANDELS: The Cosmic Assembly Near-infrared Deep Extragalactic Legacy Survey—The Hubble Space Telescope Observations, Imaging Data Products, and Mosaics," ApJS **197**, 36 (2011).

[71] R. J. Bouwens, G. D. Illingworth, P. A. Oesch, *et al.*, "UV LUMINOSITY FUNCTIONS AT REDSHIFTSz$\sim$ 4 TOz$\sim$ 10: 10,000 GALAXIES FROMHSTLEGACY FIELDS," *The Astrophysical Journal* **803**, 34 (2015).

[72] H. Yan and R. A. Windhorst, "Candidates of z ~= 5.5-7 Galaxies in the Hubble Space Telescope Ultra Deep Field," ApJ **612**, L93–L96 (2004).

[73] S. Lilly, D. Schade, R. Ellis, *et al.*, "Hubble Space Telescope Imaging of the CFRS and LDSS Redshift Surveys. II. Structural Parameters and the Evolution of disk Galaxies to z ~1^1," ApJ **500**, 75–94 (1998).

[74] S. J. Lilly, O. L. Fevre, A. Renzini, *et al.*, "zcosmos: A large vlt/vimos redshift survey covering 0 ¡ z ¡ 3 in the cosmos field," *The Astrophysical Journal Supplement Series* **172**, 70–85 (2007).

[75] D. B. Fisher, K. Glazebrook, R. G. Abraham, *et al.*, "Connecting clump sizes in turbulent disk galaxies to instability theory," *The Astrophysical Journal* **839**, L5 (2017).

[76] D. B. Fisher, K. Glazebrook, I. Damjanov, *et al.*, "DYNAMO-HST survey: clumps in nearby massive turbulent discs and the effects of clump clustering on kiloparsec scale measurements of clumps," *Monthly Notices of the Royal Astronomical Society* **464**, 491–507 (2016).

[77] H. C. Ferguson, M. Dickinson, M. Giavalisco, *et al.*, "The Size Evolution of High-Redshift Galaxies," ApJ **600**, L107–L110 (2004).

[78] R. J. Allen, G. G. Kacprzak, K. Glazebrook, *et al.*, "The size evolution of star-forming galaxies since z $\sim$ 7 using ZFOURGE," *The Astrophysical Journal* **834**, L11 (2017).

[79] J. F. Navarro, C. S. Frenk, and S. D. M. White, "The Structure of Cold Dark Matter Halos," ApJ **462**, 563 (1996).

[80] S. P. Driver, D. T. Hill, L. S. Kelvin, *et al.*, "Galaxy and Mass Assembly (GAMA): survey diagnostics and core data release," MNRAS **413**, 971–995 (2011).

[81] R. A. Windhorst, S. H. Cohen, N. P. Hathi, *et al.*, "THE HUBBLE SPACE TELESCOPE WIDE FIELD CAMERA 3 EARLY RELEASE SCIENCE DATA: PANCHROMATIC FAINT OBJECT COUNTS FOR 0.2-2 m WAVELENGTH," *The Astrophysical Journal Supplement Series* **193**, 27 (2011).

[82] S. P. Driver, S. K. Andrews, L. J. Davies, *et al.*, "MEASUREMENTS OF EXTRAGALACTIC BACKGROUND LIGHT FROM THE FAR UV TO THE FAR IR FROM DEEP GROUND- AND SPACE-BASED GALAXY COUNTS," *The Astrophysical Journal* **827**, 108 (2016).

[83] P. Madau and M. Dickinson, "Cosmic Star-Formation History," ARA&A **52**, 415–486 (2014).

[84] N. P. Hathi, J. Ryan, R. E., S. H. Cohen, *et al.*, "UV-dropout Galaxies in the Goods-South Field from WFC3 Early Release Science Observations," ApJ **720**, 1708–1716 (2010).

[85] S. L. Finkelstein, "Observational Searches for Star-Forming Galaxies at z ¿ 6," PASA **33**, e037 (2016).

[86] R. A. Windhorst, F. X. Timmes, J. S. B. Wyithe, *et al.*, "On the observability of individual population III stars and their stellar-mass black hole accretion disks through cluster caustic transits," *The Astrophysical Journal Supplement Series* **234**, 41 (2018).

[87] M. Giavalisco, M. Livio, R. C. Bohlin, *et al.*, "On the Morphology of the HST Faint Galaxies," AJ **112**, 369 (1996).

[88] S. C. Odewahn, S. H. Cohen, R. A. Windhorst, *et al.*, "Automated galaxy morphology: A fourier approach," *The Astrophysical Journal* **568**, 539–557 (2002).

[89] V. A. Taylor-Mager, C. J. Conselice, R. A. Windhorst, *et al.*, "Dependence of galaxy structure on rest-frame wavelength and galaxy type," *The Astrophysical Journal* **659**, 162–187 (2007).

[90] D. Kawata, B. K. Gibson, and R. A. Windhorst, "Cosmological simulations of the high-redshift radio universe," *Monthly Notices of the Royal Astronomical Society* **354**, 387–392 (2004).

[91] J. M. Lotz, A. Koekemoer, D. Coe, *et al.*, "The Frontier Fields: Survey Design and Initial Results," ApJ **837**, 97 (2017).

[92] T. L. Johnson, J. R. Rigby, K. Sharon, *et al.*, "Star formation at z = 2.481 in the lensed galaxy SDSS j11106459: Star formation down to 30 pc scales," *The Astrophysical Journal* **843**, L21 (2017).

[93] T. L. Johnson, K. Sharon, M. D. Gladders, *et al.*, "Star formation atz= 2.481 in the lensed galaxy SDSS j1110 = 6459. i. lens modeling and source reconstruction," *The Astrophysical Journal* **843**, 78 (2017).

[94] E. Vanzella, G. B. Caminha, P. Rosati, *et al.*, "The MUSE Deep Lensed Field on the Hubble Frontier Field MACS J0416. Star-forming complexes at cosmological distances," A&A **646**, A57 (2021).

[95] E. Vanzella, G. B. Caminha, F. Calura, *et al.*, "Ionizing the intergalactic medium by star clusters: the first empirical evidence," *Monthly Notices of the Royal Astronomical Society* **491**, 1093–1103 (2019).

[96] J. Miralda-Escude, "The Magnification of Stars Crossing a Caustic. I. Lenses with Smooth Potentials," ApJ **379**, 94 (1991).

[97] P. L. Kelly, J. M. Diego, S. Rodney, *et al.*, "Extreme magnification of an individual star at redshift 1.5 by a galaxy-cluster lens," *Nature Astronomy* **2**, 334–342 (2018).

[98] J. M. Diego, N. Kaiser, T. Broadhurst, *et al.*, "Dark matter under the microscope: Constraining compact dark matter with caustic crossing events," *The Astrophysical Journal* **857**, 25 (2018).

[99] S. A. Rodney, I. Balestra, M. Bradac, *et al.*, "Two peculiar fast transients in a strongly lensed host galaxy," *Nature Astronomy* **2**, 324–333 (2018).

[100] T. Venumadhav, L. Dai, and J. Miralda-Escudé, "Microlensing of extremely magnified stars near caustics of galaxy clusters," *The Astrophysical Journal* **850**, 49 (2017).

[101] W. Chen, P. L. Kelly, J. M. Diego, *et al.*, "Searching for highly magnified stars at cosmological distances: Discovery of a redshift 0.94 blue supergiant in archival images of the galaxy cluster MACS j0416.1-2403," *The Astrophysical Journal* **881**, 8 (2019).

[102] A. A. Kaurov, L. Dai, T. Venumadhav, *et al.*, "Highly magnified stars in lensing clusters: New evidence in a galaxy lensed by MACS j0416.1-2403," *The Astrophysical Journal* **880**, 58 (2019).

[103] Diego, J. M., "The universe at extreme magnification," *A&A* **625**, A84 (2019).

[104] R. L. Akeson, X. Chen, D. Ciardi, *et al.*, "The NASA Exoplanet Archive: Data and Tools for Exoplanet Research," PASP **125**, 989 (2013).

[105] Gaia Collaboration, T. Prusti, J. H. J. de Bruijne, *et al.*, "The Gaia mission," A&A **595**, A1 (2016).

[106] J. R. Crepp, E. J. Gonzales, E. B. Bechter, *et al.*, "The TRENDS High-contrast Imaging Survey. VI. Discovery of a Mass, Age, and Metallicity Benchmark Brown Dwarf," ApJ **831**, 136 (2016).

[107] C. Marois, B. Macintosh, T. Barman, *et al.*, "Direct Imaging of Multiple Planets Orbiting the Star HR 8799," *Science* **322**, 1348 (2008).

[108] B. S. Gaudi, S. Seager, B. Mennesson, *et al.*, "The Habitable Exoplanet Observatory (HabEx) Mission Concept Study Final Report," *arXiv e-prints* , arXiv:2001.06683 (2020).

[109] The LUVOIR Team, "The LUVOIR Mission Concept Study Final Report," *arXiv e-prints* , arXiv:1912.06219 (2019).

[110] S. Ertel, D. Defrère, P. Hinz, *et al.*, "The HOSTS Survey for Exozodiacal Dust: Observational Results from the Complete Survey," AJ **159**, 177 (2020).

[111] B. Mennesson, R. Millan-Gabet, E. Serabyn, *et al.*, "Constraining the Exozodiacal Luminosity Function of Main-sequence Stars: Complete Results from the Keck Nuller Mid-infrared Surveys," ApJ **797**, 119 (2014).

[112] S. M. Andrews, D. J. Wilner, Z. Zhu, *et al.*, "Ringed Substructure and a Gap at 1 au in the Nearest Protoplanetary Disk," ApJ **820**, L40 (2016).

[113] C. A. Grady, J. P. Wisniewski, G. Schneider, *et al.*, "The Eroding Disk of AU Mic," ApJ **889**, L21 (2020).

[114] P. Kalas, J. R. Graham, E. Chiang, *et al.*, "Optical Images of an Exosolar Planet 25 Light-Years from Earth," *Science* **322**, 1345 (2008).

[115] O. Guyon, F. Martinache, E. J. Cady, *et al.*, "How ELTs will acquire the first spectra of rocky habitable planets," in *Adaptive Optics Systems III*, B. L. Ellerbroek, E. Marchetti, and J.-P. Véran, Eds., *Society of Photo-Optical Instrumentation Engineers (SPIE) Conference Series* **8447**, 84471X (2012).

[116] S. P. Quanz, I. Crossfield, M. R. Meyer, *et al.*, "Direct detection of exoplanets in the 3-10 μm range with E-ELT/METIS," *International Journal of Astrobiology* **14**, 279–289 (2015).

[117] I. de Pater, M. H. Wong, P. Marcus, *et al.*, "Persistent rings in and around Jupiter's anticyclones - Observations and theory," Icarus **210**, 742–762 (2010).

[118] M. H. Wong, J. Tollefson, A. I. Hsu, *et al.*, "A New Dark Vortex on Neptune," AJ **155**, 117 (2018).

[119] H. Yan, D. Burstein, X. Fan, *et al.*, "Calibration of the BATC survey: Methodology and accuracy," *Publications of the Astronomical Society of the Pacific* **112**, 691–702 (2000).

[120] Z. Shang, Z. Zheng, E. Brinks, *et al.*, "Ring structure and warp of ngc 5907: Interaction with dwarf galaxies," *The Astrophysical Journal* **504**, L23–L26 (1998). Original article can be found at: http://www.journals.uchicago.edu/ApJ/–Copyright American Astronomical Society.

[121] E. Peretz, J. Mather, L. Pabarcius, *et al.*, "Mapping the observable sky for a remote occulter working with ground-based telescopes," *Journal of Astronomical Telescopes, Instruments, and Systems* **7** (2021).

[122] E. Peretz, J. C. Mather, K. Hall, *et al.*, "Exoplanet imaging scheduling optimization for an orbiting1starshade working with extremely large telescopes," *Journal of Astronomical Telescopes, Instruments, and Systems* **7**(1) (2020).

[123] E. Peretz, K. Hall, J. Mather, *et al.*, "Exoplanet imaging performance envelopes for starshade-based missions," *Journal of Astronomical Telescopes, Instruments, and Systems* **7** (2021).

[124] The LUVOIR Team, "The LUVOIR Mission Concept Study Final Report," *arXiv:1912.06219 [astro-ph]* (2019). arXiv: 1912.06219.

[125] R. M. McDermid, G. Cresci, F. Rigaut, *et al.*, "Phase a science case for mavis – the multi-conjugate adaptive-optics visible imager-spectrograph for the vlt adaptive optics facility," (2020).

[126] J. Dalcanton, S. Seager, S. Aigrain, *et al.*, "From cosmic birth to living earths: The future of uvoir space astronomy," (2015).

[127] A. I. Sheinis, M. Bolte, H. W. Epps, *et al.*, "ESI, a new keck observatory echellette spectrograph and imager," *Publications of the Astronomical Society of the Pacific* **114**, 851–865 (2002).

[128] B. Y. Chang, R. M. Huppe, C. Chase, *et al.*, "Optimization of Spectralon through numerical modeling and improved processes and designs," in *Optical Materials and Structures Technologies III*, W. A. Goodman and J. L. Robichaud, Eds., **6666**, 41 – 48, International Society for Optics and Photonics, SPIE (2007).

[129] G. W. Day and C. F. Stubenrauch, "Laser Far-Field Beam-Profile Measurement by the Focal Plane Technique," *NBS Technical Note* **1001**, 1–44 (1978).

[130] M. Young, "Mode-field diameter of single-mode optical fiber by far-field scanning," *Appl. Opt.* **37**, 5605–5619 (1998).

[131] E. M. Kim and D. L. Franzen, "Measurement of Far-Field and Near-Field Radiation Patterns from Optical Fibers," *NBS Technical Note* **1032**, 1–48 (1981).

[132] E. Richard, D. Harber, G. Drake, *et al.*, "Compact spectral irradiance monitor flight demonstration mission," in *CubeSats and SmallSats for Remote Sensing III*, *Society of Photo-Optical Instrumentation Engineers (SPIE) Conference Series* **11131**, 1113105 (2019).

[133] S. J. Schiller and J. Silny, "The Specular Array Radiometric Calibration (SPARC) method: a new approach for absolute vicarious calibration in the solar reflective spectrum," in *Remote Sensing System Engineering III*, P. E. Ardanuy and J. J. Puschell, Eds., **7813**, 108 – 126, International Society for Optics and Photonics, SPIE (2010).

[134] J. Osborn, D. Föhring, V. S. Dhillon, *et al.*, "Atmospheric scintillation in astronomical photometry," *Monthly Notices of the Royal Astronomical Society* **452**, 1707–1716 (2015).

[135] J. B. Oke and J. E. Gunn, "Secondary Standard Stars for Absolute Spectrophotometry," *The Astrophysical Journal* **266**, 713 (1986).

[136] E. Peretz, J. Mather, S. Seager, *et al.*, "Mapping the observable sky for a remote occulter working with ground-based telescopes," in *Techniques and Instrumentation for Detection of Exoplanets IX*, S. B. Shaklan, Ed., **11117**, 245 – 251, International Society for Optics and Photonics, SPIE (2019).

[137] M. K. Choi, B. J. Bos, J. L. Tveekrem, *et al.*, *Successful Use of Microporous Polytetrafluoroethylene Flexible Thin Sheets in NASAÄôs OSIRIS-REx Mission*.